THE HALL EFFECT AND THE ASSOCIATED PHENOMENA

IN CADMIUM SULPHIDE

by

M.A. SUBHAN, M.Sc.(Dacca)

Presented in candidature for the degree of

Doctor of Philosophy of the University of Durham

1969

ACKNOWLEDGEMENTS

I express my deep gratitude to Dr. J. Woods for his excellent supervision, encouragement and invaluable advice and help which I received throughout my work and the preparation of this thesis. I wish to thank Professor D.A. Wright for permitting the use of his laboratory facilities, the Ministry of Overseas Development, U.K., for financial support and the Pakistan Atomic Energy Commission for granting leave during the course of this work. I would like to thank Dr. L. Clark, Dr. K.F. Burr, M.A. Carter, D.S. Orr, M.N. Islam, F. Zanich and other members of the cadmium sulphide group for many useful discussions. The help of the Workshop staff, headed by Mr. F. Spence and Mr. R. Waite, in the construction of equipment is gratefully acknowledged. I also wish to thank Mrs. K.J. Barker for her careful typing and Miss C.A. Guyll for her assistance in drawing the diagrams.

C O N T E N T S

A B S T R A C T

Hall effect and photoHall measurements have been made on a number of crystals. These crystals were grown (in this laboratory) using a modified method of the technique of growth by vacuum sublimation.

The object of the photoHall measurements was to determine some of the parameters of the imperfection centres with energy levels in the forbidden gap in photosensitive cadmium sulphide crystals. Two crystals (crystals 78 and 79) with dark conductivities less than 10^{-7} mho cm^{-1} were chosen for the investigation. Their conductivities could be increased to 10^{-2} mho cm^{-1} by optical excitation with an intensity of 3200 ft-c.

The photoHall effect was investigated at different temperatures. Measurements were made to determine the variation in the value of Hall mobility as a function of the location of the electron Fermi level which was achieved by changing the intensity of photoexcitation. From the plots of $\frac{1}{\mu}$ versus E_{fn} (at different temperatures) four electron trapping levels with energy depths of 0·12, 0·16, 0·22 and 0·33 eV and six electron trapping levels with energy depths of 0·098, 0·13, 0·19, 0·25, 0·33 and 0·42 eV below the conduction band were obtained for crystals 78 and 79 respectively.

The photoHall data were also used to determine the charge state and the scattering cross-sections of the imperfection centres.

The experimental values of the scattering cross-sections were of the order of 10^{-11} cm^2. From a study of the temperature dependence of concentration of photoexcited carriers, the height of the energy levels of the sensitizing centres above the valence band was found to be 1·04 eV.

The Hall coefficient was also measured for a number of semiconducting samples between $14^{\circ}K$ and $300^{\circ}K$. The donor ionization energies and the donor and acceptor concentrations were determined from the variation of carrier concentration with temperature above $30^{\circ}K$. Below $30^{\circ}K$, the variation of carrier concentration with temperature was found to be dominated by an impurity band conduction mechanism (non-metallic type). Polar optical mode scattering was the dominant intrinsic scattering mechanism at the higher temperatures. The experimental mobility data could be fitted to theoretically computed values of μ assuming that polar optical mode, piezoelectric and ionized impurity scattering processes were operative. The effective mass was used as an adjustable parameter. The best fit was obtained with $m_e^* = 0{\cdot}19$ m.

CHAPTER 1

ELECTRICAL CONDUCTION IN SOLIDS

1-1. Band Theory

1-1.1. Introduction

When the component atoms are brought close together to form a solid, each energy level of the individual atom splits into a large number of closely spaced levels and gives rise to what is known as an "energy band". A knowledge of the band-theory helps to assess the electrical and optical properties of a solid. Several authors (see for example Smith[1], Cusack[2], Kittel[3], Dekker[4], etc.) have given simplified accounts of band-theory which will briefly be outlined here.

1-1.2. Sommerfeld's free electron model of a solid

To explain electrical conduction in solids several models based on the assumption that the valence electrons are free to roam among the ionic array, have been developed. Sommerfeld's[5] model is a modification of Drude's free electron theory in which the concepts of quantum mechanics were introduced by substituting Fermi-Dirac statistics for classical statistics. In this model the electrons are considered imprisoned in a potential box bounded by the wall of the solid. This model, though able to give an explanation of the small contribution of electrons to the specific heat and paramagnetism, fails to explain satisfactorily the scattering mechanism and also why some solids are good conductors and others semiconductors or insulators.

1-1.3. Band Theory Approach

(a) E-k diagram for a free electron

The energy E and momentum p of an electron of mass m in a free space are related by the expression

$$E = \frac{p^2}{2m} \tag{1.1}$$

Here E denotes the kinetic energy.

Introducing de Broglie's idea that the matter waves associated with a particle, whose wavelength λ is related to the momentum p of the particle by the relationship $\lambda = \frac{h}{p}$, the equation (1.1) becomes

$$E = \frac{\hbar^2 k^2}{2m} \tag{1.2}$$

where $k = \frac{2\pi}{\lambda}$ is defined as the wave-number. Equation (1.2) describes a parabola (fig. 1.1) with the curvature at the origin given by $\frac{d^2E}{dk^2} = \frac{\hbar^2}{m}$ which depends on mass m.

It can be shown that the solutions of the Schrödinger equation for a free electron in a field of force in which it has a potential energy V,

$$\frac{d^2\Psi}{dx^2} + \frac{8\pi^2 m}{h^2} (W-V)\,\Psi = 0 \tag{1.3}$$

are of the form $\Psi = Ae^{\pm \frac{2\pi i \sqrt{2m(W-V)}}{h} x}$ (1.4)

Substituting (1.2) i.e. $E = W-V = \frac{\hbar^2 k^2}{2m}$ in equation (1.3), the general solution for a free electron moving in a constant potential field

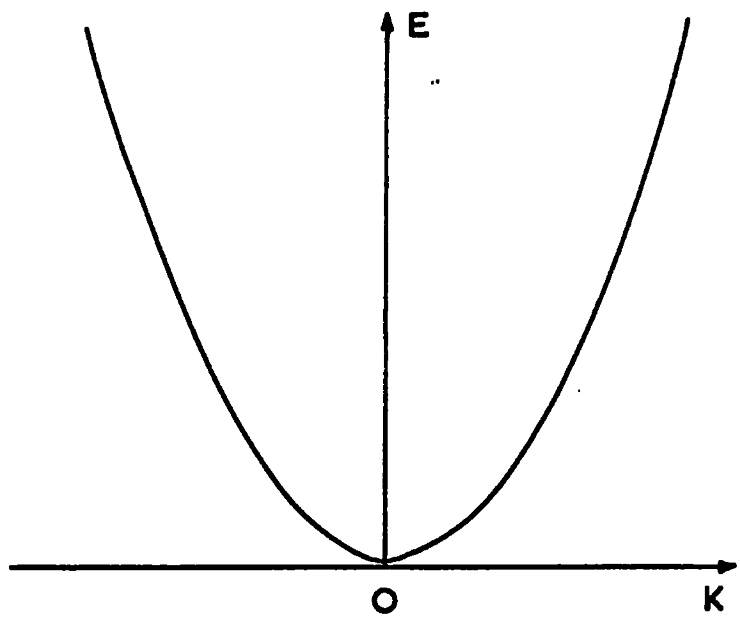

Fig. 1.1 Free electron parabola

becomes $\Psi(x) = Ce^{\pm ikx}$ (1.5)

where C is a constant.

The equation (1.5) represents the electron waves of Sommerfeld's free electron model. These are commonly referred to as Sommerfeld waves. Thus a curve of the same shape as that shown in Figure 1.1 is obtained for an electron in a field free space.

It seems that there is no upper limit to the values of either E or k that an electron can have. Because Sommerfeld's model imposes limitations on the dimension of the potential box, the energy spectrum is quasi continuous i.e. it consists of closely spaced but discrete energy levels.

(b) The Bloch Theorem

The eqn. $\Psi(x) = Ce^{\pm ikx}$ represents plane waves propagating along the x-axis with momentum $p = \hbar k$ according to de Broglie's relation.

An idealized "perfect" crystal in the absence of lattice vibrations possesses a perfect periodicity of atomic structure. Every lattice point in a three dimensional crystal lattice is described by a vector of the form

$$\underline{R}n = h\underline{a}_1 + k\underline{a}_2 + l\underline{a}_3 \qquad (1.6)$$

where h,k,l are integers and $\underline{a}_1$, $\underline{a}_2$, and $\underline{a}_3$ are called the primitive translation vectors. The atomic structure of an ideal crystal under such translation remains invariant and the resultant array is identical to the original one.

Since the crystal lattice repeats itself, the potential energy term $V(x)$ of period d in eqn. (1.3) is a periodic function such that

$$V(x) = V(x+rd) \tag{1.7}$$

where r is an integer.

F. Bloch[5] took account of the periodic potential of the crystalline lattice and showed that the solutions of the Schrödinger equation (1.3) are of the form:

$$\Psi_k(x) = U_k(x) \exp[ikx] \tag{1.8}$$

where $U_k(x)$ is a periodic function having the periodicity of the lattice in the x-direction. That means that

$$U_k(x+d) = U_k(x) \tag{1.9}$$

The wave functions given by equation (1.8), commonly called Bloch waves have the form of plane waves with propagation vector k modulated by a function whose periodicity is that of the crystal lattice.

(c) The Kronig-Penny Model

Kronig and Penny also investigated electron propagation in crystalline solids by considering an infinite series of one-dimensional square-well potentials periodically spaced as shown in Figure 1.2. A full account of the mathematical treatment of this model will be found in the references (6), (7) and (8). They used this model to obtain solutions of the Schrödinger equation in the form of Bloch functions (equation 1.8). They showed that solutions are possible only for certain electron energies which can be determined from the relation

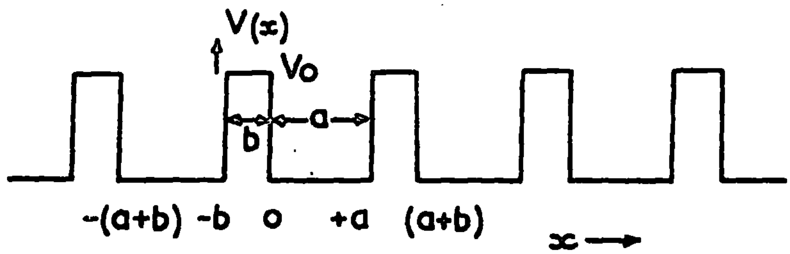

Fig. 1.2 Periodic array of potential wells

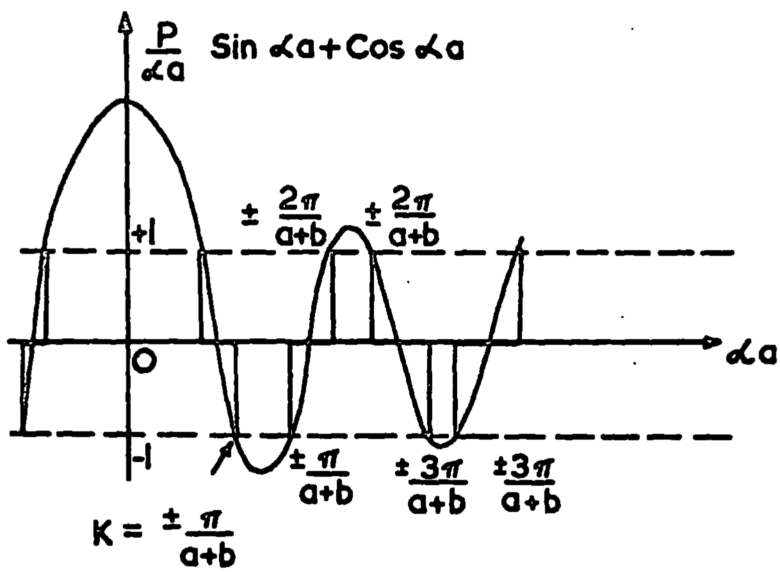

Fig. 1.3 The left hand side of equ. (1-12) is plotted as a function of αa. The allowed regions are heavily drawn.

$$\text{Cos ka} = \frac{p \text{ Sin } \alpha a}{\alpha a} + \text{Cox } \alpha a \tag{1.10}$$

$$\text{where } p = \frac{4\pi^2 ma}{h^2} V_o b \tag{1.11}$$

$$\text{and } \alpha = \frac{2\pi}{h}\sqrt{2mE} \tag{1.12}$$

To understand the real meaning of the equation (1.10), a representation of the right hand side of equation (1.10) as a function of αa for the value $p = \frac{3\pi}{2}$ is shown in Figure 1.3. Since α^2 is proportional to E, the abscissa αa is a measure of the energy. Since the left hand side of equation (1.10) can assume values between +1 and -1, only those values of αa are allowed for which the left hand side of equation (1.10) falls in this range as indicated by the horizontal lines in Figure 1.3. For values outside these limits k must be complex with non zero imaginary part and the corresponding ranges of energy represent forbidden bands in which no electron motion is possible. Thus the introduction of the very concept of the periodic potential changes the E-k diagram of Figure 1.1 by forming alternate regions of allowed and forbidden energies for electron propagation at an interval of $k = \pm \pi/d$ as shown in Figure 1.4.

From the Figure 1.3, the following conclusions can be reached:

i) The width of the allowed energy band increases with increasing E.

ii) The width of the particular allowed band decreases as the binding energy of the electrons increases.

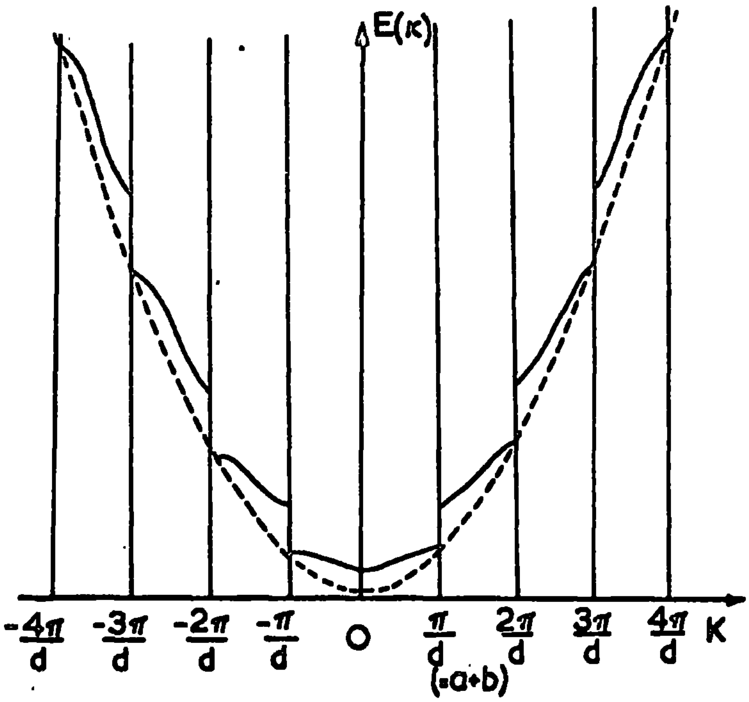

Fig. 1.4 E-K diagram modified due to periodic crystal lattice.

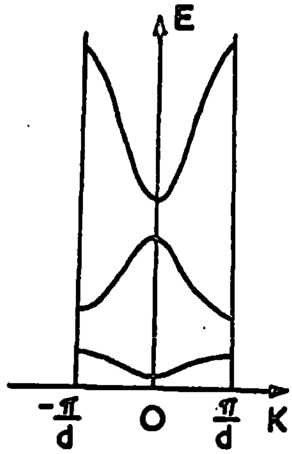

Fig. 1.5 Reduced zone propagation space.

1-1.3. Brillouin Zone

The momentum $p = \hbar k$ associated with the waves given by equation (1.8) is known as the crystal momentum and is different from the real momentum to which it is equal when $V(x)$ is constant. Also the wave function (1.8) does not define k uniquely. Let us write the wave equation (1.8) in the form:

$$\Psi_k(x) = U_k(x)e^{ikx} = [U_k(x)e^{-\frac{2\pi irx}{d}}]e^{i(k+\frac{2\pi rx}{d})}$$

$$= U_{k'}(x)e^{ik'x} \qquad (1.13)$$

$$\text{where } k' = k + \frac{2\pi r}{d} \qquad (1.14)$$

The wave function in equation (1.13) is a solution of the wave-equation for the same energy as the wave function in (1.8) and $U_{k'}(x)$ is also a periodic function of period d. Therefore the quantities k and k' are equivalent. The energy E is thus a periodic function of k with period $2\pi/d$. Thus the Bloch Theorem restricts the value of k to an interval $2\pi/d$, usually $-\pi/d \leqslant k \leqslant +\pi/d$. (1.15)

The region of k-space defined by (1.15) is referred to as the first Brillouin Zone and $k = \pm\pi/d$ as the zone boundaries. Similarly the second Brillouin Zone is defined by the segments $-2\pi/d < k < -\pi/d$ and $+\pi/d < k < +2\pi/d$; etc.

The discontinuities in the energy curve for an electron in a periodic potential (Figure 1.4) occur when k has the values

$$k = \frac{n\pi}{d} \qquad (1.16)$$

where $n = \pm 1, \pm 2, \pm 3, \ \ldots.$

Substituting the values of $k = 2\pi/\lambda$ in (1.16) we have

$$\frac{2\pi}{\lambda} = \frac{n\pi}{d}$$

$$\therefore \quad n\lambda = 2d$$

The equation (1.16) satisfies the Bragg law of reflection for an electron wave for the special case when $\theta = \pi/2$ $(n\lambda = 2d\,\mathrm{Sin}\,\theta)$.

Thus the discontinuities in the allowed energy ranges of the electrons in a crystal can be interpreted to mean either total reflection of the electrons by the planes that are normal to their direction of propagation or as Bragg reflection by the other crystallographic planes. However, the zones are functions only of the crystal structure and in all cases the boundaries of the Brillouin zones are determined by the Bragg law of reflection.

Since the wave function and hence the energy E is a multivalued function of the wave vector k, the curves of E versus k are plotted in a reduced propagation space with the values of k limited to $-\pi/d \leq k \leq +\pi/d$. This is called the <u>reduced zone representation</u> (shown in Figure 1.5) done by translating the various segments of the E versus k curves to the right or to the left, parallel to the k-axis, through distances which are integral multiples of $2\pi/d$ so that they all fit within the interval $-\pi/d \leq k \leq \pi/d$.

1-1.4. Effective Mass

Near the band edges (Figure 1.4) the energy-momentum relationship is not parabolic. As a result the group velocity of the wave packet which describes the electron motion is not expected to be identified with the classical velocity of the electron, defined as

$$v = \frac{dw}{dk} = \frac{\hbar k}{m} = \frac{p}{m} \tag{1.17}$$

Since w, the angular frequency of the de Broglie's waves is related to the energy of the particle $E = \hbar w$,

$$v = \frac{dw}{dk} = \hbar^{-1}\frac{dE}{dk} \tag{1.18}$$

The work dE done on the electron by the electric field $\mathcal{E}$ in the time interval dt is

$$dE = e\mathcal{E}\, v dt \tag{1.19}$$

Combining (1.18) and (1.19) it can be shown that

$$\hbar\frac{dk}{dt} = e\mathcal{E} \tag{1.20}$$

In a crystal therefore, $\hbar\, dk/dt$ is equal to the external force on the electron.

From the equation (1.18) and using (1.20) for dk/dt, we can show that

$$\frac{dv}{dt} = \frac{d^2E}{dk^2} \cdot \frac{e\mathcal{E}}{\hbar^2} \tag{1.21}$$

Comparing equation (1.21) with the classical equation $dv/dt = e\mathcal{E}/m$, it follows that $\hbar^2/(d^2E/dk^2)$ plays the role of the mass. Let us call this quantity the effective mass m^*:

$$m^* = \frac{\hbar^2}{d^2E/dk^2} \tag{1.22}$$

Thus the entire effect of the periodic potential is to replace the electron mass of the expression $E = \hbar^2k^2/2m$ by an effective mass m^*, so that most of the results obtained from the free electron model can be carried over to the solid. Now in the expression for energy $E = \frac{\hbar^2 k^2}{2m^*}$, m^* is consistent with equation (1.22).

At the lower edge of each band, the E versus k curve (according to Figure 1.4) resembles a parabola which corresponds to a free electron of constant mass. Higher up, a point is reached where $d^2E/dk^2 = 0$ yielding $m^* = \pm\infty$; the curvature then changes sign and d^2E/dk^2 becomes negative at the top edge. A negatively charged particle with a negative effective mass under the influence of an applied field would be expected to exhibit the same dynamical behaviour as a positively charged particle with positive mass. We shall refer to this as a hole. It is evident from the equation (1.22) that the effective mass starts at some positive value of m^* at the bottom, rises to infinity, changes sign and tends to $-m^*$ at the top edge. We can apply these concepts therefore to a whole band. The mass of an electron tends to infinity as we pass upwards towards the inflection from the bottom of the conduction band and the mass of a hole does the same as we pass downwards from the top of the valence band. It can be concluded therefore that the concept of the effective mass is only meaningful near the band edges.

1-1.5. Density of States

After establishing the rudiments of the band model, we need to consider the density of levels available to an electron and their occupation by the valence electrons in the band.

Application of ~~the~~ Pauli's exclusion principle and the uncertainty principle for electrons in a uniform potential leads to an expression for the density of states for electrons having energies between E and E + dE, for unit crystal volume,

$$N(E)dE = \frac{2\pi}{h^3} (2m)^{3/2} E^{\frac{1}{2}} dE \qquad (1.23)$$

This has been derived by considering the spherical shell between two spheres representing the region of momentum space corresponding to energies in the range E to E + dE.

When considering the density of states in bands the electron mass m in (1.23) is replaced by the effective mass m_e^* and energy must be measured from the energy E_o at the bottom of the band. Equation (1.23) then becomes

$$N(E)dE = \frac{1}{2\pi^2} \left(\frac{2m_e^*}{\hbar^2} \right)^{3/2} \left(E-E_o \right)^{\frac{1}{2}} dE \qquad (1.24)$$

The constant energy surfaces in the Brillouin zone are spherical around the point k = 0 and the distribution of levels in this region follows that of free electrons. Towards the zone boundaries, the energy contours start to bulge, the density of states curve, consequently, deviates from the free electron parabola, reaches a maximum because each elementary energy range contains successively more states than the spherical shells of the free electron theory. After this point, since only the corners of the zone are available, the density of states falls, becoming zero at the maximum energy of the band. Eventually, as the surfaces of constant energy become inverted spheres enclosing free hole states, the density of states curve again becomes parabolic, but in the reverse sense, with m in (1.23) replaced by m_h^*, the effective hole mass and E replaced by $E_I - E$ where E_I is the energy at the top of the band. Densities of states functions for different cases are shown in Figure 1.6.

It can be shown that each Brillouin zone occupies the same volume in k-space. Each Brillouin zone contains one energy level per lattice point and each energy level represents two quantum states differing in their spin quantum numbers only. Therefore, each Brillouin zone can accommodate 2N electrons, where N is the total number of primitive cells ~~atoms~~ in the crystal.

1-1.6. Conductor, Semiconductor and Insulator

On the basis of our previous discussion of the energy band model and the density of states, a proper distinction between these three groups of materials is possible. In each band there are N closely-spaced energy levels for a solid having N atoms. Since each level can accommodate two electrons according to Pauli's exclusion principle, for an atom with an odd number of valence electrons (for example, Na; $1S^2 2S^2 2P^6 3S^1$) only half of the available energy levels in the highest occupied band will be filled. As a result of this, application of an electric field to these solids can move electrons to higher unoccupied states and electronic conduction can occur. Such a solid will exhibit all the characteristic properties of a good metallic conductor.

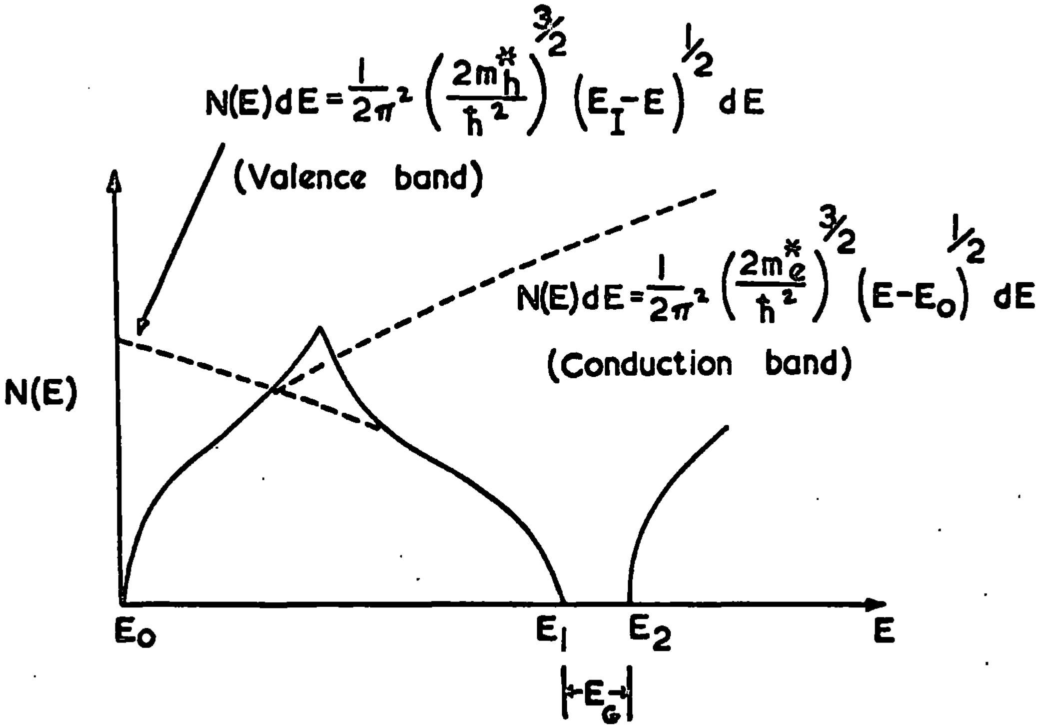

Fig. 1.6(a) Density of states curve in the Brillouin Zone. There is no band overlapping in this case.

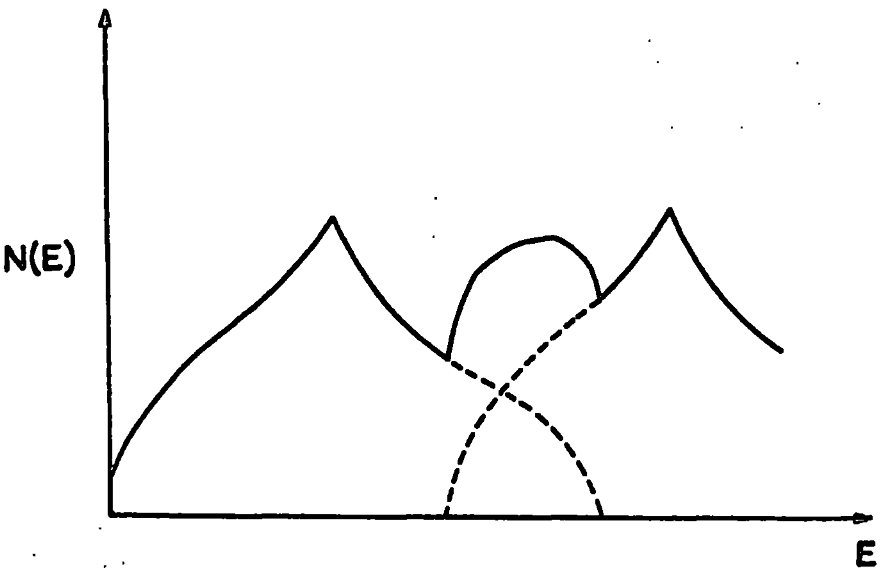

Fig. 1.6(b) Density of states curve for two overlapping bands.

According to the above discussion, in a divalent metal such as magnesium whose electronic structure is $1s^2 2s^2 2p^6 3s^2$, all available energy levels of the highest occupied band will be completely filled. In fact, the top of the highest occupied band (3s) overlaps the bottom of the (3p) band above. So the 2N electrons are therefore, in a combined band of 2N levels and the empty levels are available to allow electrical conduction to take place.

When a solid with an even number of valence electrons just sufficient to completely fill a number of energy bands, has its full band (termed the valence band) separated from the empty band (the conduction band) by a wide forbidden region ($E_G \gg kT$) there is insufficient thermal energy to excite a significant number of electrons across this region from the top of the valence band to the bottom of the conduction band. Such a material will be an <u>insulator</u>.

When this energy gap between the full and the empty bands is very small ($E_G \ll 1$ eV), at temperature above 0^{o}K, a limited number of thermally excited free electrons are available for conduction of electrical currents in the almost empty upper band. The empty states left behind near the top of the valence band allow this band to contribute to the electrical conduction by the mechanism of hole conduction. A material of this sort is called an <u>intrinsic semiconductor</u>.

The distinction between an insulator and semiconductor is of One ~~one~~ degree only. All semiconductors become ideal insulators as the temperature approaches absolute zero.

1-2. Semiconductor

In section 1-1.6 on the basis of the band theory we have discussed what is meant by a semiconductor. A solid with an energy gap $E_G < 2$ev is generally termed a semiconductor and one with $E_G > 2$ev, an insulator. Semiconductors are considered to have electrical resistivity at room temperature in the range 10^{-2} to 10^{9} ohm-cm, intermediate between good conductors ($\sim 10^{-6}$ ohm-cm) and insulators ($\sim 10^{14}$ to 10^{22} ohm-cm). There are in principle two types of semiconductors - intrinsic and extrinsic.

The name "intrinsic" implies that the semiconducting property is a property characteristic for the pure material. The value E_G/kT controls the intrinsic semiconduction. Since the thermal excitation of an electron from the valence band to the conduction band inevitably creates one and only one hole in the valence band, there will be as many holes as electrons. Another characteristic property of intrinsic semiconductors is that the current is carried by two types of carriers - electrons and holes, referred to as intrinsic charge carriers.

The characteristic properties of extrinsic semiconductors are brought about by impurities, lattice defects or lack of stoichiometry. Impurity atoms are donors if they introduce occupied energy levels in the forbidden region from which electrons can easily be excited to the conduction band. This type of semiconductor, in which the charge carriers are predominantly electrons, is called an n-type semiconductor. Some impurity atoms introduce empty energy levels to which electrons can be excited from the valence band, thereby producing free holes. This type of semiconductor where holes dominate the electrical conduction, is known as p-type.

Generally in elemental semiconductors, added impurities convert them to either n-type or p-type. On the other hand in many of the intermetallic semiconductors the lack of stoichiometric balance between the component atoms is the principal reason for their conduction. An anion vacancy in a compound semiconductor will act as a donor and a cation vacancy caused by an excess of anion can give rise to a free hole at ordinary temperature.

It is usual for semiconductors to contain both donor and acceptor impurities simultaneously. The donor electrons fill up any available acceptor levels since the crystal must attain the lowest possible energy state consistent with its temperature. Therefore, the difference between the donor and the acceptor impurity concentrations N_D and N_A determines whether the crystal is n-type or p-type. A semiconductor is said to be compensated when it is fabricated with $N_D \approx N_A$.

In addition to the shallow energy levels, there are discrete energy levels lying deep in the forbidden region. These discrete levels when they first capture electrons and subsequently capture holes, are called <u>recombination centres</u>. The probability that any localized level can capture an excess carrier is expressed in terms of capture cross-section. A recombination centre usually has a large capture cross-section both for electrons and holes. It often happens that the cross-section for capture of one type of carrier may be much larger than that for the other type of carrier.

1-2.1. Fermi Level and Free Carrier Density in an Intrinsic Semiconductor.

In an intrinsic semiconductor, the valence band is completely filled and the conduction band is completely empty at zero degree absolute. At a finite temperature, however, the thermal agitation produces a definite probability of a valence electron being excited from its band to the conduction band. Now the number of electrons in the conduction band at any temperature $T^{o}K$ can be determined by multiplying N(E), the density of available states in the conduction band by the probability f(E) that a state is occupied and integrating over all the energies greater than E_C.

The probability that an electron occupies a state of energy E is given by the Fermi-Dirac distribution:

$$f(E) = \frac{1}{1+\exp(E-E_F)/kT} \qquad (1.25)$$

Here E_F corresponds to a level of energy E which has a probability of 1/2 for being occupied and is called the "Fermi Energy Level".

Accordingly the density of electrons in the conduction band is

$$n = 2\int_{E_C}^{\infty} N(E)\ f(E)\ dE \qquad (1.26)$$

The factor 2 takes account of the spin degeneracy of a level.

Substituting the values of N(E) in the case of parabolic band structure with spherical energy surfaces given by equation (1.24) and f(E) in (1.26), we obtain

$$n = 2\left(\frac{8\pi m_e^*}{h^3}\right)\sqrt{2m_e^*(E-E_C)}\int_{E_C}^{\infty}\frac{1}{1+\exp(E-E_F)/kT}\,dE \qquad (1.27)$$

When $E-E_F \gg kT$, the probability of occupation of a level is small. Under this condition, the system is said to be non-degenerate and f(E) approaches the classical Boltzmann distribution, i.e. $f(E) \simeq \exp[-(E-E_F)/kT]$. Hence

$$n = \left(\frac{8\pi m_e^*}{h^3}\right)\sqrt{2m_e^* kT}\; e^{-(E_C-E_F)/kT}\int_{E_C}^{\infty}\left(\frac{E-E_C}{kT}\right)^{\frac{1}{2}} e^{-(E-E_C)/kT}\,dE \qquad (1.28)$$

Let $y = (E-E_C)/kT$, so that the integral takes the standard form:

$$kT\int_0^{\infty} y^{\frac{1}{2}} e^{-y}\,dy = \frac{kT\pi^{\frac{1}{2}}}{2}$$

So the equation (1.28) becomes

$$n = N_C \exp[-(E_C-E_F)/kT] = N_C \exp\left[\frac{-E_{fn}}{kT}\right] \qquad (1.29)$$

where $N_C = 2\left(\frac{2\pi m_e^* kT}{h^2}\right)^{3/2}$ is called the effective density of states in the conduction band and E_{fn} is the absolute energy difference between the Fermi level and the bottom of the conduction band.

Similarly the number of holes per unit volume in the valence band created by the thermal excitation of electrons from the valence band to the conduction band can be determined. In this case $[1-f(E)]$ represents the probability for a state of energy E to be unoccupied. The density of holes in the valence band is given by

$$p = \int_{\text{bottom}}^{E_v} N(E)[1-f(E)]dE \tag{1.30}$$

where the integration extends over the valence band. Now the density of states in the valence band according to (1.24) is

$$N(E) = \left(\frac{8\pi m_h^*}{h^3}\right)\sqrt{2m_h^*(E_v-E)}$$

Again for a non-degenerate case,

$$p = \left(\frac{8\pi m_h^*}{h^3}\right)\sqrt{2m_h^* kT}\; e^{-(E_F-E_v)/kT}\int_{-\infty}^{E_v}\left(\frac{E_v-E}{kT}\right)^{\frac{1}{2}}\cdot e^{-(E_v-E)kT}\, dE$$

On evaluating the integral, we obtain

$$p = N_v\, e^{-(E_F-E_v)/kT} = N_v \exp\left[-E_{fp}/kT\right] \tag{1.31}$$

where $N_v = 2\left(\frac{2\pi m_h^* kT}{h^2}\right)^{3/2}$, is the effective density of states in the valence band and E_{fp} is the absolute energy difference between the Fermi level and the top of the valence band.

In the case of intrinsic semiconductor n = p,

$$\therefore \qquad N_C \exp[-(E_C-E_F)/kT] = N_v \exp[-(E_F-E_v)/kT]$$

$$\text{or,} \qquad E_F = -\frac{E_G}{2} + \frac{3}{4}kT\ln\left(\frac{m_h^*}{m_e^*}\right) \tag{1.32}$$

For $m_e^* = m_h^*$, the Fermi level lies halfway between the bottom of the conduction band and the top of the valence band.

The product np has the form

$$np = n_i^2 = 4\left(\frac{2\pi kT}{h^2}\right)^3 (m_e^* \, m_h^*)^{3/2} \exp\left[-E_G/kT\right] \qquad (1.33)$$

where n_i is the density of the intrinsic carriers.

$$\therefore \quad n_i = p_i = 2\left(\frac{2\pi kT}{h^2}\right)^{3/2} (m_e^* \, m_h^*)^{3/4} \exp\left[-E_G/2kT\right] \qquad (1.34)$$

This equation shows that the concentration of carriers in an intrinsic semiconductor is a strong function of temperature, increasing as the temperature rises and is likewise strongly dependent upon the energy gap E_G, decreasing rapidly as E_G increases.

1-2.2. Free Carrier Density in an Extrinsic Semiconductor

Additions of impurities to semiconductors produce energy levels in the forbidden gap. These levels are localized about their impurity atoms for reasonably small impurity concentrations. The concentrations of electrons in the conduction band for a non-degenerate situation is still given by (1.29) i.e. $n = N_C \exp[-(E_C - E_F)/kT]$, the concentration of holes by (1.31) and the product np by (1.33). Now E_F needs to be modified because the Fermi function expresses the occupation probability associated with the impurity levels.

Let us consider an n-type semiconductor having N_D donor levels per unit volume and whose depth E_D from the conduction band is very small compared with the forbidden energy gap. At a sufficiently high temperature T all the impurities will be ionised so that $n = N_D$ and the position of the Fermi level is given by

$$-E_{fn} = kT\ln(N_D/N_C)$$

This equation shows that as N_D increases, the Fermi level moves towards the conduction band. To maintain the assumption of non-degeneracy we must have $N_D \ll N_C$. In this condition the concentration of electrons in the conduction band appears practically constant up to certain temperature and the semiconductor is said to be saturated.

It is quite impossible to prepare semiconductors which are either perfectly pure or doped with only one type of impurity. The simultaneous presence of both donor and acceptor levels in the forbidden region must be considered.

Let us assume that N_D and N_A represent the densities of donors and acceptors per unit volume and $N_D > N_A$. Also assume that the total number of ionized donors is equal to $(n + N_A)$ which is also equal to $(N_D - n_d)$ where n_d is density of neutral donors. In this condition the Fermi level lies close to the conduction band and the acceptor level is far below E_F to justify the assumption that all acceptors are fully occupied by electrons i.e. $N_A = N_A^-$.

$$\therefore \quad n + N_A^- = N_D - n_d = N_d^+ \quad \text{(say)}$$

The probability of an electron of either spin occupying a donor level is

$$f(E) = \frac{1}{1+\frac{1}{2}\exp[(E-E_F)/kT]}$$

with $E = -E_D$, the depth of the donor level from the conduction band.

The number of unionised donors n_d is given by

$$n_d = \frac{N_D}{1+\frac{1}{2}[(E-E_F)/kT]}$$

$$\therefore \quad n + N_A = N_D - n_d = \frac{N_D}{1+2\exp[(E_F+E_D)/kT]}$$

Rewriting this,

$$\frac{(n+N_A)e^{E_F/kT}}{(N_D-N_A-n)} = \frac{1}{2}\, e^{-E_D/kT} \tag{1.35}$$

If n is small so that there is no degeneracy and also $n > n_i$, then

$$n = N_C e^{E_F/kT} \quad \text{giving}$$

$$\frac{n(n+N_A)}{(N_D-N_A-n)} = \frac{N_C}{2}\exp[-E_D/kT] \tag{1.36}$$

This equation is to be examined in three fairly distinct temperature ranges.

(1) Exhaustion range when kT is greater than E_D but considerably smaller than E_G. Here $n = N_D - N_A$ and the electron concentration is essentially independent of the temperature.

(2) As the temperature is lowered, the electrons begin to freeze out into the donor levels and we enter the second range of temperature. When $n < N_D - N_A$ and $n > N_A$ the electron concentration is given by the relation

$$n = \left[\frac{N_C}{2} (N_D - N_A) \right]^{\frac{1}{2}} \exp[-E_D/2kT] \qquad (1.37)$$

(3) The third range of temperature occurs at very low temperature when the conditions $n < (N_D - N_A)$ and $n < N_A$ are satisfied. Then n becomes approximately

$$n = \frac{N_C}{2} \left(\frac{N_D - N_A}{N_A} \right) \exp[-E_D/kT] \qquad (1.38)$$

From the measurement of the carrier concentration as a function of temperature at the lower temperature region, the impurity ionization energy E_D can be determined. A plot of $\ln(nT^{-3/2})$ versus $1/T$ would be a straight line with slope $-E_D/k$ or $-E_D/2k$ depending upon the degree of compensation.

1-2.3. <u>The Quasi Fermi Levels</u>:

The relations $n = N_C \exp[-E_{fn}/kT]$ and $p = N_v \exp[-E_{fp}/kT]$ define a single Fermi level for thermal equilibrium in the dark and E_{fn} and E_{fp} give the values of the distances of the conduction and the valence bands from this level. The concept of a single Fermi level is no longer valid when the equilibrium carrier concentration is disturbed for example by irradiating the sample with light which generates free electrons and holes. Under this condition the single thermal equilibrium Fermi level is replaced by two steady-state Fermi levels known as quasi Fermi levels, one for electrons and one for holes. But the concentrations of carriers in their respective bands are still given by equations similar to (1.29) and (1.31). Thus

$$n = N_C \exp[-E_{fn}/kT] \tag{1.39}$$

and $$p = N_V \exp[-E_{fp}/kT] \tag{1.40}$$

where E_{fn} and E_{fp} are the electron and hole quasi Fermi levels.

1-3. Transport Properties

1-3.1. (a) Electrical Conductivity of a Free-Electron Gas

For an isotropic medium the electrical conductivity σ is defined by

$$J_x = \sigma \mathcal{E}_x \tag{1.41}$$

where J_x is the current density resulting from an applied electric field $\mathcal{E}_x$ in the x-direction. From an atomic viewpoint, the current can be ascribed to a flow of electrons i.e.

$$J_x = -ne\langle v_x \rangle \tag{1.42}$$

where n is the number of electrons per unit volume and $\langle v_x \rangle$ is the average velocity of the electrons in the x-direction, given by $\langle v_x \rangle = \frac{1}{n}\sum_{i=1}^{n} v_i$.

In the absence of an electric field, the electrons move in a random way with a velocity distribution appropriate to their temperature. In this condition the velocity distribution is isotropic and $\langle v_x \rangle$ vanishes.

A free electron under the influence of an external field $\mathcal{E}_x$ develops an acceleration $a_x = -e\,\mathcal{E}_x/m$, and its velocity would continue to increase with time. However Ohm's law requires that an external field should lead to an average velocity $\langle v_x \rangle$ which is proportional to $\mathcal{E}_x$. It is assumed therefore that in a collision with the lattice the electron loses all the energy it has gained from the external field and that its velocity after the collision is random. Let dt/τ express the probability for an electron to collide with the lattice during a small time interval dt. τ is a constant known as the relaxation time, and is related to the mean free time between electron collisions. Now the rate of change of the average velocity in the x-direction due to the field alone is

$$\left(\frac{\partial \langle v_x \rangle}{\partial t}\right)_{field} = \frac{-e\,\mathcal{E}_x}{m} \tag{1.43}$$

Also the rate of change of $\langle v_x \rangle$ due to collision with the lattice is

$$\left(\frac{\partial \langle v_x \rangle}{\partial t}\right)_{coll.} = -\langle v_x \rangle/\tau \tag{1.44}$$

In the steady state,

$$\frac{d\langle v_x \rangle}{dt} = 0 = \left(\frac{\partial \langle v_x \rangle}{\partial t}\right)_{field} + \left(\frac{\partial \langle v_x \rangle}{\partial t}\right)_{coll.}$$

$$\therefore \quad \langle v_x \rangle = -\left(\frac{e\tau}{m}\right)\mathcal{E}_x \tag{1.45}$$

And $$\sigma = J_x/\mathcal{E}_x = ne^2\tau/m \tag{1.46}$$

Let us define the mobility μ of a particle as the magnitude of the average drift velocity per unit field. Then from (1.45), the mobility μ is given by

$$\mu = \left[\frac{\langle v_x \rangle}{\mathcal{E}_x}\right] = \frac{e\tau}{m} \tag{1.47}$$

The expression for conductivity therefore becomes

$$\sigma = \frac{ne^2\tau}{m} = ne\mu \tag{1.48}$$

(b) Conduction Electrons in a Solid

In describing the electrical conductivity of a free electron gas we have assumed τ to be same for all free electrons. When τ is not constant but varies with the energy E, equation (1.48) needs modification. Also the free electron mass in (1.47) must be replaced by an effective mass m^*. For a metal or highly degenerate semiconductor, the presence of an external field changes the distribution of electrons effectively in an energy range of a few kT about the Fermi level E_F. In this case, equation (1.48) still holds provided the relaxation time of the electrons at the Fermi level $\tau = \tau_F$ is taken. Thus the expression for conductivity in this case becomes

$$\sigma = \frac{J_x}{\mathcal{E}_x} = \frac{ne^2\tau_F}{m^*} = ne\mu \tag{1.49}$$

Another extreme case, in which the expression for the current density needs to be simplified, occurs when the energy distribution of the electrons in the conduction band is Maxwellian. For example, in a non-degenerate semiconductor with an isotropic electron mass, the distribution function F_o in the Boltzmann transport equation for the current density

$$J_x = - \frac{e^2 \mathcal{E}_x}{3} \int_o^{\infty} \frac{\partial F_o}{\partial E} v^2 \tau (E) (8\pi/h^3) p^2 dp \qquad (1.50)$$

is $F_o = A \exp[-E/kT]$ where A is a constant, and $F_o \ll 1$. Since $F_o \ll 1$, the Fermi function satisfies the relation

$$-\left(\frac{\partial F_o}{\partial E}\right) = F_o(1-F_o)/kT \simeq F_o/kT$$

Recognising that $8\pi p^2 dpF_o/h^3$ equals the number of electrons with momentum lying between p and p + dp, integration of (1.50) gives

$$J_x = \frac{ne^2 \mathcal{E}_x \langle v^2 \tau \rangle}{3kT} = \sigma \mathcal{E}_x = ne\mu \mathcal{E}_x \qquad (1.51)$$

where n is the electron concentration in the conduction band and $\langle v^2 \tau \rangle$ is the average value of $v^2 \tau(E)$, averaged over the Maxwellian velocity distribution of the conduction electrons. Since $3kT = m^* \langle v^2 \rangle$ according to the kinetic theory, the expression for the mobility becomes

$$\mu = \frac{e}{m^*} \frac{\langle v^2 \tau \rangle}{\langle v^2 \rangle} = \frac{e}{m^*} \bar{\tau} \qquad (1.52)$$

The mobility so defined is called the conductivity mobility.

However, the relaxation time is also determined by the scattering mechanisms of the charge carriers with impurities, imperfections or aperiodicities of one sort or another in the crystal.

(c) Conduction due to both Electrons and Holes

Using equation (1.48) we can write the current densities transported by electrons and holes.

$$J_n = ne\mu_n \mathcal{E}$$

$$J_p = pe\mu_h \mathcal{E}$$

When the conductivity σ is due to both sets of carriers, as in an intrinsic semiconductor, then

$$\sigma = J/\mathcal{E} = e(n\mu_n + p\mu_h) \tag{1.53}$$

The mobilities in the above formulas are defined according to equation (1.52) as

$$\mu_n = \frac{e\,\bar{\tau}_e}{m_e^*} \quad \text{and} \quad \mu_h = \frac{e\,\bar{\tau}_h}{m_h^*}$$

1-3.2. The Hall Effect

(a) Simple Treatment

The Hall effect measurement plays a very important role in revealing the mechanism of conduction in semiconductors. By combining the data from measurements of both the Hall effect and the conductivity it is possible to determine the concentration, type and mobility of the charge carriers of a semiconductor.

We shall consider first a simple treatment in which The relaxation time τ is assumed independent of carrier energy. Thus we can consider all the charge carriers to have the same velocity component

v_x and neglect the effect of the distribution of velocities.

When a current carrier of charge e is subjected to the combined action of an electric field $\vec{\mathcal{E}}$ and a magnetic induction $\vec{B}$, the carrier is subject to a force, F, where

$$\vec{F} = me\frac{d\vec{v}}{dt} = e(\vec{\mathcal{E}} + (\vec{v} \times \vec{B})) \qquad (1.54)$$

This is known as the Lorentz force.

Consider a rectangular conductor as shown in Figure 1.7, with an applied potential difference along the x-direction. A constant magnetic field B is applied in the Z-direction. The effect of the magnetic field would be to deflect the current carriers to one side and cause the current to deviate from the direction of the electric field. The charge accumulates on the two opposite faces making one positive and the other negative, and sets up a transverse electric field. In the steady state, this transverse electric field known as the Hall field $\mathcal{E}_y$ is just sufficient to balance the deflecting effect of the magnetic field and causes the net force on the charge carriers in that direction to vanish, i.e.

$$F_y = e[\mathcal{E}_y + (\vec{v} \times \vec{B})_y] = o$$

For an n-type semiconductor, therefore, in equilibrium

$$e(v_x B_z) - e\,\mathcal{E}_y = o \qquad (1.55)$$

But the current density, $J_x = -ne\,v_x$, so that the Hall field,

$$\mathcal{E}_y = v_x B_z = -\frac{J_x B_z}{ne} = R_H J_x B_z$$

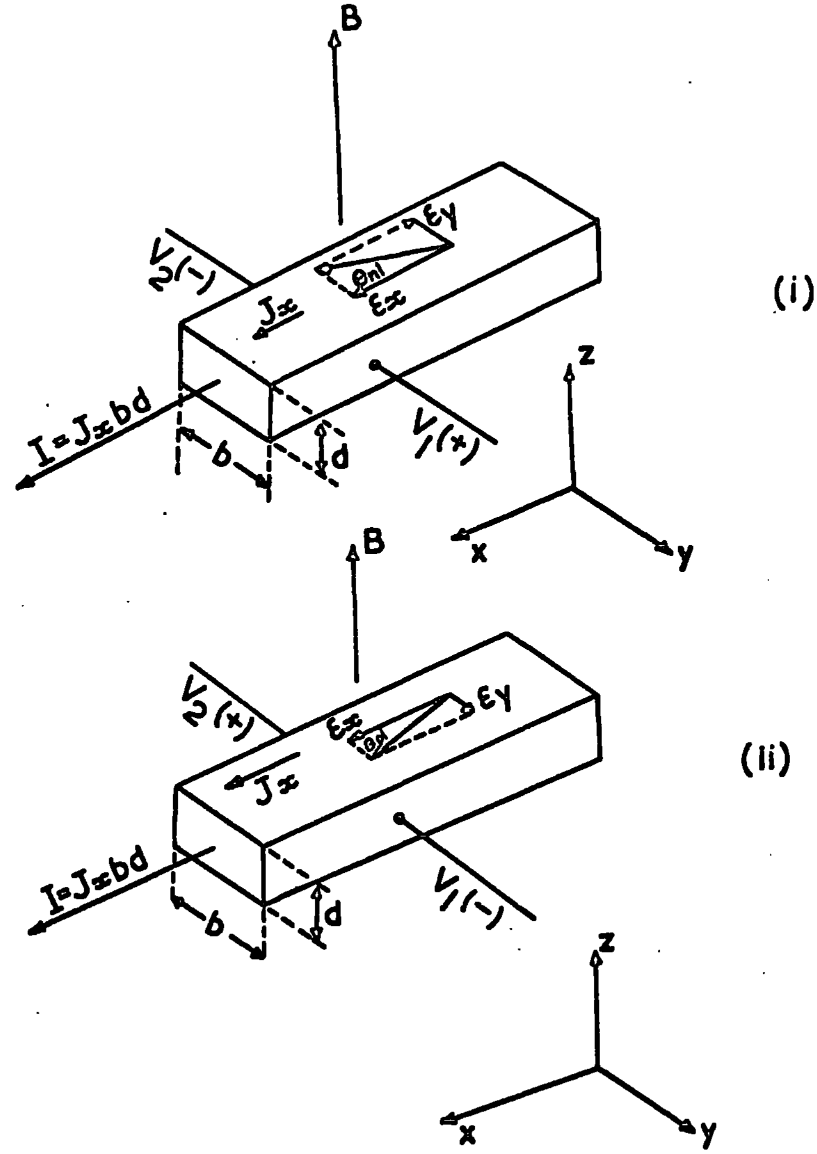

Fig. 1.7 (i) Voltage components for conduction by electrons in a magnetic field.

(ii) Voltage components for conduction by holes in a magnetic field.

where the Hall coefficient R_H for electrons is given by

$$R_H = \mathcal{E}_y / J_x B_z = -1/ne \tag{1.56}$$

The experimentally observed quantities are the Hall voltage V_H which is related to $\mathcal{E}_y$ by $\mathcal{E}_y = V_H/b$ and the total current $I = J_x bd$ where b is the sample width and d its thickness. Therefore, (1.56) becomes

$$R_H = -\frac{1}{ne} = -\frac{V_H d}{IB_z} \tag{1.57}$$

The resultant electric field due to $\mathcal{E}_x$ and $\mathcal{E}_y$ deviates from the x-direction by the Hall angle θ, where

$$\tan\theta \approx \theta = \mathcal{E}_y / \mathcal{E}_x = -R_H \sigma B_z \tag{1.58}$$

for $\mathcal{E}_y << \mathcal{E}_x$

In order to describe the mobility as measured by the Hall effect, let us introduce the term Hall mobility, μ_H, which is defined as $\mu_H = \theta / B_z = \sigma . R_H$ (1.59)

Thus from simultaneous measurements of R_H and σ, the value of μ_H can be found.

A similar situation is found in a p-type semiconductor where V_H and R_H would be reversed in sign showing that the holes dominate the electrical conduction.

(b) Two-Carrier Hall Effect

In the case of intrinsic or near intrinsic samples, where both electrons and holes are present, the Hall coefficient is a complicated average of the Hall coefficient and conductivity for each type of carrier. In this case it can be shown that

$$R_H = \frac{\sigma_n^2 R_n^2 + \sigma_h^2 R_h^2}{(\sigma_n + \sigma_h)^2} \tag{1.59}$$

The above expression may be rewritten:

$$R_H = \frac{p\mu_h^2 - n\mu_n^2}{e(n\mu_n + p\mu_h)} = \frac{1}{e} \cdot \frac{p - nb^2}{(nb+p)^2} \tag{1.60}$$

where $b = \mu_n / \mu_h$

And, therefore,

$$\mu_H = \frac{p\mu_h^2 - n\mu_n^2}{p\mu_h + n\mu_n} \tag{1.61}$$

Because of the form of the numerator in equation (1.60), the Hall voltage is generally smaller for intrinsic specimens. The sign of the Hall coefficient depends upon the relative mobilities of holes and electrons.

(c) Hall Effect - τ as a Function of Energy.

The effect of the velocity distribution has been neglected in obtaining the equations (1.57) and (1.60).

All these equations need to be modified to include that effect. In doing so, we shall assume that we are dealing with a simple n-type semiconductor with spherical energy surfaces in both conduction ~~band~~ and valence bands.

The equations describing the motion of electrons in an electric field $\mathcal{E}$ in the x-direction and the magnetic field B in the z-direction are:

$$\frac{dv_x}{dt} = -(e/m_e^*)\mathcal{E}_x - w_e v_y \tag{1.62}$$

and $$\frac{dv_y}{dt} = -(e/m_e^*)\mathcal{E}_y + w_e v_x \tag{1.63}$$

where $w_e = \frac{eB_z}{m_e}$ is the Larmor frequency for electrons.

The equations (1.62) and (1.63) can be written in the form:

$$\frac{dV}{dt} + iwV = \frac{e\mathcal{E}}{m_e^*} \tag{1.64}$$

where $V = v_x + iv_y$ and $\mathcal{E} = \mathcal{E}_x + i\,\mathcal{E}_y$.

Equation (1.64) has been solved[9] to obtain the average values for v_x and v_y by averaging over all values of E to take account of the fact that τ is a function of the carrier energy E. Writing $J_x = -ne\bar{v}_x$; etc., we have then for the current densities, assuming $w_e\,\tau \ll 1$:

$$J_x = \frac{ne^2}{m_e^*}\left(\bar{\tau}_e\mathcal{E}_x - w_e\bar{\tau}_e^{\,2}\mathcal{E}_y\right) \tag{1.65}$$

$$J_y = \frac{ne^2}{m_e^*}\left(\bar{\tau}_e\mathcal{E}_y + w_e\bar{\tau}_e^{\,2}\mathcal{E}_x\right) \tag{1.66}$$

where $\bar{\tau}_e$ and $\bar{\tau}_e^{\,2}$ are given by:

$$\bar{\tau}_e = \frac{\langle v^2\tau_e(v)\rangle}{\langle v^2\rangle} \quad \text{and} \quad \bar{\tau}_e^{\,2} = \frac{\langle v^2\tau_e^{\,2}(v)\rangle}{\langle v^2\rangle}$$

Now by putting $J_y = o$, we obtain an expression for the Hall angle θ as:

$$\tan\theta = \mathcal{E}_y / \mathcal{E}_x = -w_e \frac{\overline{\tau_e^2}}{\overline{\tau}_e}$$

$$\therefore \quad \mathcal{E}_y = R_H B_z J_x = -w_e \mathcal{E}_x \frac{\overline{\tau}_e^2}{\overline{\tau}_e}$$

$$= -B_z \cdot I_x \cdot \frac{1}{ne} \frac{\langle v^2 \rangle \langle v^2 \tau_e^2 \rangle}{\langle v^2 \tau_e \rangle^2}$$

$$\therefore \quad R_H = -\frac{r}{ne} \quad \text{where } r = \frac{\langle v^2 \rangle \langle v^2 \tau_e^2 \rangle}{\langle v^2 \tau_e \rangle^2} \tag{1.67}$$

The value of the factor r depends on the form of variation of τ with energy. The nature of this variation is determined by the nature of the electron scattering processes.

1-3.3. The Magneto-resistance Effect

In obtaining equations (1.65) and (1.66) we have neglected terms in B^2. Considering the terms in B^2, the equations (1.65) and (1.66) become

$$J_x = \frac{ne^2}{m_e^*} \left(\overline{\tau}_e \mathcal{E}_x - w_e \overline{\tau}_e^2 \mathcal{E}_y - w_e^2 \overline{\tau}_e^3 \mathcal{E}_x \right) \tag{1.68}$$

and $$J_y = \frac{ne^2}{m_e^*} \left(\overline{\tau}_e \mathcal{E}_y + w_e \overline{\tau}_e^2 \mathcal{E}_x \right) \tag{1.69}$$

From (1.68) and (1.69 by putting $J_y = o$, we obtain

$$\mathcal{E}_x = \rho_o J_x \left\{ 1 + \frac{e^2 B_z^{\ 2}}{m_e^{*2}} \quad \frac{\overline{\tau_e^{\ 3}}\ \overline{\tau_e} - (\overline{\tau_e^{\ 2}})^2}{(\overline{\tau_e})^2} \right\} \tag{1.70}$$

$$= (\rho_o + \Delta\rho) J_x$$

where $\rho_o = 1/\sigma_o$ is the zero-field resistivity.

Thus when $\Delta\sigma/\sigma_o << 1$, we have

$$-\frac{\Delta\sigma}{\sigma_o} = \frac{\Delta\rho}{\rho_o} = \frac{e^2 B_z^{\ 2}}{m_e^{*2}} \quad \frac{\overline{\tau_e^{\ 3}}\ \overline{\tau_e} - (\overline{\tau_e^{\ 2}})^2}{(\overline{\tau_e})^2} \tag{1.71}$$

If R_o is the small-field Hall coefficient i.e. $w_e\tau << 1$, equation (1.71) may be expressed in the form

$$-\frac{\Delta\sigma}{\sigma_o} = \frac{\Delta\rho}{\rho_o} = \xi_1 R_o^{\ 2} \sigma_o^{\ 2} B_z^{\ 2} \tag{1.72}$$

where the quantity ξ_1 is the magneto-resistance coefficient and is given by the equation

$$\xi_1 + 1 = \frac{\overline{\tau_e^{\ 3}}\ \overline{\tau_e}}{(\overline{\tau_e^{\ 2}})^2} \tag{1.73}$$

For non-degeneracy, ξ_1 has the values 0·57, 0·257 and 0·08 for ionized, acoustic and optical mode scattering respectively.

For a non-degenerate semiconductor with spherical constant-energy surfaces, there will be a transverse magneto-resistance given by equation (1.72) with $\Delta\sigma/\sigma_o$ proportional to $B_z^{\ 2}$, but no longitudinal magneto-resistance will be found, since J_z is not affected by the magnetic field along the z-axis.

In a strong magnetic field when $w\tau \gg 1$, the value of J_x reduces to

$$J_x = -\frac{ne^2}{m_e^*}\frac{\mathcal{E}_y}{w_e} = -\frac{ne}{B_z}\mathcal{E}_y \qquad (1.74)$$

And by putting $J_y = o$, we obtain

$$\mathcal{E}_x = -\frac{\mathcal{E}_y}{w_e}\left(\frac{1}{\bar{\tau}_e}\right) \qquad (1.75)$$

From (1.74) the Hall coefficient R becomes

$$R = \frac{\mathcal{E}_y}{B_z J_x} = -\frac{1}{ne} \qquad (1.76)$$

This result, which was obtained previously for the degenerate condition in a small magnetic field, would therefore appear to hold for any condition in a very strong magnetic field.

By Using equation (1.75) equation (1.74) can be written as

$$J_x = \left(\frac{ne^2\mathcal{E}_x}{m_e^*}\right)\Big/\left(\frac{1}{\bar{\tau}_e}\right) = \sigma_{\infty T}\,\mathcal{E}_x \qquad (1.77)$$

where $\sigma_{\infty T}$ is the conductivity in a large transverse magnetic field and is given by

$$\sigma_{\infty T} = \frac{ne^2}{m_e^*}\Big/\left(\frac{1}{\bar{\tau}_e}\right) = \sigma_o\Big/\left(\frac{1}{\bar{\tau}_e}\right)\bar{\tau}_e$$

For a metal or degenerate semiconductor $\sigma_{\infty T} = \sigma_o$.

For a non-degenerate semiconductor

$$\frac{\sigma_o}{\sigma_{\propto T}} = \left(\frac{1}{\tau_e}\right) \bar{\tau}_e = \frac{\rho_{\propto T}}{\rho_o}$$

For scattering by acoustic modes of the lattice vibration $\frac{\sigma_o}{\sigma_{\propto T}}$ is $\frac{32}{9}\pi$ and for ionized impurity scattering it is $\frac{32}{3}\pi$ showing that the conductivity reaches a saturation value independent of the field.

1-3.4. <u>Scattering Processes in Solid</u>

A charge carrier moving in a perfectly periodic lattice potential is subjected to no scattering interactions at all with the atoms of the lattice. Therefore, the collision mechanisms which do result in scattering of the charge carriers must be associated with impurities, imperfections or aperiodicities of one sort or another in a solid.

<u>(a) Scattering by Lattice Vibrations</u>

At all temperatures above the absolute zero, the atoms in a crystal vibrate about their respective mean positions. These vibrations are lattice waves and are classified as longitudinal or transverse depending on whether the direction of vibration is parallel or perpendicular to the direction of propagation of the wave. The lattice vibrations can be thought of as particle-like quanta of vibrational energy called phonons. Acoustic and optical phonons refer respectively to the in-phase and out-of-phase motion of the neighbouring ions in a lattice vibration. Electrons and holes can interact with acoustical-mode or optical mode phonons.

The interaction between charge carriers and lattice vibrations is very complex. The scattering by the longitudinal acoustic modes of the lattice vibrations is the dominant scattering process in relatively pure and structurally perfect covalent crystals, especially in the higher temperature ranges. The form of relaxation time and subsequent modifications in the expressions of the Hall coefficient and Hall mobility for acoustical mode of scattering have been described by many authors.[10,11]

Bardeen and Shockley's[12] method of calculating lattice scattering in nonpolar semiconductors is based on the concept of a deformation potential which is the change of energy of the band edge per unit dilatation due to the longitudinal waves.

The relaxation time τ for electron scattering by longitudinal acoustic modes for a semiconductor with spherical constant energy surfaces is found to be

$$\tau = \frac{\rho U_l^2 h^4}{8\pi^2 (2m_e^*)^{3/2} kT\, E_I^2 E^{1/2}} \qquad (1.78)$$

where ρ is the density, U_l is the velocity of the longitudinal phonons and E_I is an energy defined by

$$\Delta E_C = E_I \, \Delta V/V_o$$

ΔE_C is the magnitude of the change in the energy corresponding to the bottom of the conduction band due to a small change ΔV of the original volume V_o. The relaxation time then has the form

$$\tau = a\, E^{-\frac{1}{2}} T^{-1}$$

where a, is a constant.

The mobility in the range of temperature in which scattering due to longitudinal acoustic phonons predominates, is obtained from the relation for a non-degenerate semiconductor

$$\mu_L = \frac{\sigma}{ne} = \left(\frac{e}{m_e^*}\right) \langle\tau\rangle$$

$$= \frac{(8\pi)^{\frac{1}{2}}}{3} \frac{e\hbar^4 \rho U_1^{\;2}}{(kT)^{3/2} m_e^{*\,5/2} E_I^{\;2}} \qquad (1.79)$$

Thus $\mu_L \propto T^{-3/2}\, m_e^{*\,-5/2}$

The above calculations refer especially to electrons in the conduction band, but the procedure for holes in the valence band is essentially the same, with the electron mass and deformation potential constant replaced by their respective valence band analogues.

It may be shown that

$$\frac{\mu_{nL}}{\mu_{hL}} = \left(\frac{m_e^*}{m_L^*}\right)^{-5/2} \left(\frac{E_{Ie}}{E_{Ih}}\right)^{-2}$$

If $E_{Ih} \simeq E_{Ie}$, we have $\dfrac{\mu_{nL}}{\mu_{hL}} = \left(\dfrac{m_e^*}{m_h^*}\right)^{-5/2}$

To deduce the equation (1.79), the constant energy surfaces have been assumed spherical. Where the energy surfaces are not spherical, the effective mass may be replaced by an appropriate average value.

(b) Optical Mode Lattice Scattering

The temperature variation of the mobility in the range of temperatures where lattice scattering predominates, is usually rather stronger than the predicted $T^{-3/2}$ variation. The deviation involves taking account of a contribution to the scattering from optical-mode vibrations which is given by

$$\mu_0 = BT^{-\frac{1}{2}} (e^{\theta/T}-1) \tag{1.80}$$

where θ is the equivalent temperature of the optical phonons involved, and B is a constant. The observed mobility can be considered as the resultant mobility given by[13]

$$\frac{1}{\mu} = \frac{1}{\mu_L} + \frac{1}{\mu_0} \tag{1.81}$$

In ionic crystals, the atoms are dissimilar and carry opposite charges. Their displacements in the opposite directions cause an electric polarization of the lattice which scatters the charge carriers. The term polar scattering has been applied to this type of scattering which involves a Coulomb force directly. Fröhlich and Mott,[14] and Howarth and Sondheimer[15] discussed the theory in detail and showed that a perturbation theory is applicable for values of α_c less than unity.

The parameter α_c which is a measure of the strength of the interaction of the charge carriers with the polar modes is defined by

$$\alpha_c = \frac{e^2}{\hbar} \left(\frac{m^*}{2\hbar w_1} \right)^{\frac{1}{2}} \left(\frac{1}{\epsilon_\infty} - \frac{1}{\epsilon_s} \right) \qquad (1.82)$$

where ϵ_s is the static dielectric constant and ϵ_∞ is the optical dielectric constant. w_1 is the longitudinal optical-mode frequency related to θ by $\hbar w_1/kT = \theta/T$. The expression for the electron mobility due to optical mode scattering which was obtained using the perturbation theory of Fröhlich and Mott, and Howarth and Sondheimer, is in the non-degenerate case,[16]

$$\mu_{op} = \frac{1}{2\alpha_c w_1} \frac{e}{m^*} \frac{8}{3\sqrt{\pi}} \frac{X(z)}{Z^{\frac{1}{2}}} (e^z-1) \qquad (1.83)$$

where $Z = \hbar w_1/kT = \theta/T$, $X(z) = 1$ for $Z \ll 1$ and $X(z) = 3/8(\pi z)^{\frac{1}{2}}$ when $Z \gg 1$.

The "intermediate-coupling" theory developed by Lee, Low and Pines[17],[18] to replace the perturbation theory when α_c exceeds unity, results in the following expression for the mobility limited by polar scattering:

$$\mu_{I.C} = \frac{1}{2\alpha_c w_1} (e/m^*) (m^*/m_p)^2 f(\alpha_c) \exp (z) \qquad (1.84)$$

where m_p, known as the polar on effective mass, can be given to a good approximation by[17]

$$m_p = m^*(1 + \alpha_c/6) \text{ when } \alpha_c < 6.$$

$f(\alpha_c)$ is a slowly varying function of α_c, and is tabulated in reference (19).

The intermediate-coupling theory is valid for values of α_c as large as 6 but its validity is restricted to temperatures less than θ. The perturbation theory has no temperature restrictions but requires α_c to be less than unity. When α_c is small, there is little difference between equations (1.83) and (1.84) at low temperatures.

(c) Piezoelectric Scattering

An acoustic wave propagating in a piezoelectric crystal is, in general, accompanied by electrical disturbances which lead to departures from the mobility predicted by the deformation potential method of Bardeen and Shockley. Meijer and Polder[20] and Harrison[21] have developed a theory of piezoelectric scattering for crystals with the zinc blende structure using a relaxation-time approximation. The theory has been applied to cadmium sulphide by Hutson[22] who writes the piezoelectric mobility as

$$\mu_p = 1\cdot 44 \quad \epsilon_s (m/m^*)^{3/2} (300/T)^{\frac{1}{2}} \quad \left\{ \sum_{\text{modes}} \left(K^2\right)_{av} \right\}^{-1} \tag{1.85}$$

where K (the electromechanical coupling factor) is a dimensionless quantity, given by $K^2 = e^2/\epsilon_o \epsilon_s c$. Here e is an appropriate piezoelectric constant, c the appropriate elastic stiffness constant and ϵ_o the permittivity of free space. Hutson has also given the formulae for averaging the squares of the piezoelectric constants for the longitudinal and transverse modes for the case of wurzite symmetry.

(d) Charged Impurity Scattering

The effect of charged impurities in scattering charge carriers has been analyzed by Conwell and Weisskopf[23] using the theory developed by Rutherford[24] to explain the scattering of α-particles. In a semiconductor, the Coulomb potential due to charged donor and acceptor ions serves to deflect the paths of electrons and holes much as the potential of a heavy nucleus will deflect an α-particle in the Rutherford experiment. The scattering cross-section would be given by

$$\sigma(\theta) = \left(\frac{Ze^2}{2\epsilon m^* v^2} \right)^2 \operatorname{cosec}^4 \frac{\theta}{2} \tag{1.83}$$

where θ is the angle of scattering and Z is the electronic charge on the centre.

Averaging the cross-section over the velocities found in a semiconductor gives the time between collisions as

$$\tau = \frac{\epsilon^2 m^{*2} v^3}{2\pi Z^2 e^4 N} \frac{1}{\ln\left[1+\left(\frac{\epsilon m^* v^2}{2Ze^2 N^{1/3}}\right)^2\right]} \tag{1.84}$$

where N is the density of the charged imperfection centres.

Now by calculating τ by the usual averaging process over the Boltzmann distribution we obtain

$$\langle \tau_I \rangle = \frac{\langle v^2 \tau(v) \rangle}{\langle v^2 \rangle} = \frac{8\epsilon^2 (kT)^{3/2} (2m^*)^{\frac{1}{2}}}{\pi^{3/2} Z^2 e^4 N \ln\left[1+\left(\frac{3\epsilon kT}{Ze^2 N^{1/3}}\right)^2\right]}$$

whence the mobility will be given by

$$\mu_I = \frac{e\langle\tau\rangle}{m^*} = \frac{8\sqrt{2}}{\pi^{3/2}} \frac{\epsilon^2 (kT)^{3/2}}{N e^3 Z^2 m^{*\frac{1}{2}}} \frac{1}{\ln\left[1+\left(\frac{3\epsilon kT}{Ze^2 N^{1/3}}\right)^2\right]} \tag{1.85}$$

which is known as the Conwell-Weisskopf formula.

Thus $\mu_I \propto \dfrac{T^{3/2}}{Z^2 N m^{*\frac{1}{2}}}$

Since $1/\tau_i$ is proportional to the probability of scattering by mechanism i, one obtains for the case of mixed scattering by lattice vibrations and ionized impurities,

$$\frac{1}{\tau} = \frac{1}{\tau_L} + \frac{1}{\tau_I}$$

i.e. $$\frac{1}{\mu} = \frac{1}{\mu_L} + \frac{1}{\mu_I} = AT^{-3/2} + BT^{3/2} \qquad (1.86$$

For low impurity concentrations, the dominant scattering interaction is lattice scattering. At high concentration of impurity atoms, the ionized impurity scattering becomes the most dominant scattering process. In the intermediate range, both scattering interactions are important and the overall mobility μ is expressed by the relation (1.86).

(e) Neutral Impurity Scattering

Scattering by neutral impurities is analogous to the scattering of free electrons by neutral hydrogen atoms. This effect has been considered by Erginsoy[25] who found that the mobility is given by an expression with no temperature dependence.

$$\mu_N = \frac{m^* e^3}{2\epsilon_o \epsilon h^3 N} \tag{1.87}$$

where ϵ is the dielectric constant and ϵ_o is the permittivity of the free space and N is the density of neutral impurities.

Sclar[26] has done further calculations which indicate a slight temperature dependence.

(f) Other types of Scattering

Vacancies, interstitial atoms, dislocations, grain boundaries and sample surfaces can also scatter holes and electrons, although in many cases the scattering attributable to these agencies is negligible in comparison with lattice or impurity scattering.

The effect of the scattering mechanisms on mobility, relaxation time, Hall coefficient and magneto-resistance coefficients has been summarised in Table 1.1.[27]

Table 1.1. Summary of the Scattering Mechanisms

Mechanism	$\mu \propto (m^*)^x T^y$		$\tau \propto E^z$	$R_H = -r/ne$	ξ_1 (Due to transverse magneto-resistance)	
	x	y	z	r	$\omega\tau \ll 1$	$\omega\tau \gg 1$
Acoustic	-5/2	-3/2	-1/2	$3\pi/8$	0·257	$\frac{32}{9}\pi$
Polar	-3/2	Exponential	Independent	1·00 to 1·14	0·08	
Ionized Impurity	-1/2	3/2	~3/2	$315\pi/512$	0·57	$\frac{32}{3}\pi$
Neutral Impurity	1	Independent	Independent	1		
Electron-hole	-1/2	3/2	~3/2	$315\pi/512$		

References

(1) R.A. Smith - "Semiconductor", Cambridge University Press, 1961.

(2) N. Cusack - "The Electrical and Magnetic properties of Solids."

(3) C. Kittel - "Introduction to Solid State Physics". John Wiley and Sons, Inc., 1966.

(4) A.J. Dekker - "Solid State Physics". Macmillan, 1964.

(5) F. Bloch - Z. Physik 52, 555 (1928).

(6) R. de L.Kronig and W.G. Penny - Proc.Roy.Soc. (London) A.130, 499 (1931).

(7) D.S. Saxon and R.A. Hutner - Philips Res.Repts.4, 81 (1949).

(8) J.M. Luttinger - Philips Res.Repts. 6, 303 (1951).

(9) John P. McKelvey - "Solid State and Semiconductor Physics", page 283, Harper & Row, 1966.

(10) A.H. Wilson - "The Theory of Metals", 2nd edition, Cambridge Univ. Press, 1953.

(11) F. Seitz - Phys.Rev., 73, 549 (1948).

(12) J. Bardeen and W. Shockley - Phys.Rev., 80, 72 (1950).

(13) F.J. Morin and J.P. Maita - Phys.Rev., 94, 1525 (1954).

(14) H. Frölich and N.F. Mott - "Proc.Roy.Soc.A, 171, 496 (1939).

(15) D.J. Howarth and E.H. Sondheimer, Proc.Roy.Soc., A219, 53, (1953).

(16) J.A. Marley and R.C. Dockerty, Phys.Rev., 140, A304, (1965).

(17) T.D. Lee, F.E.Low and D.Pines, Phys.Rev., 90, 297 (1953).

(18) F.E. Low and D. Pines, Phys.Rev., 91, 193 (1953).

(19) F.E. Low and D.Pines, Phys.Rev., 98, 414, (1955).

(20) H.J.G. Meyer and D. Polder, Physica, 19, 255, (1953).

(21) W.A. Harrison, Phys.Rev., 101, 903, (1956).

(22) A.R. Hutson, J.Appl.Phys., 32, 2287, (1961).

(23) E.M. Conwell and V.F. Weisskopf - Phys.Rev., 94, 1525 (1954).

(24) E. Rutherford, Phil.Mag., 21, 669 (1911).

(25) C. Erginsoy, Phys.Rev.79, 1013 (1950).

(26) N. Sclar, Phys.Rev., 104, 1559 (1956).

(27) C. Hilsum and A.C. Rose-Innes, "Semiconducting III-V Compounds", Pergamon Press, 1961.

CHAPTER 2

PROPERTIES OF CADMIUM SULPHIDE

2-1. Introduction

Cadmium sulphide is a prominent member of the II-VI family of compound semiconductors. In artificially grown crystals and in most vacuum deposited films, the common crystallographic form of cadmium sulphide is the hexagonal Wurtzite structure or α-phase. The β-phase which is obtained by hydrogen sulphide precipitation from cadmium sulfate solution is of a cubic zinc-blende structure.[1] In the Wurtzite structure, the interatomic distance between the cadmium atom and its four nearest neighbours (sulphur atoms) is 2·52Å, with lattice parameters a = 4·13Å and c = 6·69Å. In the Zinc-blende structure, the interatomic distance is 2·5Å with a = 5·82Å.[2] The investigation of Rittner and Schulman[3] on the stability of the two phases indicated that cadmium sulphide crystallizes in a stable manner only in the hexagonal Wurtzite lattice.

Cadmium sulphide is in general a wide band gap semiconductor or semi-insulator. A value of 2·43 eV is usually quoted as the width of the forbidden energy gap at room temperature. A pure stoichiometric CdS-crystal is expected to have a resistivity greater than 10^{10} Ohms-cm. The important electrical and optical properties are governed by the incorporation of suitable impurities or by imperfections associated with structural deviations from the atomic arrangement of a perfect crystal.

Electrical conduction in cadmium sulphide is always n-type. This n-type semiconduction is brought about by the presence of a non-stoichiometric excess of cadmium or by the addition of impurities from Gr.III (trivalent cations, such as Al, In, Ga) and Gr.VII (halogens). The activation energies of the donor levels[4] measured in such n-type cadmium sulphide are found to be 0·03 eV.

The impurities from Gr.I and Gr.V and cation vacancies act as acceptors in cadmium sulphide and produce levels ~1·0 eV above the valence band.[5,6,7] Since the acceptor impurities produce such deep levels in cadmium sulphide, p-type conductivity is not generally observed. Cadmium sulphide heavily doped with copper shows p-type conduction which is most probably due to conduction in an impurity band.[8]

2-2. Band Structure

The band structure of cadmium sulphide arises from the orbitals of the cadmium (4d5S) and sulphur ions (3S3p) which constitute the compound. The valence band originates from the 3p atomic levels of the sulphur ions and the conduction band from the 5S atomic levels of the cadmium ions. The band structure for Wurtzite type crystals taking CdS as an example has been deduced from group theoretical considerations by Balkanski and des Cloizeaux.[9] According to them, the valence band is divided into four parts (Figure 2.1). The lowest band is due to the s-orbitals of the sulphur ions. In the presence of spin-orbit coupling the 'p' valence bands at k=o split into three bands, two of which belong

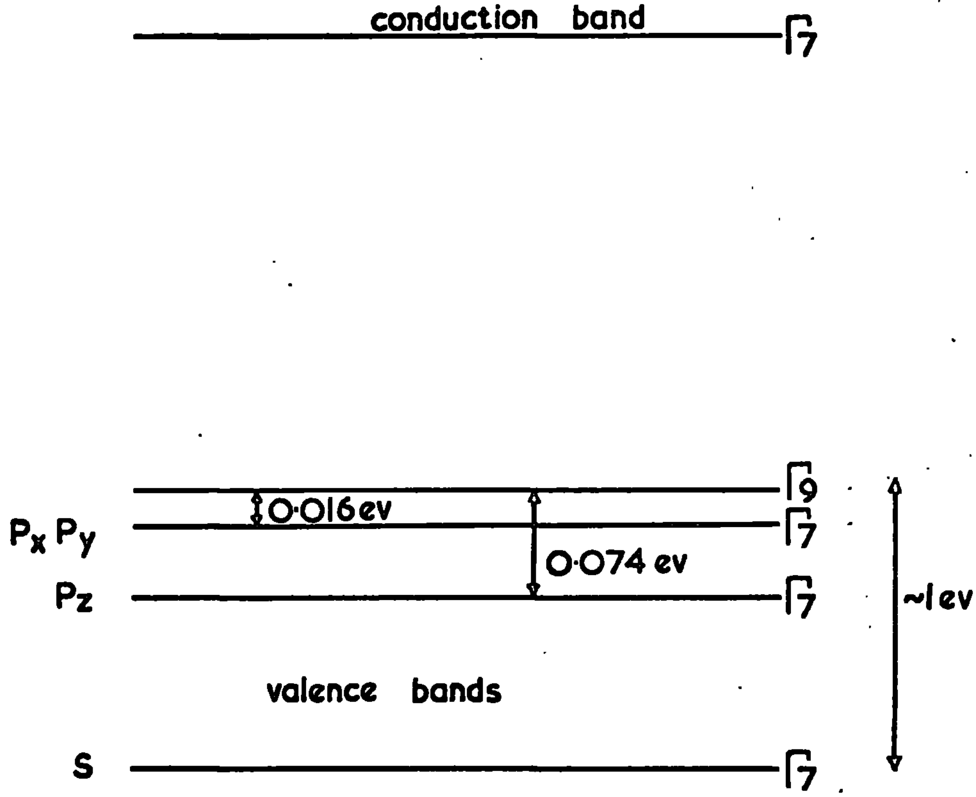

Band Structure of CdS

Fig. 2·1

to the representation Γ_7 and the third to Γ_9. Thomas and Hopfield[10] in their measurements of the reflectance and luminescence spectra of cadmium sulphide have explained the existence of three types of excitons in terms of the splitting of the valence band. Now band-to-band transitions are allowed for both modes of polarization of light for $\Gamma_7 \longrightarrow \Gamma_7$ transitions but are allowed only for light polarized perpendicular to the c-axis for $\Gamma_9 \longrightarrow \Gamma_7$ transitions. The forbidden transition $\Gamma_9 \longrightarrow \Gamma_7$ for light polarized parallel to the c-axis gives rise to anisotropies in the optical and luminescent properties. Further, the work of Balkanski and des Cloizeaux[9] and Birman[11] shows that the maximum of the upper valence band should be at $k = o$ but the two lower ones should have six minima close to $k = o$.

The shapes of the constant energy surfaces which are possible according to group theory in Wurtzite-type crystals in the conduction band have been discussed by Balkanski and des Cloizeaux[9], Birman[11], Casella[12] and Hopfield.[13] They all showed that in the absence of spin-orbit splitting the conduction band should have a minimum at $k = o$ (Figure 2.2(a)) but the inclusion of the spin-orbit coupling may lead either to toroidal energy surfaces (Figure 2.2(b)) or to a many-valley type of band structure. It is also possible in principle to have all three (shown in Figure 2.2) and/or the intermediate cases in the same crystal over different ranges of temperature. However, regarding the shape of the conduction band extrema, most of the experiments

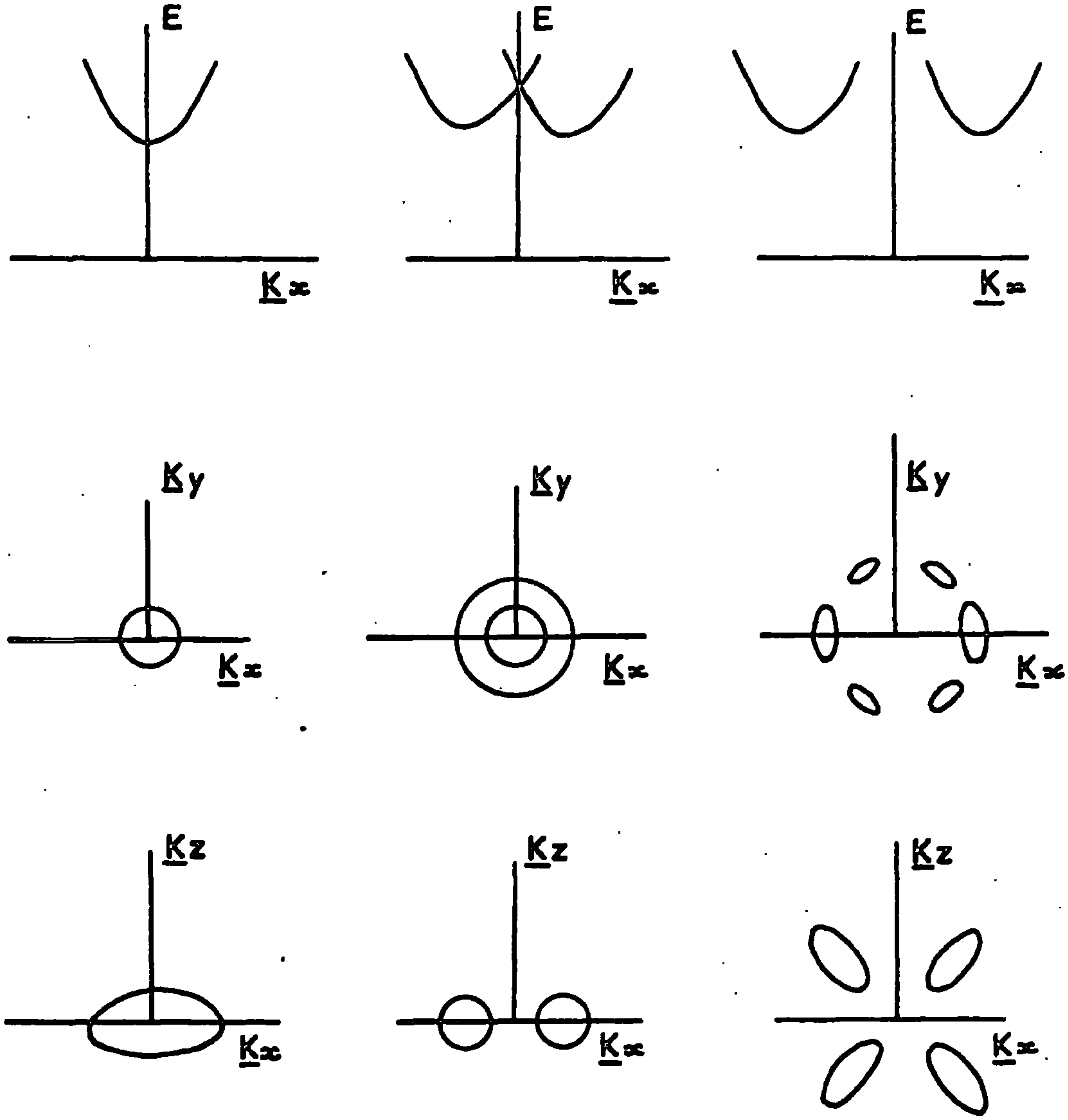

Fig. 2·2. a b c

Possible Band Structure in Wurtzite Type Crystals

a - Single ellipsoid. b - Toroid. c - Simple many valley.

The upper figures show the relationship between energy and wave number. The middle and lower ones show cross sections of constant energy.

(10,14,15,16,17,18,19,20) favour a single valley model.

2-3. Effective Mass and Mobility of Carriers

The experimental determination of the value of effective mass for electrons and holes by electrical and optical methods has been done by many workers. Kröger, Vink and Volger[21] measured the Hall effect, resistivity and thermoelectric power of both pure and doped crystals of cadmium sulphide from $20^{\circ}K$ to $700^{\circ}K$. The thermoelectric power data at room temperature and the variation of the Hall constant with temperature were explained by an effective mass ratio $m_e^*/m \approx 0{\cdot}2-0{\cdot}3$ and $0{\cdot}25$ m was given as an average. Kröger[21] et al. also found $E_D \approx 0{\cdot}02$ eV for a sample with a high impurity concentration (10^{17} cm^{-3}) and concluded that $m_e^* = 0{\cdot}12$ m by comparing the predictions of the theory of hydrogen-like donors with the experimental values. Piper and Halsted[17] found a hydrogen-like donor binding energy of $0{\cdot}032$ eV for lower impurity concentrations and obtained $m_e^*/m = 0{\cdot}20$ which is in good agreement with the optical determinations by Thomas and Hopfield,[10] and Balkanski and Hopfield.[22] Thomas and Hopfield[10] obtained values for the effective mass of holes in the valence band from the exciton absorption spectrum. The values of the effective mass parallel and perpendicular to the c-axis were found to be:

$$m_h^* \parallel \text{c-axis} = 0{\cdot}7\ m_e$$

$$m_h^* \perp \text{c-axis} = 5{\cdot}0\ m_e$$

Electron cyclotron resonance was observed in CdS by Baer and Dexter.[19] The single resonance seen in all orientations is consistent with a single-ellipsoid conduction-band model. The effective mass measured at $4{\cdot}2^{\circ}$K with the crystal c-axis parallel ($m_e^*||$) and perpendicular ($m_e^*\perp$) to the magnetic field is:

$$m_e^*|| = (0{\cdot}171 \pm 0{\cdot}003)m$$

$$m_e^*\perp = (0{\cdot}162 \pm 0{\cdot}003)m$$

There is some anisotropy, $\sim$5%, indicating that the constant energy surfaces near the conduction band are not spherical but slightly oblate. Sawamotto[20] also measured the average effective mass of photo-excited carriers at $1{\cdot}7^{\circ}$K using cyclotron resonance and found both an effective mass of $0{\cdot}17\ m_e$ and a heavier mass of $0{\cdot}81\ m_e$. The heavier mass of $0{\cdot}81\ m_e$ was attributed to holes. Zook and Dexter[16] measured the Hall mobility and magneto resistance at three different temperatures. While explaining the magnitude and temperature dependence of the electron mobility by using the theories of scattering in polar semiconductors they assumed an effective mass $m_e^* = 0{\cdot}19\ m_e$ and found a good fit with the experimental results.

The experimental values of mobility in CdS crystals are found to increase considerably as the crystal is grown in progressively purer and more perfect conditions. The Hall mobility of electrons in CdS measured by Kröger, Vink and Volger[21] in the temperature range 20°K - 700°K was found to increase from about 210 cm^2 volt^{-1}sec^{-1} at room temperature to a maximum value of 3000 cm^2/volt.sec. at 40°K.

The temperature variation was interpreted by computing a theoretical mobility μ_{th} from the relation

$$\frac{1}{\mu_{th}} = \frac{1}{\mu_{ac}} + \frac{1}{\mu_0}$$

where μ_{ac} is the mobility due to the interaction of the electrons with acoustic modes of vibration and μ_0 is determined by scattering of the longitudinal optical modes. Miyazawa, Maeda and Tomishima[23] interpreted the temperature variation of mobility in their experiment by optical mode scattering alone, but the effect of impurity scattering was taken into account at lower temperature. Piper and Halsted[17] considered polar optical mode scattering and piezoelectric scattering with only the effective mass as an adjustable parameter and were able to explain their mobility data quite well. Itakura and Toyoda[24] found in their measurements that the Hall mobility μ_H remained constant at a value of 240 cm^2 $volt^{-1}$ sec^{-1} from room temperature to 240°K and from 200°K to 50°K $\mu_H = 6{\cdot}4 \times 10^4\ T^{-3/2}$. Clark and Woods[25] measured the Hall effect of cadmium sulphide samples grown by a vapour phase technique and found that the Hall mobility of electrons obeyed the lattice scattering relationship $\mu_H \propto T^{-3/2}$ from room temperature to liquid nitrogen temperature. Spear and Mort[26] pointed out that there exists a considerable disagreement in the interpretation of the electron mobility results. They also showed that all the published data of the temperature variation of the Hall mobility of electrons follow a relationship close to $\mu_H \propto T^{-3/2}$ in the temperature range from $700^{\circ}K$ to $80^{\circ}K$.

Spear and Mort[26] measured the drift mobilities of electrons and holes in undoped CdS crystals of high resistivity over the temperature range from $500^{\circ}K$ to $80^{\circ}K$ by using fast pulse techniques. The electron mobility was found to be 265 $cm^2\ volt^{-1} sec^{-1}$ at room temperature. The hole mobilities were between 10 and 18 $cm^2\ volt^{-1} sec^{-1}$. Onuki and Hase[27] measured a hole mobility of 38 $cm^2\ volt^{-1} sec^{-1}$, which rose to 48 $cm^2\ volt^{-1} sec^{-1}$ under more intense illumination.

2-4. Photoconductivity

Photoconductivity is the increase in electrical conductivity of a photoconductor caused by radiation incident on the photoconductor. Photoconduction arises from two distinct processes: (1) the generation of excess majority and minority carriers after band-to-band transitions and (2) the production of carriers from transitions involving localized states in the forbidden band. The important parameters of a photoconductor such as speed of response, sensitivity, dark conductivity, etc. depend upon the distribution of imperfection centres in the forbidden gap. The imperfection centres are of two types: trapping centres and recombination centres. Trapping centres are those for which the probability of thermal freeing of the trapped carriers is greater than the probability of recombination with a carrier of opposite type. Recombination centres are those for which the probability of thermal freeing is less than the probability of recombination with a carrier of opposite type. Trapping centres affect the speed of response; recombination centres affect the lifetime and photosensitivity. Such imperfections in CdS may be associated with crystal defects or with incorporated impurities.

Photoconductivity per unit excitation intensity is called the photosensitivity. The imperfections that give rise to high photosensitivity have a larger capture cross-section for holes and a very small capture cross-section for electrons. The photosensitivity in CdS can be understood in terms of the model (shown in Figure 2.3a) due to Bube:[7]

(1) Levels located in the regions I and II are respectively electron and hole traps.

(2) Levels located in the region III are the recombination centres.

(3) Levels located in the region IV generally take part in the recombination process with free holes.

Recombination centres are divided into two classes (shown in Figure 2.3b). Recombination centres of class I are always present in CdS and their identity is still virtually unknown. They behave like neutral imperfections; thus, once one type of carrier is captured, there will be a strong coulomb attraction for recombination with the other type of carrier. They therefore lead to a small majority carrier lifetime for electrons. Class II centres are responsible for photosensitivity. These centres have a large capture cross-section for holes and a very small capture cross-section for electrons, perhaps less than 10^{-4} times the capture cross-section for holes. These centres known as sensitizing centres are believed to be compensated acceptor-type imperfections with

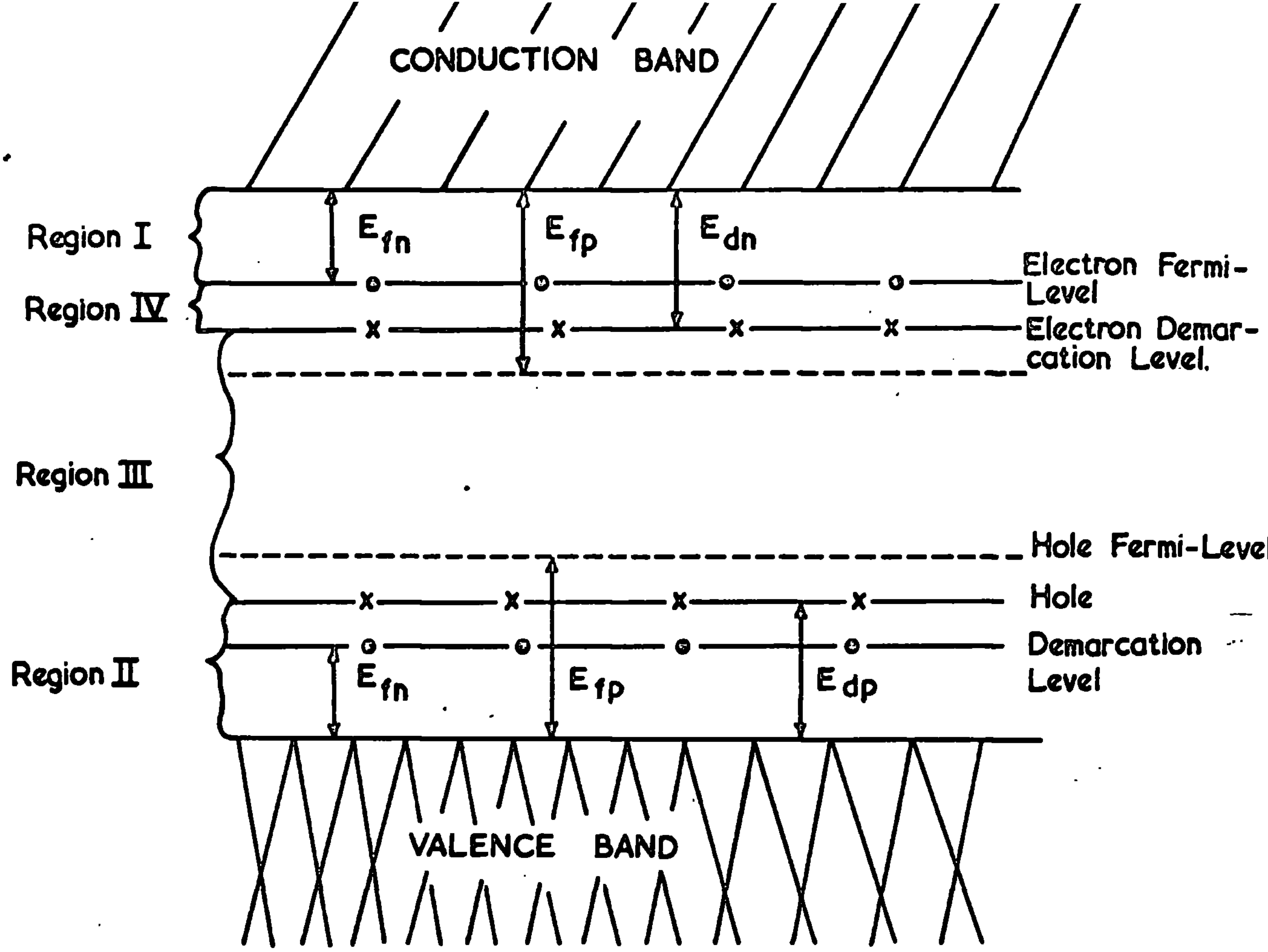

a Imperfection Sensitization of Photoconductivity

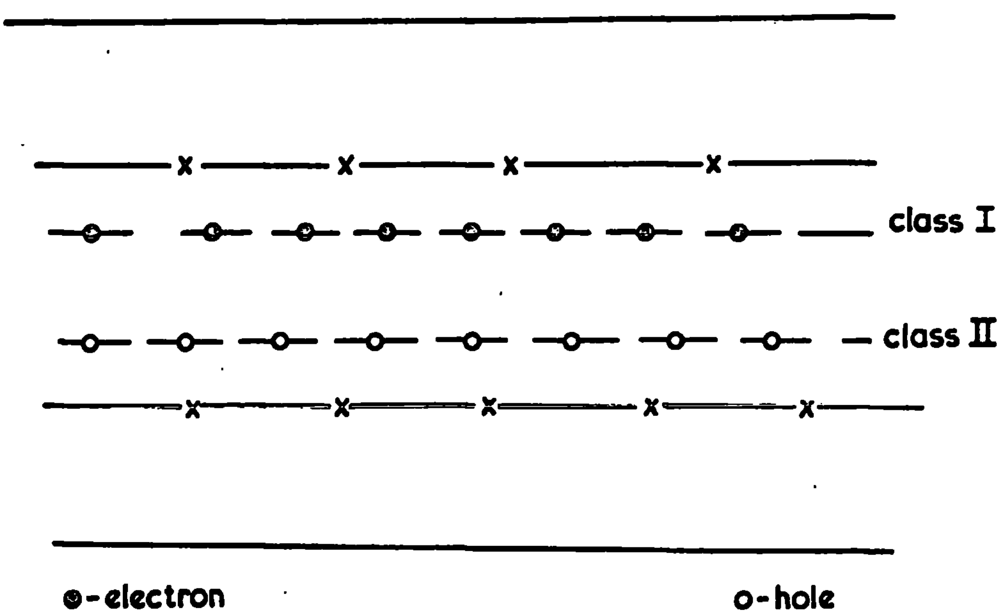

b Sensitizing Centres.

Fig. 2·3

negative charges in thermal equilibrium. Thus the addition of class II centres increases the photoconductive gain by increasing the electron lifetime and reducing the probability of a direct recombination of an electron with a hole. In CdS, impurities such as Cu or Cd-vacancies produce such sensitizing (class II) centres at a height of $\sim 1 \cdot 0$ eV above the valence band. These class II centres are also responsible for the phenomena such as (1) variation of photocurrent with a power of light intensity greater than unity, (2) temperature quenching of the photoconductivity and (3) infrared quenching of the photoconductivity. We shall describe these phenomena in the next chapter.

2-5. Photo-excited Luminescence in CdS.

(a) Edge Emission

In section 2-4 we have discussed the recombination process and its relation to photoconduction. The recombination process is accompanied by a release of energy. This may take the form of a local heating of the lattice or emission of light. The visible luminescence with photon energy close to the absorption edge is called edge emission.

The occurrence of luminescent edge emission in CdS on the long wavelength side of the absorption edge when the sample is cooled to liquid nitrogen temperature and excited with ultraviolet light was first observed by Kröger.[28] The band edge emission process illustrated in Figure 2.4 is observed as a set of bands separated by equal energy increments (300 $cm^{-1} \sim 0 \cdot 037$ eV). The first maximum corresponds to an energy close to that of the fundamental absorption edge. The edge

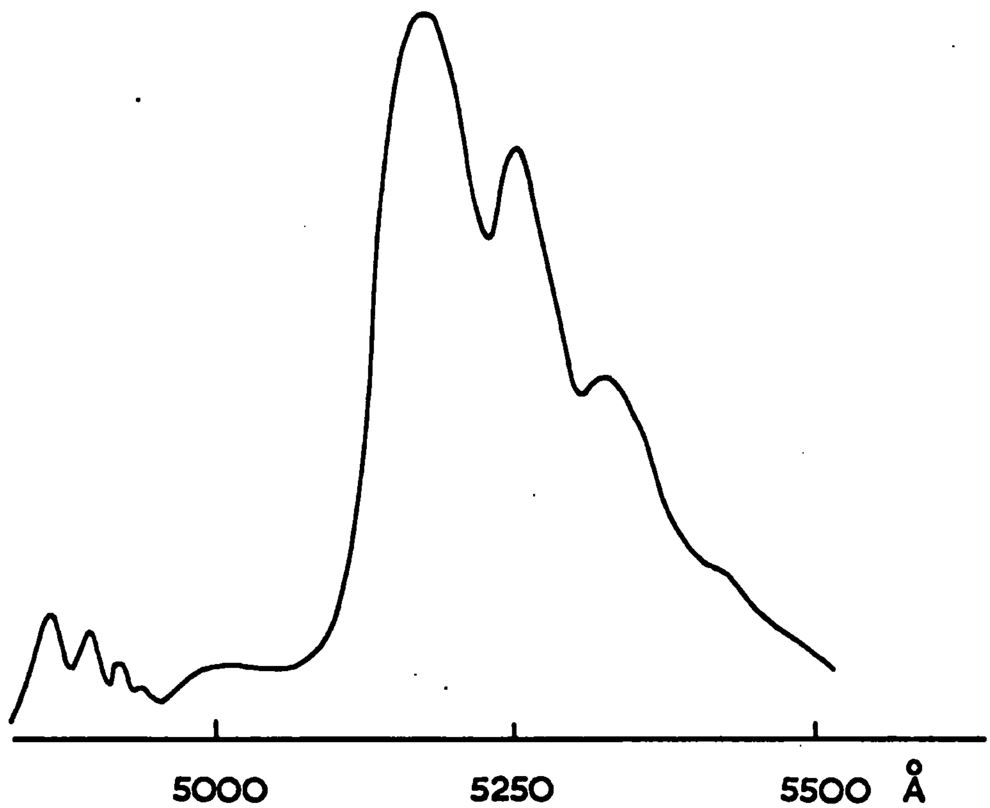

Visible Luminescence of CdS at 4·2 °K

Fig. 2·4

luminescence is assumed to be associated with a recombination process which takes place via an impurity centre with the simultaneous emission of 0,1,2,3,--- etc. LO phonons. From the infrared spectra of CdS the optical phonon frequencies were determined by Collins.[29] The value of 305 cm^{-1} for the longitudinal optical phonon found by Collins is in good agreement with the prediction by Kröger and Meyer,[30] showing that the emission is coupled to the lattice through optical phonons. The phonon energies deduced by Marshall and Mitra[31] from infrared transmission measurements confirm the association of the edge emission series with optical phonons.

Edge emission is thought to be due to recombination of a free carrier with a trapped carrier of opposite sign. Most of the works show that a defect level 0·15 eV from a band edge is responsible for edge emission. But it is not certain whether this level is near to the conduction band or to the valence band. Kulp and Kelly[32] argued from radiation damage studies in CdS that the green edge emission is due to sulphur interstitials. Similar experiments by Niekisch[33] and by Collins[29] led to the conclusion that the recombination centre was a sulphur vacancy. Marlor and Woods[34] showed that in many samples of pure and doped CdS the emission spectrum is a superposition of two separate spectra, associated with two distinct recombination routes. Their result indicated that sulphur vacancies introduce an energy level at 0·14 eV and sulphur interstials a level at 0·17 eV from a band edge. It was also observed that substitutional indium gives rise to a level

0·15 eV from a band edge. The mechahism of the green edge emission in pure and undoped crystals was also investigated by Spear and Bradberry.[35] They concluded that the luminescent centre responsible for edge emission was a centre of the class II type situated between 0·13 to 0·15 eV above the valence band.

The edge emission spectra at liquid Helium temperature sometimes show a weaker set of lines which appear to have the same spacing but are displaced slightly to shorter wavelengths. The most recent work of Thomas and Hopfield[10] shows that these lines are associated with the recombination of free excitons and excitons bound to various defects. Collins[29] argued that the blue edge emission (~ 4850 Å) observed at $4{\cdot}2^{\circ}$K was due to exciton decay. Lambe et al.[36] attributed the blue edge emission on the short wavelength side of 5000 Å to recombination at the surface. Maeda[37] observed a dominant blue peak I_2 (~ 4865 Å) with a 20°K zero-phonon peak position at $\sim 2{\cdot}395$ eV in undoped CdS single crystals which are conducting at room temperature. The I_2 line according to (10) is thought to be due to an exciton bound to a neutral donor. Hall effect and resistivity measurements in these samples are characteristic of pure CdS with a 0·033 eV donor level determining the transport behaviour. Maeda[37] also found a dominant blue peak I_1 (due to an exciton bound to a neutral acceptor) in crystals which are high resistive at 300°K but exhibit n-type photoconductivity. The I_5 line observed in crystals at $4{\cdot}2^{\circ}$K after heat treatment in a cadmium atmosphere is thought to be due to an exciton bound to a Cd-vacancy.[38]

(b) Infrared Emission

Defect levels close to a band edge give rise to edge emission. The other defect levels in the middle of the forbidden gap are thought to be responsible for emission in the infrared. The important infrared emission bands in CdS are located at 0·82 (1·51 eV), 1·02 (1·22 eV), 1·63 (0·76 eV) 1·85 (0·67 eV) and 2·05 (0·60 eV) microns.

Models proposed by Meijer,[39] Browne,[40] Garlick[41] and Broser and Schulz[42] all involve, in absorption, transitions from the top of the valence band to different ionization states of a luminescent centre. Browne[40] has proposed an energy-level scheme in which the two emission bands associated with copper in CdS are connected with the same centre, having more than one level in the forbidden gap. Maximum infrared emission is observed when the concentration of copper is approximately 100 parts per million. It is not clear whether the centre responsible for the infrared emission is a substitutional copper impurity, a cation vacancy or some more complex imperfection. Bryant and Cox[43] made an effective check on the model proposed by Browne[40] by determining whether the longer wavelength infrared excitation radiation excited only part of the infrared emission spectrum. The most significant results of their experiment were that the full infrared emission spectrum in CdS could be produced either by the 0·89 μm (1·39 eV) or by the 1·49 μm (0·83 eV) excitation bands separately. To explain the two different excitation bands for infrared emission they proposed that the same acceptor level is concerned with both emissions. The lower energy excitation and the higher energy excitation would correspond to transitions from the p-orbitals and S-orbitals respectively of the valence band states to this acceptor level. Recombination of electrons from the conduction band or a state near the conduction band to this acceptor level in the forbidden gap is responsible for "blue" emission (centred on 0·82 μm ~1·51 eV). The 'green' emission in cadmium sulphide centred on 1·02 μm (1·22 eV) is thought to be due to conduction electrons first trapped in an excited state before recombining to the same ground state.

Bryant and Cox also observed banded spectra in the 1·3 - 2·3 micron range centred on 1·63 (0·76 eV), 1·85 (0·67 eV) and 2·05 (0·60 eV) microns. They suggested that an unoccupied centre with an energy level 0·83 eV above the highest p-orbital valence band, is responsible for infra-red emission. The centre is thought to be an agglomeration of defects rather than a single defect. The banded infrared emission occurs when an electron excited to this level, returns to the p-state valence band (which is split into three components by crystal-field and spin-orbit effects).

2-6. The Acousto-electric effect in CdS

The acousto-electric effect is the interaction between sound waves and charged particles. This effect results in some interesting phenomena such as the attenuation and amplification of acoustic waves and the build up of ultrasonic flux. The attenuation of the acoustic waves explains the origin of the acousto-electric current.

This can be understood if we realize that the acoustic waves consist of a large number of phonons which impart momentum to free carriers. The transfer of momentum by the acoustic waves is manifest as the attenuation of the wave by free carriers, which can be thought of as a drag by the wave on the particles. The result is a measurable acousto-electric current or voltage. Hutson and White[44] analyzed the attenuation of acoustic waves in piezoelectric materials which they attributed to the interaction of mobile charge carriers with the strong longitudinal electric field accompanying the acoustic wave in piezoelectric crystals like CdS. Hutson, McFee and White[45] demonstrated that the attenuation of an acoustic wave could be converted to an amplification by the application of an electric field sufficiently large to cause electrons to drift faster than the velocity sound and in the same direction. If the drift velocity of the electrons is greater than the sound velocity, then those phonons which are emitted by the electrons on being scattered, are amplified. Hence this phonon mode becomes highly populated and the electron scattering increases. This tends to limit the increase in electron drift velocity above the sound velocity. A departure from Ohmic behaviour leading to current saturation and oscillation is observed.

Hutson et al.[45] reported that a substantial amplification of ultrasonic waves could be produced in photoconductive CdS by applying a dc electric field in the direction of wave propagation. Two striking results of the observation are the appearance of acoustic gain and the crossover from loss to gain at 700 volt cm^{-1}. In a 7 mm. long crystal, a gain of 18 dB was obtained at 15 MC sec^{-1} and 38 dB was obtained at 45 MC sec^{-1}. If the drift velocity v_d at crossover is equal to the appropriate CdS shear wave velocity ($v_S = 2 \times 10^5$ cm/sec) then the drift mobility $\mu = 285\ cm^2$/volt sec which agrees quite nicely with the values of Hall mobility usually obtained (see Section 2.3). An acousto-electric current saturation effect in CdS was observed by Spear and Le Comber.(46) Kröger(47) et al. observed oscillations in the current flowing in CdS under amplification conditions. Observation of current oscillations in illuminated CdS has also been reported by Okadi and Matino.(48) However, from the viewpoint of practical applications, the investigation of the acousto-electric effect is very important.

2-7. Investigation of electron-trapping Spectrum in cadmium sulphide

The distribution of electron traps in cadmium sulphide has been investigated by different workers using a wide variety of techniques. Of all the methods available that most commonly employed is the measurement of the "thermally stimulated current" one.

For thermally stimulated current measurements, the crystal is cooled to liquid nitrogen temperature and then exposed to illumination for a fixed time to fill trapping centres. The illumination is then removed and the crystal heated at a linear rate in the dark. As the crystal is heated, electrons are thermally excited from their traps into the conduction band. These excited electrons take part in electrical conduction. While the temperature is being increased, the current through the sample is monitored under constant applied field. As a set of traps begins to empty the current at first rises exponentially with temperature. Eventually a maximum is reached at a temperature T^* and thereafter the current falls as the occupancy of the traps decreases. Various methods of evaluating T.S.C. curves have been proposed and obviously there is a correlation between T^* and the trap depth. The number of trapping centres can also be calculated from the total area under the curve provided the carrier lifetime is known.

Nicholas and Woods,[49] in an exhaustive investigation, applied ten methods of analysis for the evaluation of electron-trapping parameters from conductivity glow curves. They concluded that there were at least six prominent, discrete sets of traps in cadmium sulphide with energy depths of 0·05, 0·14, 0·25, 0·41, 0·63, and 0·83 eV below the conduction band. They also suggested the following tentative identification of the defect centres associated with those trapping levels:

(i) 0·05 eV - Double negatively charged sulphur vacancy.

(ii) 0·14 eV - Also associated with sulphur vacancies.

(iii) 0·25 eV - A complex of associated sulphur vacancies.

(iv) 0·41 eV - A complex of associated cadmium and sulphur vacancies in nearest neighbour sites.

(v) 0·63 eV - Either a neutral or a positively charged cadmium vacancy.

(vi) 0·83 eV is probably the dissociation energy for a trap complex rather than the depth of a trapping level below the conduction band.

Nicholas and Woods identified six different traps but did not find trapping levels at 0·33 eV and 0·51 eV. The existence of a trapping level at 0·33 eV has been reported by many authors, namely, Brophy and Robinson[50] (noise measurements), Bube and MacDonald[51] (photo-Hall measurements), Unger[52] (photo/glow measurements), Broser[53] and Broser and Broser-Warminsky.[54] The presence of a trap at 0·51 eV has been reported twice by Trofimenko et al.[55] (activation energy plot) and Bube and MacDonald[51] (photo-Hall measurement).

Nicholas and Woods found that the trapping levels at 0·05, 0·41, 0·63 and 0·81 eV showed photochemical effects during cooling to liquid nitrogen temperature while under illumination. A detailed description of their observations on photochemical effects in cadmium sulphide can be found in reference (56). These authors also observed that no one crystal contained all the six trapping levels simultaneously. A comparison of their results with other workers who evaluated trapping parameters by various methods (from Table 2 of reference (49)) is reproduced in Table 2.1. Clearly there is a large measure of agreement over the depths of particular traps and their capture cross-sections.

Cowell and Woods[57] pointed out that trap depths obtained from thermally cleaned T.S.C. curves by using the methods advocated by Nicholas and Woods, often showed a spread of between 10 and 15% about a mean value. This scatter is not necessarily associated with any

Table 2.1

Reported by	Method of Measurement		Comparison of values of trap energy depths							
Woods & Nicholas	T.S.C. Photodecay	E T*	0·051 150	0·14 190	0·25 295	-	0·41 300	-	0·63 330	0·83 290
Woods & Wright	Bube	E T*	0·24 120	-	0·32 170	0·38 220	0·50 270	-	0·59 320	-
Niekisch	Alternating light	E E	-	0·12 -	0·22 -	0·31 -	0·40 0·45	-	0·55 0·66	0·70 0·80
Brophy et al.	Noise	E	-	-	-	0·36	0·43	-	0·60	-
Bube and Barton	Bube	E T*	0·20 100	0·25 135	0·41 180	0·44 220	0·51 270	0·58 305	0·63 350	-
Sokal'skaya	S.C.L. Currents	E	0·09	0·12	0·22	-	-	-	0·66	-
Broser et al.	T.S.C. Photodecay	E E	-	-	-	0·34 -	0·43 0·48	-	-	-
Broser	T.S.C.	E	-	-	0·22	0·31	-	-	-	-
Bube & MacDonald	PhotoHall	E	-	-	-	0·35	0·46	0·54	-	-
Franks & Keating	Franks & Keating	E	0·053	-	-	-	-	-	-	-
Driver & Wright	Primary T.S.C.	E	-	-	-	-	0·41	-	-	-
Marlor & Woods	S.C.L. Currents	E	-	-	-	-	-	-	0·61	-
Tanaka & Tanaka	-	E	-	-	-	-	0·4	-	-	-
Clayton et al.	Grossweiner	E	0·09	0·13	-	-	-	-	-	-
Smith	S.C.L. Current	E	-	-	-	-	-	-	-	0·8
Trofimenko et al.	Photo decay activation energy	E	0·045	-	0·23	-	-	0·5	-	-
Unger	Photo/glow	E	-	-	0·26	0·32	0·41	-	0·58	-
Lappe	-	E	-	-	-	-	0·41	-	-	-

E in eV. T.S.C. ≡ Thermally Stimulated Currents.

T* in ^{o}K. S.C.L. ≡ Space Charge Limited.

deficiencies in the theories underlying the various proposed methods, but rather is the result of inherent practical difficulties. Cowell and Woods used a curve-fitting technique with the methods advocated by Nicholas and Woods[49] improved the accuracy of the estimate of a trap depth of the order of 0·2 eV by 5%. The accuracy abtainable for traps with depths of the order of 0·6 eV was about 2%. The trap depths evaluated by them were 0·16, 0·18, 0·21, 0·38, 0·42, 0·63 and 0·85 eV below the conduction band.

By using slower heating rates, Cowell and Woods showed that the thermally stimulated current curve apparently due to a trap at 0·33 eV is a superposition of closely spaced T.S.C. curves. Using the curve fitting technique they were able to determine the two trap depths to be at 0·38 eV and 0·42 eV below the conduction band.

Haine and Carley-Read[58] applied a technique described as a constant-temperature method for the determination of trapping parameters. In this method, the temperature is increased until the traps begin to empty and then the temperature is held constant. The resulting current decay with time is controlled by the emptying of the trapping level. They found traps with depths of 0·18, 0·24, 0·33, 0·50, 0·60 and 0·74 eV below the conduction band. Agreement between the results of Haine and Carley-Read[58] and Cowell and Woods[57] is excellent.

2-8. Practical Applications

Cadmium sulphide is one of the best photoconductive materials known. Its sensitivity to visible light exceeds that of all other materials. By the incorporation of suitable impurities photoconductive gains as high as 10^4-10^5 can be achieved. As a photoconductor CdS could be used in devices such as infrared detectors, light meters and light-sensitive switches. In some cameras CdS is used as a light meter. CdS can also be used as a crystal counter for detecting X-rays and γ-rays. An extremely small counter of CdS could be produced to act as a personal radiation dose monitor. For an efficient crystal counter, a combination of high sensitivity and fast speed of response is required. But in cadmium sulphide a high sensitivity is associated with longer speed of response due to the presence of high density of trapping levels.

Cadmium sulphide could be used as a device based on the acousto electric amplification effect in signal processing application in which simultaneous amplification and delay are required. The performance of such acoustic amplifiers has been described by Hickernell and Sakiotes(59) and by Blötekjaer and Quate(60). Problems such as the effects of trapping levels on the acousto-electric interaction remain to be investigated and understood. The spontaneous generation of acoustic noise must be removed before such devices find successful practical applications.

Thin films of CdS are also finding practical applications of great importance in device work. CdS thin film transistors (T.F.T.), which are insulated gate field-effect transistors have been fabricated successfully from evaporated CdS with an SiO gate insulator.[61,62,63] Successful fabrication of two-terminal (Diode) and three-terminal (the space charge limited dielectric diode, a T.F.T. with pentode like characteristic) CdS thin film devices have been reported by Zuleeg.[64] An evaporated thin film of CdS on a p-type layer of copper sulphide forms a p-n junction. The photovoltaic effect in a p-n junction of CdS can serve as a useful electrical generator employing solar energy. The special aspect of CdS solar cells is that a considerable amount of photovoltaic response exists in the long wavelength side of the absorption edge of CdS, making the cells more efficient to solar radiation.

The presence of defect centres in CdS determines its electrical and optical properties. The physical and chemical identity of some of the defect centres in CdS has not yet been completely understood. A complete understanding of these defects and their control during sample preparation will provide immense possibilities of practical application of CdS to solid-state device technology.

References

(1) C.A. Escoffery, J.Appl.Phys., 35, 2273, 1964.

(2) J. Lambe and C.C. Klick, "Progress in Semiconductor", Vol.3,page 184.

(3) E.S. Rittner and J.H. Schulman, J.Phys.Chem., 47, 537, 1943.

(4) Kröger, Vink and Vander Boomgaard, Z.Phys.Chem., B203, 1, 1954.

(5) R.H. Bube, Phys.Rev. 99, 1105, 1955.

(6) R.H. Bube, Proc. IRE, 43, 1836, 1955.

(7) R.H. Bube, J.Phys.Chem.Solids, 1, 234, 1957.

(8) J. Woods and J.A. Champion, J.Elect.and Control, 7, 243, 1959.

(9) M. Balkanski and des Cloiseaux, J.Phys.Rad., 21, 825, 1960 and 22, 41, 1960.

(10) D.G. Thomas and J.J. Hopfield, Phys.Rev., 122, 35, 1961.

(11) J.L. Birman, Phys.Rev.Letters, 2, 157, 1959.

(12) R.C. Casella, Phys.Rev. 114, 1514, 1959.

(13) J.J. Hopfield, J.Phys.Chem.Solids, 15, 97, 1960.

(14) D. Dutton, Phys.Rev. 112, 785, 1958.

(15) D.G. Thomas, J.J. Hopfield and M.Power, Phys.Rev. 119, 570, 1960.

(16) J.D. Zook and R.N. Dexter, Phys.Rev. 129, 1980, 1963.

(17) W.W. Piper and R.E. Halsted, Proc. Int. Conf. on Semiconductor Physics, Prague 1960, Academic Press, New York, 1961. page 1046.

(18) W.W. Piper and D.F.T. Marple, J.Appl.Phys., 32, 2237, 1961.

(19) W.S. Baer and R.N. Dexter, Phys.Rev., 135, A1388, 1964.

(20) K. Sawamotto, J.Phys.Soc. Japan, 19, 318, 1964.

(21) F.A. Kröger, H.J. Vink and J. Volger, Philips Res.Rept. 10, 39, 1955.

(22) M. Balkanski and J.J. Hopfield, Phys.Stat.Sol., 2, 623, 1962.

(23) H. Miyazawa, H.Maeda and H. Tomishima, J.Phys.Soc. Japan, 14, 41, 1959.

(24) M. Itakura and H. Toyoda, J.Appl.Phys., 4, 560, 1965.

(25) L. Clark and J.Woods, Brit.J.Appl.Phys., 17, 319, 1966.

(26) W.E. Spear and J. Mort, Proc.Phys.Soc., 81, 130, 1963.

(27) M. Onuki and H. Hase, J.Phys.Soc. Japan, 20, 171, 1965.

(28) F.A. Kröger, Physica, 7, 1, 1940.

(29) R.J. Collins, J. Appl.Phys., 30, 1133, 1959.

(30) F.A. Kröger and H.J.G. Meyer, Physica, 20, 1149, 1954.

(31) R. Marshall and S.S. Mitra, Phys.Rev., 134, A11019, 1964.

(32) B.A. Kulp and R.H. Kelley, J.Appl.Phys., 31, 1057, 1960.

(33) E.A. Niekisch, Zeits. F.Phys.Chem., 217, 110, 1961.

(34) G.A. Marlor and J. Woods, Brit. J. Appl. Phys., 16, 797, 1965.

(35) W.E. Spear and G.W. Bradberry, Phys. Stat. Sol., 8, 649, 1965.

(36) J.J. Lambe, C.C. Klick and D.L. Dexter, Phys.Rev., 103, 1715, 1956.

(37) K. Maeda, J.Phys.Chem.Solids, 26, 1419, 1965.

(38) S. Ibuki and A. Ohso, J.Phys.Chem.Solids, 27, 1753, 1966.

(39) G. Meijer, J.Phys.Chem.Solids, 7, 153, 1958.

(40) P.F.Browne, J.Electronics, 2, 1, 1956.

(41) G.F.J. Garlick, J.Phys.Chem.Solids, 8, 449, 1959.

(42) I. Broser and H.J. Schulz, J.Electrochem. Soc., 108, 54, 1961.

(43) F.J. Bryant and A.F.J. Cox, Brit.J.Appl.Phys., 16, 463, 1965.

(44) A.R. Huston and D.L. White, J.Appl.Phys., 33, 40, 1962.

(45) A.R. Hutson, J.H. McFee and D.L. White, Phys.Rev.Letters, 7, 237, 1961.

(46) W.E. Spear and D.G. LeComber, Phys.Rev.Letters, 13, 434, 1964.

(47) H. Kröger, E.W. Prohofsky and H.R. Carleton, Phys.Rev.Letters, 12, 555, 1964.

(48) J. Okadi and H. Matino, Japan, J.Appl.Phys., 3, 698, 1964.

(49) K.H. Nicholas and J. Woods, Brit.J.Appl.Phys., 15, 783, 1964.

(50) J.J. Brophy and R.J. Robinson, Phys.Rev., 118, 959, 1960.

(51) R.H. Bube and H.E. MacDonald, Phys.Rev., 121, 473, 1961.

(52) K. Unger, Reaktions Kinetik von Electronen Prozessen in Festkorpen, (Berlin: Akademic-Verlag), page 170, 1960.

(53) J. Broser, Reaktions Kinetik von Electronen Prozessen in Festkorpen, (Berlin: Akademic-Verlag), page 45, 1960.

(54) I. Broser and R. Broser-Warminsky, Brit.J.Appl.Phys., 6, Suppl. 4, S90, 1955.

(55) A.P. Trofimenko, G.A. Fedoras and A.K. Razmadze, Soviet Physics - Solid State, 2, 1033, 1961.

(56) J. Woods and K.H. Nicholas, Brit.J.Appl.Phys., 15, 1361, 1964.

(57) T.A.T. Cowell and J.Woods, Brit.J.Appl.Phys., 18, 1045, 1967.

(58) M.E. Haine and R.E. Carley-Read, Brit.J.Appl.Phys., Ser.2, Vol.1, 1257, 1968.

(59) F.S. Hickernell and N.G. Sakiotes, Proc.IEEE, 52, 194, 1964.

(60) K. Blötekjaer and C.F. Quate, Proc.IEEE, 52, 360, 1964.

(61) P.K. Weimer, Proc.Inst.Radio Engrs., 50, 1492, 1962.

(62) W. Tantraparn and K.K. Reinhartz, Proc. N.E.C., 18, 736, 1962.

(63) J.E. Johnson, Solid State Electronics, 7, 861, 1962.

(64) R. Zuleeg, Solid State Electronics, 6, 193, 1962.

CHAPTER 3

EFFECT OF PHOTOEXCITATION ON THE PROPERTIES OF PHOTOCONDUCTING INSULATORS

3-1. Photohall Effect

3-1.1. Introduction

In high resistance crystals the measurement of the Hall effect by the conventional method is very difficult because a small voltage has to be measured at high impedance. In a photosensitive insulating cadmium sulphide crystal the impedance can be reduced by generating extra carriers by photoexcitation, then the Hall effect can be more easily investigated.

To analyse the photoconductivity process in CdS it is assumed that carriers of one type are dominant and that the mobility of these carriers is independent of the light intensity. These assumptions are true for highly pure samples. But in the case of insulators with impurity or defect centres in the forbidden gap, a change in the density of such centres by photoexcitation will lead to a change in the mobility. The application of the techniques of the photohall effect to such materials provides an opportunity to check both these normal assumptions. Photohall effects in photoconducting insulators can be summed up in the following ways:

1) Measured values of the Hall mobility, μ_H may vary with the intensity of photoexcitation L. The variation of the Hall mobility

with the intensity of photoexcitation can be expressed from the relation $\mu_H = r\mu$ as:

$$\frac{d\mu_H}{dL} = \mu \frac{dr}{dL} + r \frac{d\mu}{dL} \tag{3.1}$$

Because the value of r which is a constant, lies between 1 and 2 depending upon the scattering mechanism and band structure, the term $\mu\, dr/dL$ which involves the variation of r with L, can be neglected.

2) The variation of Hall mobility under photoexcitation can result either from (i) a change in the number or in the charge of the scattering centres, or (ii) from the initiation of two-carrier conductivity.

3) When the photoexcitation changes the effective charge of the scattering centres by adding or removing an electron from their environment, the sign of the mobility change indicates the effective charge of the scattering centre. The variation in mobility can lead to an independent determination of (i) the energy depth relative to the conduction band and (ii) the scattering cross-section of the imperfection centres. With this knowledge it may then be possible to describe the atomic configuration of the defect.

3-1.2. Scattering cross-section

The capture cross-section of an imperfection centre can be derived by equating the Coulombic attraction energy of a centre, $Ze^2/\epsilon r$, to the thermal energy of an electron:

$$Ze^2/\epsilon r = kT \tag{3.2}$$

where Z is the electronic charge on the centre, r its radius and ϵ the dielectric constant of the material. Hence the scattering cross-section S_o is

$$S_o = \pi r^2 = \frac{\pi Z^2 e^4}{\epsilon^2 k^2 T^2} \tag{3.3}$$

From the equation for the mobility resulting from Coulomb scattering in a solid derived by Conwell and Weisskopf[1] the expression for cross-section is

$S_{cw} = k_{cw} S_o$, for a singly charged centre where

$$k_{cw} = \frac{\pi^{\frac{1}{2}}}{16} \ln\left[1 + \left(\frac{3\epsilon kT}{e^2 N_I^{1/3}}\right)^2\right]$$

k_{cw} varies between 1·4 and 0·4 as N_I, the density of singly charged imperfection centres increases from 10^{12} to 10^{18} cm^{-3}, assuming $\epsilon = 10$ and $T = 300^oK$.

The quantum mechanical treatment of Brooks and Herring[2] which takes into account the shielding of scattering centres by free carriers, gives a similar result. Hence for practical purposes we can use the simplified expression for cross-section

$$S_o = Z^2 \pi e^4 / \epsilon^2 k^2 T^2 \tag{3.3}$$

At room temperature, $S \sim 10^{-12}$ cm^2 for a singly charged centre or more generally $S \sim 10^{-12} Z^2 cm^2$.

3-1.3. Two-carrier Hall Effect.

When both the carriers make an appreciable contribution to the conductivity, the measured Hall mobility μ_H is given by the equation

$$\mu_H = \frac{p\mu_h^2 - n\mu_n^2}{p\mu_h + n\mu_n} \tag{1.61}$$

However, the mobility μ_H will be independent of p and μ_h if $n \gg p$, especially in CdS where $\mu_n \gg \mu_h$.

If the photoexcitation produces comparable numbers of free electrons and holes, then the onset of two carrier conductivity will give a variation in the Hall mobility if the photoexcitation intensity is varied. Using photohall measurements, Bube et al.[3] found mobility variations in CdS indicating a hole concentration some 30 to 60 times the concentration of free electrons under conditions of infrared quenching.

With a typical ratio of $\mu_n:\mu_h$ of 10:1, the Hall mobility is reduced by 10% for $p \sim n$, and by 50% for $p \sim 10\,n$. Theoretical curves for the dependence of Hall mobility, plotted as a percentage of the electron mobility, on the hole concentration, in a system with two-carrier conductivity ~~is~~ are shown in Figure 3.1.

3-1.4. Effect of impurity centres on mobility

The variation of mobility is associated with a change in the occupancy of the imperfection centres. The photoexcitation causes this change in occupancy which in turn, causes a change in the scattering cross-section and hence the mobility. Thus the determination of the change

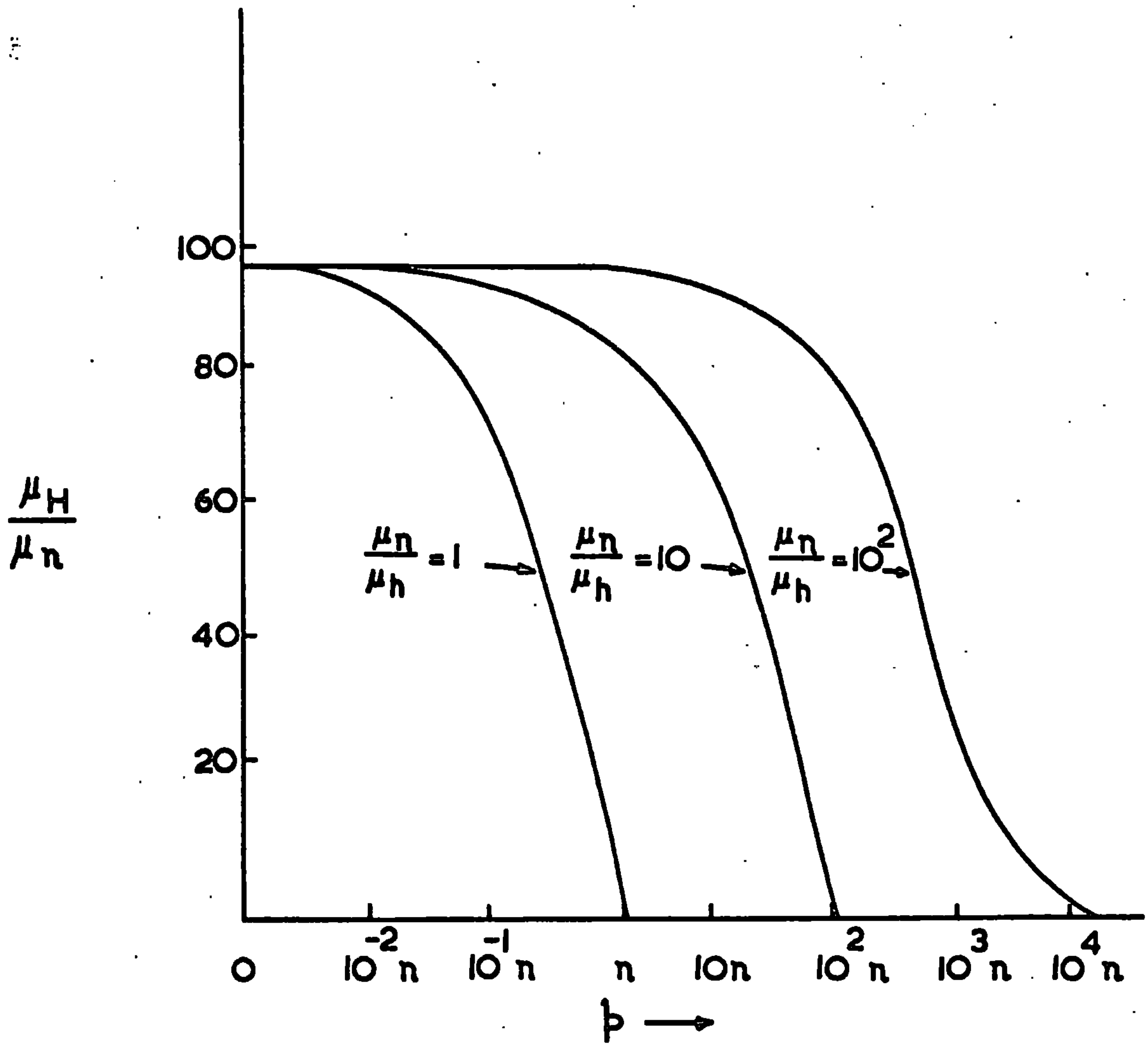

Fig. 3.1

(After Bube and MacDonald[3])

in mobility as a function of photoexcitation enables the depth and the nature of the imperfection centres to be determined. A number of possible cases in which a change in occupancy of a level will result in a change in mobility are shown in Figure 3.2.

The effect of photoexcitation on the electron mobility is described theoretically by the equation

$$\frac{1}{\mu} = \beta/\tau_o + \beta v_e \sum_i S_i(N_i - n_i) \qquad (3.4)$$

where S_i - Scattering cross-section

N_i - The density of the centres

n_i - The density of electrons in these centres.

$\beta(=m^*_e/e)$ - The proportionality factor between mobility and relaxation time which is equal in magnitude to $1{\cdot}14 \times 10^{-16}$ for cadmium sulphide in practical units.

v_e - The thermal velocity of an electron which is $\sqrt{2kT/m^*_e}$

In equation (3.4) β/τ_o represents the scattering due to all other processes such as lattice scattering, etc. Theoretical curves for the dependence of $1/\mu$ on the location of the electron Fermi level E_{fn} for cases (a), (b) and (d) of Figure 3.2 are shown in Figure 3.3.

For example, consider curve (a) of Figure 3.3, which corresponds to Figure 3.2a. Figure 3.2a represents the existence of positively charged centres (ionized donors) in the dark. The donors will be filled with electrons as the electron Fermi level approaches the

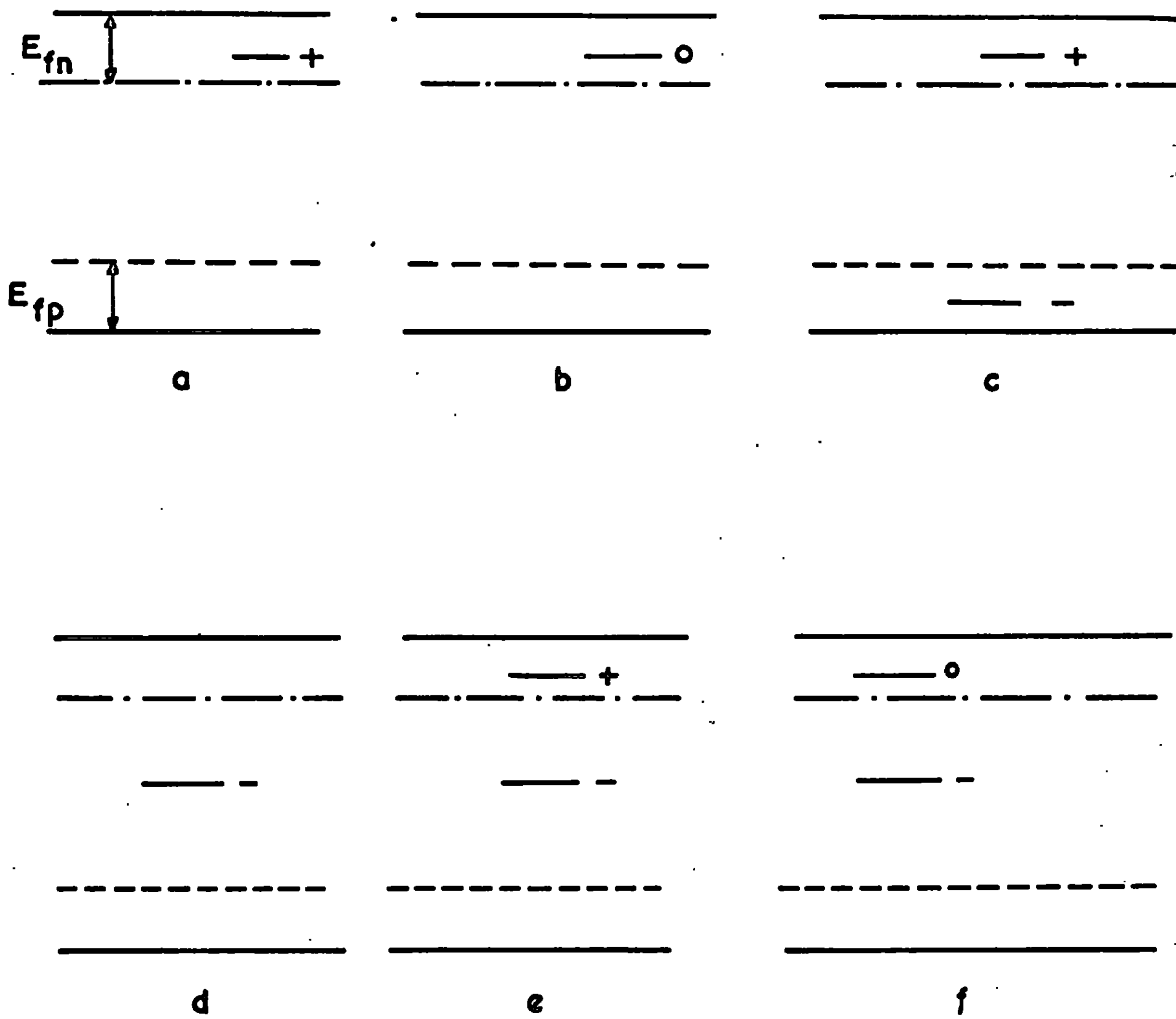

Fig. 3.2 A number of possible cases in which a change in occupancy of a level as the result of photoexcitation will result in a change in mobility.

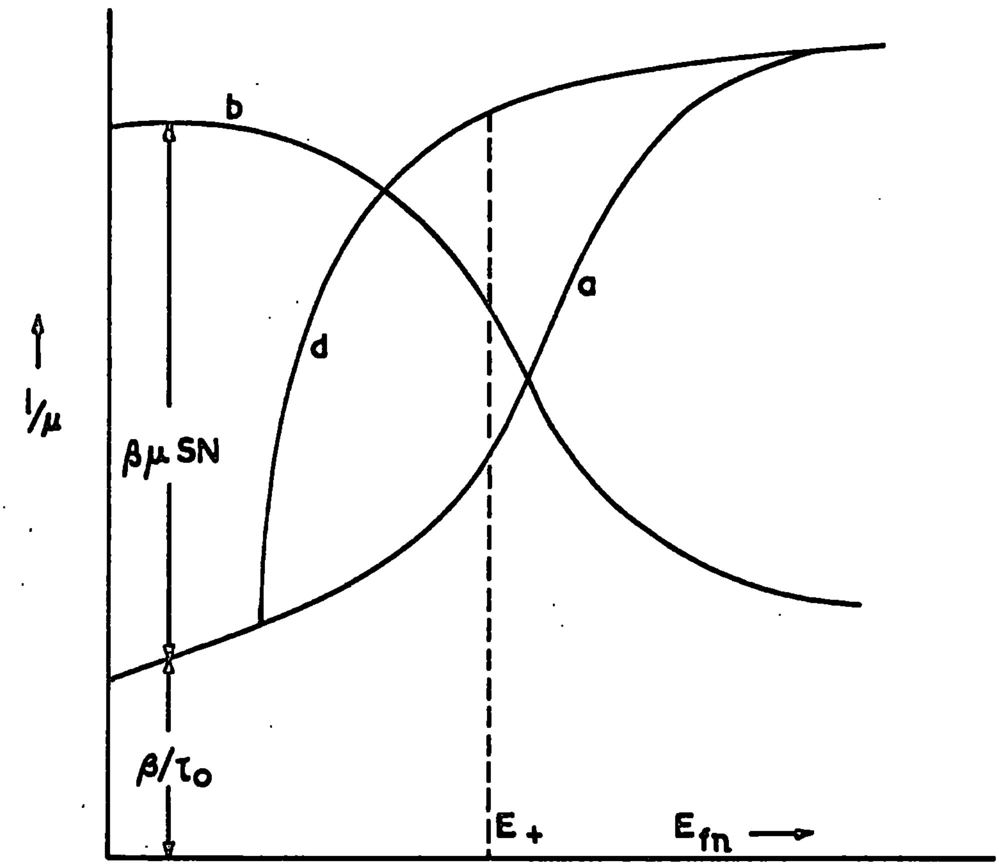

Fig. 3·3 Theoretical curves showing the dependence of $1/\mu$ on the location of the electron Fermi level for the cases of a, b and d of Fig. 3·2.

(After Bube and MacDonald[3])

conduction band under illumination. Thus their charge is removed and their scattering decreases markedly. The mobility μ is given by

$$\frac{1}{\mu} = \beta/\tau_o + \beta v_e S_+(N_+ - n_+) \qquad (3.5)$$

where N_+ is the density of the imperfection centres and n_+ the density of the electrons in these centres. The number of ionized impurity centres $(N_+ - n_+)$ can be determined from the Fermi distribution function, so that

$$(N_+ - n_+) = \frac{N_+}{1+2\ \exp[(E_+ - E_{fn})/kT]}$$

$$\therefore \quad \frac{1}{\mu} = \beta/\tau_o + \beta v_e S_+ \frac{N_+}{1+2\ \exp[(E_+ - E_{fn})/kT]} \qquad (3.6)$$

When E_{fn}, measured from the conduction band, is much less than E_+, only the scattering from the term β/τ_o remains. When E_{fn} is greater than E_+, all the terms in equation (3.6) are effective.

As E_{fn} varies from $E_{fn} \gg E_+$ to $E_{fn} \ll E_+$, $(N_+ - n_+)$ varies from N_+ through $N_+/3$ for $E_{fn} = E_+$ to $(N_+ - n_+) \longrightarrow 0$. This means that with increasing photoexcitation, the Fermi level rises and more and more imperfection centres are filled with electrons. As a result the scattering by the imperfection centres decreases and the value of the mobility increases. In fact as the Fermi level varies from $E_{fn} \gg E_+$ to $E_{fn} \ll E_+$, $1/\mu$ passes through a single step and a plot of $1/\mu$ as a function of E_{fn} gives an "S-shaped" curve. The difference between the limiting values of $1/\mu$ for small E_{fn} and large E_{fn}, i.e. $\Delta\ 1/\mu$ gives directly the values of $\beta v_e S_+ N_+$ as shown by the Figure 3.4. If N_+ is known from an alternative measurement such as thermally stimulated current measurement, a value of scattering cross-section S_+ can be calculated. A value of trap depth from the conduction band can also be found by finding the point on the curve in Figure 3.4 where $1/\mu$ has increased by $1/3\ \Delta\ 1/\mu$ from the value β/τ_o. At this point $E_{fn} = E_+$. The detailed analysis for other types of centres can be found in the reference (3).

3-2. Photoconductivity

In section 2-4 we have discussed how the presence of the class II centres in the forbidden gap gives rise to photosensitivity. These class II centres are also responsible for the observed phenomena of (i) superlinearity, (ii) thermal quenching of photoconductivity and (iii) infrared quenching. The concept of the demarcation levels (Figure 2.3) which are given by the relationships[4]

$$E_{dp} = E_{fn} + kT \ln\left(s_p/s_n\right) + \frac{3}{2} kT \ln\left(m_h^*/m_e^*\right) \qquad (3.7)$$

$$E_{dn} = E_{fp} - kT \ln(s_p/s_n) - \frac{3}{2} kT \ln(m_h^*/m_e^*) \qquad (3.8)$$

helps to explain these phenomena. Experimentally superlinearity is observed as an increase in photocurrent which is more rapid than linear with increasing light intensity at fixed temperature, as shown by the region B of Figure 3.5. In a superlinear photoconductor when the hole demarcation level is lowered through the class II centres with increasing light intensity, the class II centres convert from hole traps to recombination centres. While the class II centres are being converted from traps to recombination centres, the electron lifetime is continuously increasing and consequently the photocurrent increases superlinearly with light intensity. After full conversion of class II centres to

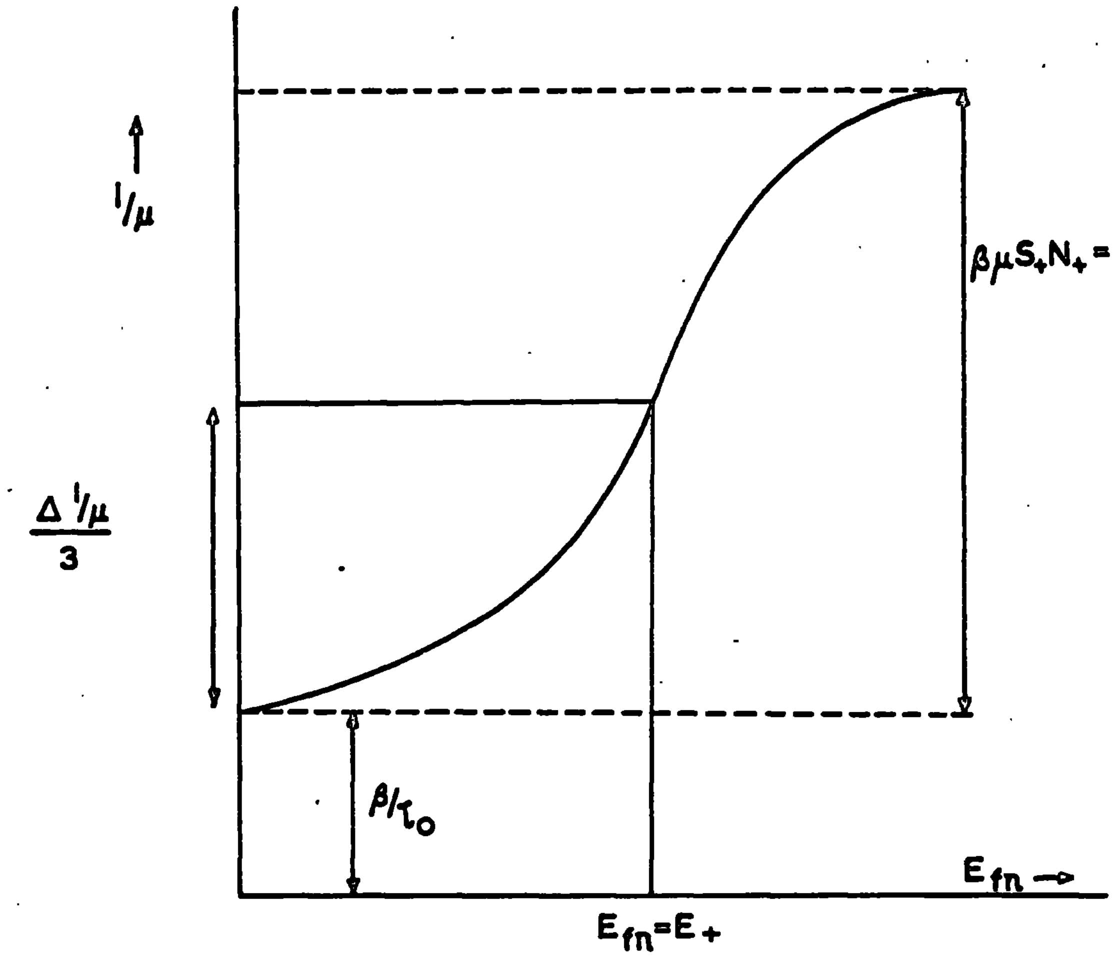

Fig. 3·4. Variation of the mobility with the variation of the location of the electron Fermi level for the case (a) of Fig. 3·2.

recombination centres, the photocurrent again increases linearly with light intensity. The three regions shown in Figure 3.5 can be described in the following way:

(1) Region A - Insensitive where the hole demarcation level lies above the class II centres.

(2) Region B - Superlinear where the hole demarcation level is being lowered through the class II centres.

(3) Region C - Sensitive where the hole demarcation level lies below the class II centres.

A variation of photocurrent can also be observed by varying the temperature at fixed light intensity. When the hole demarcation level is raised with increasing temperature at fixed light intensity, the class II centres are then converted from recombination centres to hole traps. A sharp reduction of photocurrent as shown by the transition from region C to region B of Figure 3.6 is observed. This is known as thermal quenching of photoconductivity. Region A of Figure 3.6 which shows a linear variation of photocurrent with temperature corresponds to the full conversion of class II centres into hole traps.

If the electrons are optically excited (i.e. by irradiation with infrared) from the valence band to the class II centres when these latter are occupied by holes, the holes are freed and can then be captured by class I centres. The sensitizing process is then reversed

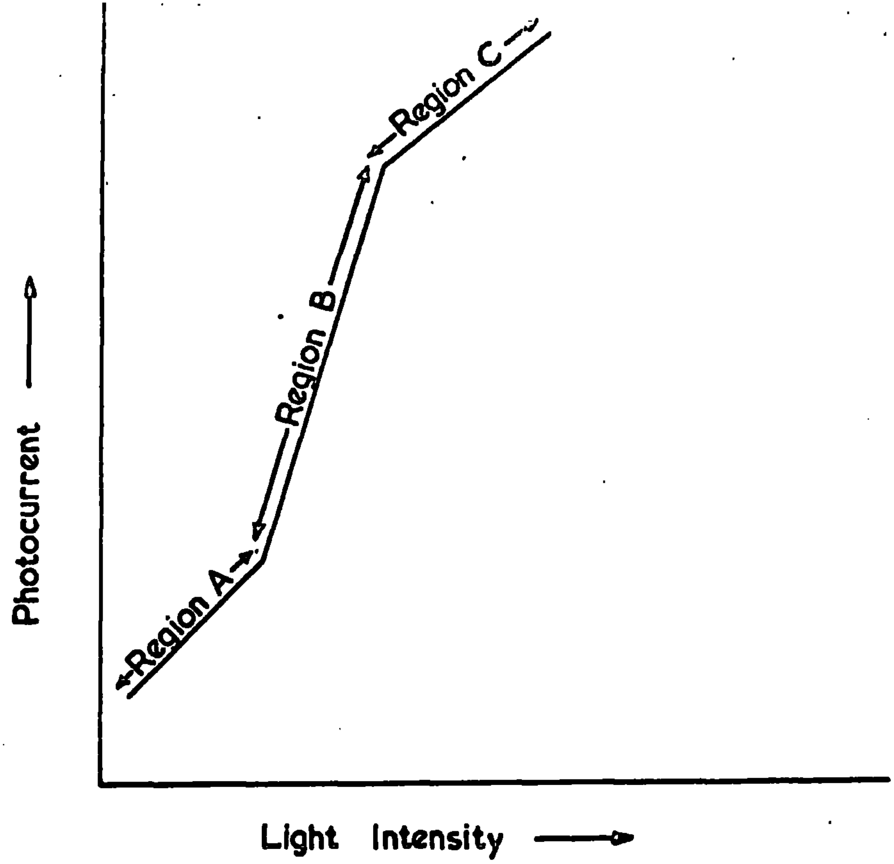

Fig. 3·5 Variation of photocurrent as a function of light intensity at fixed temperature.

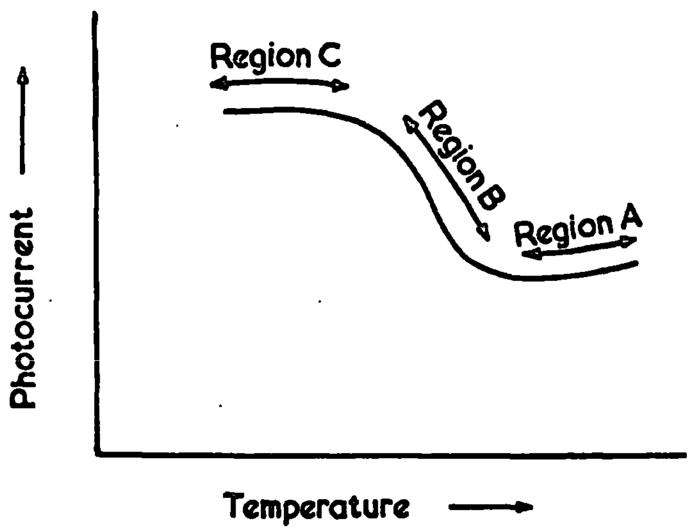

Fig. 3·6 Variation of photocurrent as a function of temperature at fixed light intensity.

i.e. optical quenching of photoconductivity occurs.

Schön[5] and Klasens[6] described such phenomena in terms of a model with two different types of centres. Using the concept of the demarcation levels defined by the equations (3.7) and (3.8), Bube considered the mathematical analysis and physical interpretation of a three level model in detail. The conclusions reached by Bube can be summed up in the following ways:

(1) The variation of the photosensitivity illustrated in Figures 3.5 and 3.6 arises from the variation of the location of the hole demarcation level through the class II centres.

(2) The break point from the region C to region B both at fixed light intensity with increasing temperature (Figure 3.6) and at fixed temperature with decreasing light intensity (Figure 3.5) occurs when the hole demarcation level associated with the class II centres is located at these levels. The condition for such breaks is that

$$\ln n = \ln\left(\frac{N_v s_p}{s_n}\right) - E_I/kT \tag{3.9}$$

where s_p/s_n is the ratio of the capture cross-section of the class II centres for holes to that for electrons, and E_I is the height of the class II centres above the valence band.

(3) The condition for the break point from region B to region A as shown by the Figures 3.5 and 3.6 is given by the equation

$$\ln n = \ln\left(N_v \frac{N_1}{N_2}\right) - \frac{E_I}{kT} \tag{3.10}$$

where N_1 and N_2 are the densities of the class I and class II centres respectively.

Now a plot of In n corresponding to the break points from region C to region B as a function of 1/T at which that break occurs for a set of curves, should yield a straight line with a slope $-E_I/k$ and an intercept at $1/T = 0$ of $\ln (N_v\ s_p/s_n)$. Similarly by plotting ln n corresponding to the break points from region B to region A as a function of 1/T at which that break occurs, a straight line should also be found with a slope E_I/k and an intercept at $1/T = 0$ of $\ln (N_v\ N_1/N_2)$.

References

(1) E. Conwell and V.F. Weisskopf, Phys.Rev. 77, 388, 1950.

(2) H. Brooks and C. Herring, Phys.Rev. 93, 693, 1954.

(3) R.H. Bube and H.E. MacDonald, Phys.Rev., 121, 473, 1961.

(4) R.H. Bube, "Photoconductivity of Solids" page 67. John Wiley & Sons, Inc.,1960.

(5) M. Schön, Physica, 20, 930, 1954.

(6) H.A. Klasens, J.Phys.Chem.Solids, 7, 175, 1958.

(7) R.H. Bube, J.Phys.Chem.Solids, 1, 234, 1957.

CHAPTER 4

THE GROWTH OF CADMIUM SULPHIDE AND SPECIMEN PREPARATION

4-1. Introduction

Cadmium sulphide crystals may be grown in a variety of ways namely, from solution,[1] by sublimation[2-7] and from the melt at high pressures.[8] Since cadmium sulphide sublimes at temperatures of about 1000°C, crystal growth techniques by sublimation have received most attention.

A number of methods of growing cadmium sulphide from the vapour phase have been reported in the literature. All these procedures are essentially modifications of two basic methods, i.e. (i) dynamic and (ii) static. In the dynamic method, the cadmium sulphide charge vapourises in the hot region of the furnace and the vapour is driven by a suitable carrier to a cooler part of the furnace where it condenses. In the static method, a temperature gradient is maintained along the sealed tube so that the charge vapourises and crystals grow at the cooler end of the tube.

4-2. Growth of flow crystals

Growing crystals of cadmium sulphide by the dynamic method of sublimation was first introduced by R. Frerichs.[2] Cadmium metal in a fused silica boat was heated in a quartz tube to about 800 to 1000°C. Hydrogen sulphide and a carrier gas were passed over heated cadmium metal. The reaction between hydrogen sulphide and cadmium vapour forms cadmium sulphide which was carried to a cooler region of the system where crystals grew generally in the form of thin rods or thin plates.

Stanley[3] used streams of oxygen-free nitrogen or argon at 175 ml. per minute to transport the vapour over a cadmium sulphide charge held at a temperature of 1000°C. Crystals with prismatic and plate-like habit were formed in the cooler part of the furnace where the temperature was 900°C.

Fochs[4] modified Stanley's method by steadily reducing the growth temperature once the temperature distribution in the growth tube had reached equilibrium. Initially, the degree of supersaturation is sufficient to cause some of the vapour to condense on suitable nucleation centres. Once this condensation has been initiated, the degree of supersaturation necessary for further growth is reduced, so that the vapour preferentially condenses on these seeded sites rather than on the adjacent parts of the silica tube. Crystals grew from the walls, remote from one another and also the growth could be extended over a comparatively larger length of the tube.

4-3.1. The Method of growing flow crystals of Cadmium Sulphide in this Laboratory.

Using a modified form of Stanley's method[3], Clark[9], Nicholas,[10] Marlor[11] and Rushby[12] grew flow crystals of cadmium sulphide with considerable success. The experimental arrangement is shown in Figure 4-1. A 32 mm. bore transparent silica tube is used as the growth tube. A charge of cadmium sulphide powder ($\sim$30 gm.) is placed inside the growth tube. A split silica liner which fits closely inside

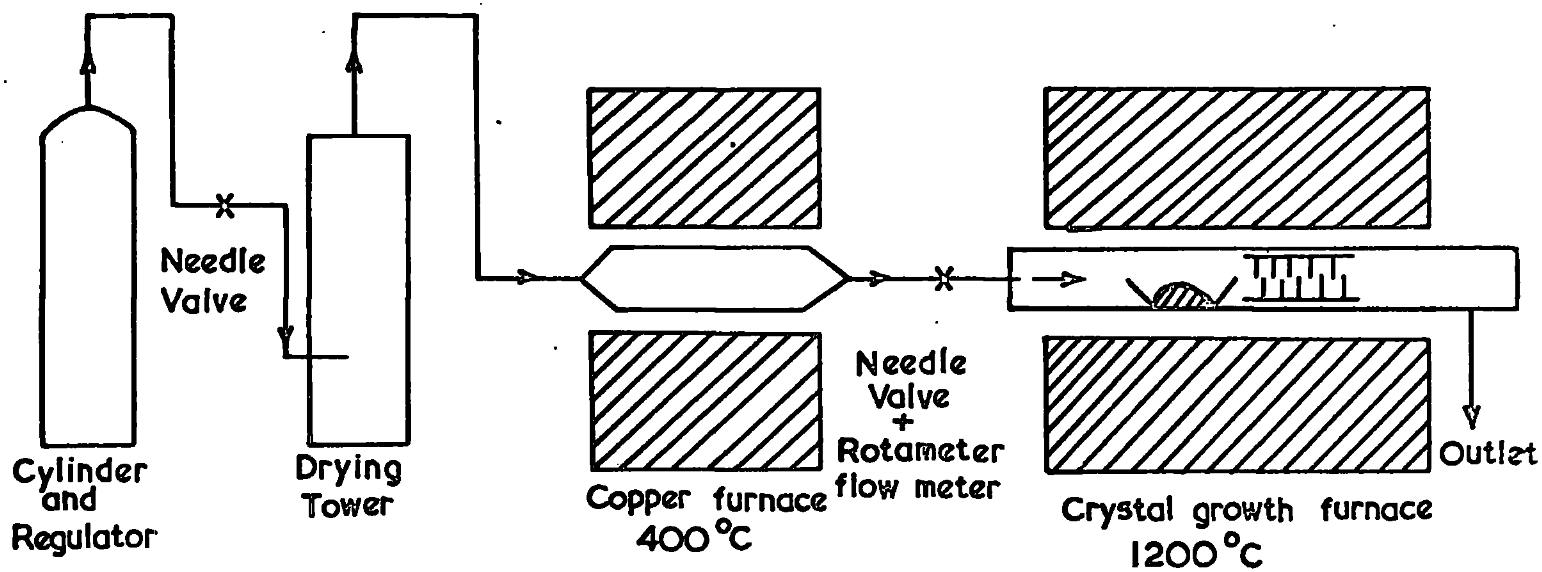

FIG. 4·1 Argon System

the growth tube, is placed close to the charge. With the growth tube in position in the furnace, the charge is at the maximum temperature ($\sim 1200^{o}C$) and the lin~~e~~ar at about $1050^{o}C$.

99·995% pure argon is used to transport the vapour over the charge. The argon from the cylinder is passed through a needle valve to reduce the pressure. This also enables fine adjustments to be made. Subsequently the argon passes first through a drying tower containing calcium aluminium silicate and then over heated copper turnings to remove water vapour and oxygen respectively. The flow of the purified argon over the heated cadmium sulphide is controlled by a second needle valve and measured with Rotameter flow meter. The flow rate remains fairly constant over 24 hours with a maximum drift of 5 ml. in the flow rate of 180 ml./min. The argon leaves the system via an outlet provided at the far end of the growth tube into the atmosphere. A quartz window enables the growth to be observed.

Initially, purified argon is allowed to flow over the charge for two hours. After that, the charge is heated at $600^{o}C$ for six hours. This is done to drive off any volatile impurities, including water vapour, chloride and organic solvents present in the original charge powder. After this period, the temperature of the charge is raised to $1200^{o}C$. A cadmium sulphide substrate on the liner which was obtained from a previous run provides nucleation centres for growth and at the same time, prevents diffusion of impurities from the silica into the crystals.[13] Two thirds of the charge powder is allowed to sublime. Crystals in the form of rods and thin plates grow radially on the wall of the liner.

4-3.2. Properties of the flow crystals

The crystals produced by this technique are in the form of rods and thin plates and are pale yellow in colouration. Some of the plates are twinned with a herringbone structure. Since the volatile impurities are driven off initially and the non-volatile impurities remain in the unsublimed residue, the degree of purity of the flow crystals should be higher than the original powder of the charge. Mass spectrometric analysis with an AEI MS7 (Fulmer Research Institute) indicates that most electrically and optically active impurities are reduced to levels below 1 p.p.m. The analysis for copper and chlorine ($\sim$1 p.p.m.) however is subject to ~~our~~ doubt and oxygen cannot be estimated at all. The crystals have a high resistivity ($\sim 10^{12}$ ohms-cm) and emit green luminescence under ultra-violet excitation ($\lambda = 3650$ Å) at 77°K. Flow crystals used as a starting charge for the growth of the boule crystals (see 4-4) were found to contain a non-stoichiometric excess of cadmium.[14]

4-4. Growth of boule crystals

Large single crystals of cadmium sulphide with centimetre dimensions are desirable for Hall effect measurements. Measurements of the Hall coefficient and resistivity lead to estimates of the carrier mobilities which provide an indication of the quality of the crystals. Large single crystals are also desirable for practical applications for example in the acousto-electric amplifier.

In recent years, several methods of growing large single crystals of CdS have been described. Clark and Woods[15] have evolved the following techniques for growing single crystal boules in this laboratory:

(1) Growth of single crystal boules by sublimation in argon.

(2) Growth by vacuum sublimation.

4-4.1(a) <u>Growth of single crystal boules by sublimation in argon</u>.

This method is a modification of that of Piper and Polich[5] and is described in detail in the paper by Clark and Woods.[7] A 12·5 cm. long and 1 cm. in diameter silica tube, sealed at one end to a conical point is used as a growth ampoule. The tube is filled with a 15 gm charge of "flow crystals". A sliding-fit quartz rod 'seal' is then inserted into the open end of the growth ampoule.

To start the run, the growth tube is evacuated and filled with purified argon. The growth tube which is sealed at one end contains argon at a pressure slightly above atmospheric. After purging for several hours while the furnace temperature is held at 150°C to drive out any moisture, the argon flow is reduced to 50 ml. per minute. After that, the apex of the growth tube and the charge are held at 1250°C and 1175°C respectively for 24 hours when all the charge sublimes to the end opposite the apex leaving a clear site for nucleation. At the same time the constriction seals itself off. The temperatures are then adjusted to the appropriate range being studied (1050-1300°C) with the apex of the growth tube at the hottest point of the furnace. When the growth tube is pulled by a motor with a speed in the range 0·5 - 3 mm./hour, the apex becomes colder than the charge, supersaturation results in growth from the tip. As the run continues, the boule crystal grows on the seed so formed, either as one single crystal or as a few sizeable crystallites. The whole procedure takes several days.

4-4.1(b) Properties of boule crystals grown in argon atmosphere.

X-ray back-reflection studies showed that the crystals produced by this method have the c-axis lying at an angle of about 25^{o} to the pulling direction. This was due to the radial temperature gradient which resulted from the practical difficulty of aligning the growth tube along the axis of the furnace. With highest furnace temperature ($1250^{o}C$) and slowest pulling rate ($0{\cdot}8$ $mm.h^{-1}$), boules 3 cm.long and 1 cm.in diameter could be grown consistently. The crystals were transparent, with a yellow-brown colouration. Resistivities were of the order of $10^{8}\,\Omega$-cm. However, the crystals grown at temperatures of $1200^{o}C$ or lower were orange in colouration. Their resistivities were non-uniform, varying from $10^{6}\,\Omega$-cm. at the surface of a boule to $1\,\Omega$-cm. at the axis. With growth temperatures in the range between $1150^{o}C$ to $1050^{o}C$ and with slowest pulling rates, small boule crystals with good yellow colouration and a high uniform resistivity ($\sim 10^{8}$ Ω-cm) were produced.

4-4.2. Growth by vacuum sublimation

(a) Method I

The purpose of the crystal growth arrangement described in Section 4-4.1(a) is to allow any non-stoichiometric excess of either element of the charge to diffuse away from the growth tube before substantial growth begins. As indicated by Somorjai and Jepsen,[16] any excess of cadmium and sulphur in the charge reduces the evaporation rate of cadmium sulphide and hence the growth rate of the boule. In an effort to reduce the growth temperature and increase the rate of material transport, Clark and Woods[7] made attempts to grow crystals in sealed evacuated tubes. The experimental arrangement was essentially the same as that described in Section 4-4.1(a) with the exception that the growth tube was sealed under high vacuum (10^{-5} Torr) instead of remaining open to an argon ambient via a constriction. A vertical furnace arrangement was used to pull the growth tube. This procedure was successful in eliminating temperature gradients across the growth face which were troublesome in the horizontal arrangement. It was found that a non-stoichiometric excess of cadmium in the flow crystals used as the starting charge reduced the evaporation rate. Hence the boule crystals could be grown successfully only if the sublimation temperature was as high as 1250-1300°C.

(b) <u>Method II</u>

At temperatures as high as 1250-1300°C silica tubing is near its softening point. Impurities present in the silica may contribute additional partial pressures during the growth. Also the presence of a non-stoichiometric excess of one of the elements in the starting charge makes the control of the growth mechanism difficult. To overcome this difficulty, Clark and Woods provided the growth ampoule with a tail which contains a reservoir of cadmium or sulphur which can be held at a fixed temperature throughout the growth cycle. The vertical furnace arrangement employed is shown in Figure 4.2 and is fully described in the paper by Clark and Woods.[15]

In this arrangement two furnaces are used. The upper furnace is the growth furnace and has a temperature profile as shown in Figure 4.2. The temperature of the lower (reservoir) furnace can be adjusted within the range 50- 775°C. This enables the tail containing the reservoir of cadmium or sulphur to be maintained at a definite temperature within the range 50-775°C and thus sustain a constant partial pressure throughout the growth period. A spacer between the two furnaces prevents excessive heat transfer. The main growth tube which is some 15 cm. long and 1·5 cm. in diameter is joined to a 4 mm. bore tube which forms the reservoir tail. The upper end of the 4 mm. bore tube which penetrates inside the growth chamber is tapered to an orifice of 1 mm. diameter to reduce the quantity of CdS which will otherwise sublime into the tail. The growth ampoule is also provided with an apex to initiate nucleation.

After evacuation to 10^{-6} Torr and baking, the growth tube is filled with excess cadmium or sulphur (0·1 gm.). This is followed by evacuation and flushing with argon. The sulphur or cadmium is then melted under vacuum to remove volatile impurities. Finally after adding 30 gms. of CdS charge crystals to the excess cadmium or sulphur, the growth tube is sealed under a high vacuum. The tube is positioned inside the furnace with the apex of the growth chamber lying below the centre of the upper furnace (Figure 4.2). The tube is then pulled through the growth furnace, the hottest point of which corresponds to 1150°C. The temperature of the reservoir

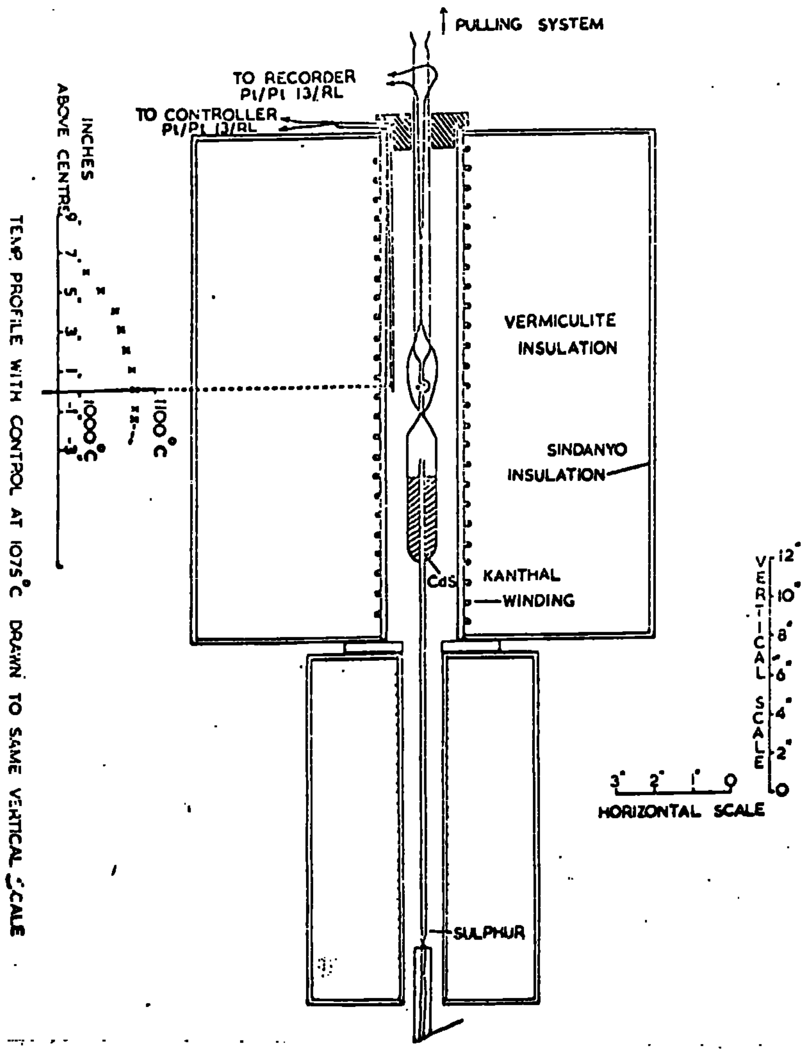

Figure 4.2. Furnace arrangement shown with growth tube in initial position.

furnace is adjusted to lie within the range 50-775°C. During the initial stage of the pull, excess cadmium or sulphur sublimes into the tail forming the reservoir from which the required partial pressure can be established. The tail temperature is held constant during the growth period. Boule crystals some 40 mm. long are produced in a period of three days.

(c) Properties of the boule crystals grown by Method II.

Boules are usually light yellow in colour although those grown in the highest pressures of cadmium are slightly darker. Crystals grown under high partial pressures of cadmium (reservoir temperature $T_{Cd} = 775^{\circ}C$) are semiconducting at room temperature with resistivities of the order of 10 Ω cm. The crystals grown in the lower pressures of cadmium ($500^{\circ}C > T_{Cd} > 300^{\circ}C$) are photosensitive semi-insulators. Two such crystals (crystals 78 and 79) were chosen for the photo-Hall measurements described in this thesis. (See Chapters 6 and 7). Crystals 78 and 79 were grown under partial pressures of cadmium when the reservoir temperature was 350°C (partial pressure of cadmium $3{\cdot}0 \times 10^{-1}$ mm. of Hg.). Their conductivities which were less than 10^{-7} mho cm^{-1} in the dark at room temperature could be increased to 10^{-2} mho cm^{-1} by illumination with light of intensity L = 3200 ft-C. Crystals grown in high pressures of sulphur vapour are insulating ($\rho = 10^{10}$-10^{12} ohm cm) and poor photoconductors. Edge emission studies made on crystals grown either in different excess partial pressures of cadmium or sulphur, have been reported in the paper by Orr et al.(17) Hall effect measurements made on a number of the semiconducting samples of cadmium sulphide will be reported in Chapter 8.

4-5. Sample preparation for Hall effect measurements

An automatic crystal cutting machine (Slicing Machine TS3 supplied by Brunner Machine Tools Ltd., London) was used to prepare Hall samples of suitable dimensions (10 mm. x 2·0 mm. x 2·0 mm.). The crystal cutting blade is a diamond wheel, 0·4 mm. thick and 120 mm. in diameter. Two speeds (6500 and 4500 r.p.m.) can be used to drive the cutting blade. During crystal cutting, a constant flow of coolant is fed to the cutting blade by an emersion pump.

The crystal was first cemented on to a piece of wood with durofix. A speed 6500 r.p.m. was used for cutting crystals of cadmium sulphide. At first a suitable piece either across the diameter or along the length of the boule crystal was cut. Then several cuts were needed to shape it as a Hall sample. Cutting was followed by grinding and polishing. Carborundum powder grades 800 and 400 was used for grinding which was done on a glass plate using water as lubricant. This brought opposite faces roughly parallel.

Final polishing was done using a precision flat lapping and polishing machine fitted with 12" diameter lapping plate. The crystal was mounted with durofix on the flat face of a special polishing jig (Figure 4.3) which held the crystal in contact with the top of the lapping plate. By using Hyprez diamond compounds, the lapping plate was found to produce a high degree of polish as well as flatness.

After polishing, the sample was etched in a chromic acid to remove the grinding damage and to clean the surfaces. The chromic acid is

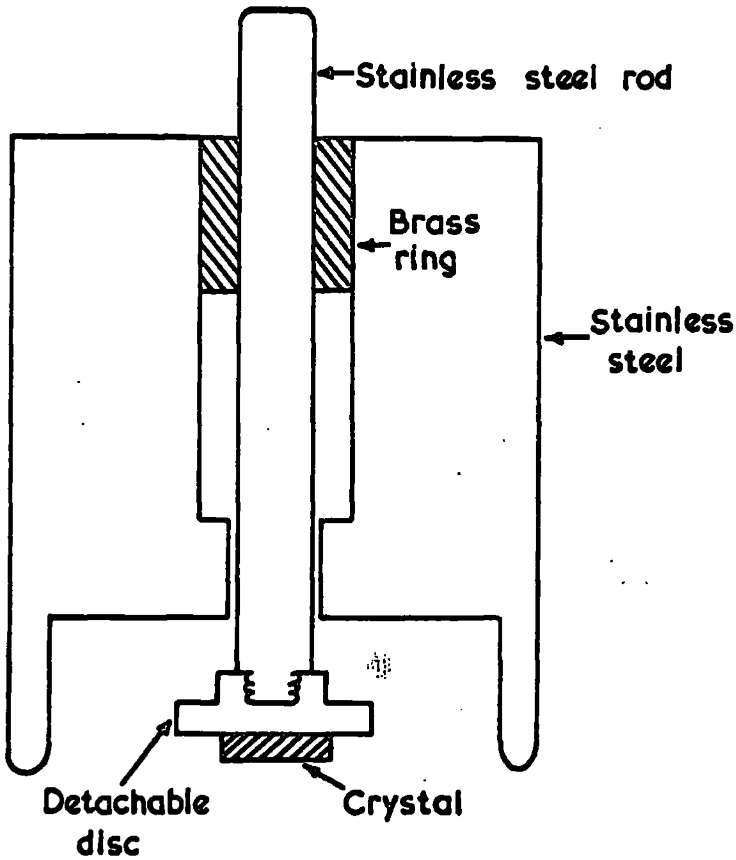

FIG. 4·3 Crystal Polishing Jig

prepared by dissolving 700 gms. of chromic oxide in two litres of distilled water. 100 ml. of concentrated sulphuric acid is added to the solution. After cooling, a small quantity of this liquid is diluted three times to obtain the required etchant. Etching was carried out at 80°C for two to five minutes. After cooling, the sample was removed, washed thoroughly in distilled water and allowed to dry. Dimensions were then measured using a vernier microscope.

4-6. Contacts

Conventional Hall effect measurements on a rectangular Hall sample require six ohmic contacts. Indium was used as the contact material since this makes good ohmic contact to cadmium sulphide[18],[19] and is convenient to apply. The contact areas were first coated with indium layers approximately 1 μm thick using high vacuum evaporation techniques. Then small pieces of indium (1 mm. slices of 1 mm.diameter) were pressed on to the evaporated layers.

After that the sample was heated to fuse the indium on to the evaporated layers. This was done in a gas tight manipulator box.[20] The manipulator box was flushed with nitrogen while heating the sample to about 165°C, just above the melting point of indium. The manipulators provide the necessary arrangements to adjust from the outside six short lengths of 30 s.w.g. tinned copper wire to the contact areas simultaneously. The net result was six ideal ohmic contacts with high mechanical strength. The ohmic nature of the contacts was determined from the verification of ohm's law both for direct and reverse current.

The contact diameter was of the order of 1 mm. except for the current contacts which covered the entire end faces of the sample. Contacts prepared in this manner have resistances less than 1% of the bulk resistance over the temperature 77–420°K.[18] Contacts should be as small as possible tending to point contacts so that they do not disturb the uniformity of the current flow. Probe contacts of 1 mm. diameter will give rise to errors in the determination of sample resistivity and Hall constant, since they act as conducting layers on the side of the sample and disturb the current flow. Zook and Dexter[21] made indium contacts on CdS as small as 0·2 - 0·3 mm. by using indium solder agitated ultrasonically with a Sonobond soldering apparatus. Even so their contacts did not approximate to point contacts and effects due to shorting of the Hall voltages by the contacts were clearly evident in the magneto resistance data. Their contacts had resistances twice as large as the sample resistance. However, these authors concluded that a lower limit to the size and resistance of the contacts was set by the requirement of low noise.

References

(1) A. Vecht and A. Apling, Phys.Stat.Sol., 3, 7, 1963.

(2) R. Frerichs, Phys.Rev., 72, 594, 1947.

(3) J.M. Stanley, J.Chem.Phys., 24, 1279, 1956.

(4) P.D. Fochs, J.Appl.Phys., 31, 1733, 1960.

(5) W.W. Piper and S.J. Polich, J.Appl.Phys., 32, 1278, 1961.

(6) L.C. Greene, D.C. Reynolds, S.J. Czyzack and W.M. Baker, J. Chem.Phys., 29, 1375, 1958.

(7) L. Clark and J. Woods, Brit.J.Appl.Phys., 17, 319, 1965.

(8) W.E. Medcalf and R.H. Fahrig, J.Electrochem.Soc., 105, 719, 1958.

(9) L. Clark, Ph.D.Thesis, University of Durham, 1965.

(10) K.H. Nicholas, Ph.D. Thesis, University of Durham, 1963.

(11) G.A. Marlor, Ph.D.Thesis, University of Durham, 1964.

(12) A.N. Rushby, Ph.D.Thesis, University of Durham, 1966.

(13) A. Vecht, B.W.Ely and A.Apling, J.Electrochem.Soc., 111, 6, 1964.

(14) J. Woods, Annual Report 1965/66, Admiralty Contract CP 11339/63.

(15) L. Clark and J. Woods, Journal of Crystal Growth, 3, 126, 1968.

(16) G.A. Somorjai and D.W. Jepsen, J.Chem.Phys., 41, 1394, 1964.

(17) D.S. Orr, L. Clark and J.Woods, Brit.J.Appl.Phys., Ser.2.Vol.1, 1609,1968.

(18) R.W. Smith, Phys.Rev., 97, 1525, 1955.

(19) C.I. Shulman, Phys.Rev., 98, 384, 1955.

(20) L. Clark and J. Woods, J.Sci.Inst., 42, 51, 1965.

(21) J.D. Zook and R.N. Dexter, Phys.Rev., 129, 1980, 1963.

CHAPTER V

EXPERIMENTAL TECHNIQUE

5-1(a) Description of the liquid helium cryostat

A metal helium cryostat for Hall effect and photoHall measurements requires the following facilities:

(1) The sample must be provided with necessary electrical leads.

(2) It must be possible to hold the temperature of the sample at any desired point.

(3) The cryostat must be provided with a window so that the sample can be illuminated from outside the cryostat.

A diagram of the cryostat specially designed and built by the Oxford Instrument Company Ltd. to meet the above requirements is shown in Figure 5.1. This cryostat was used to obtain the results described in this thesis.

The upper part of the cryostat consists of (1) helium container H, (2) nitrogen container N and (3) a space (to be called insulation space hereafter) separating the nitrogen container from the outside wall. A stainless steel tube runs through the helium container and contains exchange gas. A multiple pin socket has been provided on the top of the cryostat for electrical leads and other connections to the sample holder. All the connecting leads from the socket to the lower part of the cryostat are taken through a separate stainless steel tube as shown in the Figure 5.1.

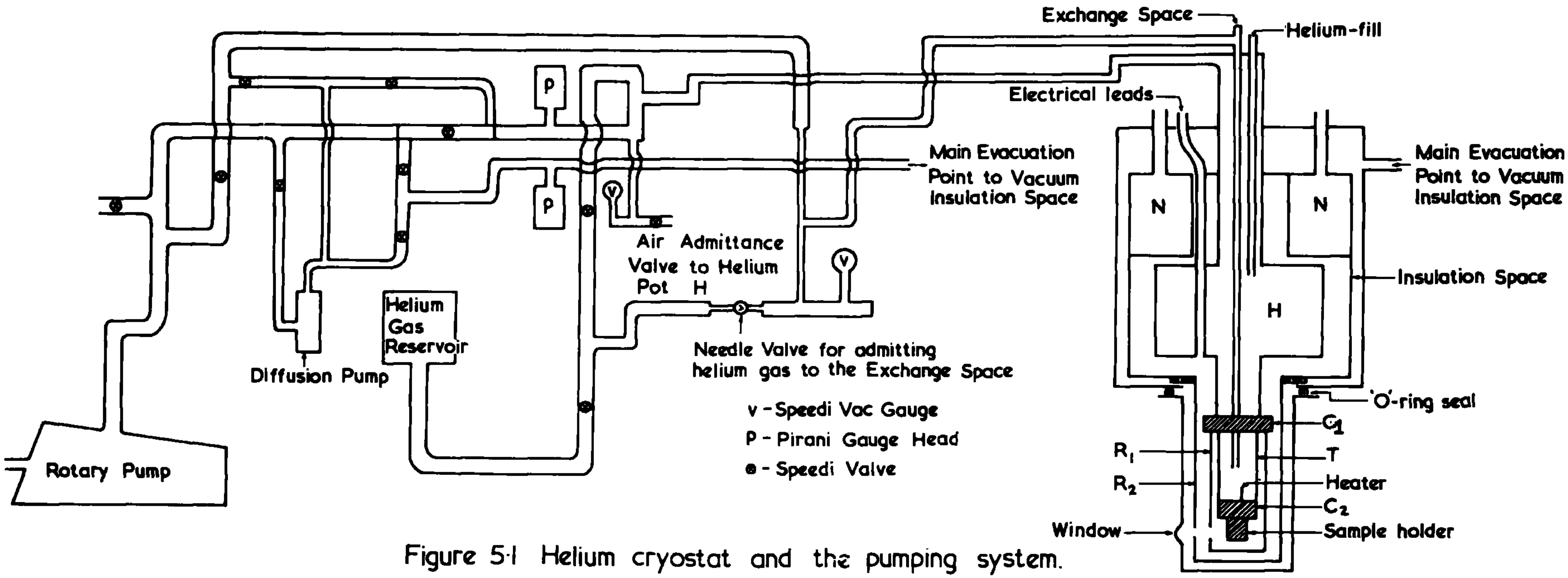

Figure 5·1 Helium cryostat and the pumping system.

The bottom of the helium container is attached to a tube T of stainless steel through a copper block C_1. The sample holder which is also a copper block is screwed to the bottom of another copper block C_2, fitted into the lower part of the tube T. The tube containing exchange gas terminates inside T. Thus the sample holder can be isolated from the refrigerant liquid by evacuating the exchange space. In order to heat the sample, a nichrome heater surrounds the shaft of the sample support which is the copper block C_2.

The sample holder is surrounded by a detachable copper radiation shield R_1 which is connected to the helium container H through the copper block C_1. The second copper radiation shield R_2, cooled by conduction from the liquid nitrogen in the container N, is also detachable. The outer casing of the tail, which is always at room temperature, is secured to the upper vacuum jacket by an 'O'-ring seal. These three components of the tail can easily be removed in order to mount a sample on the sample holder. The outer casing has been fitted with a window and the inner radiation shields contain holes to admit light to the sample.

The multiple pin socket fitted on the top of the cryostat has ten pin points. Six of these were used for providing electrical leads to the Hall sample, two for connecting the heater terminals to an outside power supply and two for a thermocouple of copper versus constantan. In addition there is a metal-ceramic seal on the side of the multiple pin socket. One gold/iron versus chromel thermocouple was brought in through this seal which carries two hollow pins.

Cotton coated, high conducting copper wire (diameter 0·03 cm) which was supplied by the London Electric Wire Company and Smiths Limited, was used for electrical leads to the Hall sample. 40 gauge (·0122 cm diameter) copper and constantan, 0·008 cm diameter gold/iron and 0·009 cm diameter chromel wiring (supplied by Johnson Matthey Metals Limited, London) were used for thermocouples. Care was taken to maintain good insulation between the two thermocouples. The junctions of the copper-constantan thermocouple were prepared in the standard way. The gold/iron and chromel were fused together by 'soft' soldering.

The reliability of the copper-constantan thermocouple was tested for known temperatures by immersing the reference junction in melting ice ($0^{o}C$) and the cold junction in dry ice and acetone ($196^{o}K$) and liquid nitrogen ($77^{o}K$). Calibration figures have been supplied by John Matthey Metals Limited for use with the gold/iron versus chromel thermocouple. The temperature indicated by the gold/iron versus chromel thermocouple was compared with the calibration figures by immersing the reference junction first in liquid nitrogen and then in liquid helium while the other junction was immersed in melting ice ($0^{o}C$) and liquid nitrogen ($77^{o}K$) respectively.

The reference junction of gold/iron versus chromel thermocouple was placed inside a 1·0 mm diameter thin walled cupro-nickel tube immersed in the liquid helium transport dewar. To read the thermocouple potentials, a 'Pye' portable potentiometer, with a sensitivity of

10 microvolts was used. The copper-constantan thermocouple was used (for temperatures above 60°K) while between liquid helium temperature and 60°K, the gold/iron versus chromel thermocouple was employed.

A thin sheet of mica on the face of the copper block of the sample holder provided good electrical insulation between the sample and the block while maintaining excellent thermal contact. The sample was illuminated by reflection from a silvered mirror placed on the face of a pole piece (of the magnet) adjacent to the window.

5-1(b) <u>Operation</u>

(1) Before evacuating the insulation space, the exchange space was filled with air and the helium container left open to the atmospheric pressure (open Air Admittance Valve to Helium pot H, Figure 5.1). The insulation space was then evacuated to 10^{-2} to 10^{-3} torr using a rotary pump.

(2) When a vacuum of 10^{-2} to 10^{-3} torr had been produced in the insulation space, the helium container and the exchange space were evacuated and then filled with helium gas from the helium gas reservoir which is connected to the system (see Figure 5.1).

(3) The nitrogen container N was then filled with liquid nitrogen. The insulation space was maintained at low pressure using the rotary pump. A few hours were needed to bring the sample temperature down to 100°K.

When the sample temperature reached 100°K, the insulation space vacuum was reduced to a pressure below 10^{-5} torr by using an oil diffusion pump. A very good vacuum in the insulation space ensures a good insulation between the outer wall and the inner chamber.

(4) To obtain further cooling, a small quantity of liquid nitrogen was poured into the helium container H. This instantly brought the sample temperature down to 77^{o}K. Any liquid nitrogen left in the helium container at this stage was boiled off by dipping a copper rod into it.

Precooling the sample to liquid nitrogen temperature prior to liquid helium transfer, is essential.

(5) The helium container H was evacuated and then filled with helium gas.

(6) At this stage the system is ready for liquid helium transfer. At first, the helium container was opened to the helium gas reservoir. Transfer of liquid helium from a travelling dewar to the container H was done using a metal syphon. Pressure was slowly built up inside the travelling dewar and transfer of liquid helium to the helium container started. When the sample had cooled down to liquid helium temperature, the syphon was withdrawn.

(7) The sample holder was then isolated from the liquid helium inside the container H by evacuating the exchange space.

(8) By energising the heater coil appropriately, the temperature of the sample could be regulated.

It was found that the temperature of the sample could be held at any desired point between liquid helium temperature and $400^{\circ}K$ within an accuracy of $\pm$ $1^{\circ}C$.

5-1(c) <u>Depth measurement of liquid helium in the helium container</u>

Access for a dip stick to the helium container H (not shown in Figure 5-1) has also been provided on the top of the cryostat so that the depth of the liquid helium inside the container H (while transferring liquid helium) could be estimated. A long dip stick sealed at one end by a rubber membrane, was lowered (open end downwards) into H through the dip stick port. Spontaneous oscillations of the membrane begin. When the lower end of the tube penetrates the liquid, this vibration drops in frequency by 30% and in intensity by 60%.[1]

5-2(a) <u>D.C. method of Hall effect measurements</u>

The Hall effect and photoHall measurements described in this thesis were made using the conventional D.C. method. Generally Hall effect measurements require six electrodes. We employed a five electrode method which is illustrated in Figure 5.2. Electrodes 1 and 2 (Figure 5.2) were for the applied voltage, 3 and 4 for the measurement of conductivity and 4 and 5 for the Hall voltage. These electrodes 4 and 5 (hereafter to be called Hall voltage probes) were aligned as closely as practicable.

The voltage was supplied to the sample from D.C. storage batteries, via variable series resistors to give coarse and fine current control (Figure 5.3). The current through the sample was determined from

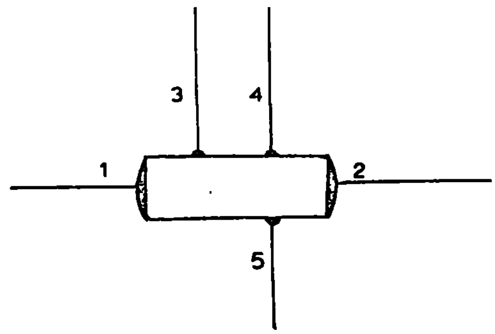

Fig. 5.2. Hall sample with five electrodes.

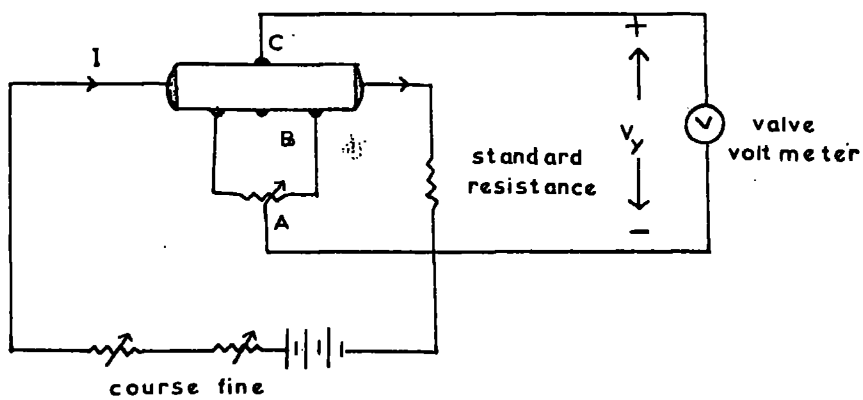

Fig. 5.3. The potentiometric method of Hall-effect measurements.

the measurements of the voltage dropped across a standard resistance, connected in series with the sample. A reversing switch was provided to change the polarity of the applied voltage.

A Philips valve voltmeter which has two ranges with input impedances of 10^6 and 10^8 ohms was used to measure the Hall voltage. D.C. voltages from ten microvolts to ten volts could be measured with the input impedance of 10^6 ohms. Voltages from 0·1 millivolt to 1000·0 volts could be determined with the 10^8 ohms impedance. The polarity of the voltage measured is indicated automatically by means of a neon tube.

The Hall contacts, in practice, are not exactly aligned on the same equipotential line, so a misalignment potential will be read by the valve voltmeter in the absence of a magnetic field. In materials like cadmium sulphide with (comparatively) small Hall effect, this misalignment potential can be much greater than the Hall voltage. In such a case, the detection of the Hall voltage signal and its measurement becomes quite difficult.

A potentiometric method as shown in Figure 5.3, can be employed to achieve an electrical balance between the Hall voltage probes. By varying the position of the moving contact on the potentiometer, the potential at point A can be made equal to that at point B which is perfectly aligned to point C (Figure 5.3).

In samples with high resistivities, the shunting effect of any practical potentiometer is too great and limits the applicability of this method. In other samples (especially the Van Der Pauw specimens, described in Section 5-2(b) only two Hall voltage probes can be provided. The misalignment voltage must then be compensated by some other arrangement. We employed the arrangements shown in Figures 5.4(a) and (b) with which it was possible to buck out all or any part of the standing voltage between the Hall probes before the magnetic field was applied.

The arrangement shown in Figure 5.4(a) uses a 'Pye' portable potentiometer as the source of the backing off voltage. The voltage at the test terminals of the potentiometer, reversed in polarity, cancels the misalignment voltage between the Hall voltage probes. An adjustment in the voltage at these test terminals can be made very accurately and comfortably over the range between ten microvolts to 1·8 volts. The use of a 'Pye' portable potentiometer as the source of the backing off voltage was suitable for low resistance Hall samples which had misalignment potentials of the order of millivolts.

In the case of high resistance ($> 10^5$ ohms) samples where the misalignment voltage between the Hall voltage probes was often greater than 1·8 volts, the arrangement shown in Figure 5.4(b) was used. Applying these methods, illustrated in Figures 5.4, the Hall voltages were readily measured with greater accuracy.

The Hall voltages were measured for both directions of sample current and magnetic field. The results were then averaged to eliminate possible errors from thermoelectric or thermomagnetic effects. The Hall coefficient R was calculated using the relation:

a)

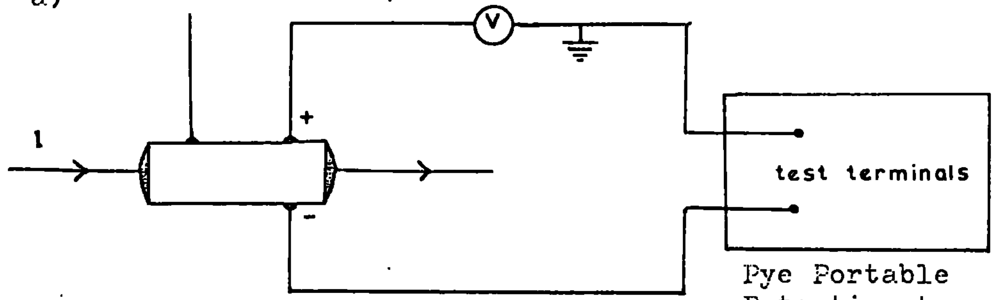

b)

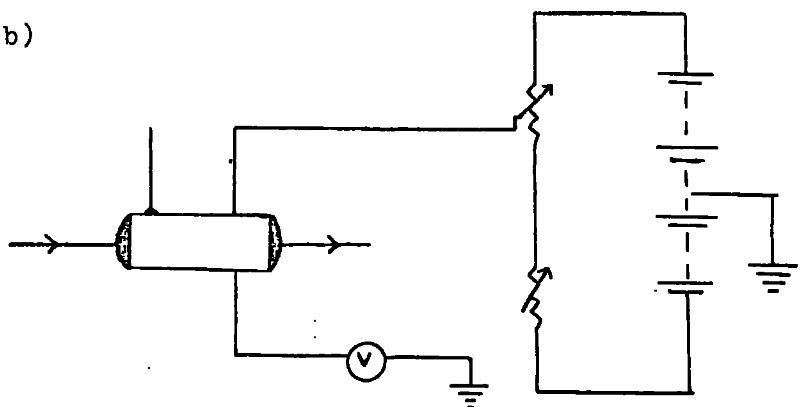

Fig. 5.4. Arrangement for cancelling out misalignment voltage between the Hall probes in the absence of a magnetic field.

$$R = \frac{d}{BI} V_H \times 10^8 \ cm^3/C \qquad (5.1)$$

where d - thickness of the Hall sample in cm

B - magnetic field, in gauss

I - current through the sample, in amperes

V_H - Hall voltage, in volts.

The conductivity σ was calculated from the formula

$$\sigma = \frac{I}{V_C} \frac{l}{wd} \ ohm^{-1} \ cm^{-1} \qquad (5.2)$$

wnere l - distance between electrodes 3 and 4 (Figure 5.2), in cm

w - width of the Hall sample, in cm

V_C - the voltage measured between the voltage probes 3 and 4 (Figure 5.2).

5-2(b) The Magnet

A 4-inch water-cooled electromagnet type A, (supplied by Newport Instruments Limited) with pole pieces 10 cms in diameter and capable of producing a magnetic field of four kilogauss with a gap of 7·5 cms between the pole-tip faces, was used for Hall effect and photoHall measurements. The current was supplied to the magnet by a power supply unit type D104, designed (by Newport Instruments Limited) to operate this magnet.

5-2(c) The Van Der Pauw Method[2]

This method allows the measurement of the resistivity and Hall mobility of a flat plate of a conducting material of arbitrary shape. Four small contacts A, B, C and D in order, are made around the perimeter of the plate. If a current I_{AB} flowing between contacts A and B produces a potential difference V_{CD} between contacts C and D then $R_{AB,CD}$ is defined as V_{CD}/I_{AB}. Similarly $R_{BC,DA}$ is defined as V_{DA}/I_{BC}, $R_{CD,AB}$ as V_{AB}/I_{CD} and $R_{DA,BC}$ as V_{BC}/I_{DA}. The resistance $R_{AC,BD}$ is defined as the ratio of the potential difference between contacts B and D to the current flowing from A to C and $\Delta R_{AC,BD}$ is the change in $R_{AC,BD}$ when the magnetic field is switched on. $\Delta R_{BD,CA}$ etc. are defined similarly. It can be shown that for any shape of plate of constant thickness d

$$\rho = \frac{\pi d}{\ln 2} \cdot \frac{R_{AB,CD} + R_{BC,DA}}{2} f\left(\frac{R_{AB,CD}}{R_{BC,DA}} \right)$$

$$\mu = \frac{d}{B} \cdot \frac{\Delta R_{AC,BD}}{\rho}$$

where f is a function satisfying the relation

$$\ln 2 \frac{R_{AB,CD} - R_{BC,DA}}{R_{AB,CD} + R_{BC,DA}} = f \text{ arc cosh} \left\{ \frac{\exp(\ln 2/f)}{2} \right\}$$

In Figure 5.5, a plot is given of f as a function of $R_{AB,CD}/R_{AC,DA}$.

Since the theory only holds for infinitely small contacts, the finite size of the contacts (usually about 1 mm square) can introduce an error. To keep this error small, the path between contacts should be made much longer than the linear dimensions of the contacts. A convenient shape of specimen is a disc with radial cuts to increase the path length between contacts as shown in Figure 5.6.

A number of samples have been cut in this shape so that the accuracy of the method could be compared with that of the conventional technique.

5-2(d) <u>A.C. method of Hall effect measurements</u>

Hall effect measurements using an A.C. method can also be made. This method shown in Figure 5.7, uses a Phase Sensitive Detector which compares a reference signal and a test signal and gives a d.c. output. An alternating current from the signal generator is supplied to the Hall sample. When a magnetic field is applied, an alternating Hall voltage of the same frequency as the current from the signal generator, appears across the Hall voltage probes. On reversing the magnetic field, the Hall effect voltage changes in phase by 180° and the component of the output from the Phase Sensitive Detector changes its sign.

Let V sin wt be the standing voltage between the Hall voltage probes with zero field applied and let v sin wt be the Hall voltage on application of a d.c. magnetic field. The total voltage

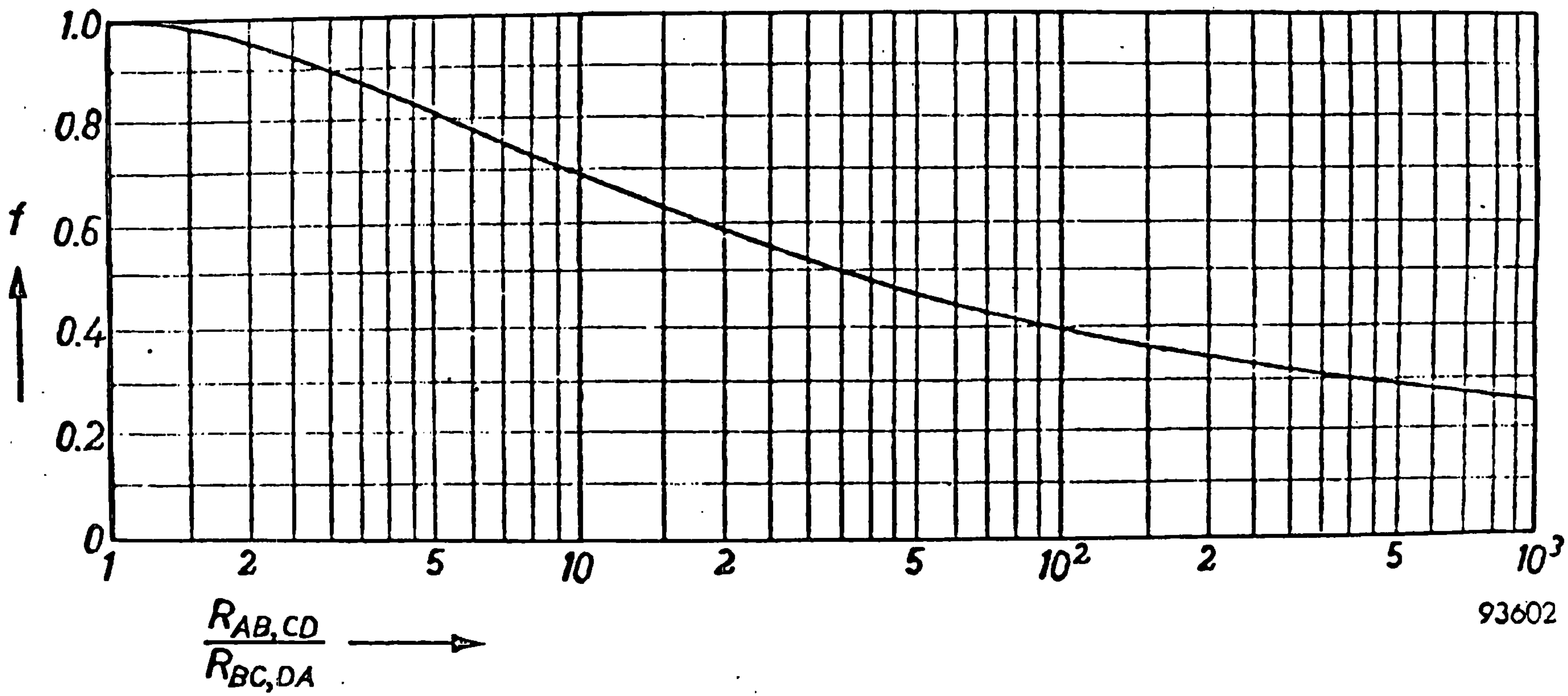

Figure 5·5 The function f used for determining the specific resistivity of the sample, plotted as a function of $R_{AB,CD}/R_{BC,DA}$.

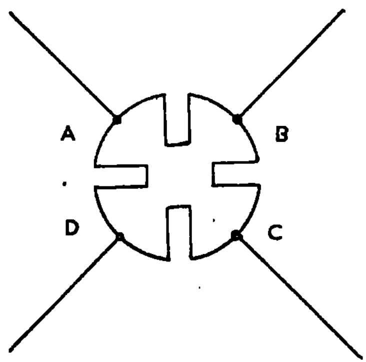

Fig. 5.6. Specimen for Van Der Pauw measurement.

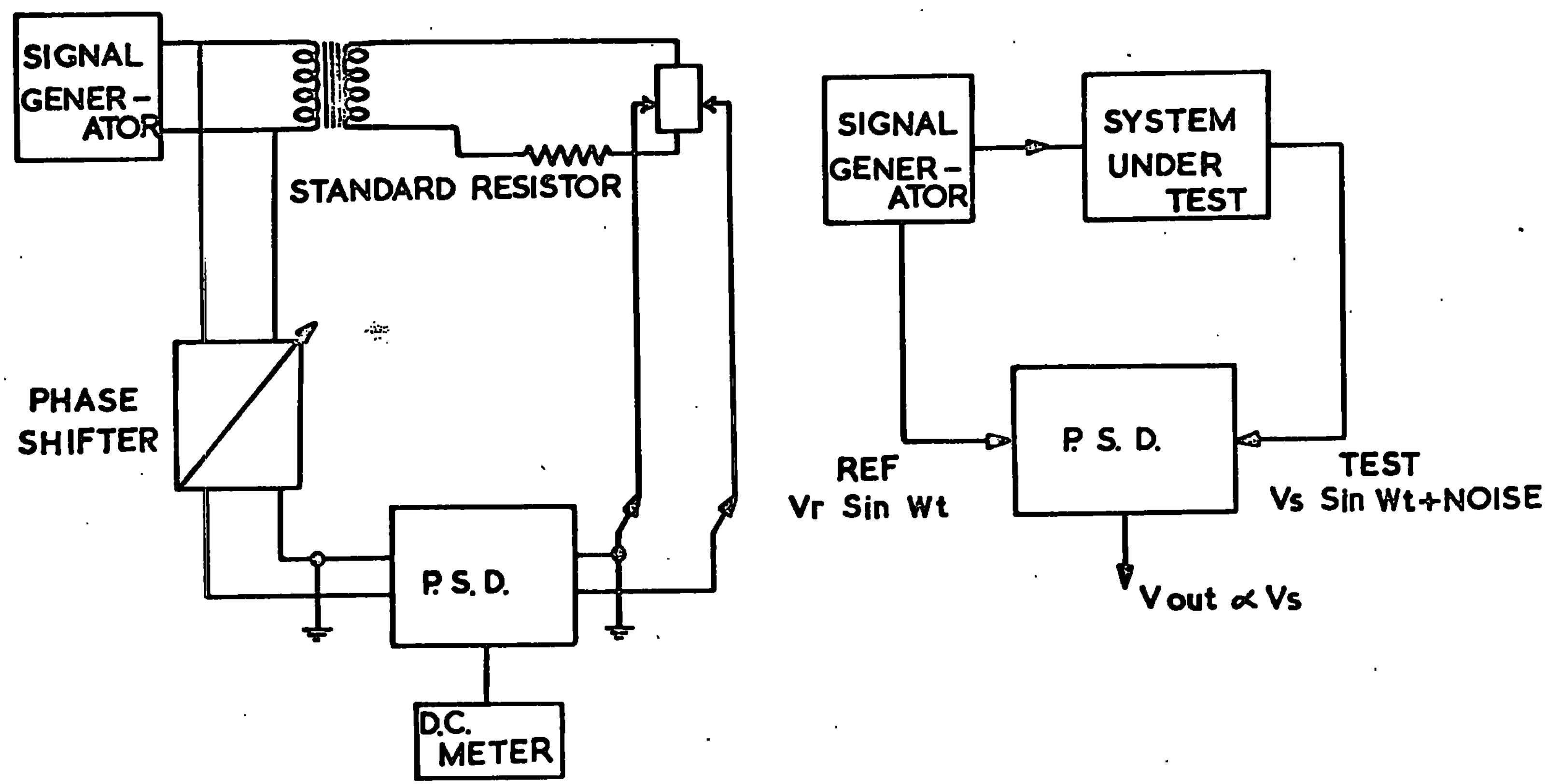

Fig. 5·7 A-C METHOD FOR HALL EFFECT MEASUREMENT.

($V \sin wt + v \sin wt$) which is observed across the Hall probes when a magnetic field is applied, is of the same frequency as the current from the signal generator (Figure 5.7). On reversal of the magnetic field, only the phase of the Hall voltage is changed by 180° and the voltage which appears between the Hall probes is

$$V \sin wt + v \sin(\pi + wt) = V \sin wt - v \sin wt$$

Thus there will be a change in the output meter reading of the Phase Sensitive Detector on reversal of the magnetic field and this is proportional to the Hall voltage only.

Some measurements have also been made using this technique in an attempt to measure Hall voltages in high impedance samples.

References

(1) J. Gaffney and J.R. Clement, Rev.Sci.Instrum., 26, 620, 1955.

(2) L.J. Van der Pauw, Philips Res.Repts. 13, 1-9, 1958.

CHAPTER 6

PHOTOHALL MEASUREMENTS

6-1. Introduction

Two photosensitive insulating cadmium sulphide crystals (crystals 78 and 79) with dark conductivities less than 10^{-7} mho cm^{-1} were chosen for photohall measurements. Both the crystals were grown by Dr. L. Clark under the same controlled partial pressures of cadmium ($3{\cdot}0 \times 10^{-1}$ mm of Hg) at a temperature of 1150°C by using the growth techniques described by Clark and Woods[1] (see Chapter 4 for crystal growth). The Hall samples prepared from the large single boules of crystals 78 and 79 had dimensions of ($0{\cdot}86 \times 0{\cdot}25 \times 0{\cdot}19$) cm^3 and ($1{\cdot}08 \times 0{\cdot}27 \times 0{\cdot}19$) cm^3 respectively. The conductivity which was less than 10^{-7} mho cm^{-1} in the dark at room temperature could be increased to 10^{-2} mho cm^{-1} by focussing light from a 500 watt d.c. tungsten lamp operated at 115·0 volts and fitted into a slide projector. To eliminate the infrared quenching and heating effects, the light from the projector was passed through a 1 cm path of 10% copper sulphate solution.

The photoHall effect was measured using a magnetic field of 3·4 kilogauss which was low enough to ensure a linear dependence of Hall voltage on magnetic field. The photoHall voltage measurements were made for both directions of sample current and magnetic field. The results were averaged to eliminate possible errors from thermoelectric or thermomagnetic effects. The intensity of illumination falling on the crystal was changed by using calibrated neutral filters. Figures 6.1 and 6.2 show the linear dependence of photoHall voltage on magnetic field at room temperature for crystals 78 and 79 respectively. The intensity of photoexcitation used for such measurements was of the order of 10^{-4} and 10^{-5} of the highest available light intensity (L = 3200 ft-C).

6-2. Variation of Hall mobility with photoexcitation

The variation in mobility is associated with a change in the occupancy of the imperfection centres. The occupancy of the imperfection centres is determined by the location of the quasi Fermi-levels. The temperature of the sample and the intensity of photoexcitation determine the location of the Fermi-levels. The variation in mobility with photoexcitation to be expected for a crystal containing two imperfection levels has been calculated and is shown in Figure 6.3.

The curve illustrated was obtained by assuming that the deeper of the two levels was positively charged when the electron Fermi-level was below it and that the shallower level was negatively charged when the electron Fermi-level was above it. The occupancy of the two levels would be determined by the intensity of the photoexcitation, and the resultant mobility can be described by an expression of the type proposed by Bube et al.[2]:

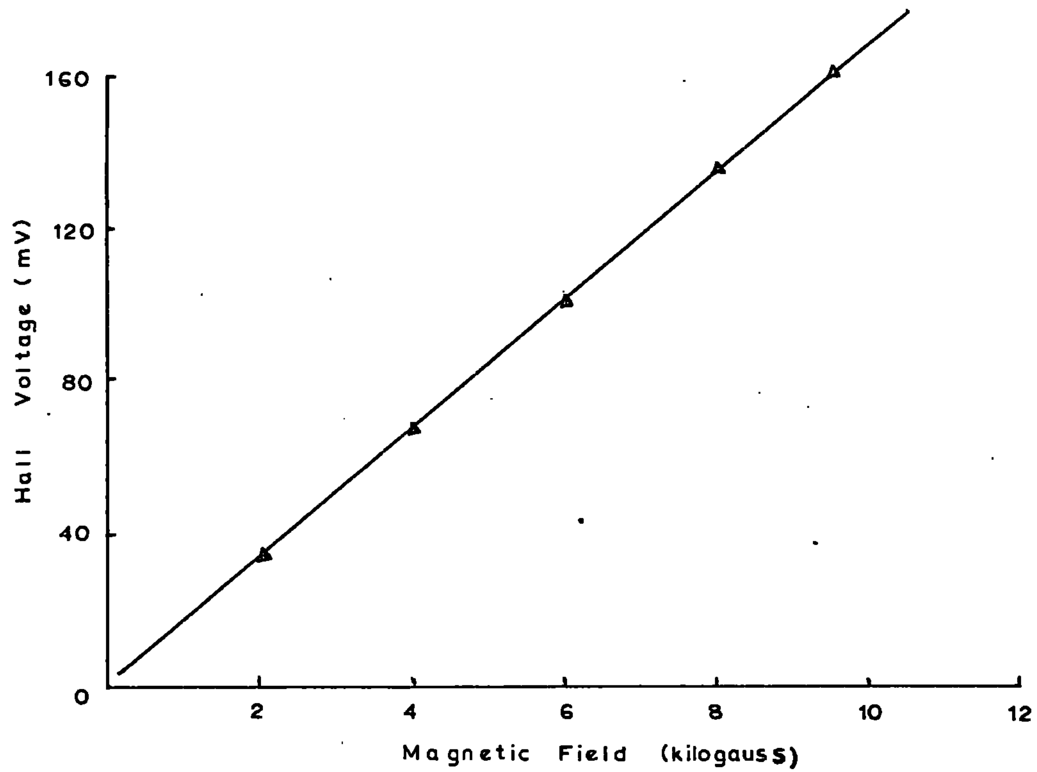

Fig. 6.1. Dependence of photoHall voltage on magnetic field strength at room temperature for crystal 78. Intensity of photoexcitation was of the order of 10^{-4} of the highest light intensity (L= 3200 ft.c).

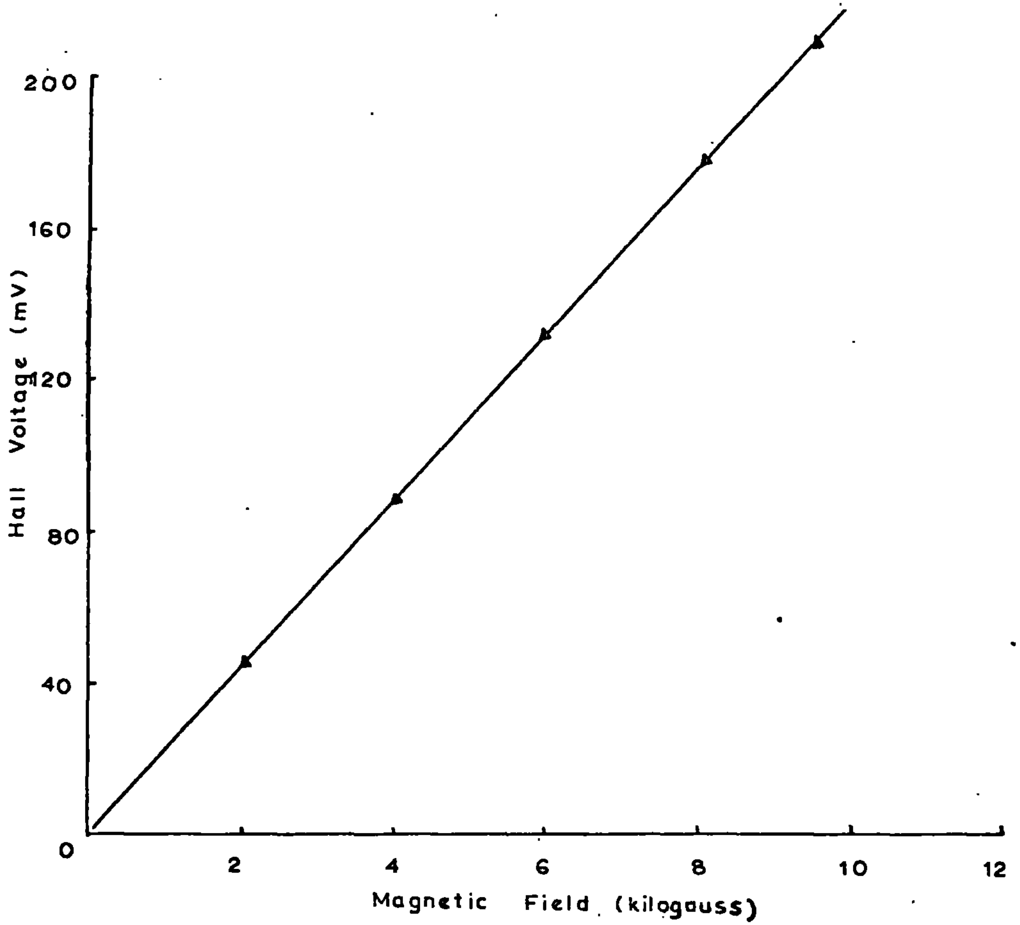

Fig. 6.2. Dependence of photo Hall voltage on magnetic field strength at room temperature for crystal 79. Intensity of photoexcitation was of the order of 10^{-5} of the highest light intensity (L=3200 ft.c.).

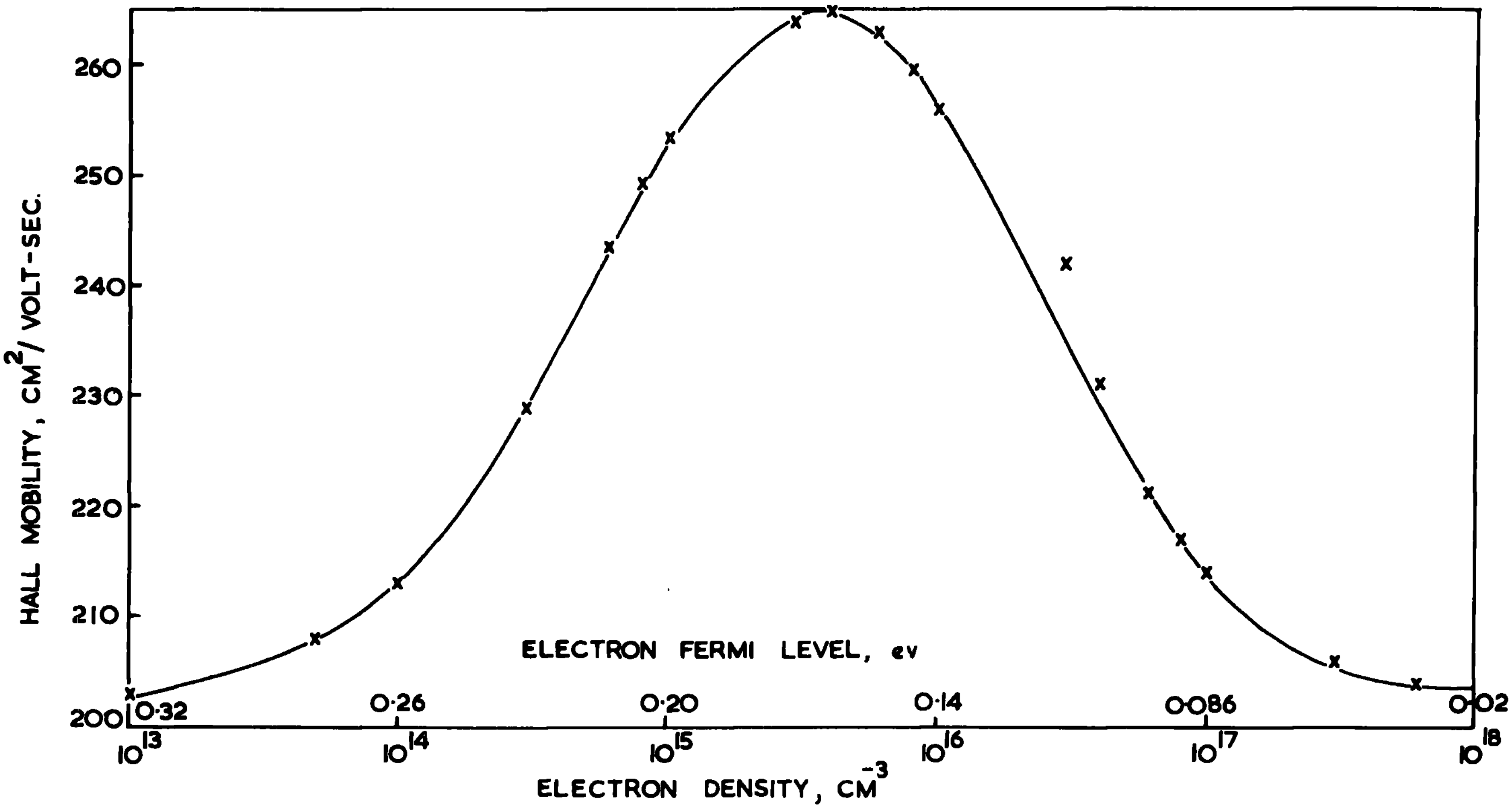

Fig. 6·3. An illustrative theoretical curve showing how the presence of two imperfection levels could vary the Hall mobility with photoexcitation.

$$\frac{1}{\mu} = \beta/\tau_o + \beta v_e S_+ N_+ \frac{1}{1+2\ \exp\left[(E_+ - E_{fn})/kT\right]}$$

$$+ \beta v_e S_- N_- \frac{1}{1+\frac{1}{2}\ \exp\left[(E_{fn} - E_-)/kT\right]} \qquad (6.1)$$

The second term on the right hand side of the expression (6.1) corresponds to scattering by positively charged centres and the third term to scattering by the negatively charged centres. When the electron concentration increases with increasing light intensity, the electron Fermi-level is raised, the second term becomes smaller and the third term larger. As a result the reciprocal mobility shows a minimum at a certain value of the electron concentration. The data used to draw the illustrated curve (Figure 6.3) were:

$\beta = \frac{m_e^*}{e} = 1\cdot14 \times 10^{-16}$ in practical units.

$m_e^* = 0\cdot2\ m$

$\beta/\tau_o = 3\cdot35 \times 10^{-3}$ (volt-sec/cm^2)

$v_e = \sqrt{2kT/m_e^*} = 2\cdot133 \times 10^7$ cm/sec.

$T = 300\cdot0^o$ K

$N_+ = N_- = 10^{17}$ cm^{-3}

$S_+ = S_- = 10^{-11}$ cm^2

$\therefore\ \beta v_e S_+ N_+ = \beta v_e S_- N_- = 2\cdot431 \times 10^{-3}$ (volt-sec/cm^2)

$E_+ = 0\cdot20$ eV

$E_- = 0\cdot10$ eV

$$n = N_C \; e^{-E_{fn}/kT}$$

$$\therefore \; E_{fn} = 2{\cdot}3026 \times \left[\log_{10}\frac{N_C}{n}\right] \times kT$$

$$N_C \text{ (for CdS at } 300^{\circ}\text{K)} = 2{\cdot}135 \times 10^{18} \text{ cm}^{-3}$$

6-3. Variation of Hall mobility with photoexcitation for crystal 78

The data reported in this Section were obtained from photoHall measurements made at a fixed temperature. The location of the electron Fermi-level was varied by changing the intensity of the photoexcitation. Since a Philips valve voltmeter with an input impedance of 100 MΩ was used to measure the Hall voltage, and the voltage drop across the potential probes, no measurements were made on samples with photoexcited conductivities less than 10^{-6} ohm^{-1} cm^{-1}.

From thermally stimulated current measurements on CdS Nicholas et al.[3] found six trapping levels in the region between 0·05 eV and 0·83 eV below the conduction band. PhotoHall measurements on crystal 78 at room temperature indicated a variation in conductivity from $4{\cdot}887 \times 10^{-3}$ to $2{\cdot}297 \times 10^{-6}$ mho cm^{-1} when the intensity of the photoexcitation was reduced from 10^{0} to 10^{-4} of the highest light intensity available (L = 3200 ft-C). The corresponding variation in electron Fermi-level was from 0·23 eV to 0·40 eV. Thus in order to observe any change in mobility as the electron Fermi-level was moved over the region from 0·05 eV to 0·80 eV, it was necessary to take several sets of measurements at different temperatures. For a particular set of measurements, the temperature of the sample was held constant and the variation in the location of the electron Fermi-level was obtained by varying the intensity of photoexcitation with calibrated neutral filters. The results were plotted in the form of $\frac{1}{\mu}$ versus E_{fn} since such curves are more susceptible to analysis. Some of the $\frac{1}{\mu}$ versus E_{fn} plots gave incomplete "S-shaped" curves, but nonetheless provided an indication of the presence of a trapping level. Further measurements were then made at other temperatures to obtain the complete "S-shaped" curve. Figures 6.4(a), (b) and (c) show a number of curves obtained from such measurements on crystal 78.

The highest temperature at which photoHall measurements were possible and where an appreciable variation in the location of the electron Fermi level could be obtained with photoexcitation was 330^{o}K. At this temperature, the variation in photoexcitation led to a change in the location of the Fermi level from 0·27 eV to 0·43 eV only (Figure 6.4(c)). The high impedance of the sample and the onset of the thermal quenching of the photoconductivity limited the measurements to values of E_{fn} below 0·43 eV.

The experimental results shown in Figures 6.4(a), (b) and (c) can be interpreted in terms of the existence of one trapping level in the case of Figure 6.4(a), two levels in the case of Figure 6.4(b) and one level in the case of Figure 6.4(c). All these levels are associated with traps which are positively charged when they lie above

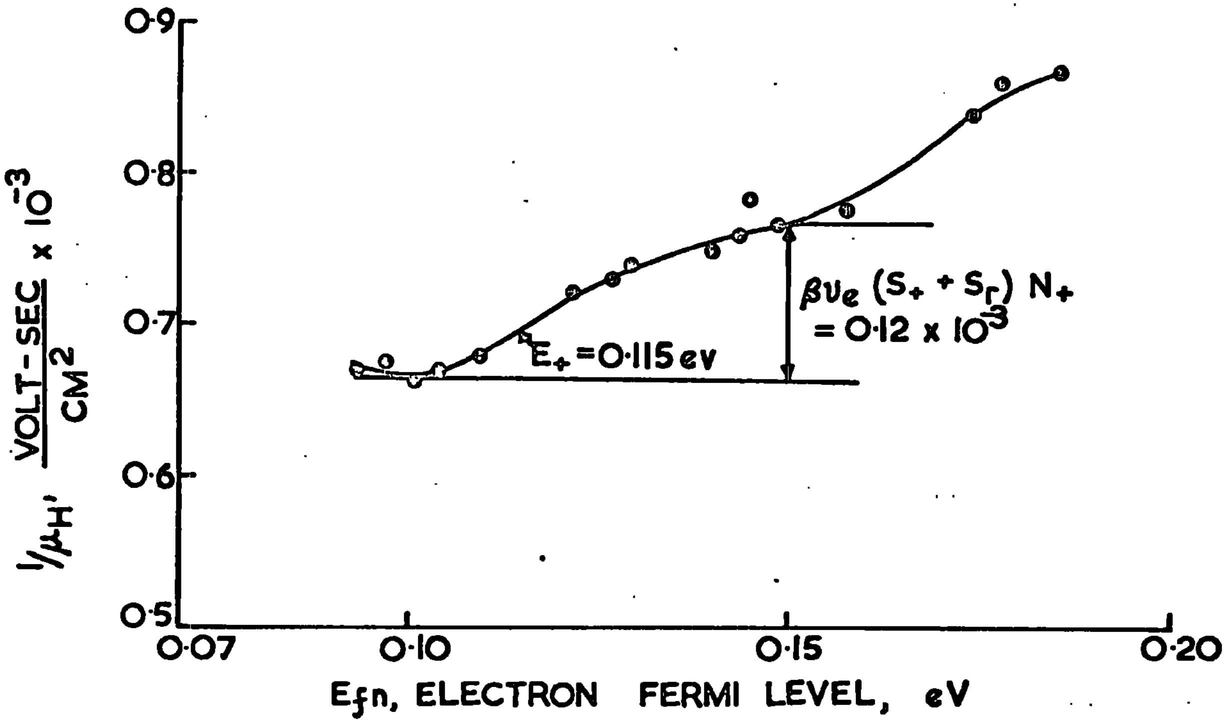

Fig. 6·4(a) Reciprocal mobility vs. location of the steady-state electron Fermi level for crystal 78. Measurement was taken when the sample temperature was 136°K.

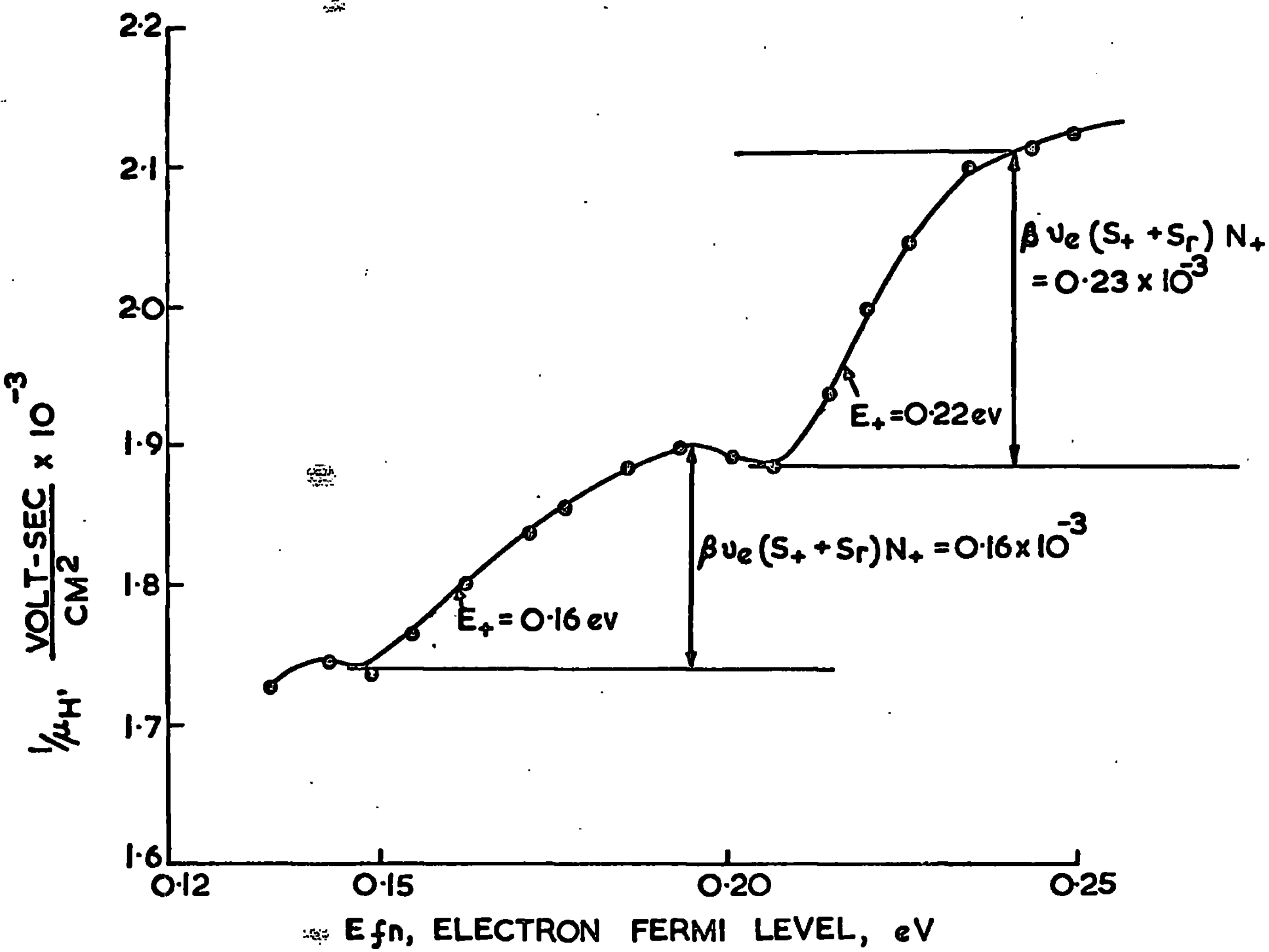

Fig. 6·4(b) Reciprocal mobility vs location of the steady-state electron Fermi level for crystal 78. Measurement was taken when the sample temperature was 193°K.

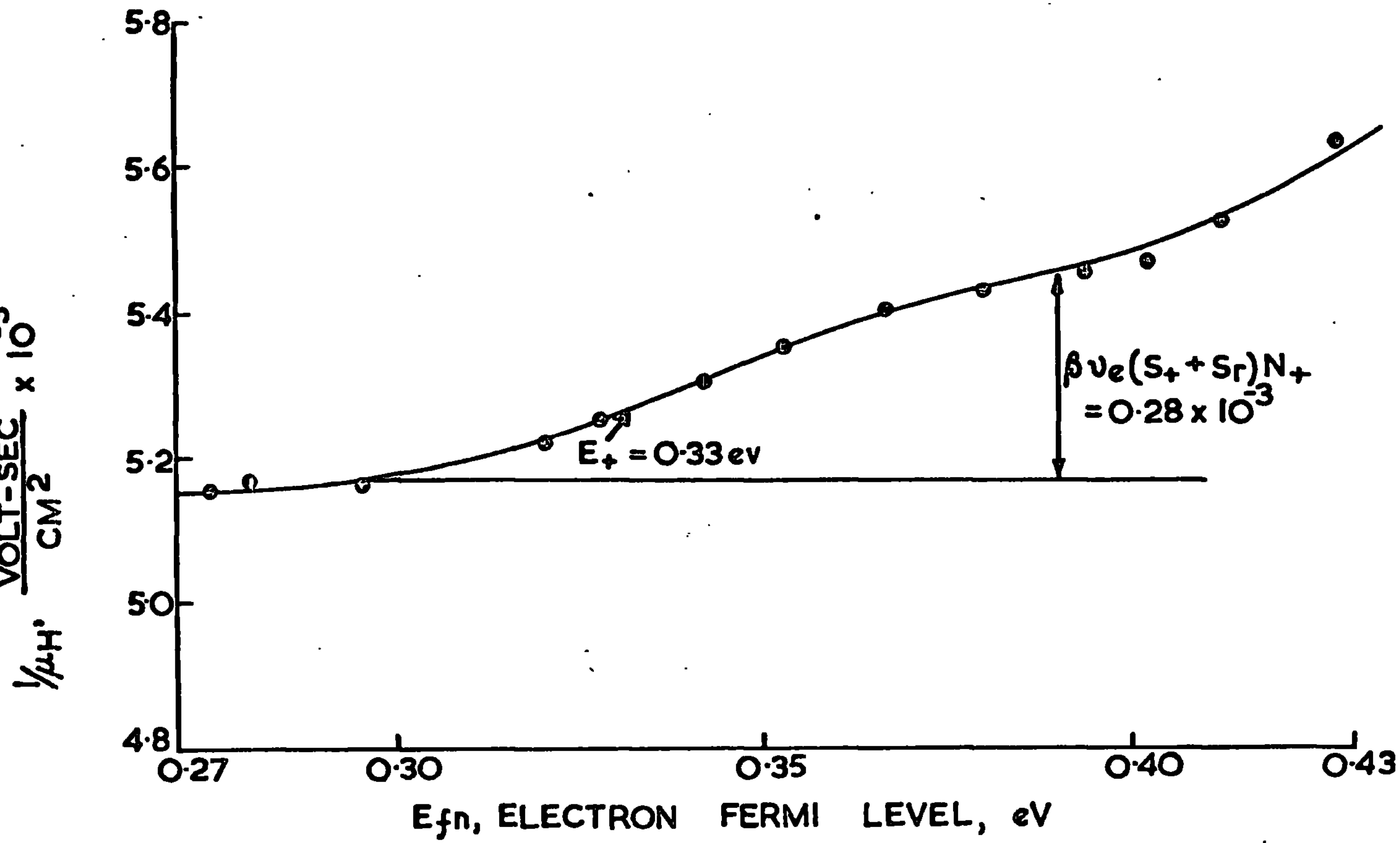

Fig. 6·4(c) Reciprocal mobility vs location of the steady-state electron Fermi level for crystal 78. Measurement was taken when the sample temperature was 330°K.

the equilibrium Fermi-level in the dark. With increasing intensity of photoexcitation the quasi Fermi-levels move towards the band edges. The photoexcited electrons are captured by the positively charged traps while the photoexcited holes are captured by the negatively charged compensated acceptors (these latter include the sensitizing centres). The anticipated variation in mobility is given by the equation

$$\frac{1}{\mu} = \beta/\tau_o + \beta v_e S_+(N_+-n) + \beta v_e S_r(N_r-p) \qquad (6.2)$$

The term β/τ_o in equation (6.2) represents the scattering due to all other processes not involved in the motion of the quasi Fermi-levels through the trapping and sensitizing levels. The change in ionized impurity scattering is described by the second and the third terms of equation (6.2).

In equilibrium in the dark, a crystal is electrically neutral. For charge neutrality, the density of positive and negative charges on imperfection centres with energy levels in the forbidden gap must be equal. In a photosensitive insulating crystal, the charges on an empty trap or ionized donor is positive. The charges on recombination centres and on hole traps are negative. It follows therefore that if N_+ is the density of singly positively charged ionized donors and N_r is the density of negatively charged recombination centres and hole traps, then $N_+ = N_r$. At any instant, the number of excess electrons and holes generated by the photoexcitation must be the same i.e. $n = p$. If n photoexcited electrons are captured by the centres which are positive, the positively charged centres are reduced to (N_+-n). If p photoexcited holes are captured by the negatively charged centres, the negatively charged defects are reduced to (N_r-p). Since the crystal must be electrically neutral, $(N_+-n) \simeq (N_r-p)$, provided the density of free carriers can be ignored.

With this assumption, equation (6.2) can be written

$$\frac{1}{\mu} = \beta/\tau_o + \beta v_e(S_r+S_+)\,(N_+-n) \qquad (6.3)$$

where N_+ - The density of the singly positively charged ionized donors (traps).

n - The density of photoexcited electrons in those centres.

S_+ - The scattering cross-section of a singly positively charged ionized donor.

S_r - The scattering cross-section of a singly negatively charged acceptor.

The number of ionized donors can be determined from the Fermi distribution function, which gives

$$(N_+-n) = \frac{N_+}{1+2\,\exp\left[(E_+-E_{fn})/kT\right]} \qquad (6.4)$$

$$\therefore \quad \frac{1}{\mu} = \beta/\tau_o + \beta v_e(S_++S_r)N_+ \quad \frac{1}{1+2\,\exp\left[(E_+-E_{fn})/kT\right]} \qquad (6.5)$$

This analysis has been applied to the experimental results of Figures 6.4(a), (b) and (c) and values of the trap depths E_+ and the corresponding values of $\beta v_e(S_+ + S_r)N_+$ have been calculated from equation (6.5). (See Section 3-1.4).

Values of the ionization energies E_+ and the products $N_+(S_+ + S_r)$ were calculated for each of the stepwise variations in the $\frac{1}{\mu}$ versus E_{fn} plots in Figures 6.4(a), (b) and (c). In order to calculate the values of the sums of the scattering cross-sections $(S_+ + S_r)$ from the values of $N_+(S_+ + S_r)$, it was necessary to know the values of N_+ from an independent measurement. Thermally stimulated current measurements were made on crystal 78 by M.A. Carter.[4] This technique can be made to yield values of the energy depths and the concentrations of imperfection centres. Trap depths determined from the photoHall data for crystal 78 agree to within 10% with those found from the analysis of thermally stimulated current curves (see Table 6.1). All the imperfection scattering parameters obtained for crystal 78 from photoHall and T.S.C. measurements are summarised in Table 6.1.

Successful evaluation of the densities of the trapping centres from the T.S.C. curves was possible for the traps with energy depths of 0·12 and 0·22 eV. The calculated values of the sum of the scattering cross-section $(S_+ + S_r)$ is the sum total of the scattering cross-sections offered by the positively and the negatively charged centres. According to the simple Rutherford model, S_+ is equal to S_r when both the centres are singly charged. This is true when the scattering centres have the spherical symmetry similar to that of a Coulombic scatterer. For spherical symmetry, the scattering radius is

Table 6.1. Summary of the imperfection scattering parameters for crystal 78

Temperature of the sample at which the photoHall measurement was made, in °K.	Trap depth from the mobility effect, in eV.	Trap depth from thermally stimulated current measurement, in eV.	The value of $\beta v_e(S_+ + S_r)N_+$ from the mobility effect, in (volt-sec)/cm^2.	Density N_+ (cm^{-3}) from thermally stimulated current measurement	Thermal velocity of an electron $v_e = \sqrt{2kT/m_e^*}$, in cm/sec.	Sum of the scattering cross-sections $(S_+ + S_r)$ in cm^2	The value of the scattering cross-section from the relation, $S = Z^2\pi e^4/\epsilon^2 k^2 T^2$ in cm^2 (for Z=1)
136°K	0·115(~0·12)	0·12	$0{\cdot}12 \times 10^{-3}$	$6{\cdot}0 \times 10^{15}$	$1{\cdot}45 \times 10^{7}$	$1{\cdot}17 \times 10^{-11}$	$4{\cdot}74 \times 10^{-12}$
193°K	0·16	0·15	$0{\cdot}16 \times 10^{-3}$		$1{\cdot}71 \times 10^{7}$		$2{\cdot}35 \times 10^{-12}$
	0·22	0·22	$0{\cdot}23 \times 10^{-3}$	$2{\cdot}0 \times 10^{15}$		$5{\cdot}60 \times 10^{-11}$	
330·0°K	0·33	0·34	$0{\cdot}28 \times 10^{-3}$		$2{\cdot}27 \times 10^{7}$		$0{\cdot}76 \times 10^{-12}$

about 10^{-5} cm and the scattering volume is then 3×10^{-17} cm^3. This means that an impurity centre will have spherical symmetry when the impurity concentration is less than about 10^{16} cm^{-3}.

With cadmium sulphide, the value of the scattering cross-section predicted by the relation,

$$S = Z^2 \pi e^4/\epsilon^2 k^2 T^2 \tag{3.5}$$

should be equal to 10^{-12} cm^2 for a singly charged centre at room temperature. If we assume $S_+ = S_r$, then $(S_+ + S_r)$ should be equal to 2×10^{-12} cm^2 when both the centres are singly charged. The experimental values of the sum of the scattering cross-section $(S_+ + S_r)$ which are of the order of 10^{-11} cm^2 (Table 6.1) can be regarded as a good agreement with the values (2×10^{-12} cm^2) predicted by the relation (3.5).

PhotoHall measurements are found more successful in evaluating the depths of the (shallower) trapping levels than the thermally stimulated current measurements. Investigations of the photoHall effect are made under the steady-state condition when the location of the electron (hole) Fermi level $E_{fn}(E_{fp})$ mostly determines the occupancy of the nearest imperfection level. A change in the value of electron mobility results principally from the change in the occupancy of this imperfection level. An analysis of μ as a function of E_{fn} according to the theory discussed in Section 3-1.4 provides imperfection scattering parameters related to this level.

Most of the methods used to calculate the trap depths from the T.S.C. measurements are based on a simple model of a single set of trapping centres in the forbidden gap. A single trap depth gives rise to a maximum at a temperature T^* in the T.S.C. curves (see Section 2-7). There is a correlation between T^* and the trap depth. The number of trapping centres of a given trap depth can be calculated from the total area under the curve provided the carrier lifetime is known.

Sometimes there are a fairly large number of discrete trapping levels in the forbidden gap. The analysis of the conductivity glow curve then becomes complicated due to the overlapping of several T.S.C. peaks. Thermal cleaning can be used effectively in certain cases to resolve the overlapping peaks but it fails if the overlapping is severe. Cleaning of a peak also involves removing more electrons from the defects being studied if the maxima are closer at the new heating rate. This results in a decrease in the number of electrons released subsequently to form the required cleaned thermally stimulated current peak. Hence the correct value of N_t is difficult to measure.

The crystal also contains recombination centres in addition to the traps and the kinetics of the emptying of traps depends on the nature of the recombination centres. In certain circumstances the free electron lifetime can change substantially and cause the temperature of the current maximum to shift; the shape of the T.S.C. curve may also be changed. These effects will create errors in the calculation of energy depths and other related trap parameters.

6-4. Variation of conductivity and carrier concentration with photoexcitation for crystal 78

The variations of conductivity σ and carrier concentration n with the intensity of photoexcitation L corresponding to the plots of $\frac{1}{\mu}$ versus E_{fn} of Figures 6.4(a), (b) and (c), are shown in Figures 6.5(a), (b) and (c). The log-log plots of n and σ versus L in Figure 6.5(a) have a slope of 0·83 from the point A to B and then a slope of 0·60 from B to C. The location of the steady-state electron Fermi-level corresponding to the breakpoint at B is 0·112 eV. This observed change in the slope can be explained by assuming that the trap with a level at 0·12 eV, changes to a Class I recombination centre as the electron Fermi-level rises above that level. The log-log plots of n and σ versus L in Figures 6.5(b) and (c) have slopes of 0·84 and 0·85 respectively and no breakpoints.

The trapping levels determined from the variation of mobility with the steady-state electron Fermi-level shown in Figures 6.4(a), (b) and (c) have been demonstrated to be positively charged in the dark. Thus with increasing light intensity, the Fermi-level rises and the trapping centres become neutral by capturing photoexcited electrons. With further rise of electron Fermi-level, they will lie between the electron demarcation level and the steady-state electron Fermi-level. The distance between the electron demarcation level and the steady-state electron Fermi-level (Figure 2.3) is given by the expression

$$E_{dn} - E_{fn} = kT \ln n_g/p_g \qquad (6.6)$$

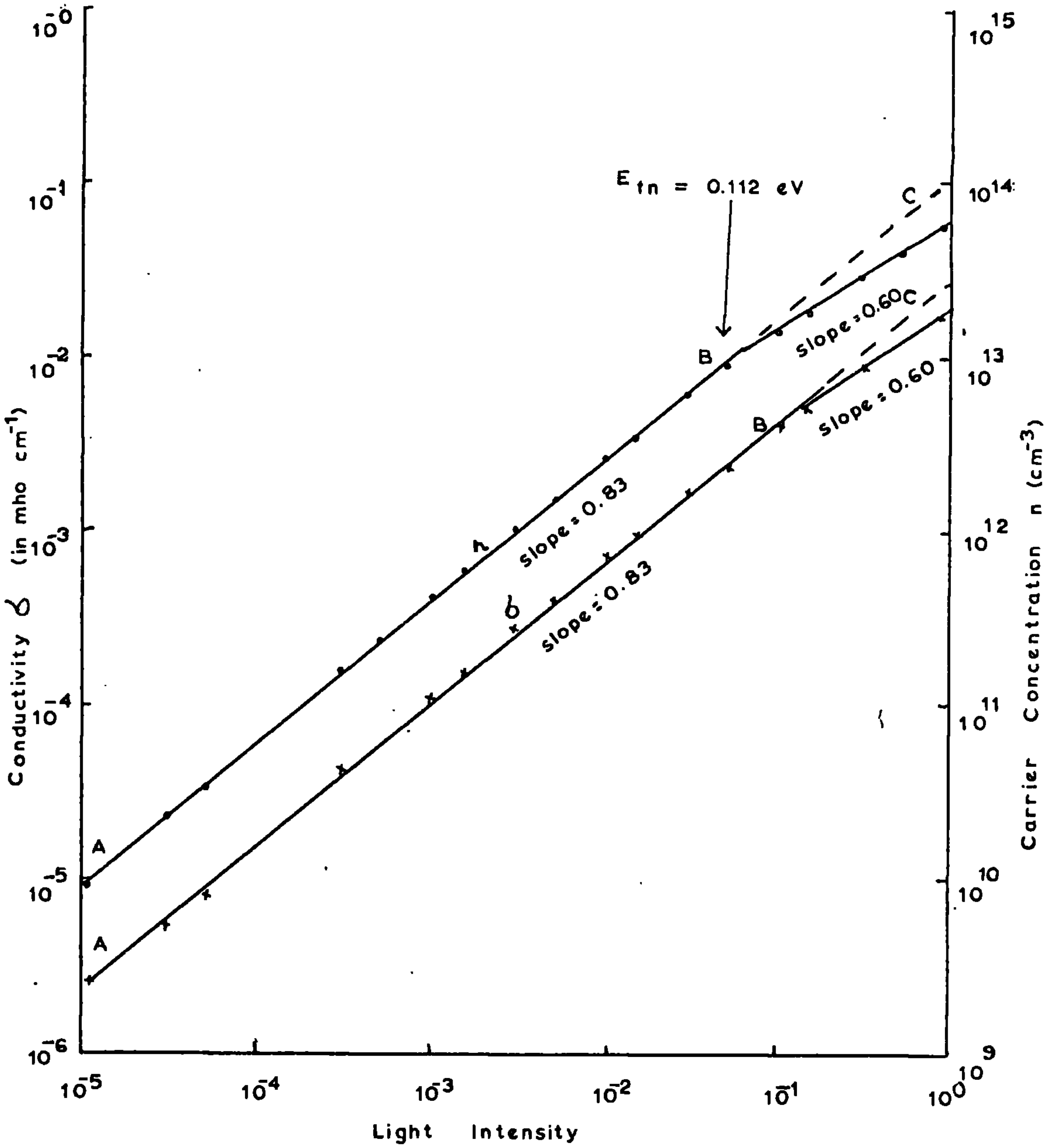

Fig. 6.5 (a). Variation of carrier concentration n and conductivity σ with the intensity of photoexcitation L for crystal 78. Measurement was taken when the sample temperature was 136°K.

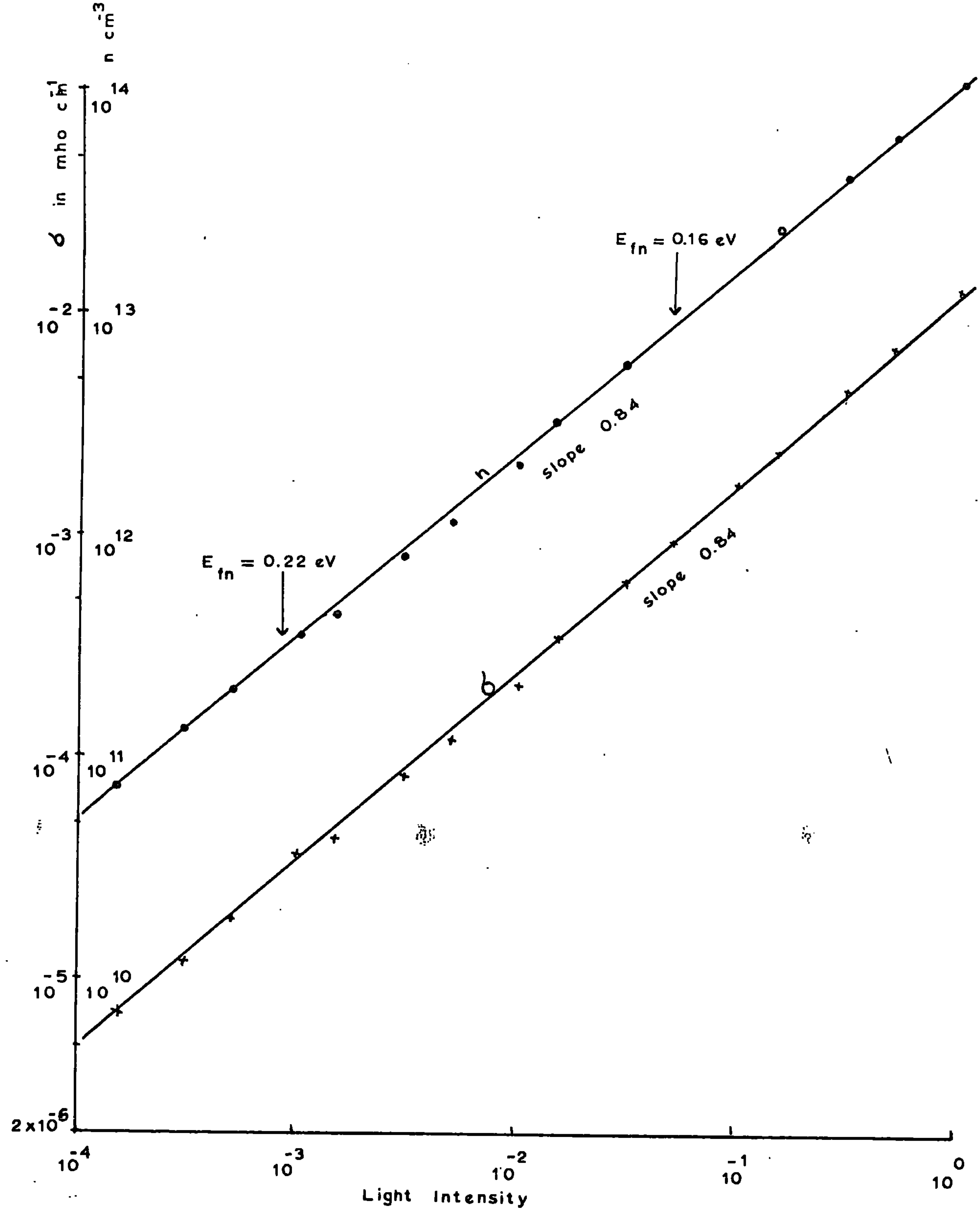

Fig. 6.5.(b) Variation of carrier conc, n and conductivity σ with the intensity of photoexcitation L for crystal 78. Measurement was taken when the sample temperature was 193°K.

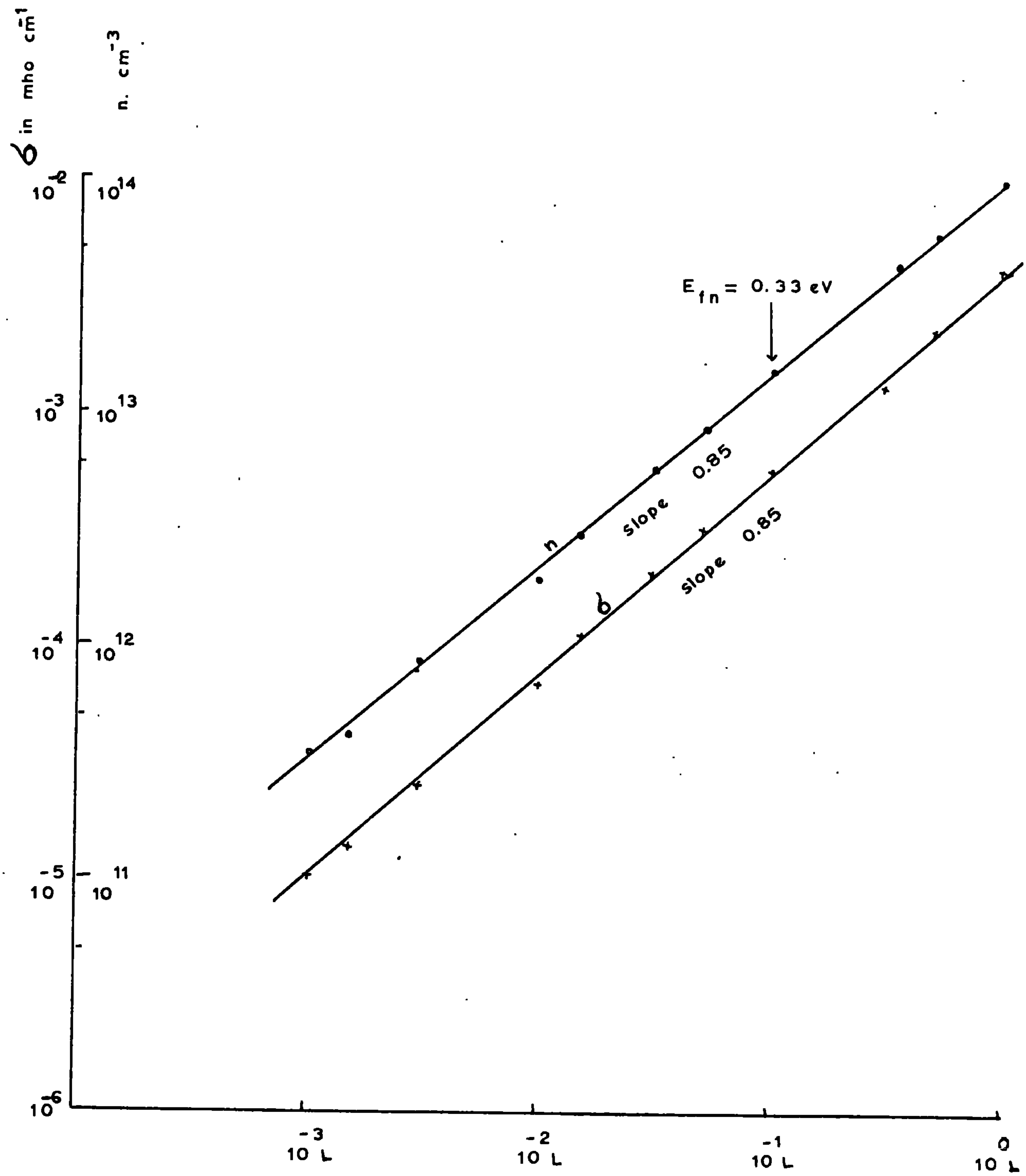

Fig. 6.5.(c) Variation of carrier conc. n and conductivity σ with the intensity of photoexcitation for crystal 78. Measurement was taken when the sample temperature was 330°K.

where n_g is the number of recombination centres occupied by electrons and p_g, the number of recombination centres occupied by holes. When $n_g = p_g$, the electron Fermi-level E_{fn} coincides with the electron demarcation level. In this condition, the neutral trapping levels will start to behave as Class I recombination centres. Once the energy levels lie well within the demarcation levels, the probability of recombination increases.

The log-log plots of n and σ versus L in Figures 6.5(b) and (c) show that no change in the slope occurred even after the electron Fermi-level crossed the position of the trapping levels at 0·22 eV and 0·16 eV (Figure 6.5(b)) and 0·33 eV (Figure 6.5(c)) while approaching the conduction band as the light intensity was increased. It may be that the trapping levels at 0·16, 0·22 and 0·33 eV do not promote significant recombination of Class I type whereas the trapping level at 0·12 eV does, although it is difficult to understand why this should be.

6.5 Variation of Hall mobility with photoexcitation for crystal 79

PhotoHall measurements on crystal 79 at room temperature indicated a variation in conductivity from $1{\cdot}67 \times 10^{-2}$ mho cm^{-1} to $5{\cdot}82 \times 10^{-6}$ mho cm^{-1} when the intensity of photoexcitation was reduced from 10^{0} to 10^{-5} of the original intensity (L = 3200 ft-C). The corresponding variation in electron Fermi level was from 0·226 eV to 0·42 eV. The experimental procedure to determine the trap depth from the variation of Hall mobility as a function of the steady-state electron

Fermi level for crystal 79 was the same as that described for crystal 78. The highest temperature at which photoHall measurements were possible for an appreciable change in the location of the electron Fermi level with photoexcitation was 340°K. Figures 6.6(a), (b) and (c) show three plots of $\frac{1}{\mu}$ versus E_{fn} corresponding to three sets of photoHall measurements made at temperatures of 148·6°K, 220°K and 340°K. A plot of $\frac{1}{\mu}$ versus E_{fn} (Figure 6.9) which will be discussed in Section (6.7), was also obtained from the photoHall measurements when the sample temperature was 98·7°K.

The plots of $\frac{1}{\mu}$ versus E_{fn} shown in Figures 6.6 can be interpreted by proposing the existence of one level in the case of Figure 6.6(a), two levels in the case of Figures 6.6(b) and 6.6(c); all of which are positively charged in the dark. The scattering effect for each of these levels can be described by the expression (6.5). Following the procedure described in Section 6.3, values of E_+ and $\beta v_e(S_+ + S_r)$ have been determined for each stepwise variation of $\frac{1}{\mu}$ versus E_{fn} (Table 6.2).

Thermally stimulated current measurements were also made on crystal 79 to obtain values of the energy depths and the concentration of imperfection centres. Although several overlapping peaks were observed in the T.S.C. curve (Figure 6.7), it was only possible using thermal cleaning to resolve completely four of these. The trap depths were 0·1, 0·13, 0·16 and 0·6 eV below the conduction band. The sum of the scattering cross-sections $(S_+ + S_r)$ has been calculated for the trap with a depth of 0·13 eV only. A summary of the calculated trapping parameters for crystal 79 is given in Table 6.2.

Table 6.2. Summary of the imperfection scattering parameters for crystal 79

Temperature of the sample at which the photoHall measurement was made, in ^{o}K.	Trap depth from the mobility effect, in eV.	Trap depth from thermally stimulated current measurement, in eV.	The value of $\beta v_e(S_+ + S_r)N_+$ from the mobility effect, in (volt-sec)/cm^2.	Density of N_+(cm^{-3}) from thermally stimulated current measurement.	Thermal velocity of an electron $v_e = \sqrt{2kT/m_e^*}$, in cm/sec.	Sum of the scattering cross-sections $(S_+ + S_r)$ in cm^2.	The value of the scattering cross-section from the relation $S = Z^2 \pi e^4/\epsilon^2 k^2 T^2$ in cm^2 (for Z = 1).
148·6	0·13	0·13 0·16	$0{\cdot}48 \times 10^{-3}$	10^{16} 7×10^{14}	$1{\cdot}503 \times 10^{7}$	$2{\cdot}80 \times 10^{-11}$	$3{\cdot}94 \times 10^{-12}$
220·0	0·19 0·25		$0{\cdot}58 \times 10^{-3}$ $0{\cdot}28 \times 10^{-3}$		$1{\cdot}83 \times 10^{7}$		$1{\cdot}81 \times 10^{-12}$
340·6	0·33 0·42		$1{\cdot}8 \times 10^{-3}$ $5{\cdot}4 \times 10^{-3}$		$2{\cdot}28 \times 10^{7}$		$7{\cdot}53 \times 10^{-13}$
		0·60		3×10^{13}			

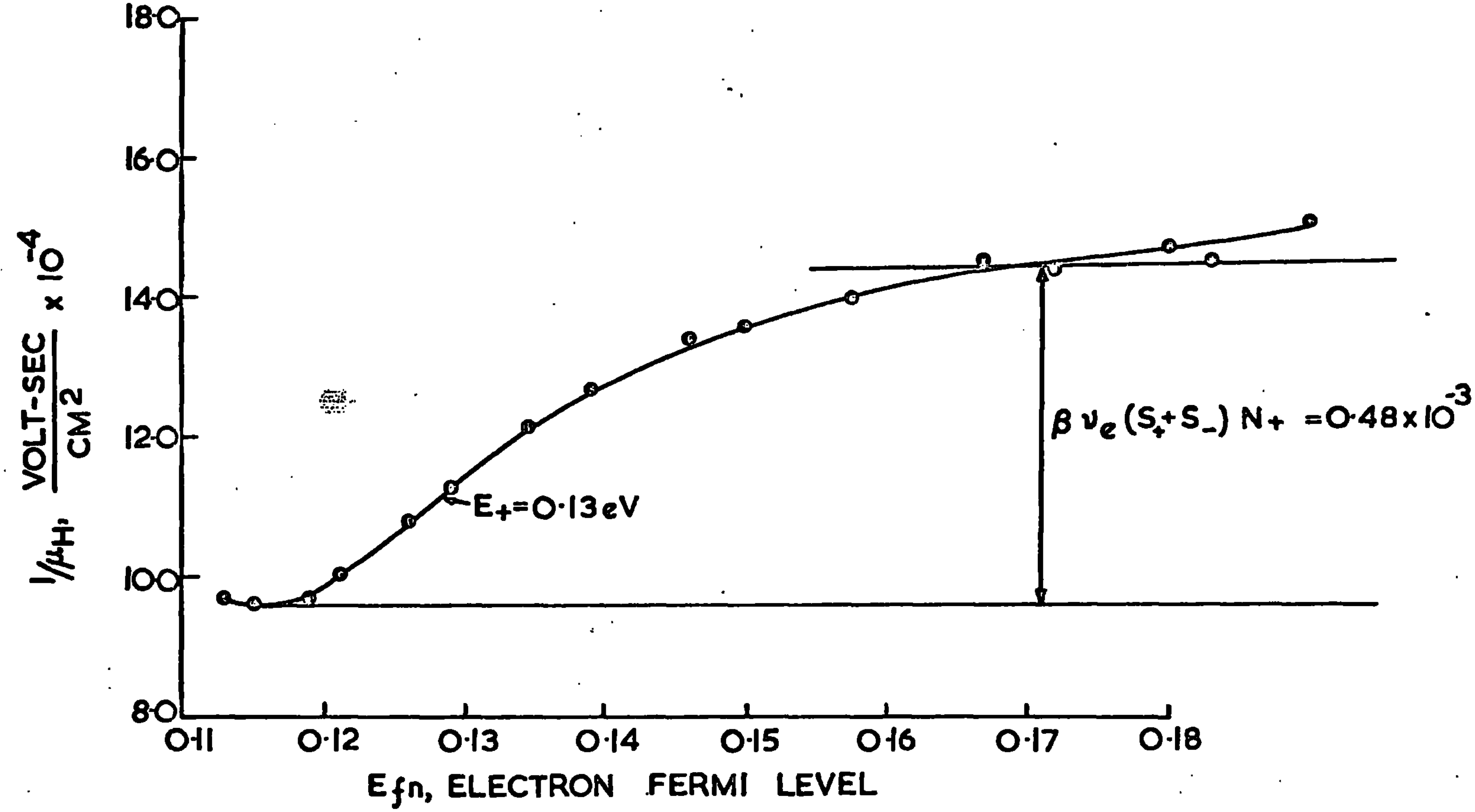

Fig. 6·6(a) Reciprocal mobility vs location of the steady state electron Fermi level for crystal 79. Measurement was taken when the sample temperature was 148·6°K.

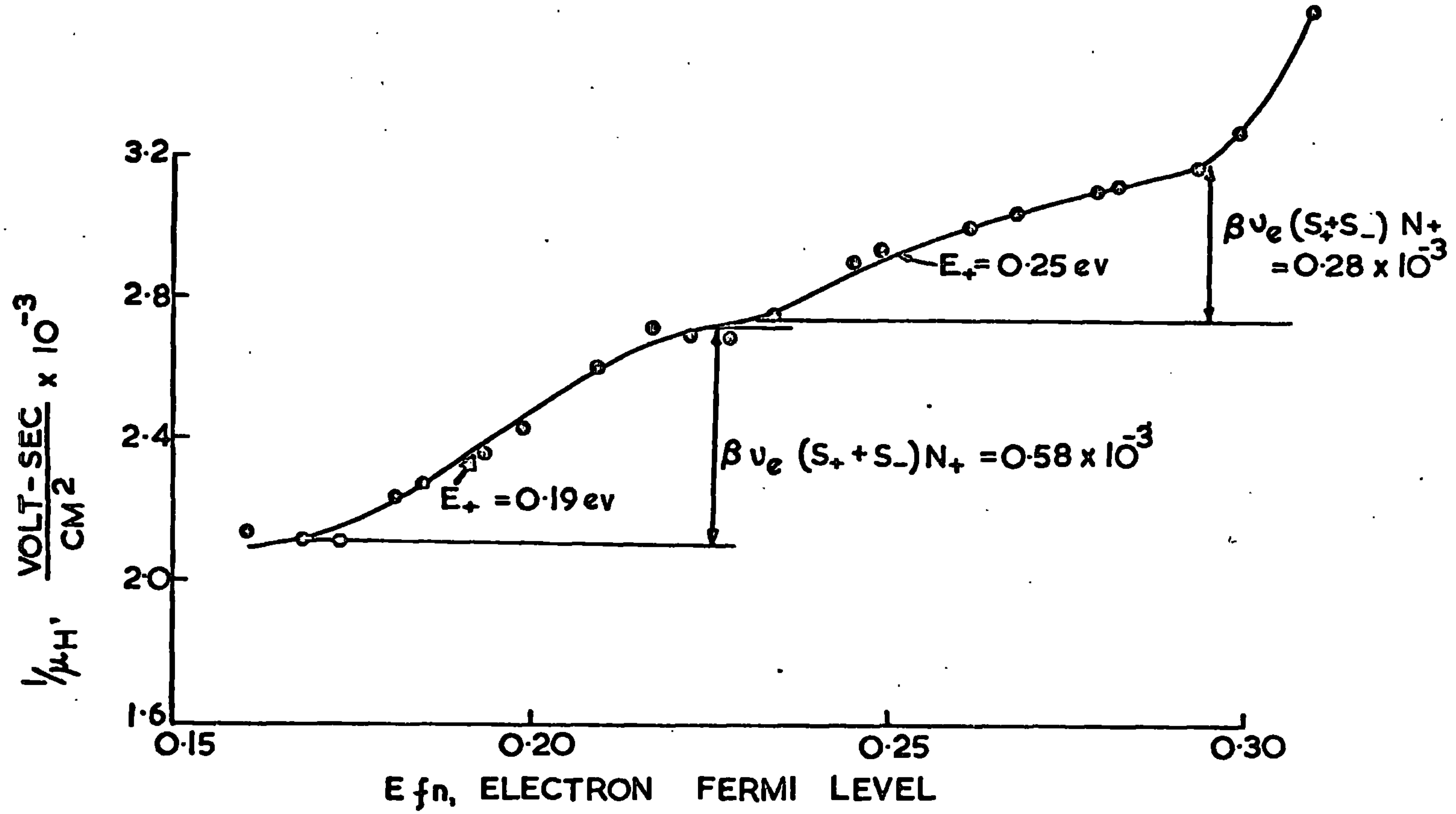

Fig. 6·6 (b) Reciprocal mobility vs location of the steady-state electron Fermi level for crystal 79. Measurement was taken when the sample temperature was 220·0°K.

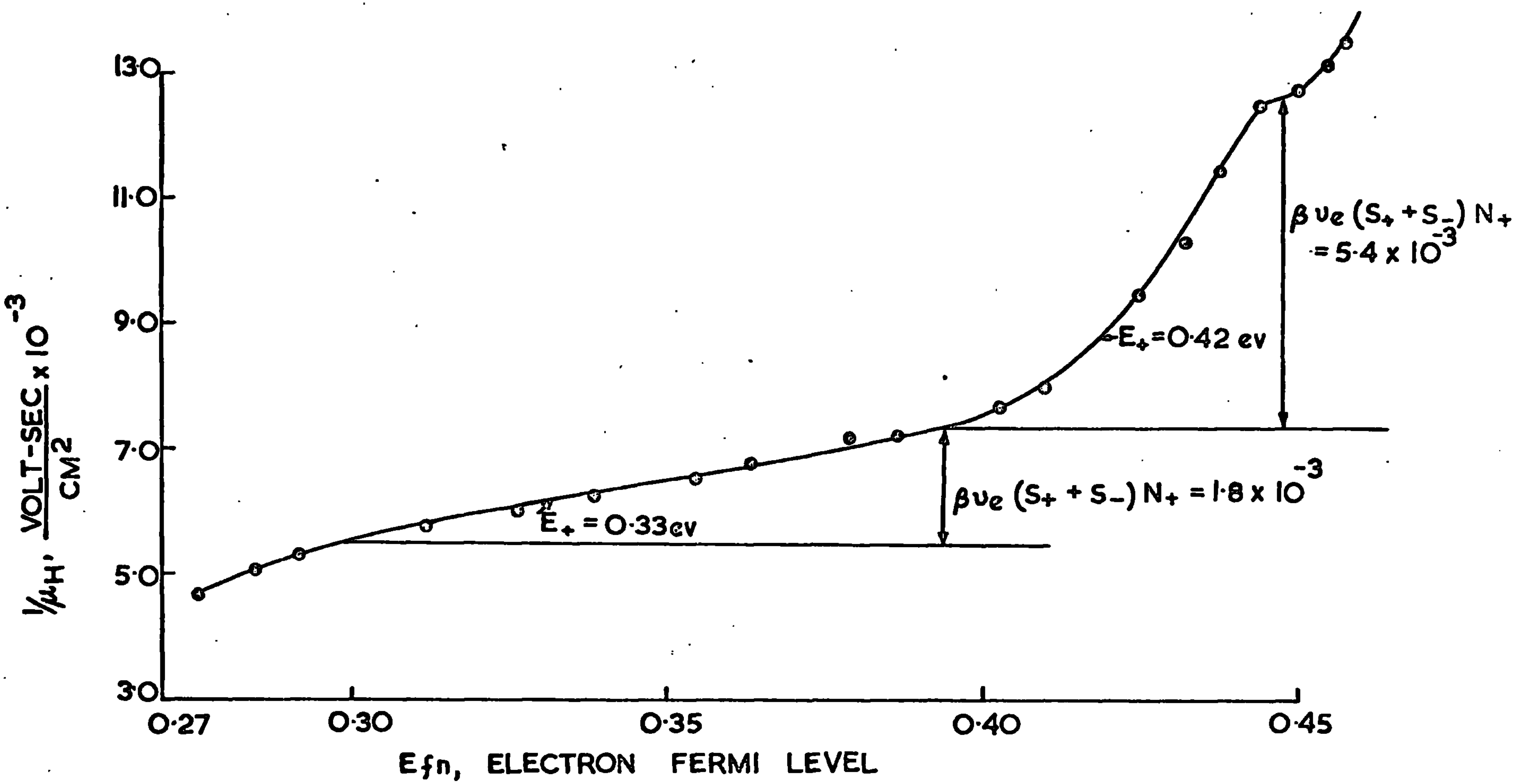

Fig. 6·6 (c) Reciprocal mobility vs location of the steady-state electron Fermi level for crystal 79. Measurement was taken when the sample temperature was 340·6 °K.

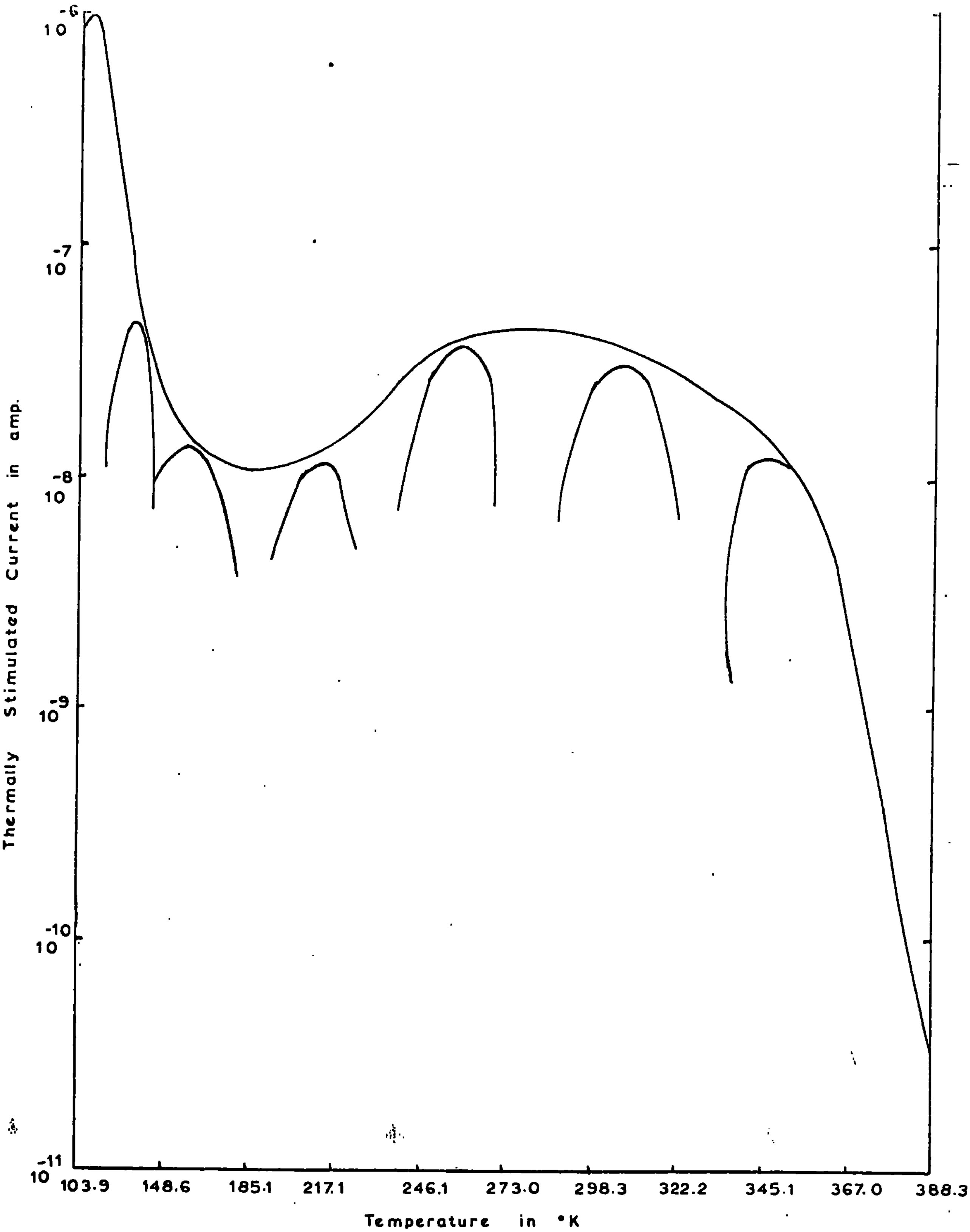

Fig. 6.7. Thermally stimulated current for the crystal 79.

6-6. Variation of conductivity and carrier concentration with photoexcitation for crystal 79

The variation of conductivity σ and carrier concentration n as a function of the light intensity L corresponding to the $\frac{1}{\mu}$ versus E_{fn} curves illustrated in Figures 6.6(a), (b) and (c), is shown in Figures 6.8(a), (b) and (c). The curves of n and σ versus L of Figure 6.8(a) have a slope of 0·86 from A to B and then a slope of 0·46 from B to C. A similar change of slope in the plots of n and σ versus L was also observed for crystal 78 (Figure 6.5(a)).

The location of the steady-state electron Fermi level corresponding to the breakpoint at B (Figure 6.8(a)) is 0·13 eV. The corresponding plot of $\frac{1}{\mu}$ versus E_{fn} shown in 6.6(a) demonstrates the existence of a trapping level at a height of $\sim$0·13 eV below the conduction band. Similarly the curves of n and σ versus L of Figure 6.8(b) have a slope of 0·84 from A to B and then a slope of 0·60 from B to C. The breakpoint at B of Figure 6.8(b) occurs when the location of the steady-state electron Fermi level is 0·193 eV below the conduction band, which is the depth of a trapping level shown in Figure 6.6(b).

The curve of n versus L of Figure 6.8(c) has a slope of 0·47 from A to B, a slope of 0·78 from B to C and then a slope of 0·5 from C to D. The breakpoints at B and C correspond to steady-state electron Fermi energies of 0·43 eV and 0·31 eV respectively. The change in the slope at C can be accounted for by assuming that the centres at 0·33 eV (Figure 6.6(c)) change from trapping centres to Class I type

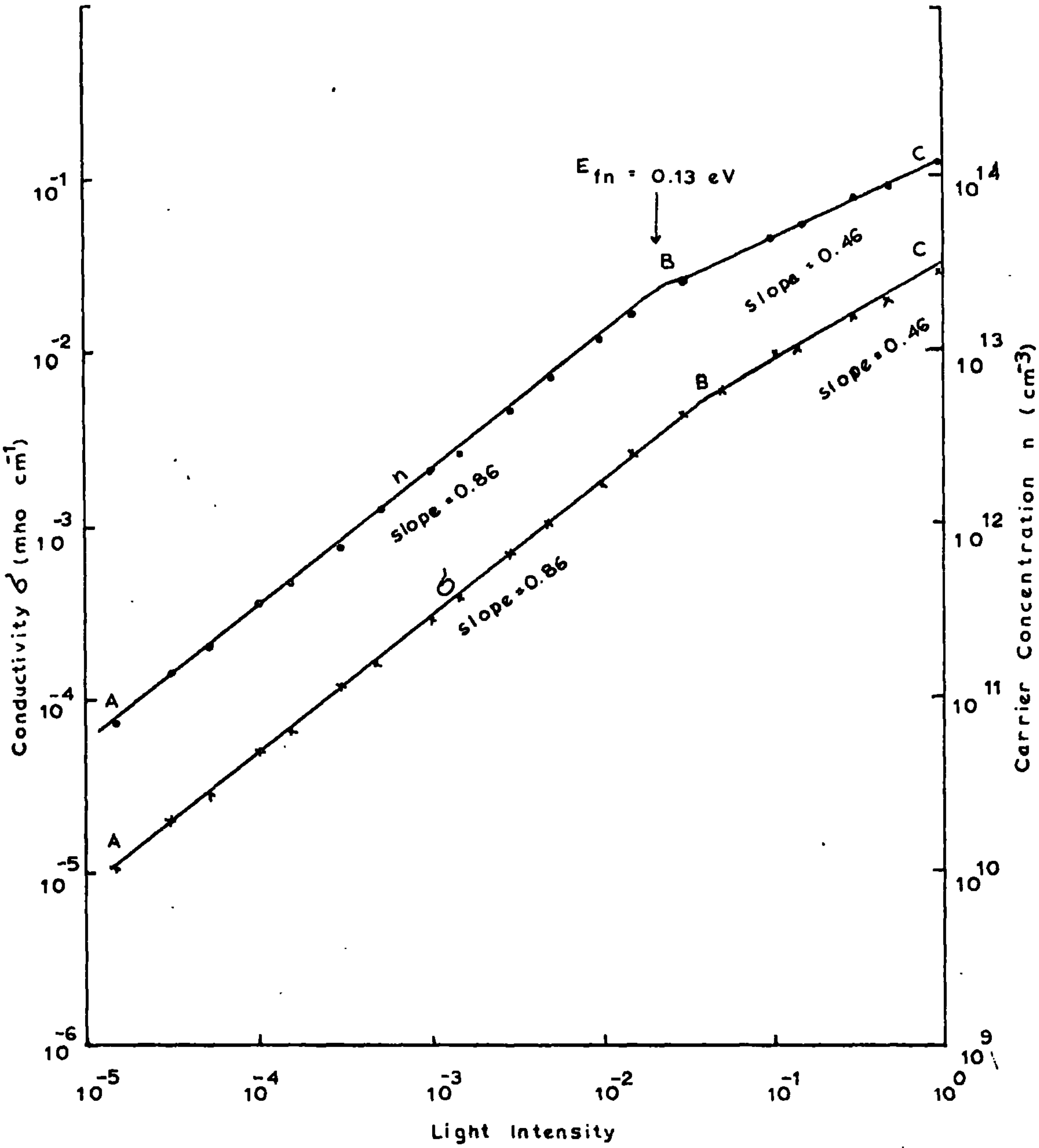

Fig. 6.8 (a). Variation of carrier concentration n and conductivity σ with the intensity of photoexcitation L for crystal 79. Measurement was taken when the sample temperature was 148.6°K.

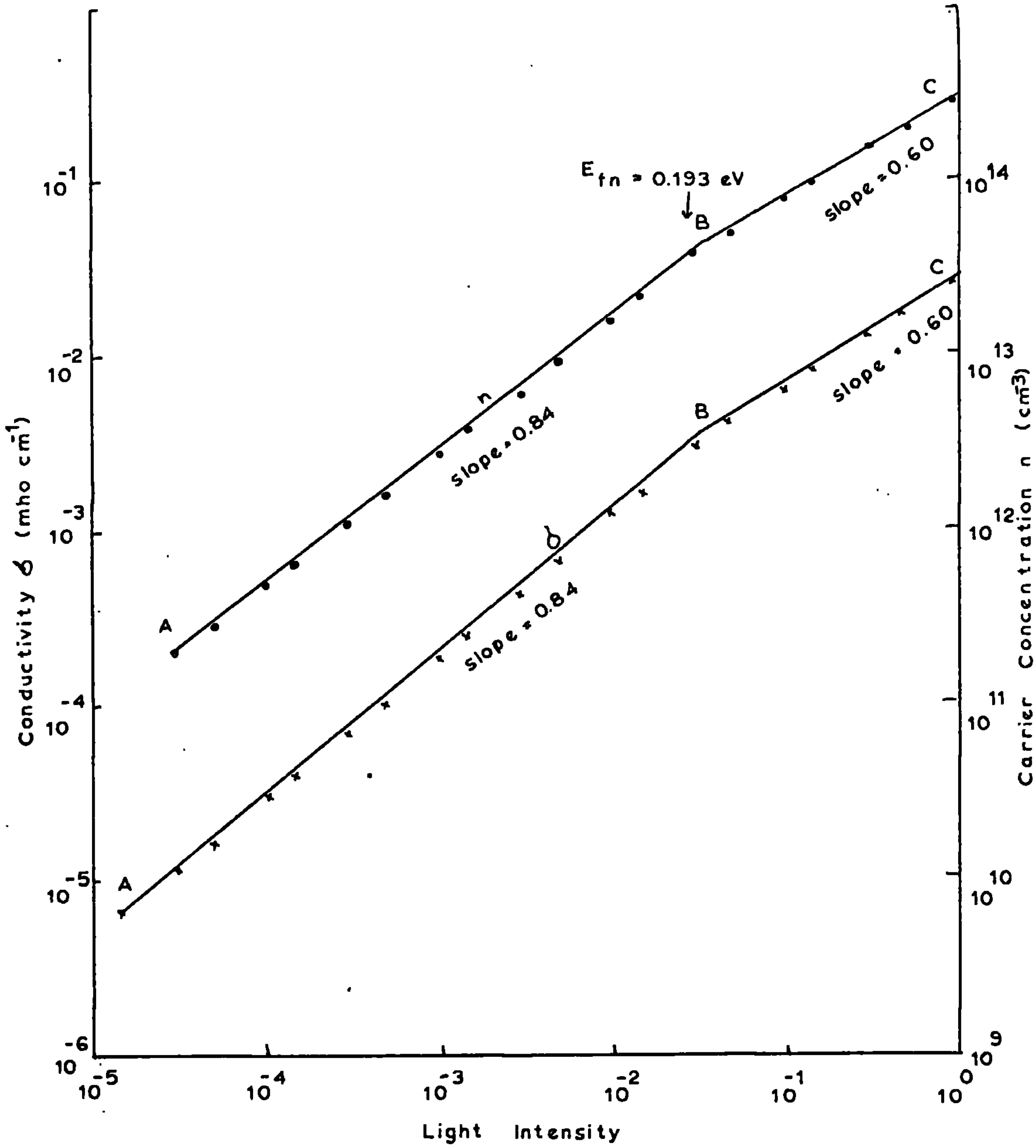

Fig. 6.8 (b). Variation of carrier concentration n and conductivity δ with the intensity of photoexcitation L for crystal 79. Measurement was taken when the sample temperature was 220°K.

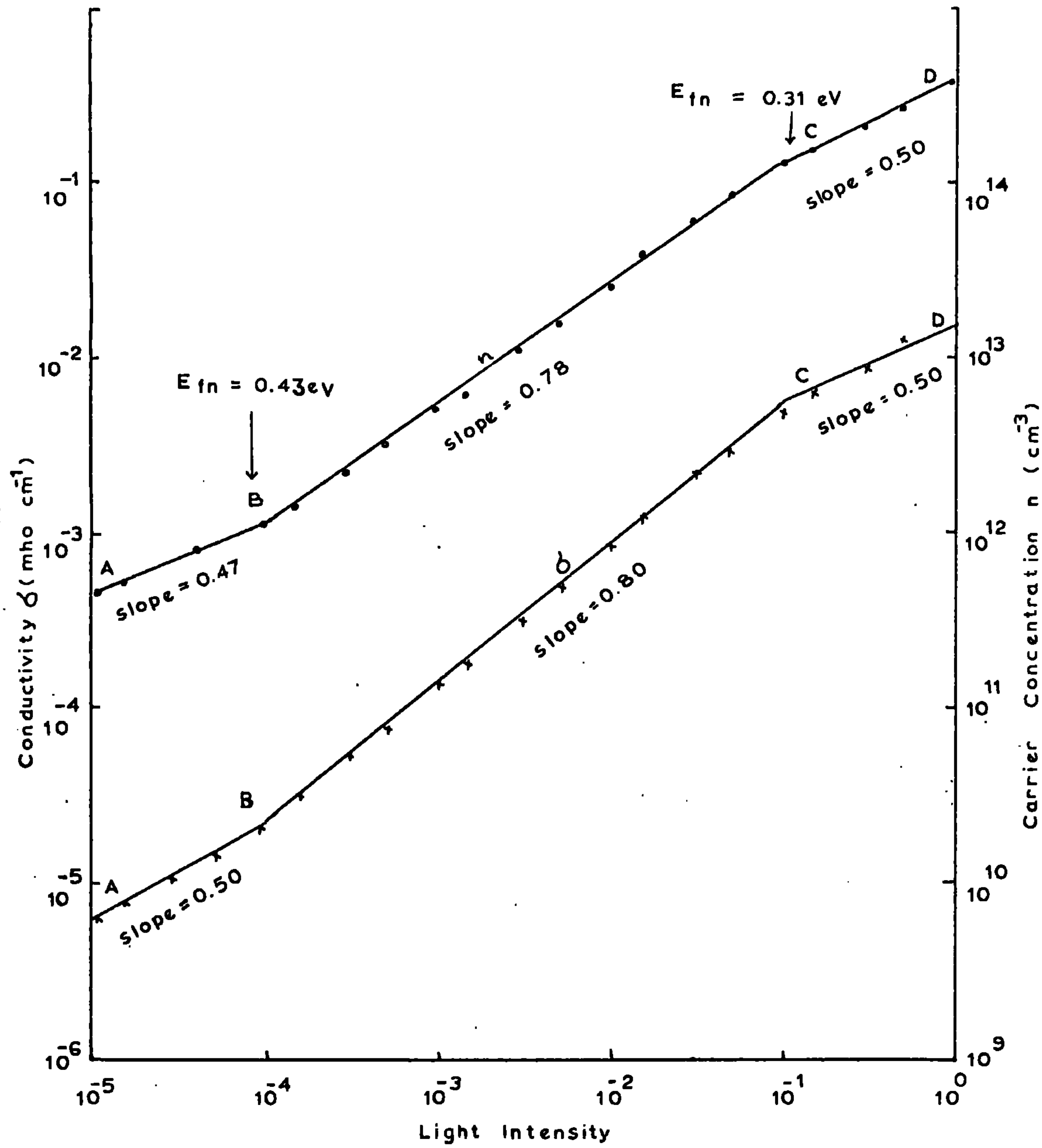

Fig. 6.8 (c). Variation of carrier concentration n and conductivity σ with the intensity of photoexcitation L for crystal 79. Measurement was taken when the sample temperature was 340°K.

recombination centres as the electron Fermi level rises through them.

The location of the steady-state electron Fermi level corresponding to the breakpoint at B is 0·43 eV, which coincides with one of the two trapping levels determined from the mobility effect (Figure 6.6(c)). However, the location of the hole demarcation level (calculated from the relation $E_{dp} = E_{fn} + kT \ln S_p/S_n$) corresponding to the breakpoint at B was found to be 0·97 eV assuming that S_p/S_n was 10^8, a value suggested for doubly charged Class II sensitizing centres[5] (see Chapter 7). If the energy level associated with the Class II sensitizing centres in cadmium sulphide is taken to lie 1·1 eV[6] above the valence band, then the hole demarcation level corresponding to the breakpoint at B of Figure 6.8(c), would almost coincide with the energy levels of the Class II centres

Further increase of the intensity of photoexcitation corresponding to the intensity at B of Figure 6.8(c) would push the electron Fermi level towards the conduction band and the hole demarcation level towards the valence band. As the hole demarcation level would be lowered through the Class II sensitizing centres, the free electron lifetime would increase continuously and consequently the free electron concentration would increase superlinearly with light intensity (see Section 3-2). At the same time, the electron Fermi level would rise through the trapping centres at 0·43 eV below the conduction band. The trapping centres with levels at 0·43 eV might promote significant recombination of Class I type and thus reduce the free electron lifetime (see Section 6-4). However, such an effect would be swamped by the Class II sensitizing centres. Thus it is suggested that Class II recombination centres are responsible for the increase in slope of the (n,σ) versus light intensity curves at breakpoint B, Figure 6.8(c).

6-7. Variation of Hall mobility with photoexcitation for crystal 79 at 98·7°K

Figure 6.9 shows a plot of $\frac{1}{\mu}$ versus E_{fn} obtained from photoHall measurements made when the sample temperature was 98·7°K. The shape of this curve can be interpreted by assuming the existence of a trapping centre which is neutral in the dark. In this case the anticipated variation in mobility with photoexcitation can be written

$$\frac{1}{\mu} = \beta/\tau_o + \beta v_e S_r (N_r - p) + \beta v_e S_- n \tag{6.7}$$

where

- n - The density of electrons in the neutral imperfection centres.
- S_- - The scattering cross-section of the centres which become negative after capturing photoexcital electrons.
- N_r - The density of negative charges due to negatively charged acceptors in the dark.
- S_r - The scattering cross-section of a singly negatively charged acceptor (the recombination centres).

In equation (6.7), the second term corresponds to scattering by negatively charged compensated acceptors (the recombination centres) and the third term to scattering by neutral imperfection centres

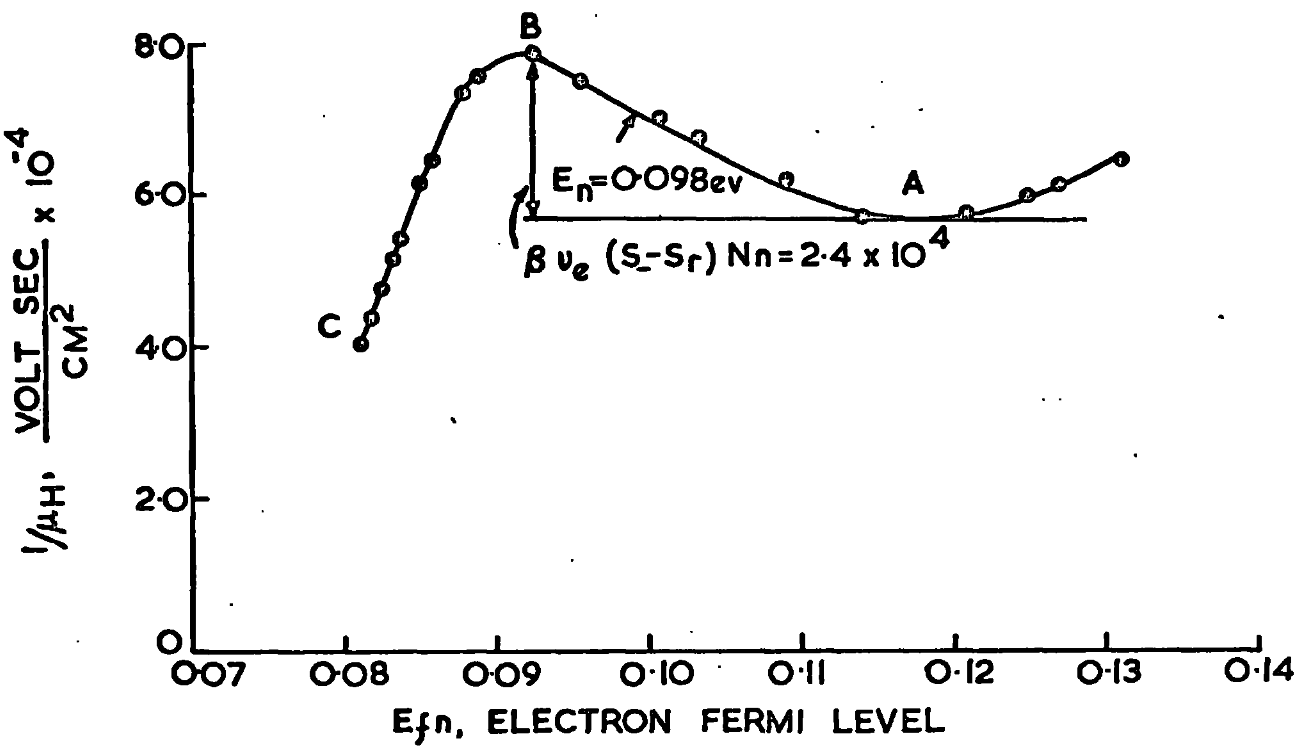

Fig. 6·9 Reciprocal mobility vs location of the steady state electron Fermi level for crystal 79. Measurement was taken when the sample temperature was 98·7°K.

which become negative on capturing photoexcited electrons. Since the system must be electrically neutral in the dark, it follows that there must be some positively charged traps which are probably very shallow. Photoexcited electrons are mainly captured by the neutral imperfection centres because they are nearer to the steady-state electron Fermi-level. The very shallow positively charged traps remain virtually unoccupied by photoexcited electrons, so they play no essential part in determining the variation of Hall mobility. The term β/τ_o includes their contribution to the scattering as well as that of all the other processes such as lattice scattering, etc. At any instant the number of excess electrons and holes generated must be the same, i.e. n = p. Equation (6.7) can, therefore, be written

$$\frac{1}{\mu} = \beta/\tau_o + \beta v_e S_r N_- + \beta v_e (S_- - S_r) n \qquad (6.8)$$

In equation (6.8), the term $\beta v_e (S_- - S_r) n$ is the only one which can change with light intensity. To explain the variation of mobility with photoexcitation shown in Figure 6.9 it is necessary to assume $S_- - S_r > 0$. If both centres are simple coulombic, then the two-cross-sections would be roughly equal but differences can occur (see later).

In equation (6.8), n represents the density of the occupied centres which become negatively charged after capturing photoexcited electrons. n can be determined from the Fermi distribution function.

$$n = \frac{N_n}{1+\frac{1}{2}\exp\left[(E_{fn}-E_n)/kT\right]} \tag{6.9}$$

where N_n is the density of the neutral imperfection centres and E_n, the depth of such centres from the conduction band. Substituting the value of n, equation (6.8) becomes

$$\frac{1}{\mu} = \beta/\tau_o + \beta v_e S_r N_- + \beta v_e (S_- - S_r) \frac{N_n}{1+\frac{1}{2}\exp\left[(E_{fn}-E_n)/kT\right]} \tag{6.10}$$

This equation satisfactorily describes the type of behaviour illustrated in Figure 6.9 where the region from A to B provides a value of $\Delta\frac{1}{\mu}$ equal to $\beta v_e(S_- - S_r)N_n$ which is the difference between the limiting values of $\frac{1}{\mu}$ for small E_{fn} and large E_{fn}. A value of trap depth can also be found from the region AB in Figure 6.9. This is given by the position of the Fermi level at the point where $\frac{1}{\mu}$ has increased by $\frac{2}{3}\,\Delta\,\frac{1}{\mu}$ from the point A. At this point $E_{fn} = E_n$ and $\frac{2}{3}\,\Delta\,\frac{1}{\mu} = \frac{2}{3}\,\beta v_e(S_- - S_r)N_n$.

To calculate the value of $(S_- - S_r)$, it is necessary to know the value of N_n, the density of the imperfection centres. A value of E_n of 0·098 eV was calculated from Figure 6.9. A trapping level at a height of 0·1 eV below the conduction band was also found by M.A.Carter[4] from the analysis of thermally stimulated current data and is almost certainly the same trapping level. So by taking the value of N_n derived from the T.S.C. measurements, namely $4{\cdot}92 \times 10^{16}$ cm^{-3}, the calculated value of $(S_- - S_r)$ was found to be $3{\cdot}5 \times 10^{-12}$ cm^2. Table 6.3 summarises the

TABLE 6.3

Temperature of the sample at which the measurement was made, in ^{o}K.	Trap depth from mobility effect in eV.	Trap depth from thermally stimulated current measurement, in eV.	The value of $\beta v_e(S_- - S_r)N_n$ from the mobility effect, in (volt-sec)/cm^2.	Density N_n (cm^{-3}) from thermally stimulated current measurement	Thermal velocity of an electron, $v_e = \sqrt{2kT/m_e^*}$, in cm/sec.	The value of $(S_- - S_r)$ in cm^2.
$98 \cdot 7^{o}$K	0·098 eV	0·10	$2 \cdot 4 \times 10^{-4}$	$4 \cdot 92 \times 10^{16}$	$1 \cdot 23 \times 10^{7}$	$3 \cdot 50 \times 10^{-12}$

scattering parameters. The calculated value of $(S_{-}-S_{r})$ is of the same order as the thermal values of scattering cross-section predicted by equation (3.5) for a singly charged centre. In the case of cadmium sulphide, the value of the scattering cross-section predicted by equation (3.5) is equal to 10^{-12} cm^{2} for a singly charged centre at room temperature.

The log-log plots of carrier concentration n as a function of light intensity L (Figure 6.10) corresponding to the plot of $\frac{1}{\mu}$ versus E_{fn} of Figure 6.9, show a slope of 0·8 from A to B, and then a break to a slope of 0·26 from B to C. The location of the steady-state electron Fermi-level at the breakpoint B is 0·09 eV.

Positively charged ionized donor levels in the dark (Figures 6.6(a), (b) and (c)) were found to behave as recombination centres of Class I type when the electron Fermi-level crossed them as the intensity of photoexcitation was increased (Figures 6.7(a), (b) and (c)). Positively charged ionized donors become neutral on capturing photoexcited electrons when the Fermi-level moves towards them. These neutral centres are likely to behave as recombination centres of Class I type when the Fermi-level crosses them. However imperfection centres associated with the trapping level at 0·1 eV which have been demonstrated to be neutral in the dark would have been expected to act as Class II centres and increase the free electron lifetime and an upward kink at B.

Obviously these centres promote fast recombination once they become substantially filled with electrons. It is difficult to understand however the mechanism by which a neutral centre can reduce the free

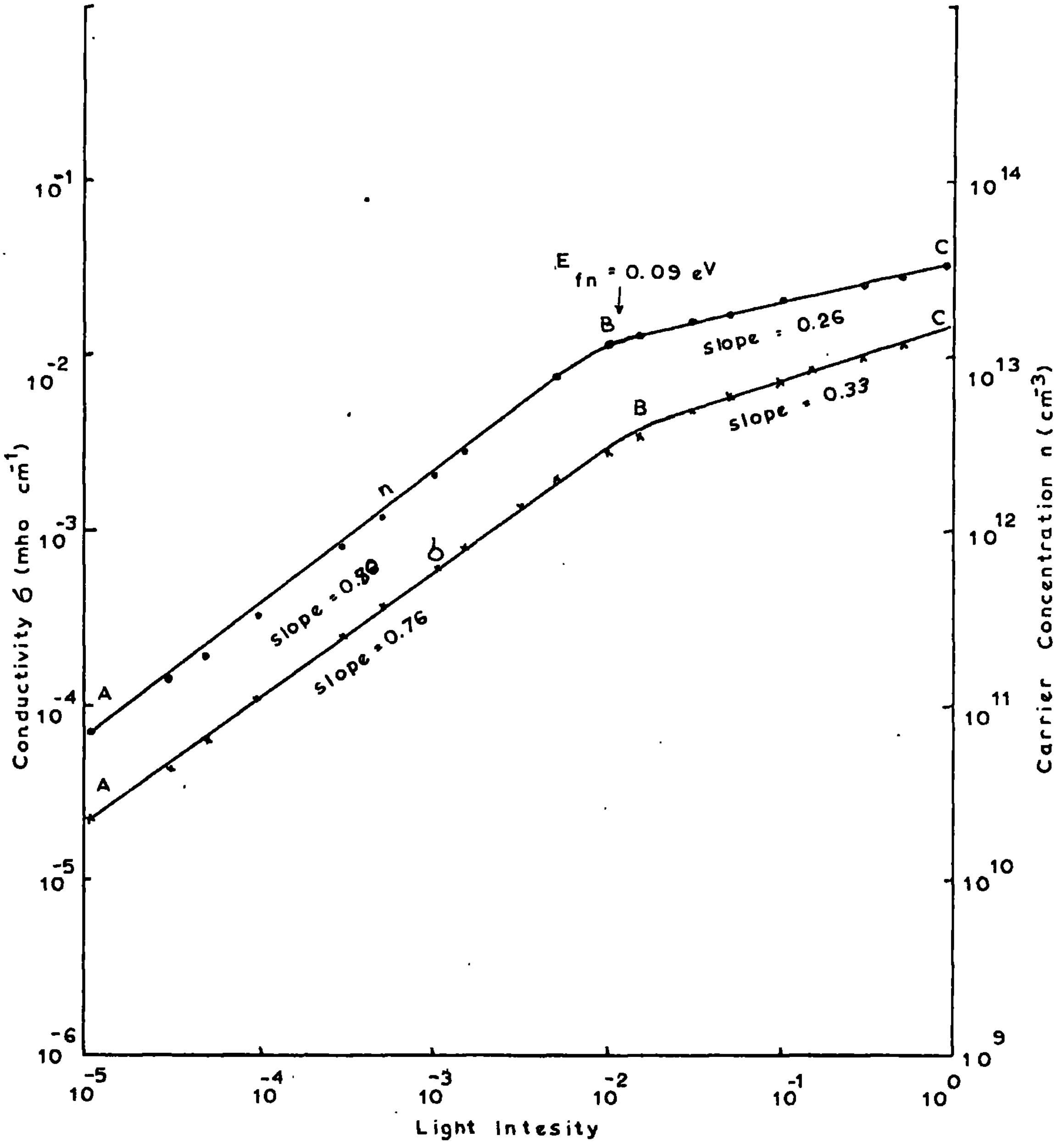

Fig. 6.10. Variation of carrier concentration n and conductivity σ with the intensity of photoexcitation L for crystal 79. Measurement was taken when the sample temperature was 98.7°K.

electron lifetime by accelerating the recombination of electrons.

6.8. Conclusions

(i) Validity of PhotoHall and T.S.C. methods

The application of photoHall measurements to the determination of the various parameters related to trapping levels is based on the concept of quasi Fermi levels. When the equilibrium carrier concentration is disturbed for example, by irradiating the sample with light which generates free electrons and holes, the single thermal equilibrium Fermi level is replaced by two steady-state Fermi levels known as quasi Fermi levels, one for electrons and one for holes (see Section 1-2.3). The steady-state Fermi level essentially describes the occupancy of the levels lying between the corresponding band edge and the Fermi level. The occupancy of the levels lying between the two steady-state Fermi levels is determined by the recombination processes.

Bube applied a Fermi level method of analysing thermally stimulated current curves by assuming that the Fermi level is located at the trapping level when the conductivity is a maximum.(7) A Fermi level method of analysis requires a steady-state condition as in photoHall measurements. Since the T.S.C. type of measurement (see Section 2-7) is done under non-steady state conditions, Fermi level analysis of the T.S.C. curves is only valid for fast retrapping which is a quasi steady-state. Under fast retrapping, steady-state conditions exist because the defect levels are at all times in thermal equilibrium with the conduction band.

Boer et al.[8] consider a two level scheme with emptying traps and recombination centres which have a much lower probability of capture of the free electrons than the trapping levels. They show that

$$E_{Bor} = kT^{*} \log \frac{N_C}{n^{*}} \frac{\eta}{1-\eta} \qquad (6.11)$$

where n^{*} is the density of the electrons in the conduction band when the stimulated current reaches a maximum and η is the fraction of filled traps at the corresponding temperature T^{*}. Bube assumes that the defect levels are approximately half full at the current maximum. This is equivalent to requiring that at the current maximum, the electron Fermi level coincides with the defect levels i.e. that the occupancy at the maximum current η is one half. With this assumption, equation (6.11) reduces to

$$E_B = kT^{*} \log \frac{N_C}{n^{*}} \qquad (6.12)$$

Equation (6.12) has been found to be a good approximation for very fast retrapping but gives incorrect results for slow retrapping. Boer et al.[8] showed that the occupancy at the peak maximum is less than 1/2 and is of the order of 1/10 to 1/100. Nicholas and Woods[3] showed that the analysis of trap depths from the T.S.C. curves (traps at 0·05 eV, 0·14 eV and 0·25 eV) using equation (6.12) leads to values of energy depths which are consistently too large (see also Table 11.1 of reference (9)).

The depths of the traps in crystals 78 and 79 which were presented earlier have been determined from an analysis of thermally stimulated current data, on the assumption that retrapping is negligible.

The validity of the assumption can be tested in a variety of ways (M.A. Carter, Ph.D.Thesis). In fact, the calculation of trap depths from the plot of $\frac{1}{\mu}$ versus E_{fn} for crystal 78 shows very good agreement with the thermally stimulated current measurements and reinforces our belief in the validity of the assumptions made both in the evaluation of photoHall and T.S.C. data.

(ii) Incidence of traps in different crystals

Crystals 78 and 79 were grown under nominally identical conditions (see Section 6-1). Both crystals therefore should have identical trapping spectra. A comparison of the traps identified in crystals 78 and 79 is shown in Table 6.4. PhotoHall measurements were successfully applied to investigate trapping levels in the region from 0·09 eV to 0·43 eV and from 0·08 eV to 0·46 eV below the conduction band for crystals 78 and 79 respectively. The traps with energy depths of 0·13, 0·25 and 0·33 eV were found to exist in both samples (Table 6.4). It had been hoped to extend the measurements to crystals grown in a variety of partial pressures of sulphur and cadmium to study the incidence of particular traps, but time has been too short to permit this to be done.

(iii) Limitation of the PhotoHall method

The evaluation of trap depths by the application of photoHall measurements is only possible for traps with low energies (< 0·5 eV). In applying this method to a deeper level, a number of experimental difficulties will arise. Suppose, there exists an electron

Table 6.4. A comparison of trap depths for crystals 78 and 79

Crystal 78		Crystal 79	
Trap depth from the mobility effect, in eV.	Trap depth from thermally stimulated current measurement, in eV.	Trap depth from the mobility effect, in eV.	Trap depth from thermally stimulated current measurement, in eV.
0·115 (~ 0·12)	0·12	0·098	0·10
0·16	0·15	0·13	0·13
0·22	0·22		0·16
0·33	0·34	0·19	
		0·25	
		0·33	
		0·42	
			0·60

trapping level in the forbidden gap some 0·60 eV below the conduction band. At room temperature, the carrier concentration corresponding to the location of the steady-state Fermi level at 0·60 eV is $2{\cdot}04 \times 10^{8}$ cm^{-3}. The corresponding value of conductivity would be $3{\cdot}26 \times 10^{-9}$ mho cm^{-1} for a value of Hall mobility 100 cm^2/volt-sec. The measurement of the photoHall effect would be very difficult because a small voltage would have to be measured at high impedance.

The problem of impedance may be overcome by increasing the temperature which will cause the Fermi level to move away from the band edge. To evaluate the trap depth of a level at 0·60 eV from an "S-shaped" curve which results from the plot of $\frac{1}{\mu}$ versus E_{fn}, it might be possible to make the photoHall measurements at 450°K with a carrier concentration of 10^{13} cm^{-3}, say, under conditions of maximum intensity of illumination. The corresponding location of the steady-state electron Fermi level at 450°K would then be 0·50 eV and at lower light intensities E_{fn} would pass this value. At this temperature for E_{fn} = 0·50 eV and $S_p/S_n = 10^8$ (see Chapter 7 for the value of S_p/S_n), the corresponding location of the hole demarcation level E_{dp} $(= E_{fn} + kT \ln S_p/S_n)$ would be 1·21 eV above the valence band. If the height of the Class II sensitizing centres is taken equal to 1·1 eV[6], then the hole demarcation level would lie above the Class II sensitizing centres. This would quench the photocurrent and prohibit the successful measurement of the photoHall effect.

(iv) Comparison with other workers

PhotoHall measurements have also been made successfully on photosensitive insulating crystals of cadmium sulphide by Bube et al.[2] Their results summarised in Table 6.5, show three trapping levels with depths of 0·35, 0·46 and 0·54 eV (column 2 of Table 6.5) which were obtained from the stepwise variation of $\frac{1}{\mu}$ versus E_{fn} (Figure 7 of reference (2)). In their calculations Bube et al. assumed an electron effective mass $m_e^* = 0 \cdot 4$ m. A recalculation of their results using $m_e^* = 0 \cdot 2$ m, the correct value, yields trap depths of 0·32, 0·43 and 0·51 eV. Two of these levels at 0·33 and 0·41 eV coincide with those obtained from photoHall measurements reported here on crystals 78 and 79 (Table 6.4).

(v) Uniformity of Samples and Giant scattering centres

The photoHall data can also be used to determine both the charge state and the scattering cross-section of the imperfection centres. The scattering cross-section is the effective area offered by an individual imperfection centre to deflect the course of the conduction electrons. Bube et al.[2] found from their photoHall measurements that all the calculated scattering cross-sections were of the order of 10^{-10} cm^2 or about 10^2 times larger than expected value from simple theoretical calculations. This large scattering effect was attributed to the removal of the charge on inhomogeneously distributed scattering imperfection centres by photoexcitation. Weisberg[10] has shown that an inhomogeneous distribution of charged imperfections can lead to a so-called giant scattering cross-section per defect which is two orders of magnitude greater than that of a Coulombic centre.

The calculation of scattering cross-sections from the data reported here shows that their magnitude is of the order of 10^{-11} cm^2.

Table 6.5. Summary of the imperfection scattering parameters reported by Bube et al[2]

Trap depth from mobility effect, eV	Trap depth from thermally stimulated current, eV	Density from thermally stimulated current, cm^{-3}	Sum of scattering cross-sections, $(S_+ + S_r)$, cm^2
	0·20	$2 \cdot 2 \times 10^{15}$	
	0·25	$9 \cdot 1 \times 10^{15}$	
0·35	0·40	10^{15}	4×10^{-10}
0·46	0·46	$3 \cdot 0 \times 10^{15}$	$1 \cdot 1 \times 10^{-10}$
0·54	0·55	$3 \cdot 3 \times 10^{15}$	$0 \cdot 8 \times 10^{-10}$

This can be considered reasonably close to the expected values from theoretical calculations. A good agreement between the calculated and theoretically expected values of scattering cross-sections can therefore be taken to imply a high degree of uniformity in the resistivity of the crystal and a homogeneous distribution of imperfection centres.

When the imperfection centres are inhomogeneously dispersed, the resistivity in the case of photosensitive insulating crystals can vary markedly from region to region in the dark. According to Weisberg, this fluctuation in resistivity will form localized "space-charge" regions. Photoexcitation erases the inhomogeneities by reducing the space-charge region but a comparatively larger effect will be found in the variation of Hall mobility. A mapping of potential distribution to check the uniformity in resistivity of all samples has been made along the current axis at room temperature using a voltage probe and a micromanipulator. The measurement was made for the worst possible condition i.e. when the intensity of photoexcitation was of the order of 10^{-4} and 10^{-5} of the original light intensity. The potential distribution as a function of distance is illustrated in Figures 6.11(a) and (b) and indicates excellent uniformity of both samples.

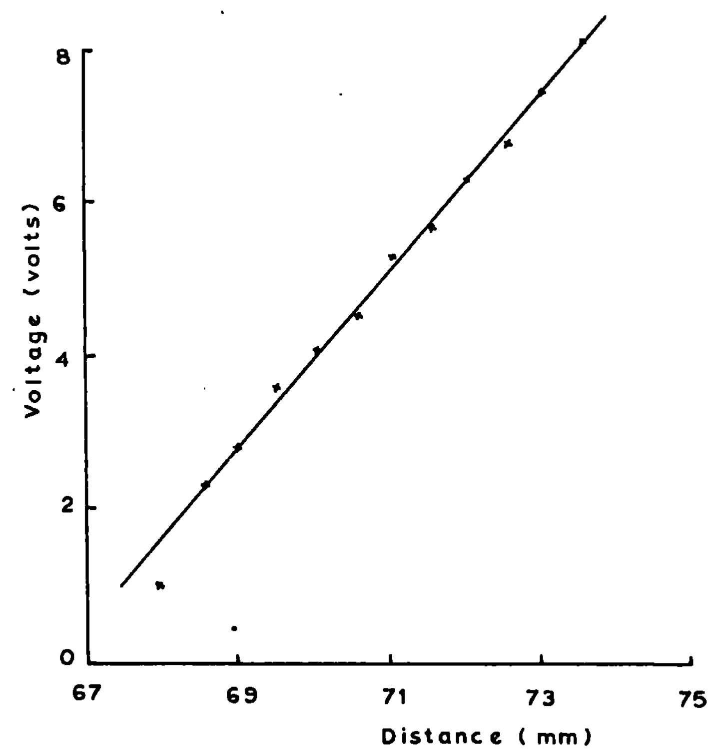

Fig. 6.11(a). Mapping of potential distribution along the current axis for crystal 78. Intensity of photoexcitation was of the order of 10^{-4} of the original light intensity.

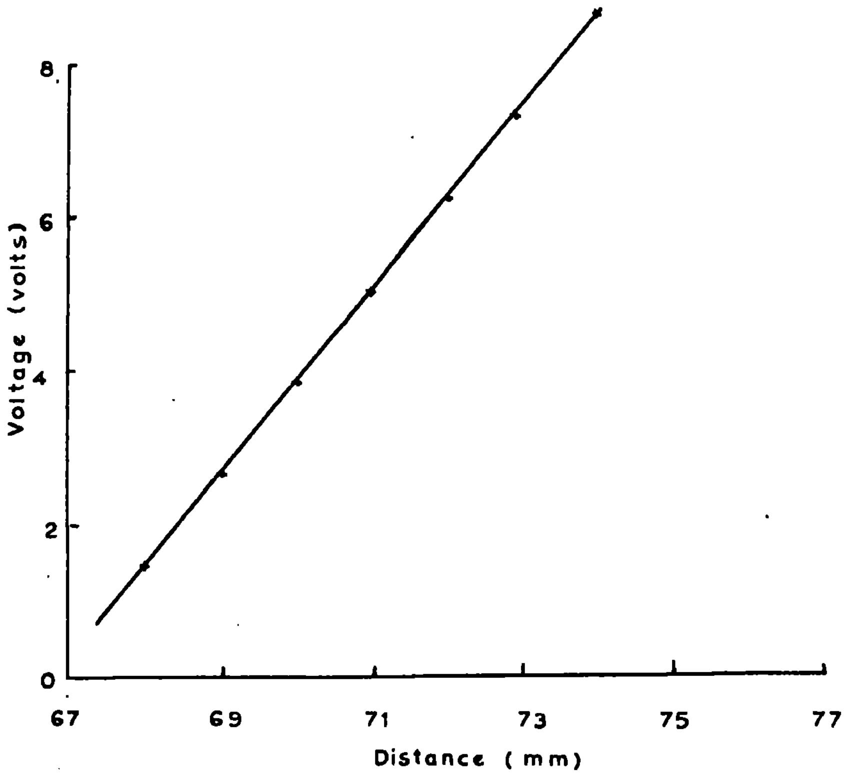

Fig. 6.11(b). Mapping of potential distribution along the current axis for crystal 79. Intensity of photoexcitation was of the order of 10^{-5} of the original light intensity.

References

(1) L. Clark and J. Woods, J.Crystal Growth, 1968.

(2) R.H. Bube and H.E. MacDonald, Phys.Rev., 121, 473, 1961.

(3) K.H. Nicholas and J. Woods, Brit.J.Appl.Phys., 15, 783, 1964.

(4) M.A. Carter is a research student of this department.

(5) R.H. Bube, J.Appl.Phys., 32, 1707, 1961.

(6) R.H. Bube, "Photoconductivity of Solids" John Wiley & Sons Inc. London, 1960, page 353.

(7) R.H. Bube, J.Chem.Phys., 23, 18, 1965.

(8) K.W. Boer, S.Oberlander and J. Voigt, Ann.Phys., 2, 136, 1958.

(9) K.H. Nicholas, Ph.D. Thesis, University of Durham, 1963.

(10) L.R. Weisberg, J.Appl.Phys., 32, 1707, 1961.

CHAPTER 7

TEMPERATURE DEPENDENCE OF PHOTOHALL DATA

7-1. Introduction

The results described in this chapter were also obtained from the photoHall measurements made on crystals 78 and 79. In Section 2-4, we have shown that the presence of Class II centres (known as sensitizing centres) increases the photosensitivity. The technique of photoHall measurements was applied to determine the depth of the sensitizing centres from the top of the valence band. The variations of the Hall mobility and carrier concentration with temperature under constant excitation with the highest light intensity (L = 3200 ft-C) were also measured.

7-2. Thermal quenching of photoconductivity for crystal 78.

To observe the thermal quenching of photoconductivity, photo-Hall measurements were made with increasing temperature at a variety of fixed light intensities on crystal 78. Thermal quenching of photoconductivity (Section 3-2) occurs when the hole demarcation level rises through the class II centres. This occurs when the temperature is increased while the light intensity remains constant. The class II centres are then converted from recombination centres to hole traps. When this process of conversion from recombination centres to hole traps continues, a continuous decrease in the value of the free electron lifetime τ_n occurs. Again a steady value of τ_n which is smaller than the value when the class II centres act as recombination centre, is attained (region A of Figure 3.6) after full conversion of class II centres from recombination centres to hole traps. A change in the value of free electron lifetime τ_n will be reflected in the data of photo-Hall measurements because the total number of photo-generated free electrons in the steady state is given by $n = F\tau_n$ where F is the total rate of generation of free carriers per second. The onset of a decrease in carrier concentration with increasing temperature at constant light intensity occurs when the hole demarcation level associated with the class II centres is located at the energetic position of these levels.

The variation of carrier concentration with increasing temperature at different fixed light intensities for crystal 78 is illustrated by the set of curves in Figure 7.1. The breakpoint corresponding

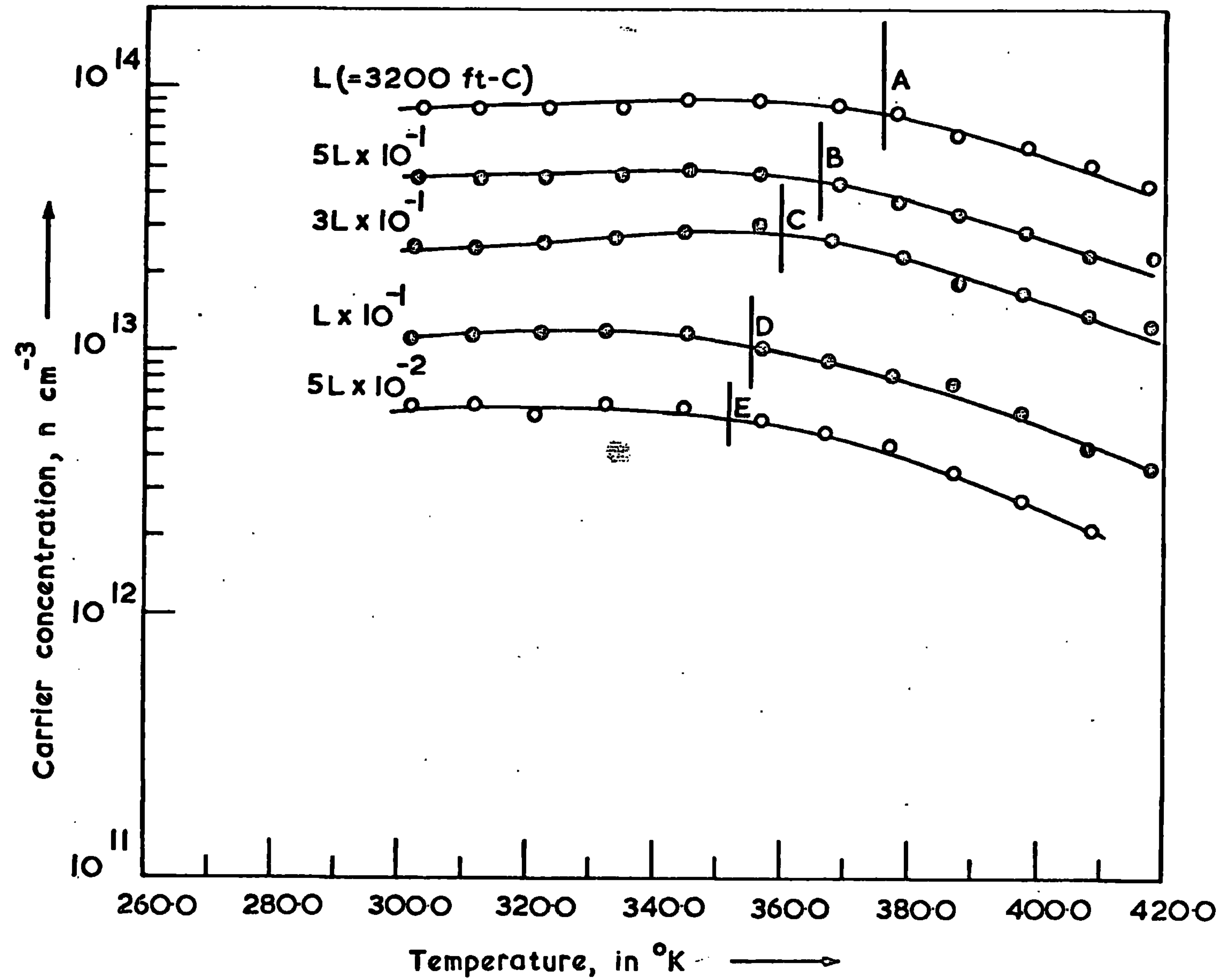

Fig. 7·1. Variation of carrier concentration as a function of temperature at different fixed light intensities for crystal 78.

to the onset of a decrease in carrier concentration with increasing temperature was evident in all the curves in Figure 7.1 at A, B, C, D and E. A plot of $\ln n$ at the breakpoints, as a function of $1/T$, at which those breakpoints occurred, is shown in Figure 7.2. From the slope of the straight line (Figure 7.2) which is equal to E_I/k according to the theory discussed in Section 3-2, a value of E_I, the height of the sensitizing centres above the valence band was found to be 1·02 eV. This is in good agreement with the value of 1·1 eV found (for the position of the sensitizing centres above the valence band) from the measurements of optical and thermal quenching of photoconductivity by Bube[1] and others.[2], [3], [4]

A plot of the values of E_{fn} at the breakpoints in Figure 7.1 as a function of temperature is also shown in Figure 7.3. A straight line is expected to be obtained from such a plot because the electron Fermi level E_{fn} at the breakpoint is related to the hole demarcation level E_{dp} by the relation

$$E_{fn} = kT\ln(S_p/S_n)-E_{dp} \tag{7.1}$$

The slope of the straight line from such a plot should be equal to $-k\ln(S_p/S_n)$ and the intercept at T = 0 to E_I. Accordingly, a straight line, drawn only through four points, was obtained in Figure 7.3. The value of S_p/S_n was found to be $2{\cdot}07 \times 10^8$ and that of E_I was 1·04 eV. The value of E_I as 1·04 eV is in fair agreement with the value of E_I(~1·02 eV) obtained from the slope of the straight line in Figure 7.2.

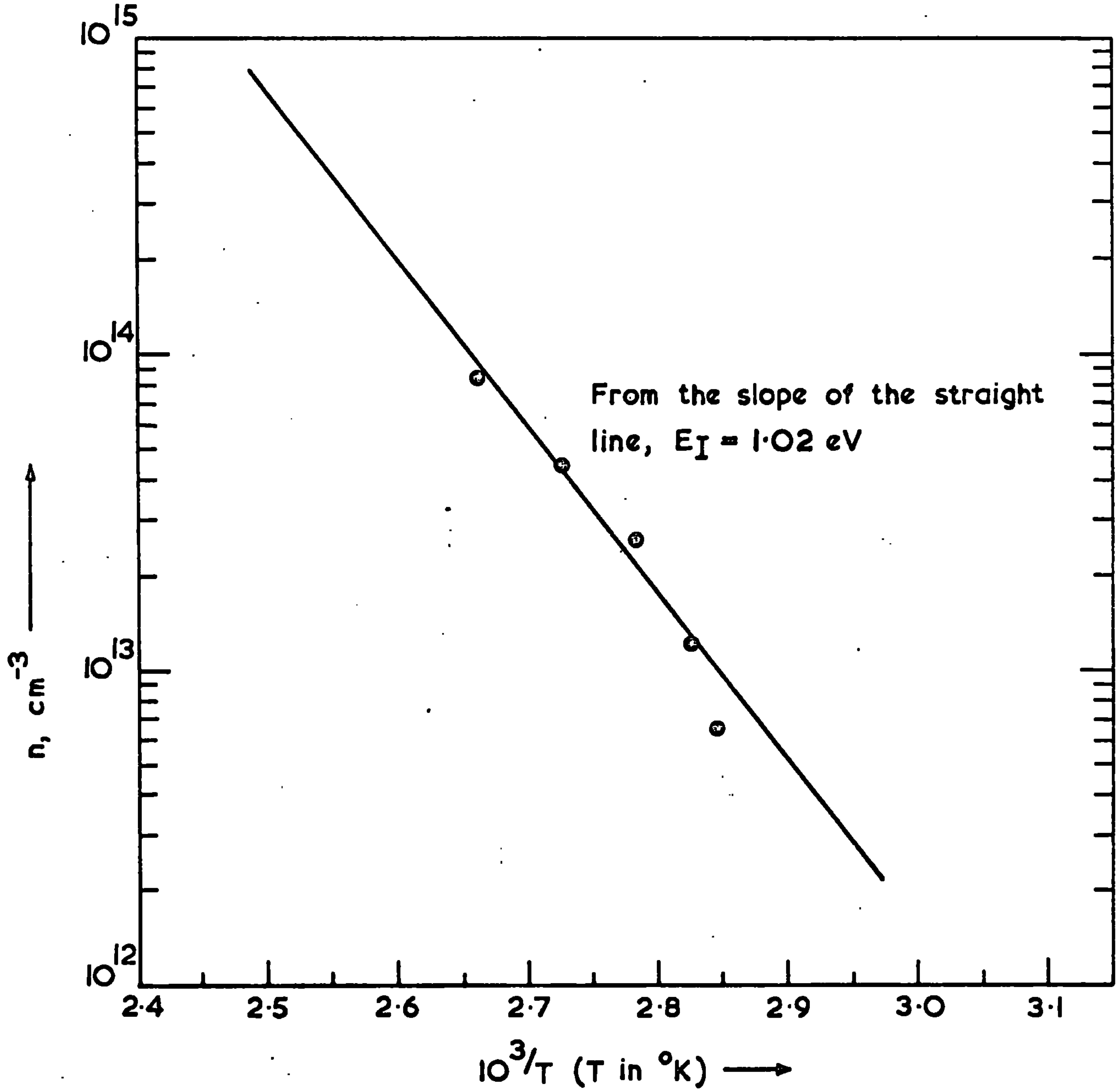

Fig. 7·2. A plot of ln n at the breakpoints A,B,C,D and E of Fig. 7·1 as a function of reciprocal temperature.

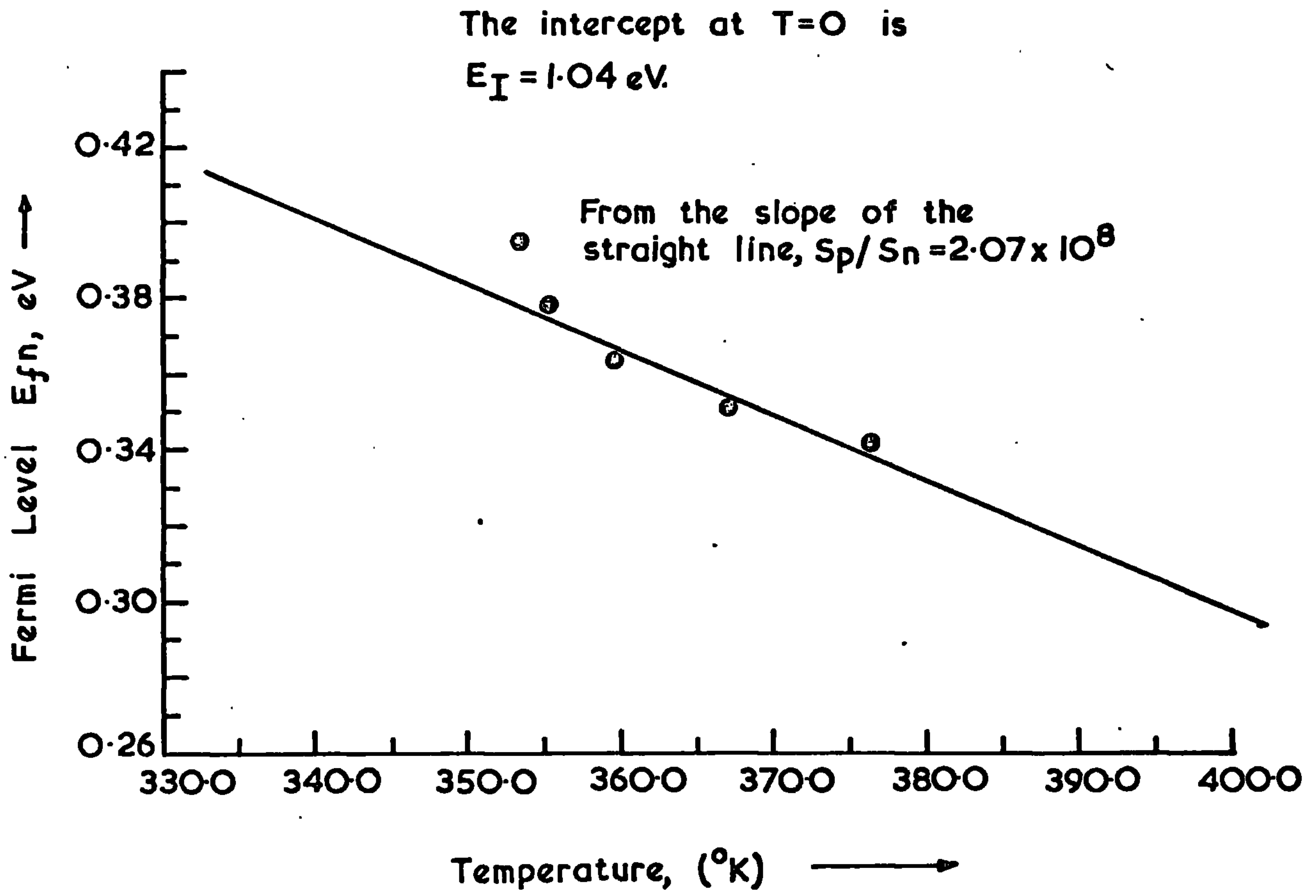

Fig. 7·3. A plot of E_{fn} at the break points A,B,C,D and E of Fig. 7·1 as a function of temperature.

The value of $S_p/S_n (\sim 2{\cdot}07 \times 10^8)$ agrees with the value of $S_p/S_n (\sim 4 \times 10^8)$ obtained by Bube.[4] Bube attributed the high value of $S_p/S_n (\sim 4{\cdot}0 \times 10^8)$ to doubly negatively charged sensitizing centres. Crystals 78 and 79 were as grown crystals. Cadmium vacancies would be expected to be present and act as sensitizing centres in this type of photosensitive insulating crystal. Since CdS is a divalent compound, cadmium vacancies are likely to be doubly negatively charged.

From the known values of E_{fn} at the breakpoints in Figure 7.1, the corresponding height of the hole demarcation level E_{dp} was also calculated by using the relation $E_{dp} = E_{fn} + kT\ln(S_p/S_n)$ for four values of S_p/S_n namely 10^5, 10^6, 10^7 and 10^8. The calculated values of E_{dp} are presented in Table 7.1. If the hole ionization energy of the sensitizing centres in cadmium sulphide is taken to be 1·1 eV above the valence band, then the calculated values of E_{dp} at the breakpoints in Figure 7.1 were found near to 1·1 eV (Table 7.1) when $S_p/S_n = 10^8$.

7-3. Thermal quenching of photoconductivity for crystal 79.

The variation of the carrier concentration with increasing temperature at different fixed light intensities is illustrated by the curves in Figure 7.4. All these curves except the bottom one in Figure 7.4 showed a decrease in carrier concentration with increasing temperature. However the breakpoints were not so well defined as in Figure 7.1. By taking the points marked by F,G,H,I,J,K,L and M as breakpoints, attempts were made to determine the values of E_I and S_p/S_n as was done in the previous section.

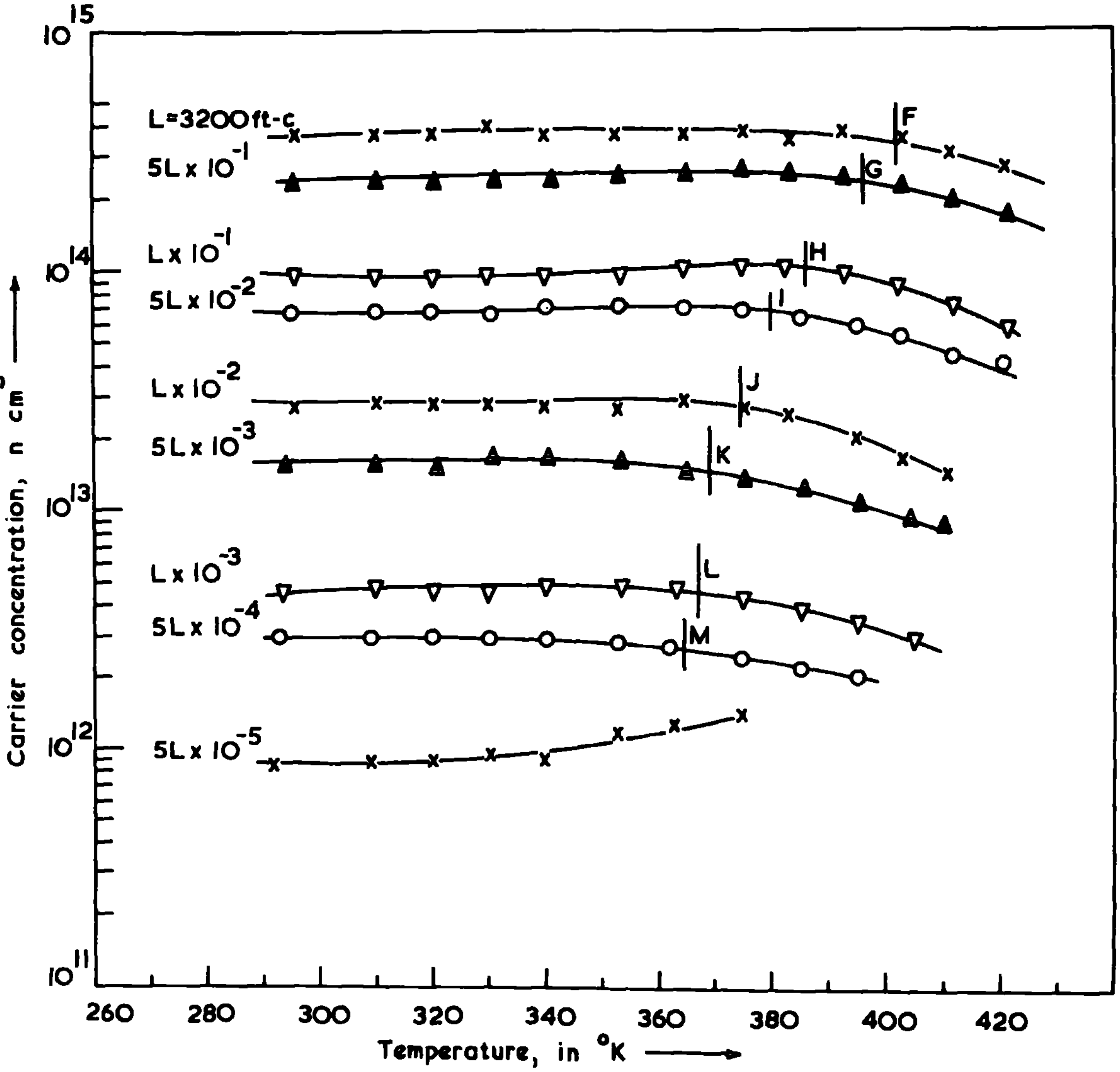

Fig. 7·4 Variation of carrier concentration as a function of temperature at different fixed light intensities for crystal 79.

Table 7.1. Calculation of the location of hole demarcation level E_{dp} corresponding to the breaks A,B,C,D and E of Figure 7.1

Intensity of photo-excitation	Breakpoint	E_{fn} at the breakpoint, eV	$E_{dp} = E_{fn} + kT \ln S_p/S_n$			
			$S_p/S_n = 10^5$	$S_p/S_n = 10^6$	$S_p/S_n = 10^7$	$S_p/S_n = 10^8$
L (=3200 ft-C)	A	0·340eV	0·72eV	0·79eV	0·86eV	0·94eV
$5L \times 10^{-1}$	B	0·350eV	0·72eV	0·79eV	0·86eV	0·93eV
$3L \times 10^{-1}$	C	0·363eV	0·72eV	0·79eV	0·86eV	0·93eV
$L \times 10^{-1}$	D	0·378eV	0·73eV	0·80eV	0·87eV	0·94eV
$5L \times 10^{-2}$	E	0·395 eV	0·75eV	0·82eV	0·89eV	0·96eV

A plot of lnn at the breakpoints marked by F,G,H,I,J,K,L and M in Figure 7.4, as a function 1/T is shown in Figure 7.5. A twofold linear dependence was found. The values of E_I calculated from the slopes of the straight lines YZ and XY in Figure 7.5 were found to be 0·99 eV and 2·34 eV respectively. The value of E_I of 0·99 eV is within 5% agreement with the value of 1·03 eV (a mean value of 1·02 eV and 1·04 eV) obtained in the previous section for crystal 78. The value of E_I as 2·34 eV, which seems close to the value of the energy band gap (2·4 eV) for CdS, cannot be explained at present by any known theory.

Figure 7.6 shows a plot of E_{fn} at the breakpoints in Figure 7.4 as a function of temperature. A twofold linear dependence was also found in this case. The slope of the straight line YZ in Figure 7.6 gave a value of S_p/S_n of $7{\cdot}78 \times 10^7$ while the intercept of the straight line at T = 0 was 0·98 eV. The intercept of the second straight line XY (in Figure 7.6) at T = 0 was 2·38 eV.

The values of S_p/S_n($\sim 7{\cdot}78 \times 10^7$) and E_I($\sim$ 0·98 eV) obtained from the straight line YZ in Figure 7.6 are in agreement with the values of S_p/S_n ($\sim 2{\cdot}07 \times 10^8$) and E_I ($\sim$ 1·03 eV, a mean value of 1·02 eV and 1·04 eV) obtained for crystal 78. These values are also in agreement with the values ($E_I \sim 1{\cdot}1$ eV and $S_p/S_n \sim 4 \times 10^8$) obtained by Bube.[4] From the known values of E_{fn} at the breakpoints in Figure 7.4, the corresponding values of the hole demarcation level E_{dp} were calculated for four values of S_p/S_n as 10^5, 10^6, 10^7 and 10^8 (Table 7.2). It was also found that the calculated values of E_{dp} were near to 1·1 eV when S_p/S_n was taken to be 10^8(Table 7.2).

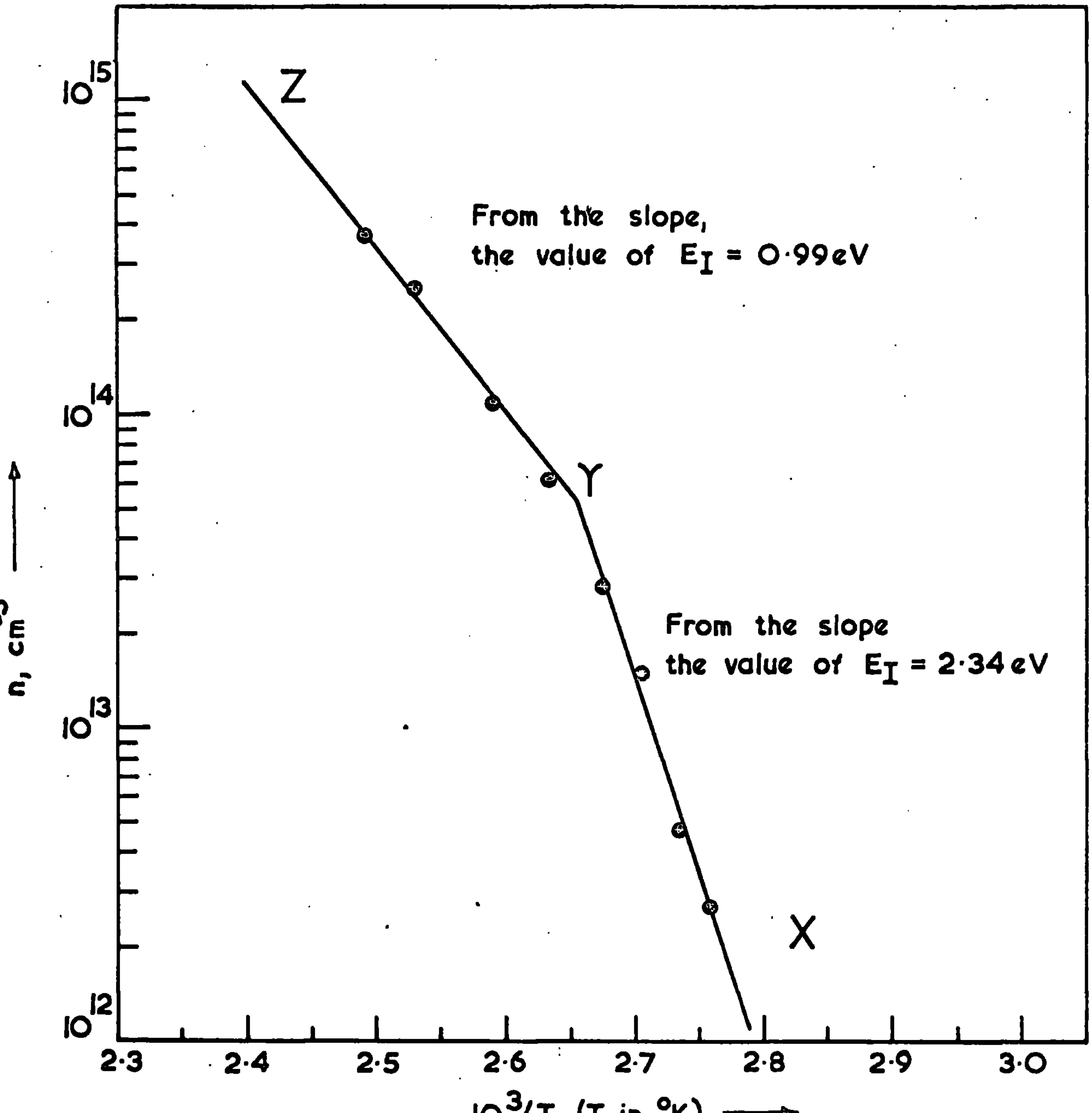

Fig. 7·5. A plot of ln n at the breakpoints F,G,H,I,J,K,L and M of Fig. 7·4. as a function of reciprocal temperature.

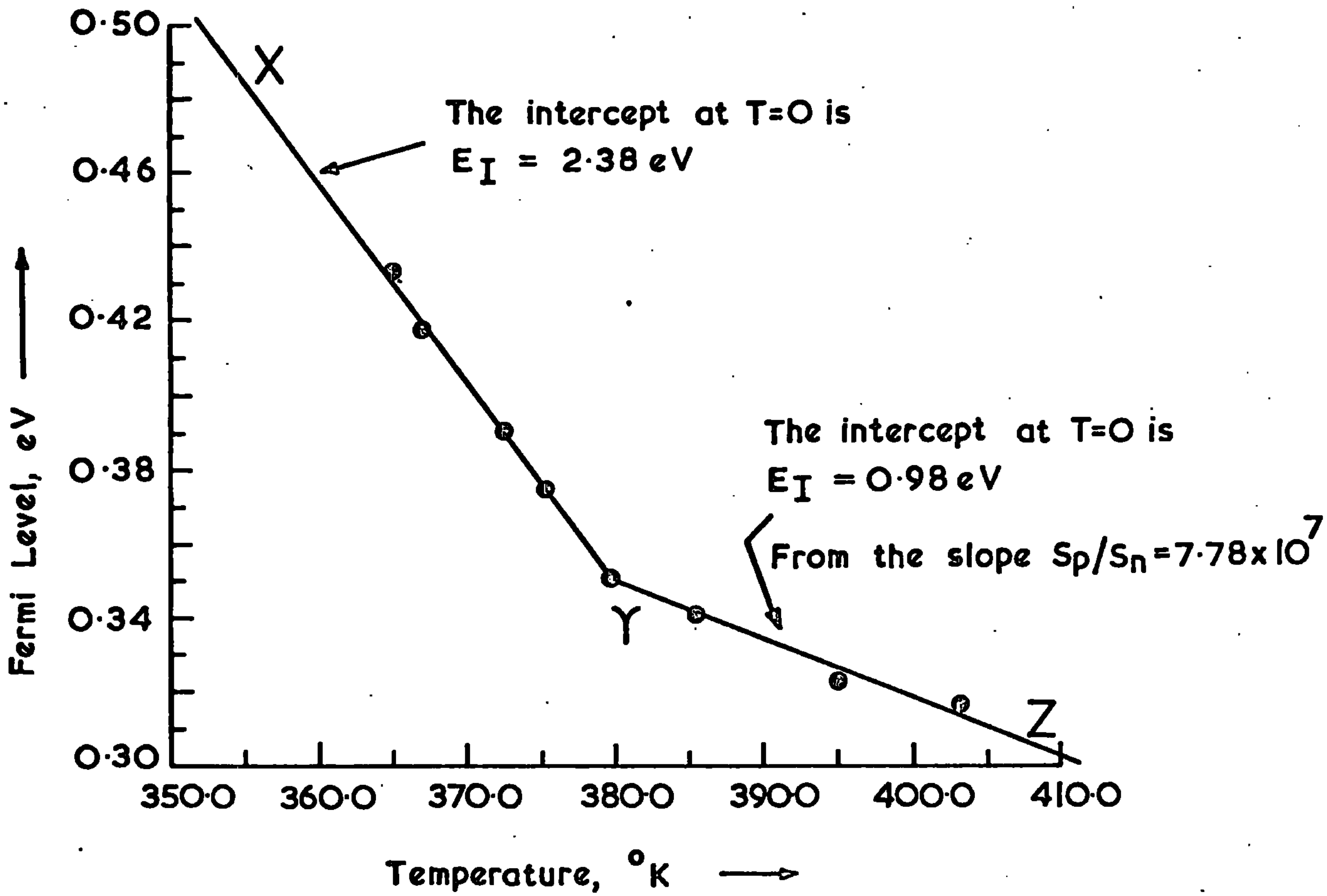

Fig. 7·6 A plot of E_{fn} at the breakpoints F,G,H,I,J,K,L, and M of fig. 7·4 as a function of temperature.

Table 7.2. Calculation of the location of hole demarcation level E_{dp} corresponding to the breaks of Figure 7.4

Intensity of photo-excitation	Breakpoint	E_{fn} at the breakpoint, eV	$E_{dp} = E_{fn} + kT\ln S_p/S_n$ when			
			$S_p/S_n = 10^5$	$S_p/S_n = 10^6$	$S_p/S_n = 10^7$	$S_p/S_n = 10^8$
L(=3200 ft-C)	F	0·317	0·72eV	0·80 eV	0·88eV	0·96eV
$5L \times 10^{-1}$	G	0·322	0·71eV	0·78eV	0·87eV	0·95eV
$L \times 10^{-1}$	H	0·340	0·72eV	0·80eV	0·87eV	0·95eV
$5L \times 10^{-2}$	I	0·350	0·73eV	0·79eV	0·87eV	0·95eV
$L \times 10^{-2}$	J	0·375	0·74eV	0·81eV	0·89eV	0·97eV
$5L \times 10^{-3}$	K	0·390	0·74eV	0·83eV	0·91eV	0·98eV
$L \times 10^{-3}$	L	0·417	0·75eV	0·85eV	0·92eV	1·000eV
$5L \times 10^{-4}$	M	0·432	0·77eV	0·86eV	0·94eV	1·02eV

According to the model put forward by Bube (Section 3-2), the condition for the breakpoint which corresponds to the onset of superlinearity or thermal quenching of photoconductivity is that

$$\ln n = \ln(N_v\, S_p/S_n) - E_I/kT \tag{3.9}$$

Equation (3.9) does not predict the possibility of a twofold linear dependence as shown in Figure 7.5. There was also some indication of twofold linear dependence in Figure 7.2 where a straight line was drawn through four points only.

L. Kindleysides[5] also found a similar twofold linear dependence in one of his CdSe crystals. The upper breakpoints of superlinearity observed in CdSe (Figure 11.2.2 of reference (5)) were plotted in the form of $\ln n$ against $1/T$. The slope of the line at high illumination intensities (high values of n) yielded a value of E_I of 0·58 eV. This value is in excellent agreement with value of 0·6 eV found by Bube.[6] The slope of the line at low light intensities yielded an energy of 1·13 eV. Kindleysides assumed that this value of 1·13 eV might be associated with the new Class I centres which were created photochemically when the sample was cooled from 400°K under continuous photoexcitation.

It appears therefore that equation (3.9) may not be adequate to explain such a breakpoint at low intensities. However, before drawing any conclusion about the possible cause of twofold linear dependence further work is required on a number of photosensitive insulating crystals of CdS.

7-4. Variation of Hall mobility with temperature under constant photoexcitation for crystals 78 and 79.

The variation of Hall mobility with temperature under constant photoexcitation using the highest light level available (L = 3200 ft-C) is presented in Figures 7.7 and 7.8 for crystals 78 and 79 respectively. Hall mobility for crystal 78 was measured from $36^{\circ}K$ to $300^{\circ}K$. For crystal 79, Hall mobility measurements were made from $80^{\circ}K$ to $300^{\circ}K$ only.

In the case of crystal 78, the Hall mobility could be described by the relation $\mu_H = 5{\cdot}67 \times 10^7 T^{-2{\cdot}2}$ from $300^{\circ}K$ to $90^{\circ}K$ and by $\mu_H = 2{\cdot}43 T^{1{\cdot}5}$ from $90^{\circ}K$ to $36^{\circ}K$ (Figure 7.7). For crystal 79, the dependence of Hall mobility on temperature from $300^{\circ}K$ to $80^{\circ}K$ was $\mu_H = 1{\cdot}49 \times 10^7 T^{-1{\cdot}92}$ (Figure 7.8). From $300^{\circ}K$ to $90^{\circ}K$ Hall effect measurements on crystal 78 under constant photoexcitation using an intensity of light 1000 ft-C was also made by M.N. Islam.(7) The dependence of Hall mobility on temperature found from his measurements was $\mu_H = 1{\cdot}5 \times 10^7 T^{-1{\cdot}91}$.

The relation $\mu_H = 2{\cdot}43 T^{1{\cdot}5}$ (Figure 7.7) indicated that the photoHall mobility at low temperature under constant photoexcitation was limited by ionized impurities. A dependence of photoHall mobility on temperature varying approximately as $\mu_H \propto T^{-2{\cdot}0}$ in the temperature range from $300^{\circ}K$ to $90^{\circ}K$ (Figures 7.7 and 7.8) is difficult to explain by any particular scattering mechanism. A combination of scattering mechanisms due to lattice vibrations and the change of nature of the scattering centres on photoexcitation might give a $T^{-2{\cdot}0}$ law dependence.

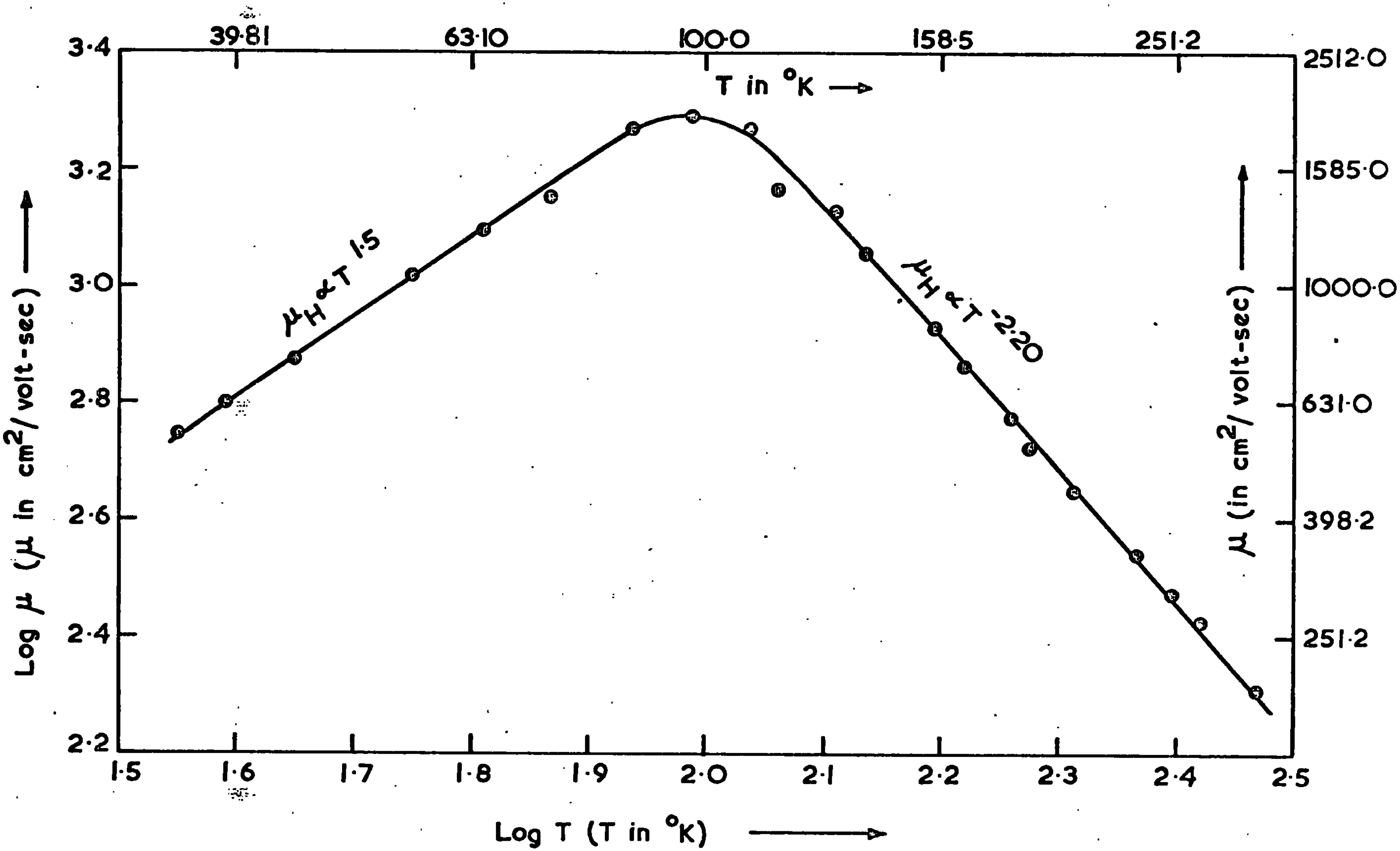

Fig. 7·7 Variation of Hall mobility with temperature for crystal 78 under constant photoexcitation of highest light level (L = 3200 ft. c)

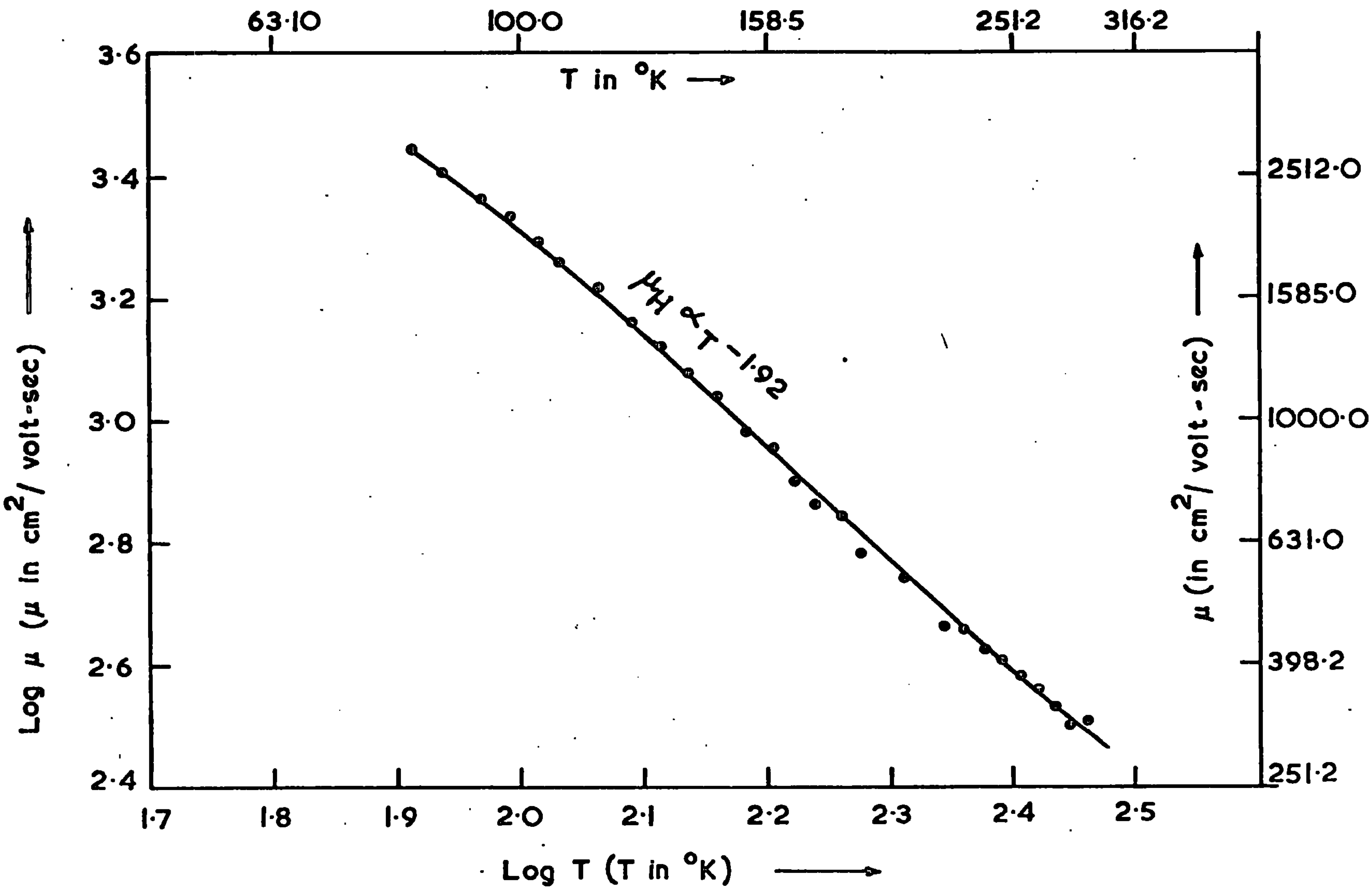

Fig. 7·8. Variation of Hall mobility with temperature for crystal 79 under constant photoexcitation of highest light level (L=3200 ft-C)

7-4. Variation of carrier concentration at low temperatures under constant photoexcitation.

The variation of carrier concentration with temperature under constant photoexcitation at the highest light level (L = 3200 ft-C) is presented for crystals 78 and 79 in Figures 7.9 and 7.10 respectively. The curve in Figure 7.9 shows that the carrier concentration remained constant down to 145.0°K and then started to decrease. Again at very low temperature from 80°K to 36°K it remained constant. A decrease in carrier concentration at temperatures below 160°K was also observed for crystal 79 (Figure 7.10). In the case of crystal 79, measurements were limited to a lower temperature 82°K.

In a semiconductor, as the temperature is lowered, the electrons from the conduction band begin to freeze out into the donor levels. A decrease in carrier concentration with decreasing temperature therefore is to be expected in a semiconductor. In photosensitive insulators, a decrease in carrier concentration with decreasing temperature under constant photoexcitation is expected to be dominated by recombination processes. To interpret the data presented in Figures 7.9 and 7.10, a qualitative explanation was developed using information on the quenching of edge emission (See Section 2-5a).

Efforts were made to calculate the location of the hole Fermi level E_{fp} corresponding to point A in Figure 7.9 by using the relation[8]

$$E_{fp} = E_{fn} + kT\ln\{ (m_h^*/m_e^*)^{3/2} \tau_n/\tau_p \} \qquad (7.2)$$

where τ_n and τ_p are the free carrier lifetimes for electrons and holes respectively. Equation (7.2) involves the unknown parameters τ_n and τ_p. The electron lifetime τ_n in a photosensitive insulating crystal of CdS is

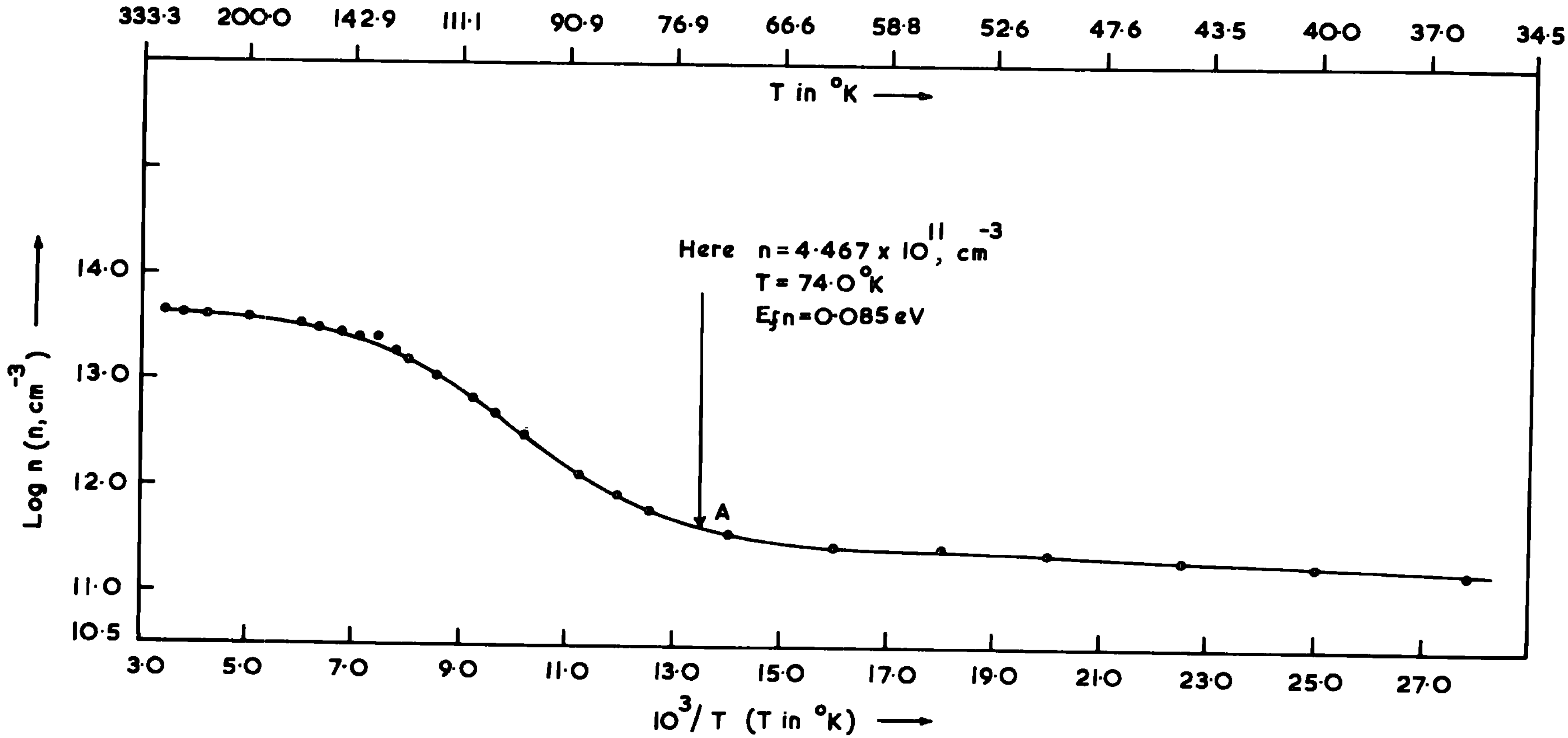

Fig. 7·9. Variation of carrier concentration with temperature for crystal 78 under constant photoexcitation of highest light level (L = 3200 ft-c)

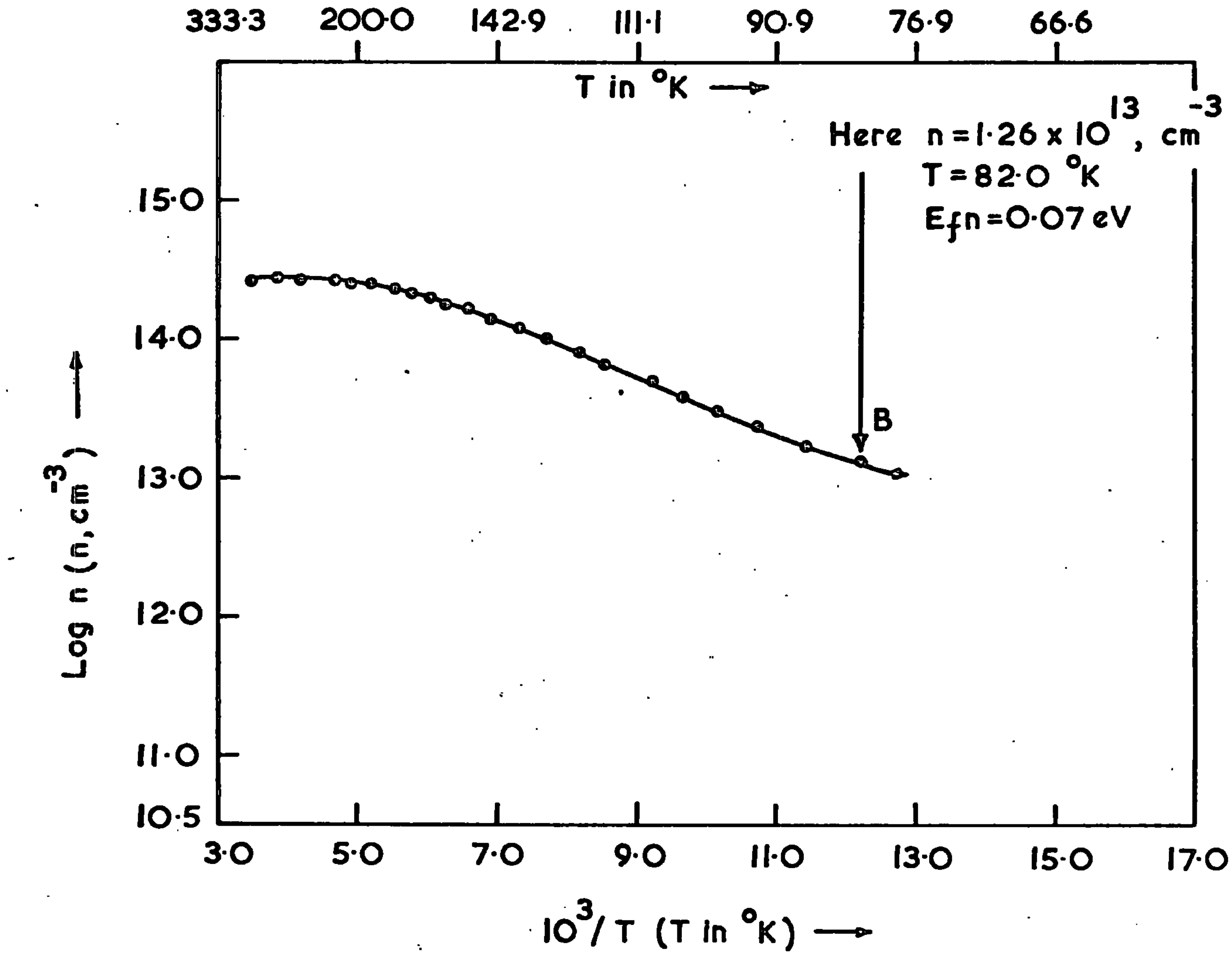

Fig. 7·10. Variation of carrier concentration with temperature for crystal 79 under constant photoexcitation of highest light level (L = 3200 ft-c) considered to be in the range of 10^{-2} to 10^{-3} second while hole lifetimes are typically shorter than 10^{-8} second.[9] Assuming $m_h^*/m_e^* = 3{\cdot}5$ (see Section 2-3) and $\tau_n/\tau_p = 10^5$, the value of E_{fp} at A in Figure 7.9 was found to be 0·17 eV. The value of E_{fp} at B in Figure 7.10 was also found to be 0·17 eV.

Edge emission is thought to be due to recombination of a free carrier with a trapped carrier of opposite sign. Most investigators[10-12] believe that a defect level some 0·15 eV from a band edge is responsible for edge emission. From a systematic investigation of photoconductive, transport and luminescent properties in the temperature range between 77°K and 130°K on a number of pure and undoped crystals of CdS and the dependence of those properties on heat treatment (350°C), Spear and Bradberry[12] concluded that the luminescent centre responsible for edge emission was a centre of the Class II type situated between 0·13 and 0·15 eV above the valence band.

Spear and Bradberry built up their interpretation primarily on the basis of the observed superlinearity in the curves of electron density n versus photoexcitation density F in conjunction with the temperature dependence of the electron density in the luminescent temperature range from 115°K to 77°K (Figures 4 and 5 of reference (12)). Their photoconductivity measurements showed a pronounced increase of carrier concentration with decreasing temperature in the temperature range between 115°K to 77°K. Thermal quenching of carrier concentration n around 90°K observed by them

(Figure 4 of reference (12)) suggests that the Class II centres predominantly involved here should lie much closer to the valence band. The data presented in Figures 7.9 and 7.10, on the contrary, show a decrease in carrier concentration with decreasing temperature under constant photoexcitation (L = 3200 ft-C).

The increase in carrier concentration with decreasing temperature under constant photoexcitation of highest light level F_{max}(= 4·0 x 10^{18} photons cm^{-3} sec^{-1}) observed by Spear and Bradberry (Figure 4 of reference (12)) might be due to the fact that the density of the deeper Class II centres perhaps did not exceed significantly the density of the other centres. Addition of centres of the Class II type with levels situated between 0·13 eV and 0·15 eV, and with significantly higher density than the deeper Class II centres (lying at a height of 1·1 eV above the valence band), in this condition, would dominate the photoconductivity mechanism and increase the free electron lifetime.

Room temperature measurements on crystals 78 and 79 showed that the conductivity which was less than 10^{-7} mho cm^{-1} in the dark, could be increased to 10^{-2} mho cm^{-1} by using the highest light level available (L = 3200 ft-C). It could be assumed that this large photosensitivity was due to the presence of a high density of deeper Class II centres. If a shallower level of Class II type even of comparable density with the density of deeper Class II level and situated between 0·13 eV and 0·15 eV above the valence band, when added to the deeper Class II level, would take part in the population distribution of hole but would not increase the free electron lifetime. Then the transitions of electrons from the conduction band to this defect level (shallower Class II type centre) would reduce the carrier concentration in the conduction band. This might be the possible mechanism in the reduction of carrier concentration observed in the data presented in Figures 7.9 and 7.10.

The calculated values of E_{fp} at A and B in Figures 7.9 and 7.10 are close to the value of a defect level at 0·15 eV, thought to be responsible for edge emission. Several assumptions regarding the values of m_h^*/m_e^* and τ_n/τ_p were made. If these assumptions were found reasonable, it could be said that a hole trap at or near to 0·15 eV above the valence band was responsible for the observed decrease of carrier concentration (Figures 7.9 and 7.10) at low temperature.

References

(1) R.H. Bube, Phys.Rev., 99, 1105, 1955.

(2) E.A. Taft and M.H. Hebb, J.Opt.Soc.Am., 42, 249, 1952.

(3) R.H. Bube and A.B. Dreeben, Phys.Rev., 115, 1578, 1959.

(4) R.H. Bube, J.Appl.Phys., 32, 1707, 1961.

(5) L. Kindleysides, Ph.D.Thesis, University of Durham, 1969.

(6) R.H. Bube, J.Phys.Chem.Solids, 1, 234, 1957.

(7) M.N. Islam is a research student of this department.

(8) R.H. Bube, "Photoconductivity of Solids", John Wiley and Sons, Inc., 1960, page 55.

(9) A. Rose, "Concepts in Photoconductivity and Allied Problems", John Wiley and Sons, Inc., London, 1963, page 43-44.

(10) G.A. Marlor and J. Woods, Brit.J.Appl.Phys., 16, 797, 1965.

(11) B.A. Kulp and R.H. Kelley, J.Appl.Phys., 31, 1057, 1960.

(12) W.E. Spear and G.W. Bradberry, Phys.Stat.Sol., 8, 649, 1965.

CHAPTER 8

HALL EFFECT MEASUREMENTS ON SEMICONDUCTING SAMPLES OF CADMIUM SULPHIDE

8-1. Introduction

Hall effect measurements were made on a number of semiconducting crystals of cadmium sulphide. The crystals were grown by L.Clark and K.F. Burr. Hall samples of proper dimensions were prepared from large single boule crystals which were grown at a temperature of 1150°C by using the growth technique of Clark and Woods[1] which was described in Chapter 4.

Samples chosen for Hall effect measurements were grown either by using (i) electronic grade powder from Derby Luminescent Ltd. or (ii) British Drug Houses' Optran grade lumps as the starting material. Flow crystals were grown first by the argon flow technique (See Section 4-3.1). Then these flow crystals were used as the starting charge for growing boule crystals. In some cases, the Optran material was used as supplied for growing boule crystals (crystal 107). Crystal 182 was grown from charges to which 1000 p.p.m. by weight of Cu_2S had been added. Mass spectrographic data on crystal 182 show that very little copper was incorporated in the boule (Cu concentration ~0·8 p.p.m.)[2]. To grow crystal 229 doped with chlorine, flow crystals prepared from B.D.H. Optran powder were used as the starting charge to which $CdCl_2$ 1000 p.p.m. by weight was added. The dimensions and the growth parameters of the crystals selected for Hall effect measurements are given in Table 8.1.

Table 8.1. Dimensions and Growth conditions

Sample No. according to growth run	Dimensions (cm^3)	Growth Conditions					
		Description of the charge powder used to grow crystals	Any other material added to the charge powder	Growth temperature (0^oC)	Grown either in excess cadmium or sulphur	Reservoir Temperature (0^oC)	Equivalent partial pressures (Torr)
167	0·84x0·27x0·24	B.D.H. Optran + flow process	-	1150·0	Cadmium	650	180·00
107	0·80x0·21x0·14	B.D.H.Optran	-	1150·0	Cadmium	550	30·00
148	0·89x0·28x0·19	Derby Luminescents Ltd+ flow process	-	1150·0	Cadmium	450	4·5
183	0·80x0·20x0·17	B.D.H. Optran + flow process	-	1150·0	Cadmium	50	10^{-9}
182	0·75x0·23x0·15	B.D.H. Optran + flow process	Cu_2S, 1000 p.p.m. by weight	1150	Sulphur	250	12·0
229	0·90x0·22x0·18	B.D.H. Optran + flow process	$CdCl_2$ 1000 p.p.m. by weight	1100	Cadmium	550	30·0

Only samples with uniform resistivity were used for the Hall effect measurements. The potential distribution along the current axis was determined using a voltage probe and a micromanipulator. The Hall effect measurements were carried out in the helium cryostat described in Section 5.1. The Hall effect measurements were made over the temperature range from 14^{o}K to 300^{o}K for crystals 167 and 182 and from 25^{o}K to 300^{o}K for crystal 183. The temperature range of measurements for crystals 148, 107 and 229 was from 65^{o}K to 300^{o}K only. Hall voltages were measured using a magnetic field of 3·3 kilogauss which was low enough to ensure a linear dependence of Hall voltage on magnetic field. The voltage measurements were made for both directions of sample current and magnetic field. The results were then averaged to eliminate possible errors from thermoelectric or thermomagnetic effects.

The Hall voltage and the voltage dropped across the voltage probes were measured with a Philips valve voltmeter which has two measuring ranges with input impedances of 10^{6} and 10^{8} ohms. Using the range with an input impedance of 10^{6} ohms, D.C. voltages from 10 micro volts to 10 volts can be measured. The range with an input impedance of 10^{8} ohms measures D.C. voltages from 0·1 millivolt to 1000 volts. The room temperature resistivities of the Hall samples chosen were in the range from $3{\cdot}0 \times 10^{-2}$ to 4·0 ohm cm (Table 8.2). At low temperatures as the carriers froze out the resistivities increased. The highest resistivity achieved was 10^{5} ohm cm. in crystal 167 at 14^{o}K. The ranges with

TABLE 8.2

Sample No.	Room Temperature ($300^{o}K$) values of			Range of the temperature variation of carrier concentration chosen to calculate the slope ($=E_D/k$)	Donor ionization energy, E_D, from the slope of the plot of log n vs $10^3/T$ (Slope equal to E_D/k), eV	Donor concentration $N_D(cm^{-3})$	Acceptor concentration ($N_A(cm^{-3})$)	N_D-N_A	Compensation N_A/N_D	N_D/N_A	Relative intensities of I_2/I_1, from edge emission at liquid helium temperature
	Carrier concentration, $n(cm^{-3})$	Conductivity σ (in mho cm^{-1})	Hall mobility μ_H (in cm^2/volt.sec)								
167	$2{\cdot}40 x 10^{16}$	1·31	356·34	50 - 34·0°K	0·029	$2{\cdot}55 x 10^{16}$	$1{\cdot}47 x 10^{15}$	$2{\cdot}40 x 10^{16}$	0·06	17·3	480
107	$9{\cdot}0 x 10^{15}$	$4{\cdot}56 x 10^{-1}$	320·30	75 - 64·0°K	0·021	$1{\cdot}73 x 10^{16}$	$8{\cdot}25 x 10^{15}$	$9{\cdot}10 x 10^{15}$	0·48	2·03	50
148	$4{\cdot}4 x 10^{16}$	2·02	286·93	75 - 64·0°K	0·021	$5{\cdot}88 x 10^{16}$	$1{\cdot}51 x 10^{16}$	$4{\cdot}37 x 10^{16}$	0·27	3·89	
183	$4{\cdot}8 x 10^{15}$	$2{\cdot}41 x 10^{-1}$	333·30	50 - 34·0°K	0·020	$8{\cdot}31 x 10^{15}$	$3{\cdot}52 x 10^{15}$	$4{\cdot}79 x 10^{15}$	0·42	2·36	
182	$4{\cdot}0 x 10^{15}$	$2{\cdot}44 x 10^{-1}$	383·02	57 - 37·0°K	0·020	$7{\cdot}4 x 10^{15}$	$3{\cdot}4 x 10^{15}$	$4{\cdot}0 x 10^{15}$	0·46	2·18	
229	$9{\cdot}40 x 10^{17}$	33·49	224·03	Degenerate							

input impedances of 10^6 and 10^8 ohms were used for Hall effect measurements at higher and lower temperatures respectively.

8-2(a) <u>Variation of carrier concentration with temperature</u>

The variation of carrier concentration n as a function of temperature is shown in Figure 8.1 for the various crystals examined. The carrier concentration was calculated using the expression $n = r/(R_H e)$ where R_H is the Hall coefficient and e is the charge on the electron. The factor 'r' is the ratio of the Hall mobility μ_H to drift mobility μ. The value of 'r' lies between 1 and 2 depending upon the scattering mechanism and band structure (see Table 1.1). In cadmium sulphide crystals, the scattering mechanism is limited by different processes over different temperature regions, strictly therefore the value of 'r' should be changed to match the dominant scattering mechanism in different temperature ranges. Owing to the difficulty of compounding scattering mechanisms, the values of n plotted in Figure 8.1 were obtained using the simplifying approximation that r = 1 at all temperatures.

The experimental results presented in Figure 8.1 show that the room temperature carrier concentrations for crystals 148, 167, 107, 183 and 182 varied from 4×10^{16} to $4{\cdot}0 \times 10^{15}$, cm^{-3}. These carrier concentrations remained almost constant down to 200°K in crystals 148, 167, 107 and 182. In crystal 183, the carrier concentration was constant down to 100°K. However, a decrease in carrier concentration with decreasing temperature is evident in all five crystals below 100°K.

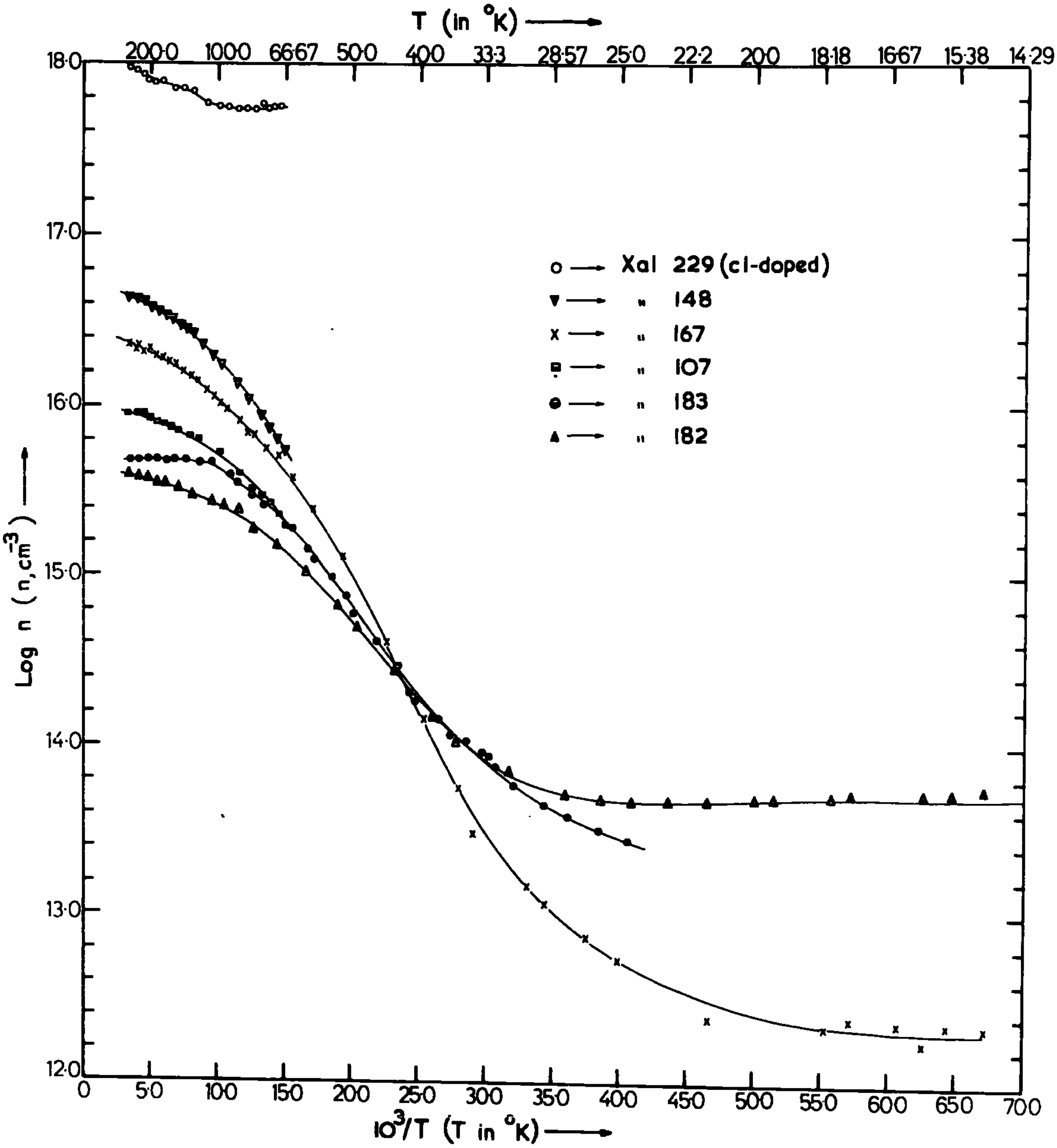

Fig. 8·1. Temperature variation of free carrier concentration.

It is also apparent from the curves in Figure 8.1 that the plot of log n versus 1/T exhibits a linear section over a certain portion of the lower temperature range. This linear section extends from 50°K to 35°K for crystal 167 and from 55°K to 35°K for crystals 182 and 183. The linear sections of the plot of log n versus 1/T for crystals 148 and 107 occur between 85°K and 65°K, and 80°K and 65°K respectively. Figure 8.1 also shows another interesting feature namely the strong departure from linearity at temperatures in the neighbourhood of 25°K. The linear decrease is followed by a region in which the carrier concentration remains almost constant down to 14°K.

Crystal 229 which was doped with chlorine had a high concentration, 10^{18} cm^{-3}, of conduction electrons at room temperature. This concentration showed little change as the temperature was reduced to 65°K. This phenomenon is undoubtedly attributable to metallic impurity conduction which is due to charge transport in an impurity band. At high donor densities, the overlapping of the wave functions of the donor electrons forms an impurity band[3] which can merge with the conduction band. The electrons move in this impurity band without activation into the conduction band.

Crystals 148, 167, 107 and 183 were undoped as-grown. Crystal 182 was grown from a charge to which copper was added in the form of Cu_2S. The n-type semiconduction observed in these crystals, therefore, can be attributed to the presence of sulphur vacancies which act as donors in cadmium sulphide. Edge emission studies by Orr et al.[4]

indicate that such semiconducting crystals of CdS also contain acceptors. The electrons released by donors must be shared between the acceptor states and the conduction band. Since these crystals show n-type semiconduction, the concentration of donors N_D must be greater than the concentration of acceptors N_A. Let us assume that the donor impurities are associated with a single donor energy level at a depth E_D below the conduction band. The variation of carrier concentration n with temperature T for a partially compensated n-type semiconductor which is non-degenerate, can be expressed by the equation (see Section 1-2.2):

$$\frac{n(N_A+n)}{(N_D-N_A-n)} = \frac{N_C}{2} \exp(-E_D/kT) \qquad (1.36)$$

In equation (1.36), the spin degeneracy factor has been taken equal to 1/2 by assuming a single-valley conduction band for cadmium sulphide.

At least three distinct regions of the curves of Figure 8.1 have to be examined, and in each range equation (1.36) is modified accordingly. The regions are discussed below.

(1) The exhaustion range when kT is greater than E_D but considerably smaller than E_G. Here $n = N_D-N_A$ and the electron concentration n is essentially independent of the temperature. This range is evident in the curves of Figure 8.1 at temperature above 200°K for crystals 148, 167, 107 and 182 and above 100°K for crystal 183.

Thus values of N_D-N_A were obtained from the room temperature measurements of carrier concentration (cm^{-3}) and recorded in Table 8.2.

(2) As the temperature is lowered, the electrons begin to freeze out into the donor levels and we enter the second range of temperature. In this range, $n < N_D-N_A$ and $n > N_A$, equation (1.36) which under these conditions reduces to

$$n = \left[\frac{N_C}{2} (N_D-N_A) \right]^{\frac{1}{2}} \exp(-E_D/2kT) \qquad (1.37)$$

The extent of the intermediate region described by the equation (1.37) depends upon the degree of compensation. Equation (1.37) describes the behaviour of crystals with negligible compensation and is not valid for highly compensated samples.

(3) The third range of interest occurs at very low temperatures when the conditions $n < (N_D-N_A)$ and $n < N_A$ are satisfied. Then equation (1.36) leads to the following approximate expression for the carrier concentration, viz.

$$n = \frac{N_C}{2} \left(\frac{N_D-N_A}{N_A} \right) \exp(-E_D/kT) \qquad (1.38)$$

From the measurement of the carrier concentration as a function of temperature over the lower temperature region, the donor ionization energy E_D can be determined. A plot of $\ln(nT^{-3/2})$ versus $1/T$ should produce a straight line with a slope of $-E_D/k$ or $-E_D/2k$

depending upon the degree of compensation. Since the degree of compensation is difficult to determine in semiconducting crystals of CdS, most investigators[5-10] have used the equation (1.38) to describe the linear section of the log n versus 1/T plot observed at lower temperatures.

To interpret the temperature variation of carrier concentration, the curves are generally plotted in the form of log n versus 1/T. The right hand side of equation (1.38) contains N_C, which varies as $T^{3/2}$, and $\exp(-E_D/kT)$, which defines the donor activity. In principle, the curves should be plotted as $\log(nT^{-3/2})$ versus 1/T instead of log n versus 1/T. At very low temperatures, the exponential term increases so rapidly that the contribution of the $T^{-3/2}$ term is swamped and a logarithmic plot of carrier concentration n versus 1/T has a nearly uniform slope of E_D.

The expression (1.38) has been applied to the linear sections of the plots of log n versus 1/T observed at lower temperatures in Figure 8.1, so that the gradients of the linear sections are equal to $-E_D/k$. This provides us with the donor ionization energies E_D directly. For crystal 167, E_D was found to be 0·029 eV, for crystals 148 and 107, E_D = 0·021 eV and for crystals 182 and 183, E_D = 0·020 eV. If the donors are considered to be hydrogen-like impurities, then an estimate of the activation energy can be obtained from the relation[6]

$$E_{hydrogenic} = \frac{m_e^* e^4}{2h^2 \epsilon_s^2} \qquad (8.1)$$

where m_e^* is the electron effective mass and ϵ_s, the static dielectric constant. If the values of m_e^* and ϵ_s for cadmium sulphide are taken to be $0{\cdot}2m$ and $10{\cdot}33$[11] respectively, then $E_{hydrogenic} = 0{\cdot}026$ eV.

A wide range of values has so far been reported for the donor ionization energies in cadmium sulphide by the various investigators. Kröger et al.[5] found $E_D = 0{\cdot}02$ eV for samples with 3×10^{17} cm^{-3} conduction electrons at room temperature. Piper and Halsted[6] observed a donor level at 0·032 eV in samples with a carrier concentration of 10^{15} cm^{-3}. Itakura and Toyoda[7] measured the Hall effect in a crystal which had 10^{17} conduction electrons at room temperature. The plot of lnn versus 1/T showed two slopes: one of 0·014 eV from 200°K to 50°K and the other of 0·007 eV from 50°K to 10°K. Itakura and Toyoda interpreted their results indicating the presence of two types of donor with concentrations of $1{\cdot}5 \times 10^{17}$ cm^{-3} for that with a level at 0·014 eV, and more than 10^{16} cm^{-3} for that with a level at 0·007 eV. Clark and Woods[8] measured the Hall effect of cadmium sulphide with a carrier density of 2×10^{16} carriers/cm^3 at room temperature and observed a donor level E_D at 0·016 eV. Measurements by Woodbury[12] on high purity cadmium sulphide crystals of 10^{15} cm^{-3} free carriers at room temperature gave a value of 0·024 eV as the donor ionization energy. Crandall[10] observed a donor level at 0·021 eV in a sample with a room temperature carrier concentration of $6{\cdot}9 \times 10^{15}$ cm^{-3}.

Donor ionization energies for CdS can also be determined from optical measurements. From an investigation of the absorption and fluorescent spectra of cadmium sulphide platelets (impurity concentration 10^{17} cm^{-3}), Thomas and Hopfield[13] calculated a value of 0·033 eV for the binding energy of a hydrogenic donor. Maeda[14] observed a dominant blue peak I_2 ($\sim$4865 Å) at 20°K in the luminescence emission spectra of undoped cadmium sulphide single crystals which were conducting at room temperature. The I_2 line according to Thomas and Hopfield,[13] is due to recombination of an exciton bound to a neutral donor. From Hall effect and resistivity measurements on these samples, a donor level was found at 0·033 eV. From edge emission studies on a number of semiconducting samples of cadmium sulphide, Colbow[15] obtained donor binding energies between 0·028 eV and 0·032 eV and gave 0·0305 $\pm$ 0·0005 eV as an average value.

Approximate values for the densities of acceptors and donors N_A and N_D were also obtained by fitting the expression (1.38) to the linear sections of the plots of log n versus 1/T. in Figure 8.1. The values of N_D-N_A used in the expression (1.38) were obtained from the saturated part of Figure 8.1. A value of 0·2m was used for the density of states mass m_e^* to calculate N_C. The calculated values of N_A were found to be higher than the values of carrier concentration in the linear sections of Figure 8.1 as is required for equation (1.38) to be valid. Values of E_D, N_D-N_A, N_D and N_A together with the room temperature values of carrier concentration, conductivity and mobility are given in Table 8.2.

One of the objects of the research described in this chapter was to determine how the donor and acceptor concentrations, N_D and N_A varied with the conditions under which the crystals were prepared. All the crystals 167, 107, 148 and 183 were grown under various partial pressures of cadmium (see Table 8.1). To compare N_D and N_A for these crystals with the conditions under which they were grown, a plot of N_D and N_A as a function of T_{cd} (reservoir temperature, see Section 4-4.2(b)) is shown in Figure 8.2, where it can be seen that N_A varied more rapidly than N_D with T_{cd}. Both donor and acceptor concentrations reached a maximum when $T_{cd} = 450^{\circ}C$. For values of T_{cd} between $550^{\circ}C$ and $650^{\circ}C$, N_D remained practically constant, whereas the value of N_A decreased with increasing T_{cd} in the range $450^{\circ}C$ to $650^{\circ}C$. Crystal 182 which was grown with $T_S \sim 250^{\circ}C$, was found to have a donor concentration (see Table 8.2) approximately twice that of the acceptors.

The decrease of N_A with increasing T_{cd} (Figure 8.2) is in excellent agreement with the prediction of the results of the edge emission studies made in this laboratory. In studying edge emission, Orr et al.[4] found that the intensity of the green emission decreased as T_{cd} increased to $775^{\circ}C$. The magnitude of the intensity of the green emission was also proportional to the intensity of the I_1 line which is due to recombination of excitons bound to neutral acceptors. The decrease in the density of green emission was interpreted due to a decrease of acceptor concentration N_A as T_{cd} increased, which is now confirmed.

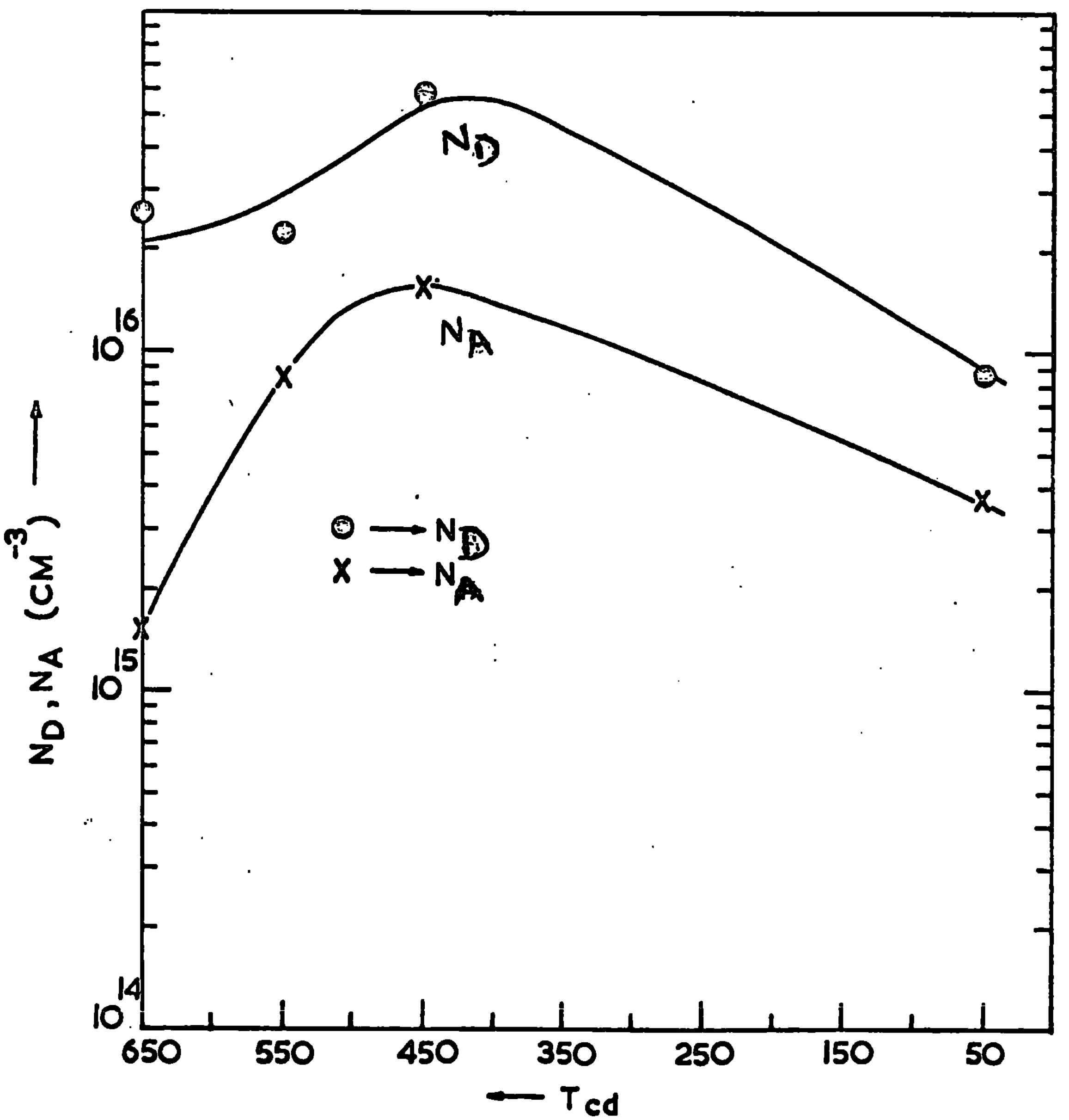

Fig. 8·2. Curves illustrate the variations of donor and acceptor concentrations N_D and N_A with the partial pressures of cadmium.

The values of N_D and N_A calculated from the curves of Figure 8.1 have also been compared with the results of edge emission studies. The intensities of the $I_2(\lambda = 4867$ Å) and the $I_1(\lambda = 4889$ Å) exciton emission components of the edge emission, excited by 3650 Å radiation, was measured (by D.S.Orr) for a number of cadmium sulphide crystals at liquid helium temperatures. I_1 and I_2 lines are due to recombination of excitons bound to neutral acceptors and donors respectively. Their relative intensities give an (approximate) indication of the relative concentration of acceptors and donors. The values of I_2/I_1 for crystals 167 and 107 (only information available at the moment) are given in Table 8.2. The agreement between I_2/I_1 and N_D/N_A for crystals 167 and 107 are reasonably satisfactory.

8-2(b) <u>Impurity band conduction (non-metallic type)</u>

As mentioned in Section 8.2(a), the plots of log n versus 1/T for crystals 167, 182 and 183 (Figure 8.1) exhibit a departure from linearity at very low temperatures (near 30°K for crystals 182 and 183 and near 25°K for crystal 167). In this temperature range the carrier concentration remains almost constant as the temperature is decreased down to 14°K. Hall effect measurements were made successfully for crystal 167 and 182 down to 14°K and for crystal 183 to 25°K. Hall effect measurements on cadmium sulphide at liquid helium temperatures have also been made by several investigators.[5,6,7,10,16] Their results show that the mobility reaches a maximum in the neighbourhood of 40°K and then decreases rapidly. The Hall coefficient also reaches a maximum in the neighbourhood of 30°K and then saturates or decreases with decreasing temperature. Equation (1.36) can be used to interpret the Hall effect data until the departure from linearity occurs.

The saturated region observed in the plot of log n versus 1/T in the neighbourhood of 14 to 30°K (Figure 8.1) can be explained in terms of a non-metallic, impurity conduction mechanism which is described fully in the paper by Mott and Twose.[3] This explanation for the formation of a conducting impurity band at lower temperatures in a partially compensated semiconductor with a majority carrier concentration as low as 10^{16} cm^{-3}, is different from the metallic type conduction exhibited by crystal 229 with $10^{18}cm^{-3}$ donors (Figure 8.1). As mentioned in Section 8.2(a), metallic type impurity conduction is due to charge transport in an impurity band which is formed by the overlapping of the wave functions of the charge carriers. The impurity band may also overlap the neighbouring band edge. In contrast, non-metallic type impurity conduction is due to a phonon-activated hopping motion of a charge carrier from one occupied impurity site to a neighbouring unoccupied site.

For example, in a partially compensated n-type semiconductor $(N_D > N_A)$ conduction electrons freeze out into the donor levels with decreasing temperature. The compensating acceptor impurities, however, always remain occupied with electrons. Some of the donor impurities, therefore, remain unoccupied even at the absolute zero of temperature.

Impurity conduction arises from the fact that a net transport of electrons even at very low temperature can occur from occupied to unoccupied donor centres without activation into the conduction band. The transport of electrons is considered to take place by tunnelling., an activation energy still exists because of the need to overcome the Coulomb barriers associated with the compensating acceptor impurities. A phonon is emitted or absorbed to conserve energy.

At low temperatures where impurity conduction becomes dominant, variation of the Hall coefficient can be used to indicate the occurrence of this phenomenon. Normally the Hall coefficient reaches a maximum and then either saturates or decreases with decreasing temperature. The activation energy for the impurity conduction process appears in the variation of conductivity as a function of reciprocal temperature. (See Section 8-4). The Hall coefficient maximum occurs at a temperature where charge transport in the conduction band and that through the impurity levels contribute almost equally to the electrical conductivity.(3)

The plot of log n versus 1/T (Figure 8.1) shows that the Hall coefficient maximum occurs at 28^{o}K and 22^{o}K for crystals 182 and 167 respectively. The temperature T_S at which this Hall coefficient maximum occurs, depends upon the impurity concentration and degree of compensation K. The temperature T_S can be correlated with the degree of compensation K with the following relationship:(3)

$$\exp(-\epsilon_3/kT) \sim K^{\frac{1}{2}} \tag{8.2}$$

where ϵ_3 is the activation energy associated with the phonon-activated hopping process of the donor electrons (for n-type semiconductor). We were only able to make Hall effect measurements down to 14°K and a value of ϵ_3 could not be obtained. To determine the value of ϵ_3, from the variation of conductivity σ versus 1/T, measurements have to be made down to below liquid helium temperature.[10] However, this conduction process will be discussed briefly in Section 3.4 where the variation of conductivity with reciprocal temperature for all the crystals will be described.

8-3.1. Temperature variation of the Hall mobility

The experimental variation of the Hall mobility μ_H with temperature for crystals 182, 183, 167, 107, 148 and 229 is shown in Figure 8.3 (which is a plot of Log μ_H versus Log T). As mentioned in Section 8-1, the Hall effect measurements for crystals 182 and 167 and for crystal 183 were successfully made down to 14°K and 25°K respectively. For crystals 107, 148 and 229, the lowest temperature reached was 60°K. The Hall mobility μ_H was calculated using the relation $\mu_H = R_H x \sigma$ where R_H is the Hall coefficient and σ, the conductivity. The results presented in Figure 8.3 showed that with decreasing temperature, the Hall mobility μ_H for crystals 182, 183 and 167 increased, reached a maximum in the neighbourhood of 50°K and then decreased rapidly. For crystals 107 and 148, the Hall mobility μ_H increased with decreasing temperature down to

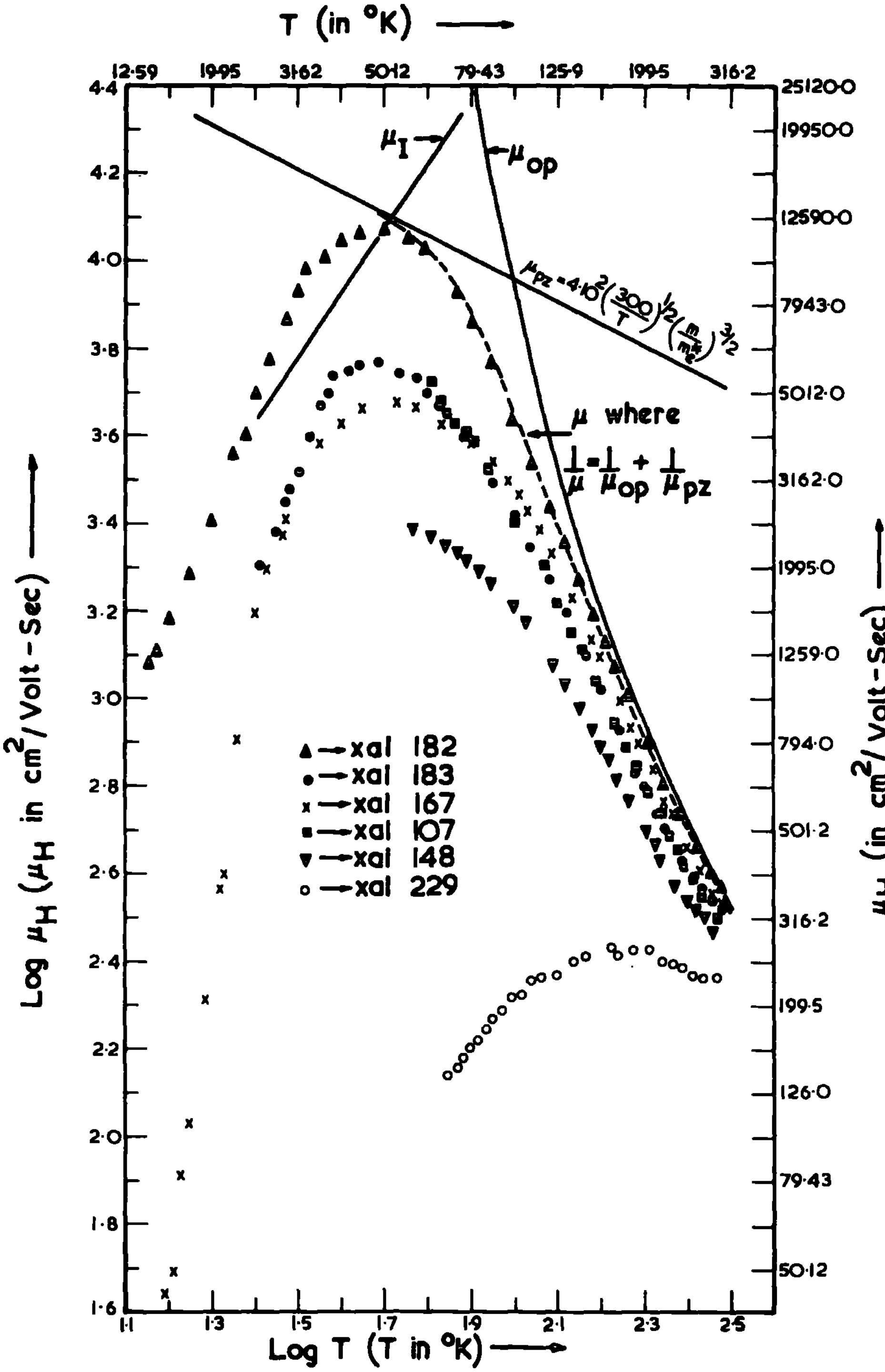

Fig. 8·3 Temperature variation of the Hall mobility. The symbols ▲, ●, x, ■, ▼ and ○ represent the experimental values of the Hall mobilities for crystals 182, 183, 167, 107, 148 and 229 respectively. The broken curve is the theoretical value of the electron mobility due to the combined effects of the polar optical mode (μ_{op}) and piezoelectric (μ_{pz}) scattering assuming $m_e^*/m = 0{\cdot}18$. μ_{pz} was calculated from the relation:

$$\mu_{pz}=4{\cdot}0\times10^2\left(\frac{300}{T}\right)^{1/2}\left(\frac{m}{m_e^*}\right)^{3/2}$$

$60^{\circ}K$. Relatively small changes in the variation of the Hall mobility with temperature were observed for crystal 229.

In an ionic crystal like cadmium sulphide where the neighbouring atoms are dissimilar and carry opposite charges, polar optical mode scattering is expected to dominate the intrinsic scattering mechanism at higher temperatures (see Section 1-3.4(b)). Howarth and Sondheimer[17] discussed the theory in detail and showed that a perturbation theory is applicable for values of α_c less than unity. The parameter α_c which is a measure of the strength of the interaction of the charge carriers with the polar modes is defined by the expression (1-82).[18]

$$\alpha_c = \frac{e^2}{\hbar^2}\left(\frac{m^*}{2\hbar w_l}\right)^{\frac{1}{2}}\left(\frac{1}{\epsilon_\infty} - \frac{1}{\epsilon_s}\right) \qquad (1.82)$$

where ϵ_s is the static dielectric constant and ϵ_∞, the optical dielectric constant. w_l is the longitudinal optical-mode frequency related to Debye temperature θ by $\hbar w_l/kT = \theta/T$.

The value of α_c for cadmium sulphide is calculated to be 0·80 when the following values are used in equation (1.82):

$\epsilon_s = 10{\cdot}33$ [11]

$\epsilon_\infty = 5{\cdot}24$ [19]

$w_l = 5{\cdot}75 \times 10^{13}\ \mathrm{sec}^{-1}$ [20]

$m_e^* = 0{\cdot}2m$

The values of α_c are found to be 0·78 and 0·76 if the electron effective mass m_e^* for cadmium sulphide is taken to be 0·19m and 0·18m respectively. It will be shown later that the theoretically computed values of mobility μ give a good fit to the experimental data for values of the electron effective mass m_e^* of 0·19m and 0·18m.

Since the value of α_c is less than unity for cadmium sulphide, the expression (1.83) (see Section 1-3.4(b)) can be used to describe the electron mobility due to polar optical mode scattering. Expression (1.83) which was obtained using the perturbation theory of Fröhlich and Mott and Howarth and Sondheimer, becomes in the non-degenerate case:[21]

$$\mu_{op} = \frac{1}{2\alpha_c w_1} \cdot \frac{e}{m_e^*} \cdot \frac{8}{3\sqrt{\pi}} \cdot \frac{X(z)}{Z^{\frac{1}{2}}} (e^z-1) \qquad (1.83)$$

where $Z = \hbar w_1/kT = \theta/T$, $X(z) = 1$ for $Z \ll 1$ and $X(z) = 3/8(\pi z)^{\frac{1}{2}}$ when $Z \gg 1$. θ is the characteristic temperature of the longitudinal optical phonons and is equal to 440°K for cadmium sulphide.

Different values of the coupling constant α_c for cadmium sulphide have previously been reported by different investigators. Zook and Dexter[22] gave a value of α_c of 0·3 and Piper and Halsted[6] mentioned that the coupling constant α_c for cadmium sulphide is less than 0·4. Devlin[23] gave a value of α_c equal to 0·71. Devlin used 9·30 and 5·20 as the values of the static dielectric and the optical dielectric constants respectively in his calculation. Zook and Dexter[22] obtained the following expression after simplification for the mobility due to polar optical mode scattering:

$$\mu_{op} = \left(16{\cdot}91/\theta^{\frac{1}{2}}\right)\left(\frac{1}{\epsilon_{\alpha}} - \frac{1}{\epsilon_{s}}\right)^{-1}\left(\frac{m}{m_e^*}\right)^{3/2}\left(e^{\theta/T} - 1\right) \qquad (8.1)$$

$$\text{cm}^2/\text{volt-sec.}$$

we compared the values of μ_{op} calculated using equation (8.1) with those obtained using equation (1.83). In fact, equations (8.1) and (1.83) were found to give the same values of μ_{op} at a particular temperature.

There is little information available about the scattering of electrons in cadmium sulphide by the deformation potential associated with the acoustic mode lattice vibrations. Bardeen and Shockley showed that the mobility of carriers in a single band due to deformation potential scattering is given by[24]

$$\mu_{ac} = 3{\cdot}2\text{x}10^{-5}\ dv_s^2\ (m/m_e^*)^{5/2} \Big/ T^{3/2}E_{IC}^2 \quad \text{cm}^2/\text{volt-sec.} \qquad (8.2)$$

where d is the density of the material, v_s is the velocity of sound and E_{IC} is the deformation potential of the conduction band for dilational strain measured in eV per unit dilation. An estimate of E_{IC} can be obtained from Gutsche's experiments on the effects of pressure on cadmium sulphide. Gutsche obtained the following information:

$$\text{compressibility} = -\frac{1}{V}\frac{dV}{dP} = 5{\cdot}6\times10^{-13}\ (\text{dynes/cm}^2)^{-1}$$

$$\left(\frac{dE_G}{dP}\right)_T = 4{\cdot}5\times10^{-12}\ \text{eV/dynes cm}^{-2}$$

But $\frac{dE_G}{dP} = -E_{IG}\frac{1}{V}\frac{dV}{dP}$ where E_{IG} is the change in the forbidden band gap per unit dilation. From the data quoted above, E_{IG} is of the order $\sim 8{\cdot}0$ eV.

If it is assumed that $E_{IC} \sim 1/3\ E_{IG}$,[23] then according to equation (8.2) the electron mobility at 300°K would be $3{\cdot}30 \times 10^4$ cm^2/volt-sec. if it were limited by deformation potential scattering alone. This value is much higher than that observed at room temperature which is ~ 400 cm^2/volt.sec. Onodera[26] showed that acoustic mode scattering in cadmium sulphide has little effect on the electrical mobility. He stated that the temperature variation of the mobility due to acoustic mode scattering would be $\mu_{ac} = 2{\cdot}8 \times 10^7 \times (300/T)^{3/2}$ cm^2/volt-sec.

In the light of the above discussion, the direct effect of deformation potential scattering on the mobility will be assumed negligible.

A much more significant indirect effect is expected to arise in cadmium sulphide from the acoustic mode lattice vibrations. Since the material has no inversion symmetry, a piezoelectric polarization is developed by the strain associated with the acoustic mode vibrations.

Thus an acoustic wave propagating in cadmium sulphide, is in general accompanied by electrical disturbances which lead to departures from the mobility predicted by the deformation potential model of Bardeen and Shockley. Piezoelectric scattering becomes dominant at lower temperatures in a highly perfect crystal. The theory of piezoelectric scattering has been applied to cadmium sulphide by Hutson[27] who writes the piezoelectric mobility as

$$\mu_{pz} = A\ (m/m_e^*)^{3/2}\ (300/T)^{1/2} \tag{1.85}$$

where the factor A is a constant which is determined by the piezoelectric and the dielectric constants and which is equal to:

$$A = 1{\cdot}44\,\epsilon_s \left\{ \sum_{\text{modes}} \left(K^2 \right)_{av} \right\}^{-1} \tag{1.85a}$$

In relation (1.85a), K (the electromechanical coupling factor) is a dimensionless quantity given by $K^2 = e^2/(\epsilon_o \epsilon_s C)$. Here e is an appropriate piezoelectric constant, C the appropriate stiffness constant and ϵ_o the permittivity of free space. The first value of 'A' given by Hutson was $1{\cdot}20\times10^2$. Later on, he found this value to be too low to describe piezoelectric scattering in cadmium sulphide. He improved his estimate by taking the spherical average of the square of the electromechanical coupling (see appendix of reference (27)) and obtained a new value of 'A' as $4{\cdot}0\times10^2$.[27]

The values of the donor N_D and acceptor N_A concentrations obtained in section 8.2 (Table 8.2) from the analysis of the temperature variation of the carrier concentration showed that samples 182, 183, 167, 107 and 148 were partially compensated. Thus the effect of the ionized impurity scattering on the electrical mobility in our crystals must be considered. The mobility associated with ionized impurity scattering was calculated using the well-known Brooks-Herring (B-H) formula which takes into account the temperature variation of the number of ionized centres N_I and also the shielding of the scattering centres by free carriers. The expression for mobility due to ionized impurity scattering is[24]

$$\mu_I(\text{B-H}) = 3{\cdot}2\times10^{15}\left(\frac{m}{m_e^*}\right)^{\frac{1}{2}} \frac{\epsilon_s^2\, T^{3/2}}{Z^2 N_I} \Bigg/ \log\left[1{\cdot}3\times10^{14}T^2\left(\frac{m_e^*}{m}\right)\Big/ n\right] \quad \text{cm}^2/\text{volt-sec.} \tag{8.4}$$

where N_I is the concentration of ionized centres, n the carrier concentration and Z, the electronic charge on the ionized centre. The value of N_I at a particular temperature T was obtained from the knowledge of acceptor N_A (from the Table 8.2) and carrier concentration n by putting $N_I = 2N_A + n$.

The Hall mobility data presented in Figure 8.3 show a wide variation from crystal to crystal at lower temperatures which could be due to ionized impurity scattering. An attempt was made to interpret the mobility data by combining effects of the polar optical mode (equation

(1.83)), piezoelectric (equation (1.85)) and ionized impurity (equation (8.4)) scattering. The resultant mobility μ was computed assuming that the reciprocals of the mobilities are additive i.e. ($\mu^{-1}=\mu_{op}^{-1}+\mu_{pz}^{-1}+\mu_{I}^{-1}$). To calculate μ_I using equation (8.4), the ionized impurity centres were assumed to be singly charged.

The variation of the Hall mobility with temperature for crystal 182 down to 50°K can be explained by a combination of polar optical mode and piezoelectric scattering. The broken line (shown in Figures 8.3 and 8.3(a)) which fits the experimental values very nicely, was computed theoretically from the relation $\mu^{-1}=\mu_{op}^{-1}+\mu_{pz}^{-1}$ using an electron effective mass value of 0·18m in equations (1.83) and (1.85). A value of $4{\cdot}0 \times 10^2$ was used for A in equation (1.85) to calculate μ_{pz}. If m_e^* was taken equal to 0·19m, then the experimental value of the Hall mobility at 300°K was found to be higher than the theoretical value due to polar optical mode scattering. At 300°K, calculated values of μ_{op} from equation (1.83) for $m_e^* = 0{\cdot}19m$ and 0·18m come out to be 349·00 and 380·00 (in cm^2/volt-sec) respectively. The experimentally obtained value of the Hall mobility at 300°K for crystal 182 was 383·00 cm^2/volt-sec (Table 8.2). This value is closer to the theoretical value of μ_{op} with $m_e^* = 0{\cdot}18m$.

At temperatures below 50°K, the calculated values of μ_I for crystal 182, using equation (8.4) for $m_e^* = 0{\cdot}18m$, were found to be lower than the experimental values (Figures 8.3 and 8.3(a)). When μ_I^{-1} was added to μ^{-1} (= $\mu_{op}^{-1}+ \mu_{pz}^{-1}$), the experimental values of the Hall mobility in the neighbourhood of 50°K were still higher than the theoretical values.

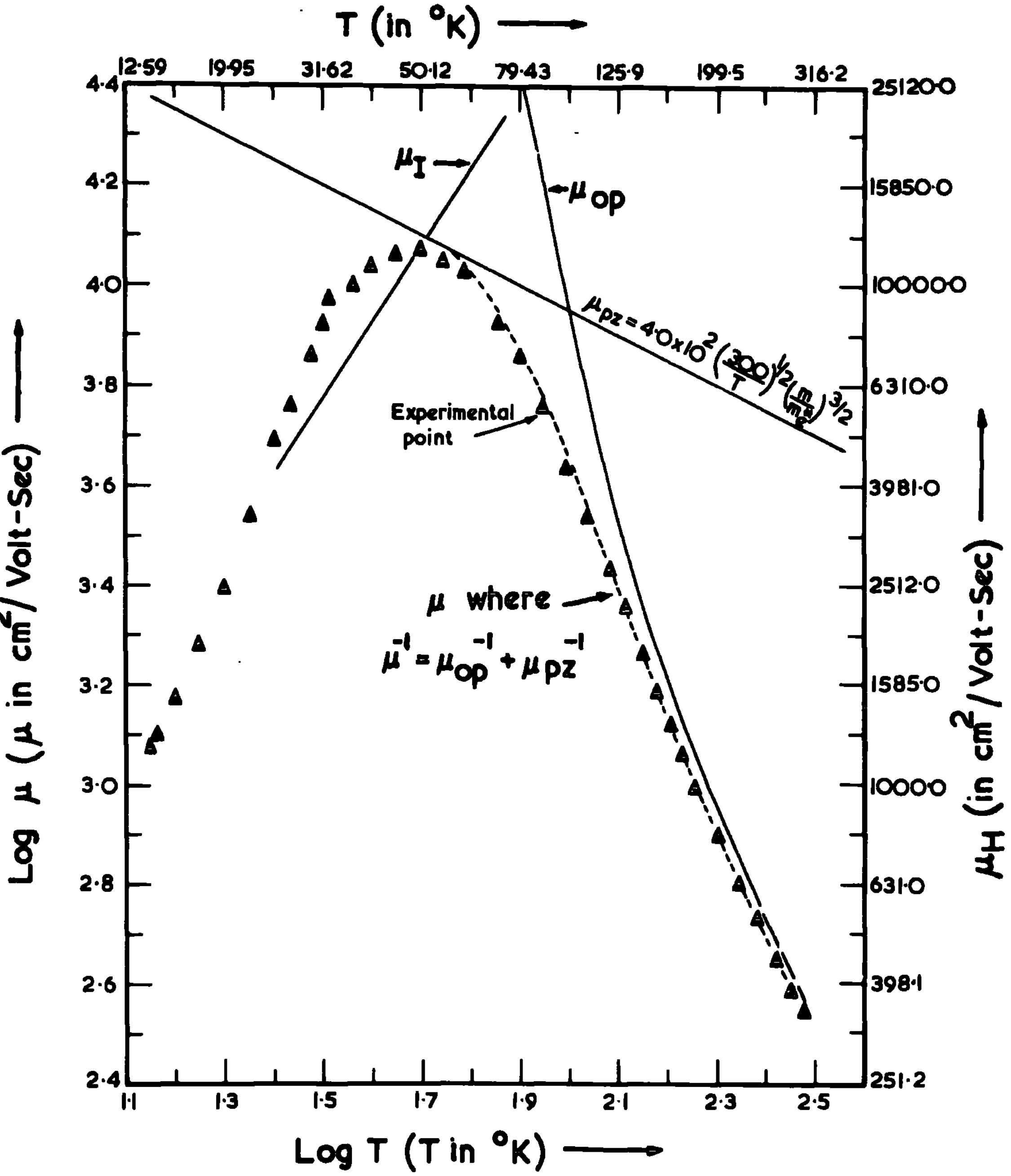

Fig. 8·3(a) Temperature variation of the Hall mobility for crystal 182. The broken curve shows the theoretically computed values of the electron mobility μ due to the combined effects of the polar optical mode (μ_{op}) and piezelectric (μ_{pz}) scattering assuming $m_e^*/m = 0{\cdot}18$. μ_{pz} was calculated from the relation:

$$\mu_{pz} = 4{\cdot}0 \times 10^2 \left(\frac{300}{T}\right)^{1/2} \left(\frac{m}{m_e^*}\right)^{3/2}$$

However, the computed values of $\mu(\mu^{-1}=\mu_{op}^{-1}+\mu_{pz}^{-1})$ for temperature above 68^{o}K did not change significantly from the values shown by the broken line in Figures 8.3 and 8.3(a). This indicated that the effect of ionized impurity scattering on the intrinsic scattering mechanisms for crystal 182 was not appreciable.

The temperature variation of the Hall mobility data for crystals 183, 167, 107 and 148 are also shown separately in Figures 8.3(b), (c), (d) and (e) respectively. The theoretically computed values of $\mu(\mu^{-1}=\mu_{op}^{-1}+\mu_{pz}^{-1}+\mu_{I}^{-1})$ were fitted to the experimental points of the Hall mobility data for crystal 183 using $m_e^* = 0{\cdot}19m$ and a value of A of 3×10^2. The values of μ shown by the broken line in Figure 8.3(b), in fact, described the temperature variation of μ_H convincingly down to 30^{o}K for crystal 183.

A best fit between the theoretical values of $\mu(\mu^{-1}= \mu_{op}^{-1}+\mu_{pz}^{-1}+\mu_{I}^{-1})$ and the experimental points of the Hall mobility data for crystal 167 was found for $m_e^* = 0{\cdot}19m$ and $A = 3{\cdot}5 \times 10^2$. For crystal 167, theoretically computed values of $\mu(\mu^{-1}=\mu_{op}^{-1}+\mu_{pz}^{-1}+\mu_{I}^{-1})$ shown by the broken line in Figure 8.3(c) described the temperature variation of μ_H down to 80^{o}K only. Below 80^{o}K the calculated mobility $\mu(\mu^{-1}=\mu_{op}^{-1}+\mu_{pz}^{-1}+\mu_{I}^{-1})$ was much higher than the experimental values (Figure 8.3(c)).

With crystal 107, the theoretically computed values of $\mu(\mu^{-1}=\mu_{op}^{-1}+\mu_{pz}^{-1}+\mu_{I}^{-1})$ fitted very well to the experimental points for $m_e^* = 0{\cdot}19m$ and $A = 3{\cdot}2 \times 10^2$ (Figure 8.3(d)). With crystal 148, however, a good

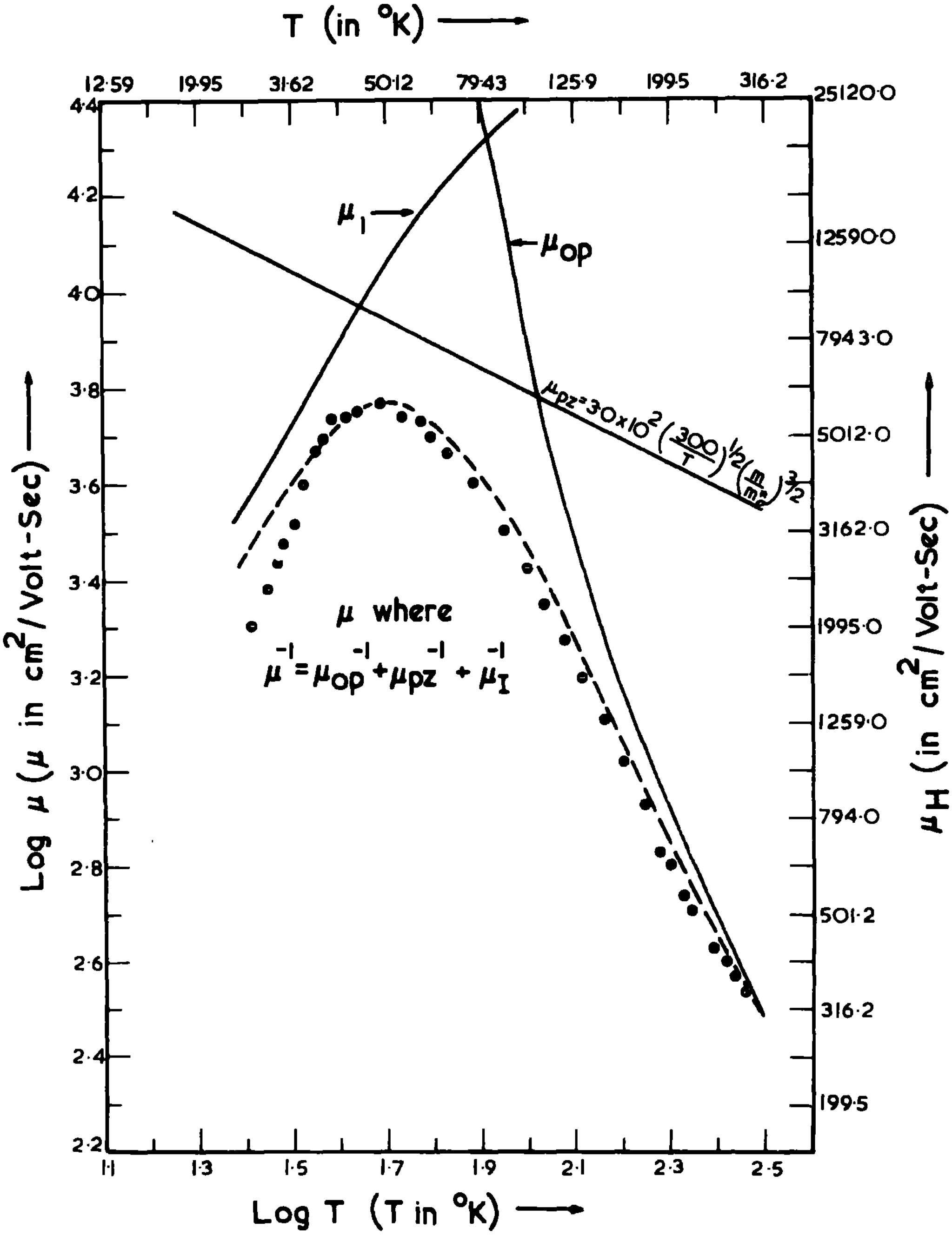

Fig. 8·3 (b) Temperature variation of the Hall mobility for crystal 183. The broken curve shows the theoretically computed values of the electronic mobility μ due to the combined effects of the polar optical mode (μ_{op}), piezoelectric (μ_{pz}) and ionized impurity scattering (μ_I) assuming $m_e^*/m = 0{\cdot}19$. μ_{pz} was calculated from the relation:

$$\mu_{pz} = 3{\cdot}0 \times 10^2 \left(\frac{300}{T}\right)^{1/2} \left(\frac{m}{m_e^*}\right)^{3/2}$$

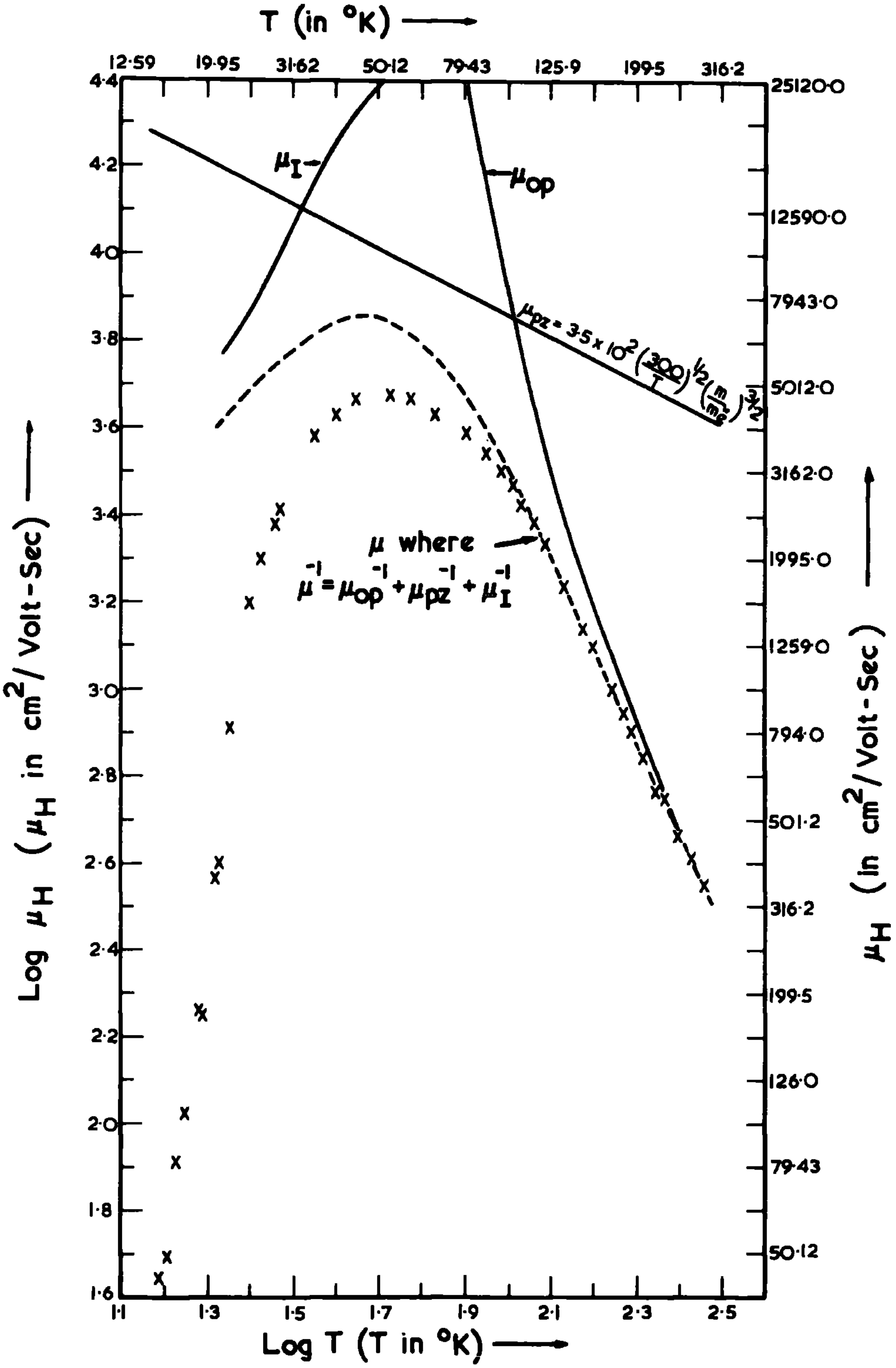

Fig. 8·3(c) Temperature variation of the Hall mobility for crystal 167. The broken curve shows the theoretically computed values of the electron mobility μ due to the combined effects of the polar optical mode (μ_{op}), piezoelectric (μ_{pz}) and ionized impurity scattering (μ_I) assuming $m_e^*/m = 0·19$. μ_{pz} was calculated from the relation:

$$\mu_{pz} = 3·5 \times 10^2 \left(\frac{300}{T}\right)^{1/2}\left(\frac{m}{m_e^*}\right)^{3/2}$$

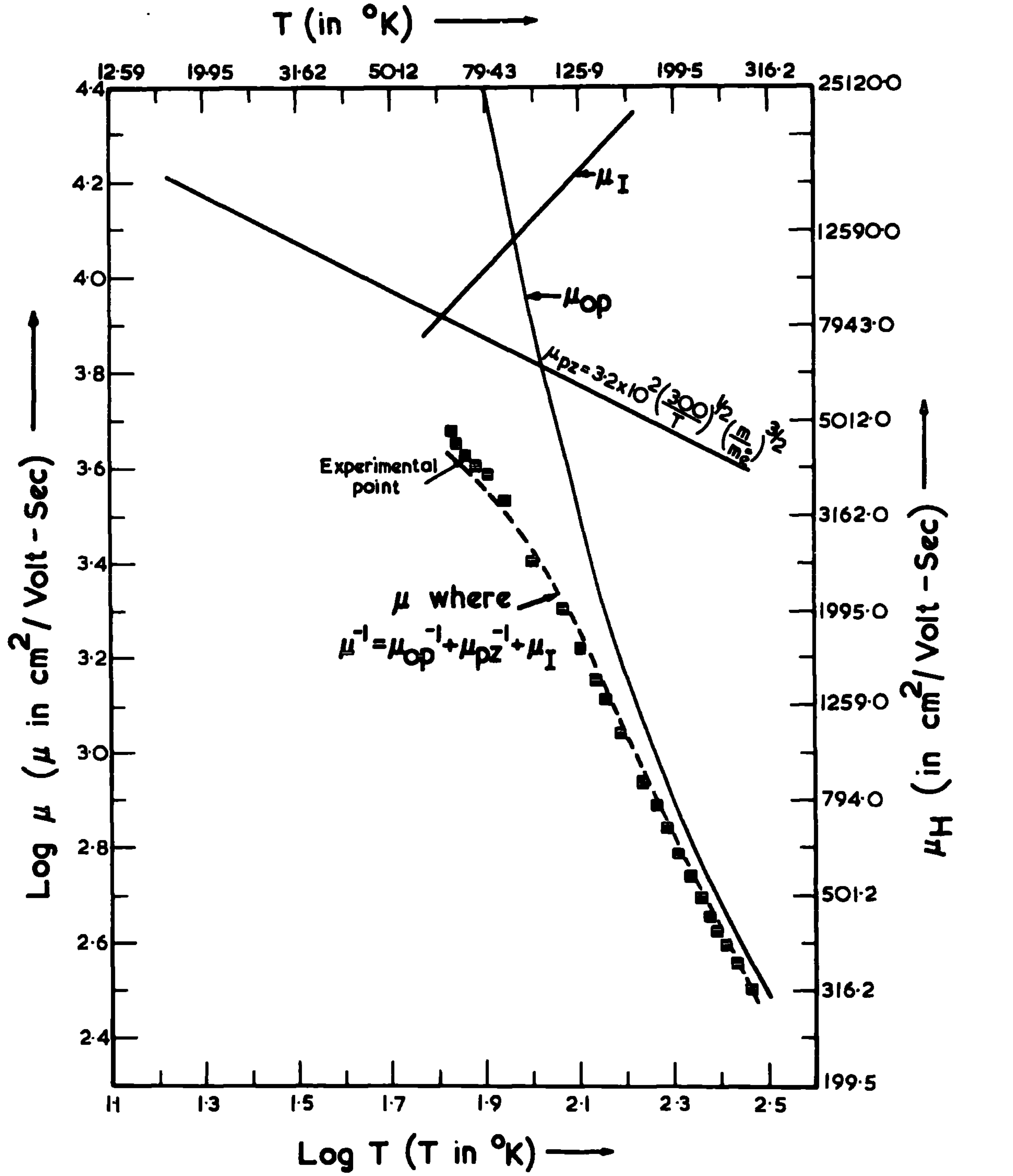

Fig. 8·3 (d) Temperature variation of the Hall mobility for crystal 107. The broken curve shows the theoretically computed values of the electrical mobility μ due to the combined effects of the polar optical mode (μ_{op}), piezoelectrical (μ_{pz}) and ionized impurity scattering (μ_I) assuming $m_e^*/m = 0{\cdot}19$. μ_{pz} was calculated from the relation :

$$\mu_{pz} = 3{\cdot}2 \times 10^2 \left(\frac{300}{T}\right)^{1/2} \left(\frac{m}{m_e^*}\right)^{3/2}$$

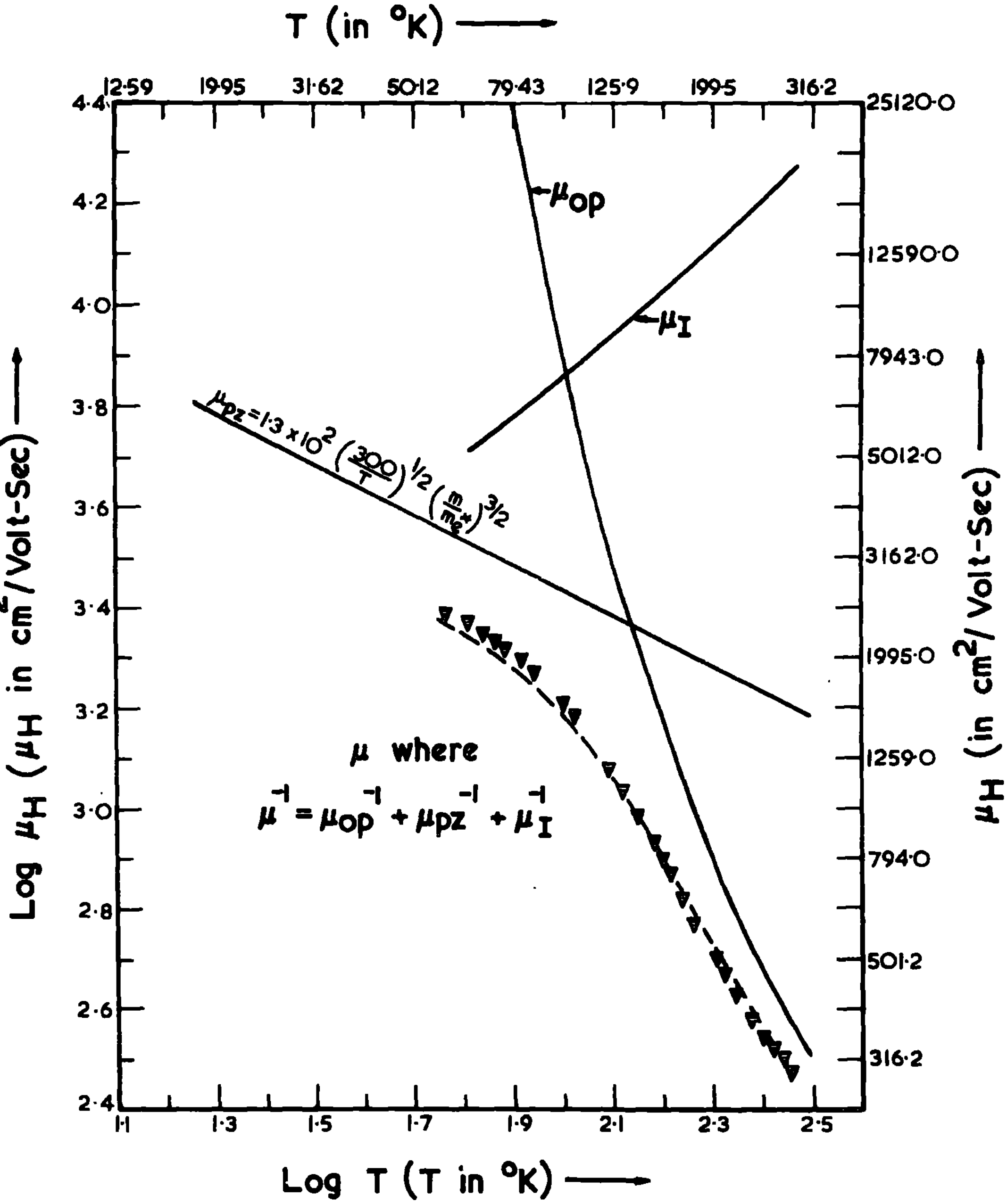

Fig. 8·3(e) Temperature variation of the Hall mobility for crystal 148. The broken curve shows the theoretically computed values of the electron mobility μ due to the combined effects of the polar optical mode (μ_{op}), piezoelectric (μ_{pz}) and ionized impurity scattering (μ_I) assuming $m_e^*/m = 0{\cdot}19$. μ_{pz} was calculated from the relation:

$$\mu_{pz} = 1{\cdot}3 \times 10^2 \left(\frac{300}{T}\right)^{1/2} \left(\frac{m}{m_e^*}\right)^{3/2}$$

fit was only possible for $m_e^* = 0{\cdot}19m$ when the value of 'A' in equation (1.85) was chosen equal to $1{\cdot}3 \times 10^2$ (Figure 8.3(e)). Possible reasons for the variation in the values of 'A' will be discussed later.

8-3.2. Discussion

(a) Previous work

Much of the previous work on cadmium sulphide has been concerned with the intrinsic scattering mechanisms[23] (Section 2.3). Piper and Halsted made Hall effect measurements down to 15°K on a number of crystals with different impurity concentrations. The Hall mobility of their best sample reached a maximum at 50°K and then decreased with decreasing temperature. The Hall mobility data of their other samples show a wide range of values and a similar temperature variation. Our mobility data (Figure 8.3) are in fact, consistent with the mobility data of Piper and Halsted.

Piper and Halsted[6] described the temperature variation of the Hall mobility of their best crystal using a combination of polar optical (μ_{op}) and piezoelectric (μ_{pz}) scattering with $m_e^* = 0{\cdot}16m$. To calculate μ_{pz}, a value of 'A' equal to $1{\cdot}2 \times 10^2$ was used in equation (1.85). Their theoretically computed values of $\mu(\mu^{-1}=\mu_{op}^{-1}+\mu_{pz}^{-1})$ fitted the experimental points very closely down to 70°K. Their value of the effective mass for electrons ($m_e^* = 0{\cdot}16m$) could be increased if a higher value of 'A' were used in equation (1.85). To describe the temperature variation of the Hall mobility in their other samples, the effect of ionized impurity scattering had to be taken into account. Zook and Dexter[22] pointed out that the wide range of mobilities reported by Piper and Halsted,[6] could be explained by the varying amount of ionized impurity scattering in different samples. However, Piper and Halsted did not discuss how well their theoretically computed values of $\mu(\mu^{-1}=\mu_{op}^{-1}+\mu_{pz}^{-1}+\mu_{I}^{-1})$ agreed ~~well~~ with the experimental points for their samples.

Zook and Dexter[22] interpreted their Hall mobility data at 77°K in a similar way combining polar optical mode and piezoelectric scattering and using an electron effective mass of 0·19m. Devlin[23] used a variational method to find the combined effect of the two scattering mechanisms (thus avoiding the assumption that the mobilities add reciprocally) in an undoped crystal of cadmium sulphide. His Hall effect measurements were limited to liquid nitrogen temperature. The combination of polar optical mode and piezoelectric scattering assuming $m_e^*/m = 0{\cdot}20$ was found to describe the temperature dependence of the Hall mobility down to 80°K.

Kobayashi[29] measured the electron Hall mobility in insulating crystals of cadmium sulphide using the blocking electrode method of Redfield[30] and under continuous photoexcitation. In his measurements which were made down to 1·5°K, the effect of ionized impurity scattering was absent. Kobayashi described the temperature variation of the Hall mobility above 150°K in terms of optical mode scattering and below 25°K by the piezoelectric scattering alone. Between these two temperatures, three scattering processes (optical mode, deformation potential and piezoelectric scattering) were considered to contribute almost equally. In order to obtain the best agreement between the theoretical mobility and the experimental points over the whole range of temperature, Kobayashi took $m_e^* = 0{\cdot}16m$, $A = 2{\cdot}5 \times 10^2$ for $\mu_{pz}(\perp C)$, $A = 1{\cdot}7 \times 10^2$ for $\mu_{pz}(\parallel C)$ and $\mu_{Hd} = 7{\cdot}0 \times 10^6\ T^{-3/2}\ cm^2$/volt-sec where μ_{Hd} is the Hall mobility limited by deformation potential scattering only. A structurally perfect crystal of cadmium sulphide is a good insulator. The effect of impurity scattering would be expected to be negligible in an insulating crystal of cadmium sulphide. The absence of impurity scattering in the Hall mobility data of Kobayashi which were measured under conditions of photoexcitations could also be attributed to the neutralization of the compensated acceptors by the trapped holes.

(b) <u>The present work</u>

The temperature variation of the Hall mobility data for crystals 182, 183, 167, 107 and 148 (Figure 8.3) have beem shown to have a straight forward interpretation down to $50^\circ K$. The temperature variation of the Hall mobility data for crystal 182 down to $50^\circ K$ can be compared with the data reported by Piper and Halsted(6) (for their best crystal) and Devlin.(23) The best crystal of Piper and Halsted had 5×10^{15} carriers, cm^{-3} at room temperature. The crystal 182 had 7×10^{15} carriers, cm^{-3} at room temperature (see Table 8.2). As shown earlier, the theoretically computed values of the mobility for crystal 182 which were due to the combined effects of the polar optical mode and piezoelectric scattering

($\mu^{-1}=\mu_{op}^{-1}+\mu_{pz}^{-1}$) with m_e^*/m = 0·18 were found to fit the experimental points down to 50°K (Figure 8.3(a)). In view of our earlier discussion of the results of Piper and Halsted[6] and Devlin,[23] this agreement for crystal 182 is very acceptable.

To interpret the Hall mobility data for crystals 183, 167, 107 and 148, it was necessary to include the effect of ionized impurity scattering. In fact, the theoretically computed values of μ(where $\mu^{-1}=\mu_{op}^{-1}+\mu_{pz}^{-1}+\mu_{I}^{-1}$) assuming m_e^*/m = 0·19 described the experimental data for crystal 183 down to 30°K (Figure 8.3(b)) very satisfactorily and for crystals 107 (Figure 8.3(d)) and 148 (Figure 8.3(e)) down to 60°K. With crystal 167, a fit between the theoretically computed values of $\mu(\mu^{-1}=\mu_{op}^{-1}+\mu_{pz}^{-1}+\mu_{I}^{-1})$ and the experimental points was possible down to 80°K only (Figure 8.3(c)). The Hall mobility of crystal 229 which is a completely degenerate semiconductor, was affected by the impurity banding effects and showed little dependence on temperature (Figure 8.3). The best value of the electron effective mass m_e^* obtained was 0·19m for crystals 183, 167, 107 and 148 and 0·18m for crystal 182. A value of 0·18m agrees with the values for m_e^* obtained from optical and the electrical studies of cadmium sulphide by different investigators.[6,13,22,31-33]

Some anomaly is apparent in comparing the experimental Hall mobility data with the theoretically computed values of μ at the lowest temperatures for crystals 182 and 167 (Figures 8.3(a) and (c)). However, there was a good fit between the theoretical and the experimental values for crystal 183 down to 30°K (Figure 8.3(b)). The probable reason for the discrepancy is difficult to assess. Lambe and Klick[34] pointed out that the lower temperature mobility measured by Kröger et. al.[5] varies as T^3 which is difficult to interpret theoretically. Toyotomi and Morigaki[16] and Crandall[10] mentioned similarly rapid decreases in the Hall mobility at lower temperature. Itakura and Toyoda[7] concluded that the rapid temperature dependence of the Hall mobility below $50^{o}K$ was not understood.

The temperature variation of the carrier concentration for crystals 182, 183 and 167 (Figure 8.1) was found to give rise to conduction via impurity band (non-metallic type) (see Sections 8.2(a) and 8.2(b)) in the neighbourhood of $30^{o}K$ to $14^{o}K$. Evidence of a similar type of impurity conduction is evident in the results of Kröger et. al.,[5] Piper and Halsted,[6] Toyotomi and Morigaki,[16] Crandall[10] and Itakura and Toyoda.[7] In the impurity conduction band regime, the observed Hall mobility μ_H has two components: the conduction band Hall mobility and the impurity band Hall mobility.[3] It is difficult to separate these two components and assess the contribution of the impurity band conduction process but it is clear that the existence of this latter process could be responsible for the discrepancies between the calculated and the experimental mobilities at low temperature. Further, the effect of neutral impurity scattering (see Section 1-3.4(a)) has also been ignored although this would not be expected to lead to a rapid temperature dependence.

It should be pointed out here that in order to obtain good agreement between the theoretically and the experimental data of the Hall mobility, some adjustment in the values of 'A' in equation (1.85) had to be made. The values of 'A' were found to lie in the range from $4{\cdot}0 \times 10^2$ to $1{\cdot}3 \times 10^2$ for crystals 182, 183, 167, 107 and 148. The value of 'A' given by Hutson was $4{\cdot}0 \times 10^2$ taking the spherical average of the square of the electromechanical coupling constant and assuming that the crystal was elastically and dielectrically isotropic. Piper and Halsted[6] and Kobayashi[29] (their results were discussed earlier in this section) also used values of 'A' in equation (1.85) different from the value suggested by Hutson.[27]

There are a number of reasons for supposing that the value of 'A' may vary from sample to sample. For example, the piezoelectric constants used by Hutson in his calculation of the spherical average of the electromechanical coupling constant (see appendix of reference (27)) were obtained from piezoelectric measurements made on crystals annealed in sulphur and which inconsequence are highly insulating. It is possible that the value of the piezoelectric coupling constant will be different in samples with higher conductivities because of the shielding out of the piezoelectric field by the free carriers. Further, the expression for 'A' involves piezoelectric, elastic and dielectric constants. Devlin[23] pointed out that the exact calculation of the transport properties which would allow for the anisotropy of the piezoelectric, elastic and dielectric constants is very complicated in detail and has not as yet been carried out. The value of 'A' may therefore depend on the crystallographic orientation of the sample.

Another possibility is suggested by the work of Rozyonyi and Foster[35] on thin film transducers who showed that adjacent regions in cadmium sulphide films could produce piezoelectric voltages of opposite sign because of C-axis polarity inversion between them. Thus the quantity 'A' may well vary from crystal to crystal if large single crystals contain an appreciable number of anti-phase boundaries.

Following these suggestions, it is proposed to make piezoelectric measurements on insulating and semiconducting samples of cadmium sulphide to determine whether finite values of conductivity affect the electromechanical coupling constant. Similarly an electron microscope investigation of thin slices of single crystal boules is in hand to study the incidence of anti-phase boundaries.

8-4. Temperature dependence of conductivity

The temperature dependence of the electrical conductivity of crystals 182, 183, 167, 107 and 148 is shown in Figure 8.4. The data presented in Figure 8.4 show that the conductivity increased as the temperature dropped from 300°K to 100°K, even though the carrier concentration remained constant over this temperature range (Figure 8.1). This behaviour reflects the increase in mobility ($\sigma = ne\mu$) with decreased scattering of carriers by the thermal vibrations of the crystal lattice. The conductivity reached a maximum in the neighbourhood of 100°K and then

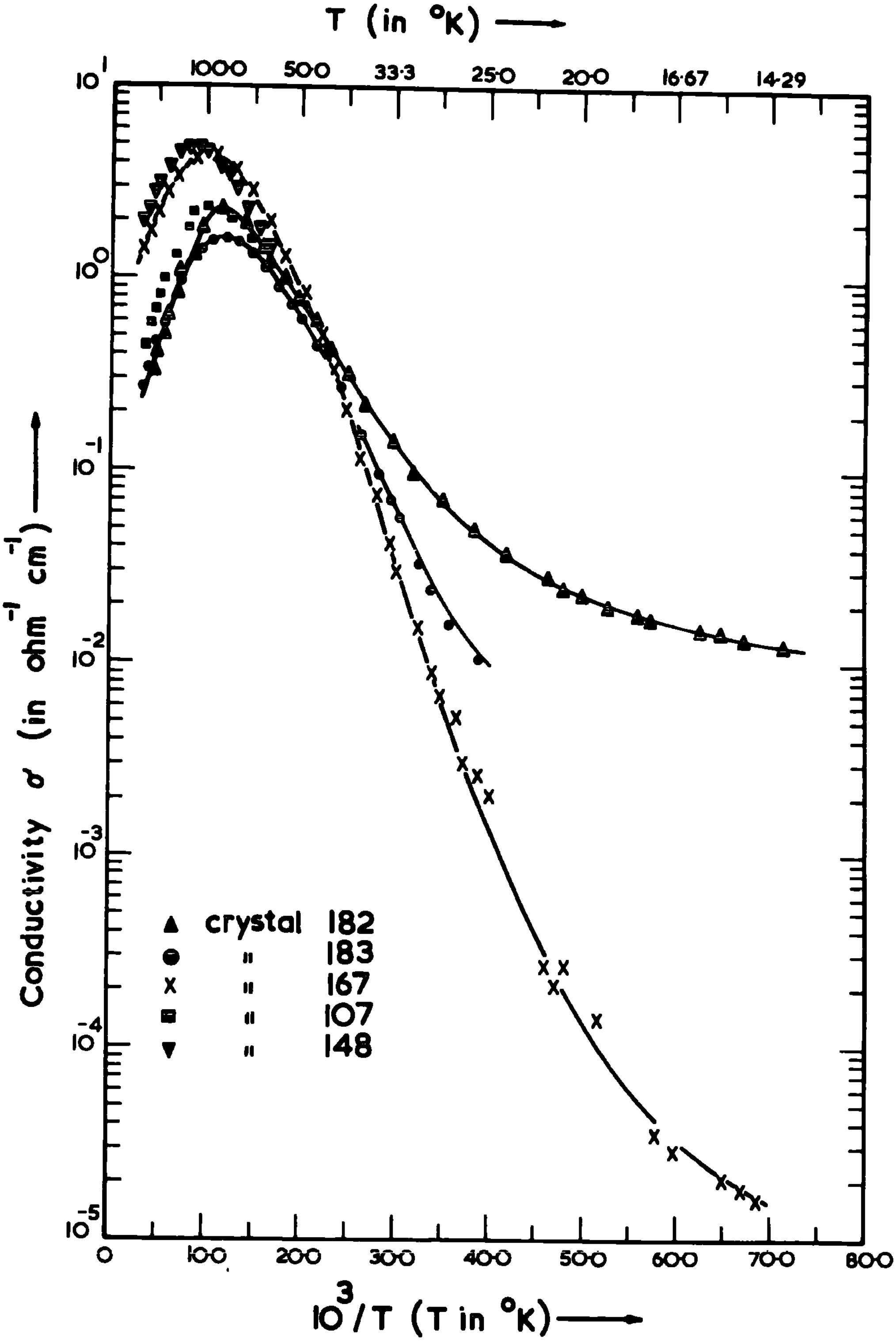

Fig. 8·4. The electrical conductivity σ as a function of temperature for crystals 182, 183, 167, 107 and 148.

decreased with decreasing temperature (Figure 8.4).

At very low temperatures the slopes of the curves for crystals 182 and 167 are very different. The overall dependence of conductivity on temperature(Figure 8.4) from 100°K down to 25°K could be ascribed to the combined effects of two phenomena. (i) A drop in the concentration of the conduction electrons in this temperature range (Figure 8.1) was observed due to the de-ionization of the donor impurities. (ii) The Hall mobility reached a maximum and then decreased as impurity scattering became more pronounced. The temperature variation of carrier concentration (Figure 8.1) showed a saturated region from the neighbourhood of 25°K to 14°K for crystals 182 and 167. The decrease in conductivity for crystals 182 and 167 observed in this temperatuer range was due to the decrease in the Hall mobility (Figure 8.3).

Much of the previous work has been concerned with the temperature variation of conductivity and a discussion of this phenomenon is appropriate here. The temperature dependence of the conductivity is usually expressed as[3]

$$\sigma = C_1 \exp(-\epsilon_1/kT) + C_2 \exp(-\epsilon_2/kT) + C_3 \exp(-\epsilon_3/kT) \qquad (8.6)$$

where the C's are assumed to depend only slowly on temperature. In equation (8.6), ϵ_1 is the activation energy to excite an electron from a donor to the conduction band and ϵ_3 is the activation energy associated with the phonon-assisted hopping motion of donor electrons from an occupied to an unoccupied donor (see Section 8-2(b)). ϵ_2, the activation energy which appears in the so-called "intermediate concentration range" is difficult to discuss. In germanium, ϵ_2 is found to appear in plots of σ versus $1/T$ for samples with carrier concentration in the range between 2×10^{16} to 2×10^{17} cm^{-3} at room temperature.[3] ϵ_2 has been interpreted in different ways by different investigators, a discussion of which will be found in the literature.[36]

The temperature dependence of the carrier concentration of crystals 182, 183 and 167 was found to give rise to impurity band conduction (non-metallic type) in the range 25°K to 14°K (Figure 8.1). A brief discussion of impurity conduction (non-metallic type) has been given in Section 8-2(b). To determine the value of ϵ_3, which is the activation energy of the impurity band conduction, from the variation of conductivity σ versus $1/T$, measurements have to be made down to below liquid helium temperatures. Our measurements were, however, limited to 14°K only.

An analysis of the temperature dependence of the conductivity data (Figure 8.4) was made to yield the values of ϵ_1 and ϵ_2 for crystals 182 and 167 and ϵ_1 for crystal 183. The values of ϵ_1 and ϵ_2

were determined from the slopes of the conductivity versus 1/T curve using equation (8.6). The conductivity versus 1/T plots (Figure 8.4) shows the following slopes: 16·5 meV (ϵ_1) from 66°K to 30°K and 2·3 meV (ϵ_2) from 25°K to 14°K for crystal 182; 27 meV (ϵ_1) from 50°K to 25°K and 6·1 meV from 18°K to 14°K for crystal 167 and 18 meV (ϵ_1) from 60°K to 30°K for crystal 183. No attempt was made to determine the values of ϵ_1 from σ versus 1/T (Figure 8.4) for crystals 107 and 148, measurements for which were limited to 60°K only.

The values of ϵ_1 calculated from the variations of σ versus 1/T (Figure 8.4) for crystals 182, 183 and 167 differ from the values of E_D determined from the variation of log n versus 1/T (Figure 8.1) by 10 to 20% (see Table 8.2). In the temperature range considered, the carrier concentration is, in general, given by

$$n = \left((N_D - N_A)/N_A\right) \left(\frac{2\pi m_e^* kT}{h^2} \right)^{3/2} \exp(-E_D/kT) \qquad (1.38)$$

If we use the value of n in the expression $\sigma = ne\mu$ and compare this with $\sigma = C_1 \exp(-\epsilon_1/kT)$, then ϵ_1 will be equal to E_D only when the electrical mobility varies as $T^{-3/2}$. The mobility observed (for CdS) does not vary as $T^{-3/2}$ in the temperature range considered here (Figure 8.3) so that values of ϵ_1 determined from $\ln\sigma$ versus 1/T curves give only approximate estimates of the donor activation energy for cadmium sulphide.

Crandall[10] made Hall effect and conductivity measurements from 300^{o}K to 1·8^{o}K on an undoped crystal of cadmium sulphide with $n = 6{\cdot}9 \times 10^{15}$ cm^{-3} and $\mu = 350{\cdot}00$ cm^{2}/volt-sec. at room temperature. A donor level E_D of 0·021 eV, believed to be due to excess cadmium, was found by Crandall from the variation of the Hall coefficient versus 1/T. Crystal 182 which has $n = 4{\cdot}0 \times 10^{15}$ cm^{-3} and $\mu = 383{\cdot}00$ cm^{2}/volt-sec. at room temperature and a donor level E_D of 0·02 eV, is comparable with the crystal of Crandall. Crandall observed three distinct slopes in the variation of σ versus 1/T curve (for his crystal): 18 meV (ϵ_1) from 50^{o}K to 22^{o}K, 2·6 meV (ϵ_2) from 22^{o}K to 4^{o}K and 0·66 meV (ϵ_3) from 3^{o}K to 1·8^{o}K. The values of ϵ_1 and ϵ_2 for crystal 182 are 16·5 meV and 2·3 meV respectively. The lower energy ϵ_3 (= 0·66 meV) (Crandall's results) was attributed to hopping conduction.

8-5. Summary

Hall effect measurements have been made successfully on a number of doped and undoped crystals of cadmium sulphide between 300^{o}K and 14^{o}K. The analysis of the temperature dependence of the free electron concentration (Figure 8.1) using equation (1.36) yielded values of the donor ionization energy E_D, and the donor N_D and acceptor N_A concentrations (see Table 8.2). The values of N_D and N_A calculated from the curves of Figure 8.1 have been compared with the intensities of the I_2 and I_1 lines obtained from edge emission studies by D.S.Orr. The values of the ratios of I_2/I_1 were found to agree reasonably satisfactorily with those of

N_D/N_A for the two crystals 167 and 107 for which complete data are available (Table 8.2).

The variation of the carrier concentration at low temperature showed a saturated region in the neighbourhood of 30^oK to 14^oK (Figure 8.1). This can be explained in terms of a non-metallic, impurity conduction mechanism which is described fully in the paper by Mott and Twose[3] (see Section 8-2(b)).

The Hall mobility data were found to have a straight forward interpretation down to 50^oK (see Section 8-3.1). The theoretically computed values of the electrical mobility μ assuming polar optical mode (μ_{op}) and piezoelectric (μ_{pz}) scattering ($\mu^{-1} = \mu_{op}^{-1}+\mu_{pz}^{-1}$) with $m_e^* = 0{\cdot}18m$ described the experimental mobility data down to 50^oK well for crystal 182 (Figure 8.2(a)). To obtain agreement between the theoretical and the experimental values of the mobility data for crystals 183, 167, 107 and 148, the effect of ionized impurity scattering μ_I was also taken into consideration. The theoretically computed values of $\mu(\mu^{-1} = \mu_{op}^{-1}+\mu_{pz}^{-1}+\mu_I^{-1})$ assuming $m_e^* = 0{\cdot}19m$ described the experimental mobility data for crystals 107 and 148 down to 60^oK (Figures 8.2(d) and 8.2(e)), for crystal 167 down to 80^oK (Figure 8.2(c)) and for crystal 183 down to 30^oK (Figure 8.2(b)).

The electron effective mass used in the analysis of the Hall mobility data is in agreement with the values obtained from the electrical and optical measurements.[6,13,22,31-33]

An analysis of the temperature dependence of conductivity data was also discussed in Section 8-4. The values of activation energy of donor impurities calculated from the curves σ versus 1/T (Figure 8.4) for crystals 182, 183 and 167 agree within 10 to 20% with the values of E_D (Table 8.2) calculated from the plots of log n versus 1/T (Figure 8.1).

(1) L. Clark and J. Woods, Journal of Crystal Growth, 3, 126, 1968.

(2) K.F. Burr and J. Woods, "Progress Report on growth and doping of cadmium sulphide single crystals", Department of Appl.Physics and Electronics, University of Durham, February, 1969.

(3) N.F. Mott and W.D. Twose, Advances in Physics, 10, 107, 1961.

(4) D.S. Orr, L. Clark and J. Woods, Brit.J.Appl.Phys., Ser.2, Vol.1, 1609, 1968.

(5) F.A. Kröger, H.J. Vink and J. Volger, Philips Res.Repl., 10, 39, 1955.

(6) W.W. Piper and R.E. Halsted, Proc.Int.Conf.on Semiconductor Physics, Prague 1960, Academic Press, New York, 1961. page 1046.

(7) M. Itakura and H. Toyoda, J.Phys.Soc., Japan, 18, 150, 1963.

(8) L. Clark and J. Woods, Brit.J.Appl.Phys., 17, 319, 1966.

(9) G.P.O. Telecommunications Headquarters, Research Report No.47.

(10) R.S. Crandall, Phys.Rev., 169, 577, 1968.

(11) D. Berlincourt, H. Jaffe and L.R. Shiozawa, Phys.Rev., 129, 1009, 1963.

(12) H.H. Woodbury, page 586 in Physics and Chemistry of II-VI Compounds, ed. M.Aven and J.S. Prener (North-Holland Publishing Co., Amsterdam, 1967).

(13) D.G. Thomas and J.J. Hopfield, Phys.Rev., 128, 2135, 1962.

(14) K. Maeda, J. Phys.Chem.Solids, 26, 1419, 1965.

(15) K. Colbow, Phys.Rev., 141, 742, 1966.

(16) S. Toyotomi and K. Morigaki, J.Phys.Soc., Japan, 25, 807, 1968.

(17) D.J. Howarth and E.H. Sondheimer, Proc.Roy.Soc., A219, 53, 1953.

(18) A.C. Beer, "Galvanomagnetic Effects in Semiconductors", Academic Press, 1963. page 289.

(19) S.J. Czyzak, W.M. Baker, R.C. Crane and J.B. Howe, J.Opt.Soc.Am. 47, 240, 1957.

(20) R.J. Collins, J.Appl.Phys., 30, 1135, 1959.

(21) J.A. Marley and R.C. Dockerty, Phys.Rev., 140, A304, 1965.

(22) J.D. Zook and R.N. Dexter, Phys.Rev., 129, 1980, 1963.

(23) S.S. Devlin, "Physics and Chemistry of II-VI Compounds", ed. M.Aven and J.S. Prener (North-Holland Publishing Co., Amsterdam, 1967). page 551 (Table 11.1).

(24) C. Hilsum and A.C. Rose-Innes, "Semiconducting III-V Compounds", Pergamon Press, 1961, page 114.

(25) E. Gutsche, Naturwissenschaften, 45, 486, 1958.

(26) Y. Onodera, J.Phys.Soc., Japan, 20, 633, 1965.

(27) A.R. Hutson, J.Appl.Phys., 32, 2287, 1961.

(28) A.R. Hutson, Phys.Rev.Letters, 4, 505, 1960.

(29) K. Kobayashi, "II-VI Semiconducting Compounds", 1967 International Conference, ed. D.G. Thomas. page 755.

(30) A.G. Redfield, Phys.Rev., 94, 526, 1954.

(31) M. Balkanski and J.J. Hopfield, Phys.Stat.Sol., 2, 623, 1962.

(32) W.S. Baer and R.N. Dexter, Phys.Rev., 135, A1388, 1964.

(33) K. Sawamotto, J.Phys.Soc., Japan, 19, 318, 1964.

(34) J. Lambe and C.C. Klick, "Progress in Semiconductors, Vol.3, page 184.

(35) G.A. Rozgonyi and N.F. Foster, J.Appl.Phys., 38, 5172, 1967.

(36) E.A. Davies and W.D. Compton, Phys.Rev., 140, A2183, 1965.

CHAPTER 9

CONCLUSIONS

9-1. PhotoHall measurements

One of the objectives of the investigation described in this thesis was to use photoHall measurements to determine various electron trapping parameters. The present work has proved that the method is very successful in realising this objective.

With insulators with impurity or defect centres in the forbidden gap, a change in the density of filled traps following photoexcitation leads to a change in mobility. An estimate of the energy depths of the imperfection centres relative to the conduction band can then be made from the measured variation of electrical mobility with photoexcitation.

The evaluation of trap depths by this method has proved possible for traps with low ionization energies ($< 0{\cdot}5$ eV). Results obtained from photoHall measurements have been supported by an independent investigation of T.S.C. In fact, the trap depths calculated from photoHall data for crystal 78 are in excellent agreement with the T.S.C. measurements (Section 6.3).

The photoexcitation changes the effective charge of the scattering centres by adding or removing an electron from their environment; so the sign of the mobility change indicates the effective charge on the imperfection centres. The photoHall data have been used to determine both the charge state and the scattering cross-sections of the imperfection centres. The experimental values of scattering cross-sections are of the order of 10^{-11} cm^2 which can be considered reasonably close to the values ($\sim 10^{-12}$ cm^2) expected from theoretical calculations. Good agreement between the experimental and theoretical values of the scattering cross-sections can be taken to imply that the crystal has a high degree of uniformity and a homogeneous distribution of imperfection centres. This has been confirmed by making a mapping of the potential distribution along the current axis at room temperature (under the worst possible condition of illumination). The potential distribution as a function of distance indicates excellent uniformity of the crystals (Section 6-8(v)).

The presence of Class II centres in the forbidden gap of an insulator like cadmium sulphide gives rise to high photosensitivity. The technique of photoHall measurement has also been used to determine the height of the sensitizing centres above the top of the valence band. The temperature dependence of the photoexcited carrier concentration yielded a value of 1·04 eV for the height of these centres above the valence band (Sections 7-2 and 7-3). This value agrees well with that of 1·1 eV found from measurements of the optical and thermal quenching of photoconductivity.[1][2]

9-2. <u>Nature of the defect centres</u>

The photoHall measurements indicated the presence of four electron trapping levels with energy depths of 0·12, 0·16, 0·22 and 0·33 eV in crystal 78 and six electron trapping levels with energy depths of 0·098, 0·13, 0·19, 0·25, 0·33 and 0·42 eV in crystal 79. The traps with energy depths of 0·13, 0·25 and 0·33 eV were found therefore in both the samples. The exact atomic nature of these defect centres is very difficult to determine. Some suggestions can only be made based on circumstantial evidence obtained from photoHall measurements.

The values of trap depth were obtained from "S-shaped" curves which resulted from plotting $\frac{1}{\mu}$ versus E_{fn}. From the variation of Hall mobility with photoexcitation the imperfection centres associated with the trapping levels at 0·13, 0·16, 0·19, 0·25, 0·33 and 0·42 eV were recognised as being singly positively charged when they lie above the equilibrium Fermi level in the dark.

The trapping levels are probably associated with intrinsic crystal defects. The simplest types of crystal defect with the required property of being positively charged in the dark, are an anion (sulphur) vacancy or anion vacancy-impurity complex, either without any trapped electrons (doubly positively charged) or with one trapped electrons (singly positively charged). Another possibility is that the centres might be cadmium-interstitials. Recently Woodbury et al.[3] have indicated that interstial cadmium and sulphur atoms are probably neutral and do not form trapping levels in the forbidden gap of cadmium sulphide.

In general, a centre such as an anion vacancy which is singly positively charged would be expected to be paramagnetic in character. It is hoped that electron spin resonance measurements which it is planned to make on these samples, will be able to establish the symmetry of these centres. In this respect, a correlation between photoHall and e.s.r. measurements will be very useful.

The nature of defect centres identified in this work can be compared with the observations of Nicholas and Woods[4] and Cowell.[5] Nicholas and Woods concluded from T.S.C. measurements that the defect levels at 0·05 and 0·15 eV were associated with isolated sulphur vacancies. They also proposed a tentative identification of the defect level at 0·25 eV as a complex of associated sulphur vacancies. Cowell found a series of trapping levels at 0·18, 0·21, 0·39 and 0·42 eV in cadmium-rich samples and concluded that they were due to sulphur vacancies. These observations can be considered to be in good agreement with the results of the present photoHall measurements.

The photoHall measurements also showed that crystal 79 contained an imperfection level at 0·098 eV below the conduction band. The centre involved was neutral in the dark. A sulphur vacancy with a level at this energetic position would be positively charged and a cadmium vacancy doubly negatively charged in the dark. Therefore, it may be that this imperfection level at 0·098 eV is associated with a complex of sulphur and cadmium vacancies.

The information obtained from photoHall measurements was also used to determine E_I, the height of the Class II centres above the valence band. A value of S_p/S_n, which is the ratio of the capture cross-sections of the Class II centres for holes to electrons could also be obtained. The value of E_I was found to be 1·04 eV and that of S_p/S_n

was ~10^8. Bube[6] attributed the high value of S_p/S_n (~$4{\cdot}0 \times 10^8$) to doubly negatively charged sensitizing centres. Crystals 78 and 79 were as-grown crystals. Cadmium vacancies would be expected to be present and act as sensitizing centres in this type of photosensitive insulating crystal. Since cadmium sulphide is a divalent compound, cadmium vacancies are likely to be doubly negatively charged.

9-3. Hall effect measurements

Thermal equilibrium Hall effect measurements were made on a number of semiconducting samples of cadmium sulphide in the temperature range from 14°K to 300°K. All these samples were grown in this laboratory using the method described in the literature by Clark and Woods.[7] The object of the investigation was to assess the quality of the crystals and to determine the dominant carrier scattering mechanisms.

The n-type semiconduction observed in the as-grown, undoped crystals was attributed to the presence of sulphur vacancies which act as donors. An anion vacancy (sulphur) in II-VI compounds captures two electrons to maintain charge neutrality in the crystal. The second trapped electron can be released thermally and thus contribute to electrical conduction. The semiconducting samples of cadmium sulphide also contain acceptors. The value of the activation energy E_D of the donor level and the concentration of donors and acceptors N_D and N_A were determined from the variation of carrier concentration with temperature. The donor ionization energies were found to lie in the range 0·02 eV to 0·029 eV. The variation of carrier concentration below 30°K was found to be dominated by an impurity band conduction mechanism (non-metallic type).

The incorporation of a halogen ion in cadmium sulphide results in the formation of a centre consisting of the halogen ion and an electron bound to the centre:

$$S^{-2} = Cl^{-1} + e$$

Thus the halogen ion replaces sulphur and acts as a donor. A halogen-doped sample is expected to have the same activation energy of the donor level as an as-grown semiconducting sample. Hall effect measurements on samples doped with chlorine have established this.[8] We have made Hall effect measurements on a sample of cadmium sulphide which was heavily doped with chlorine. Due to impurity band conduction (metallic type), the carrier concentration showed little change with temperature and the activation energy of the donor level was not obtained from the plot of log n versus 1/T.

Another expected effect of the incorporation of halogen donors is the formation of cadmium vacancies for charge compensation. Thus the sensitizing centres are produced by the normal process of donor incorporation.

The calculated values of N_D and N_A were compared with the results of edge emission studies. Reasonable agreement was found between the ratios of I_2/I_1 and N_D/N_A. The I_1 and I_2 emission lines are due to recombination of excitons bound to neutral acceptors and donors respectively. Their relative intensities therefore, give an (approximate) indication of the relative concentration of acceptors and donors. The way in which the donor and acceptor concentrations varied with the conditions under which these crystals were grown, were also determined.

The high values of the electron mobilities indicate a high degree of crystalline perfection in our crystals. Polar optical mode scattering was found to be the dominant intrinsic scattering mechanism at higher temperatures. The Hall mobility data were fairly straight forward to interpret down to 50^{o}K. The theoretical values of the electrical mobility μ were computed assuming polar optical mode, piezoelectric and ionized impurity scattering ($\mu^{-1}=\mu_{op}^{-1}+\mu_{pz}^{-1}+\mu_{I}^{-1}$) . Good fit with the experimental curves was obtained with $m_e^* = 0{\cdot}19$ m at least down to temperatures of 50^{o}K. Although the effect of ionized impurity scattering was evident in the variation of mobility with temperature below 50^{o}K, the mobility variation in that region is not clearly understood. This is due to the onset of the impurity band conduction process at low temperatures.

The value of effective mass ($m_e^* = 0{\cdot}19$ m) used in the computation of the theoretical values of the electrical mobility is in good agreement with the values obtained from other electrical and optical measurements.

9-4. Suggestions for future work

PhotoHall effect should be measured on crystals grown in a wide variety of partial pressures of cadmium and sulphur to study the incidence of particular traps.

Hall effect measurements using an A.C. method have been made at room temperature on semiconducting samples of cadmium sulphide.

Using a suitable impedance converter this method will enable the Hall voltage of samples with resistivities up to 10^7 to 10^8 ohms-cm to be measured and thus extend the number of samples which can be studied.

Galvanomagnetic effects could also be measured to study the symmetry of the energy band structure.

References

(1) R.H. Bube, Phys.Rev., 99, 1105, 1955.

(2) R.H. Bube and A.B. Dreebeen, Phys.Rev., 115, 1578, 1959.

(3) H.H. Woodbury and R. Hall, Phys.Rev. Letters, 17, 1093, 1966.

(4) K.H. Nicholas and J. Woods, Brit.J.Appl.Phys., 15, 783, 1964.

(5) T.A.T. Cowell, Ph.D.Thesis, University of Durham, 1968.

(6) R.H. Bube, J.Appl.Phys., 32, 1707, 1961.

(7) L. Clark and J. Woods, J.Crystal Growth, 1968.

(8) F.A. Kröger, H.J. Vink and J. Volger, Philips Res.Rpt.10, 39, 1955.